Morphological control of $LiNi_{0.8}Mn_{0.1}Co_{0.1}O_2$ cathodes for lithium-ion cells using biotemplating

Ryan Emmett

For the degree of Doctor of Philosophy

Supervisors – Dr Rebecca Boston, Dr Alisyn Nedoma

University of Sheffield

Faculty of Engineering

School of Chemical, Materials and Biological Engineering

December 2024

Abstract

The novel biotemplating method was used to synthesise NMC811 such that particle morphology would be manipulated, performance of the cathode increased, and lithium-ion cells improved to help reach the goal of net-zero. NMC811, defined by a high specific capacity of >200 mAh/g but a poor capacity retention and structural stability, was synthesised using either dextran or sodium alginate, preheated at 300 °C for 2h and calcined at 800 °C using nitrate precursors or 850 °C using acetate precursors for 2 h under O_2. The resulting layered, organised NMC811 indicated high layering and low mixing of Li^+ and Ni^{2+} cations with nanoscale octahedral and rounded primary particles of average diameter 600 to 1000 nm. When cycled to 4.2 V at 0.1 C resulted in specific capacities as high as 240 mAh/g with capacity fade of 30 mAh/g over 50 cycles when using sodium alginate or 150 mAh/g specific capacity with a capacity fade of 10 mAh/g over 50 cycles when using dextran. Plate and nanowire novel morphologies were also observed when using dextran and sodium alginate respectively. Sodium alginate and κ-carrageenan were also used to dope NMC811 with sodium and sulfur respectively. 10% Na-doped and 0.5% S-doped NMC811 were viable, exhibiting layered, organised NMC811 structures with sodium peroxide/sodium carbonate and lithium sulfate secondary phases respectively, and exhibiting morphological control of nanoscale, octahedral primary particles. Novel microwire morphologies were also observed when biotemplated with κ-carrageenan. When cycled to 4.2 V at 0.1 C, specific capacities of 170 mAh/g and 150 mAh/g with capacity fade of 10 mAh/g and 40 mAh/g after 50 cycles were observed when doping with sodium alginate and κ-carrageenan, respectively. Using the novel biotemplating method, nanoscale novel morphologies can be synthesised and NMC811 specific capacity and capacity retention increased, while cathode synthesis is more inexpensive and quicker.

Acknowledgements

I would like to thank my supervisors Dr Rebecca Boston and Dr Alisyn Nedoma for providing me with the opportunity to study a PhD at the university of Sheffield, for providing support and direction in my transition from an engineering master's student to a materials and chemistry PhD student, and for being patient with my specific style of work.

I wish to thank the Faraday Institution for funding my PhD, for providing numerous opportunities to train and grow as both a person and a professional, and for making it possible to share my work in places as far away as Dublin and Hawai'i. I would also like to thank the rest of Faraday Cohort 3 for making our many training days so enjoyable.

I would like to give thanks to the Sustainability Oxide Processing Group and associated people both past and present (Becca Huang, Yining Li, Pha Thibthong, George Wilson, Silvija Zilinskaite, Steph Mudd, Enrique Casanas, Pooja Kumari, Shuchi Vaishnav, Jess Andrews, Laura Wheatcroft, Daniel Martin, and Babatunde Adebayo) for all the wonderful meals over the last 4 years and for creating such a wonderful and unique office to work in.

Thank you to all the staff of the Sir Robert Hadfield Building, Sorby Centre, and Royce Discovery Centre who have helped me with my work during my project. Without your knowledge of materials and chemistry I would have struggled even more with the transition from engineer to material scientist.

Thank you to Sheffield University Sub Aqua Club and the many friends I have played tabletop games with (you know who you are) for making Sheffield so welcoming and providing me the opportunity to have numerous new adventures.

Finally, thanks to my parents Dean and Annette Emmett for their continued support and love while doing my PhD and in life, and a special thank you to Amy Hammond, Zoe Scarlett, and Adam Higginbottom (who demanded I have a duck in my thesis, so "duck") for all the laughs, support, coffee breaks and nights in.

Contents

Contents of Figures

1 Literature Review

1.1 Net zero and the role of electrochemical storage

As of 2024, the United Nations' Emissions Gap Report 2024 predicts a likely global temperature increase of 3.1 °C by 2100 with the current emissions regulations in place [1]. As of 2023, the United Kingdom is a significant polluter with 384.2 $MtCO_2e$ of greenhouse gases emitted over the calendar year [2]. While a reduction of 52.7% when compared to emissions in 1990 and 14.2% less emissions than in 2019, further work is required to make the UK's 2050 net zero target [3]. During 2023, emissions from domestic transport made up 29.1% of the UK's total greenhouse gas emissions making it the largest emitting sector. Reducing greenhouse gas emissions from domestic transport is therefore one of the most effective ways of reaching net zero. One of the currently used methods to reduce greenhouse gas emissions emitted by transport is the widescale replacement of internal combustion engine (ICE) vehicles with electric vehicles (EVs). As of October 2024, the UK government plans to phase out all new ICE vehicles by 2035 [4] to help towards the 2050 net zero goal. Therefore, as of 2035 all new production cars in the UK will be EVs.

1.2 Cell Chemistries

Cells are a form of electrochemical storage. Cells work by converting chemical potential energy into electrical energy, and consist of two terminals – one positive, one negative, two electrodes – a positive cathode and a negative anode, and an electrolyte [5]. When a cell is discharged atoms in the cathode will ionise and the ions conduct from the anode, through the electrolyte, to the cathode, Figure 1. The free electrons produced during ionization will travel from the negative to the positive terminal through whatever conductive matter the terminals are connected to, at which point ions in the cathode regain the electrons. When charged this process occurs in reverse.

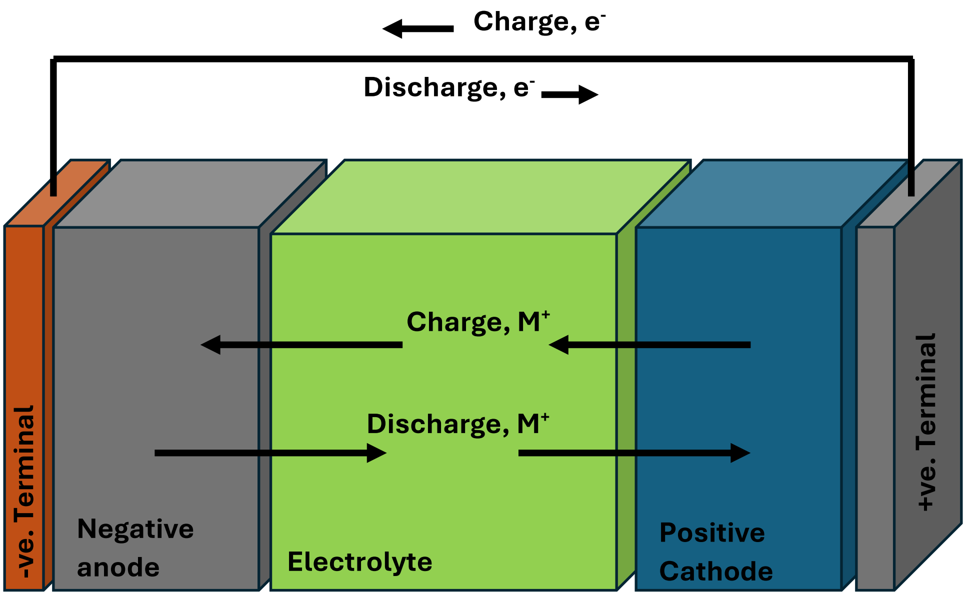

Figure 1 Electrochemical cell diagram

Numerous cell chemistries have been researched, each with different applications. Lithium-ion cells are currently employed in portable electronic devices, power tools, electrical vehicles, and are being investigated for possible use in grid storage [6]. Sodium-ion cells are being investigated as potential replacements for lithium-ion cells in electronic devices and EVs, but due to a lower volumetric energy density and being currently 3x heavier than lithium ion cells are mainly being investigated for use in such applications as large scale energy storage, grid backup systems, and microgrids [7]. In the past nickel metal hydride cells were used in portable electronics and hybrid vehicles but have since been outclassed [8], while lithium-sulfur cells meanwhile are being targeted for use in space, aviation, and defence due to being light weight [9].

1.2.1 Lithium-ion cells

Lithium-ion cells have numerous benefits that make them attractive for use in application such as EVs. This includes a high cell potential, high volumetric capacity, high energy density and power density,

Figure 2, and the ability to cycle at a high c-rate [10]. Disadvantages include high cost, issues with the supply of raw materials, and safety issues. Overall, the benefits have been seen to outweigh the negatives which have led to an adoption over other cell chemistries, with the ability of lithium-ion cells to be cycled at operating voltages above 4 V, gravimetric capacities of 250 Wh/kg and volumetric energy densities of 650 Wh/L, and specific capacities of 230 mAh/g when using high Ni cathodes [11]. Due to high capacities and energy densities almost all EVs presently sold in the UK are powered by lithium-ion cells. Improving lithium-ion cells is therefore beneficial towards ensuring the government's 2035 phase-out and 2050 net zero goal [4][6]. It is indicated though that the pipeline from the mining of materials to producing cells has a significant carbon footprint [12], and the concentration of raw materials in locations such as China and the Americas [13] are leading researchers to investigating other cell types.

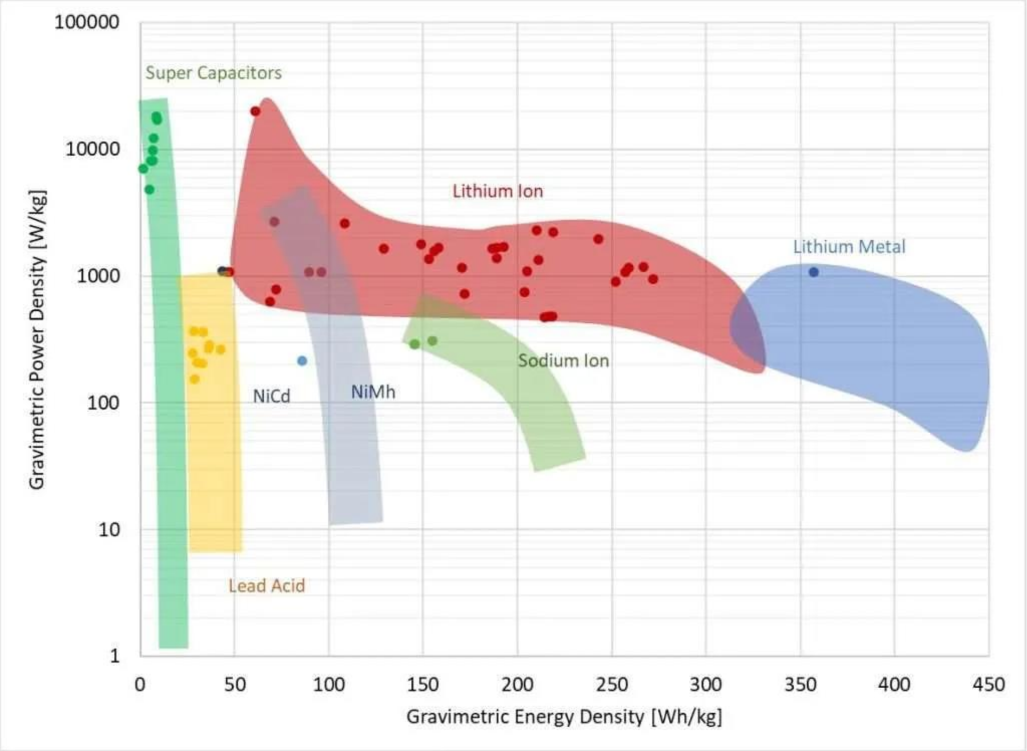

Figure 2 Comparison of Current Cathode Chemistries [14]

1.2.2 Sodium-ion cells

Sodium-ion cells, while reaching commercialisation and being seen as being very similar and a viable alternative to lithium-ion due to being relatively inexpensive, sodium having greater availability, safer, and greener, suffers from a poorer energy density and cycling life [15]. Current sodium ion cells have exhibited capacities of between 120 and 145 mAh/g and capacity retentions of between 70 and 89% depending on the cathode used while also being cycled at lower operating potentials, below 4 V, relative to lithium-ion cells [16]. Along with energy densities of between 130 and 200 Wh/kg and low electronic conductivity this makes sodium-ion more suitable for stationary energy storage systems rather than for in EVs, however use in lower power EVs may be feasible [17]. While also being theoretically cheaper, due to still being in the early phases of commercialisation they are still more expensive per kW/h compared to lithium-ion.

1.2.3 Lithium-sulfur (LiS) cells

Lithium-Sulphur cells, in development since the 2000s, exhibit high energy density upwards of 300 Wh/kg [18] and theoretically boast a very high theoretical capacity of 1675 mAh/g, a high abundance of sulfur, a lower required operating voltage, higher safety, lower cost, are environmentally friendly, and high energy density [19]. The reality is however that lithium-sulfur cells currently have poor cycle life, low efficiency, and struggle to utilise active material. This along with that fact that sulfur acts as an ionic and electronic insulator, high volume change, loss of active material, poor cycling stability and parasitic reactions with the cathode make current lithium-sulfur cells not viable [20][21]. As such, sulfur-doping current viable chemistries, such as NMC811, may prove a useful intermediate step between improving existing lithium-ion cathodes and developing lithium-sulfur cells.

1.2.3.1 Other cell chemistries

Before the advent of lithium-ion, other cell chemistries were considered the norm. While being cheaper and safer, nickel metal-hydride has a lower power density vs. lithium-ion cells as well as having a lower discharge rate and is susceptible to the memory effect [22]. Capacity values of up to 60 mAh/g were stated which is no longer viable for use in applications such as EVs [8]. nickel cadmium also suffer from low power density and energy density vs. lithium ion cells as well as being expensive and very environmentally damaging [23] [24] [8]. Lead-acid batteries have similar disadvantages with energy densities of between 33 to 42 Wh/kg and 50 to 70 Wh/L, power densities of 180 W/kg, and a 300 cycle maximum lifetime [25] [24].

As of 2024 therefore, for high energy density applications lithium-ion remains the optimum selection for uses such as EVs despite rapid advancements in sodium-ion and lithium-sulfur cells.

1.2.4 Discussion of Lithium-ion Cells vs. Alternative Cell Chemistries

When selecting cell chemistry one parameter was to decide on whether to further optimise existing chemistries or aim to further research chemistries currently within the development stage. Both have advantages, with currently under development sodium-ion chemistries being cheaper and more sustainable compared to current lithium-ion chemistries [15], and lithium-sulfur cells exhibiting energy densities of 300 Wh/kg and specific capacities of 1675 mAh/g in addition to improved safety and lower costs [18] [19]. When it came to deciding however, optimisation of current lithium-ion chemistries was selected. Reasons for this include that the timescale for improving net zero technologies is growing small, with the UK targeting the phase out of ICEs and net zero by 2035 and 2050 respectively [3] [4], and that among the biggest concerns amongst consumers are charge life/range in addition to cost [26], [27]. It was therefore decided to select a chemistry that was able to be improved in minimal time and that already started at a high performance baseline.

As such, development of lithium-ion cells were chosen due to a high specific capacity, up to 230 mAh/g when using high Ni cathodes, as well as a high energy density allowing for use in current portable electrical devices and vehicles [11]. Sodium-ion cells, while gaining traction, have lower energy densities (130 – 200 Wh/kg), specific capacities (120 – 145 mAh/g) and are more suited to stationary energy storage while lithium-sulfur is currently too early in development to be viable [16]. Both sodium-ion and lithium-sulfur cells while being cheaper in the future will also currently have an increased price per kW/h due to being in development [17]. With older chemistries (lead-acid, Ni metal hydride, Ni-Cd) already being outpaced by lithium-ion, it makes lithium-ion the current chemistry of choice for reducing greenhouse emissions [24].

1.3 Cathodes

When investigating different positive electrodes, or cathodes, for use in lithium-ion cells each material has advantages and disadvantages. In a lithium-ion cell, lithium acts as the charge carrier Li^+, which when discharging delithiates at the negative anode and lithiates at the positive cathode. Common materials for the electrodes and terminals are outlined in Table 1:

Positive Terminal	**Positive Electrode** [28]	**Electrolyte**	**Negative Electrode** [29]	**Negative Terminal**
Aluminium (Al)	Lithium Iron Phosphate (LFP)	Lithium Hexafluorophosphate ($LiPF_6$)	Graphite (C_6)	Copper (Cu)
	Lithium Nickel Manganese Cobalt Oxide (NMC)		Silicon (Si)	
	Lithium Cobalt Oxide (LCO)		Titanium Oxide (TiO_2)	
	Lithium Manganese Oxide (LMO)			
	Nickel Cobalt Aluminium Oxide (NCA)			

Table 1 Outline of possible materials for Lithium-ion cell components

1.3.1 Nickel Manganese Cobalt Oxide (NMC)

Nickel Manganese Cobalt Oxide, or NMC, is a high energy density cathode that boasts a high cathode potential and specific capacity, with his cathode being seen as a substitute for high cobalt cathodes such as lithium cobalt oxide, or LCO. This cathode is however relatively more expensive, prone to thermal degradation, and has low capacity retention due to oxygen loss during cycling. Most commercially available NMC consists of polycrystalline secondary particles made up of nanoscale primary particles. This results in low tap density compared to LCO, and influences energy density, cycling stability and rate capacity [30]. The high energy density of around 300 Wh/kg is a suitable compromise for the cathode’s shortcomings, however it is observed that NMC cathodes are extremely subject to particle morphology and the method of synthesis used. High mixing of Li and metal layers and poor stoichiometry control may also occur when synthesising high nickel NMC cathodes under solid state synthesis [31].

NMC, Figure 3 [32], consists of the same layered oxide structure as LCO cathodes with alternating layers of lithium and transition metals (nickel, manganese, and cobalt) and layers of oxygen between each layer (i.e. Li-O-TM-O). NMC811 has the rhombohedral space group $R\overline{3}m$, where a=b/=c and α=β=90 ° and γ=120 °. Valence states of high Ni NMC consist of Ni^{2+} and Ni^{3+}, Mn^{4+}, and Co^{3+} when the cathode is fully lithiated [33].

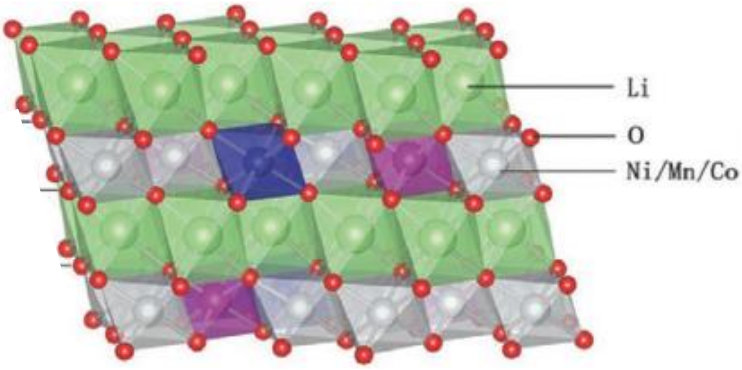

Figure 3 Layered structure of NMC cathode [32]

The high capacity of NMC is a result of the shifting valence states of Ni, with Ni^{2+} shifting to Ni^{3+} and Ni^{3+} to Ni^{4+} during discharge as redox occurs. When charging, the reverse occurs as Ni^{4+} shifts to Ni^{3+} and Ni^{3+} shifts to Ni^{2+}. Degradation of the NMC occurs during this redox process where Ni^{4+} may also shift to Ni^{2+} and form nickel oxide (NiO) [34].

Stability of the NMC cathode is due to the presence of manganese, with a low proportion of manganese in NMC leading to high degradation. When redox occurs Mn^{3+} shifts to Mn^{4+} transferring electrons to Ni^{2+} [33] This not only causes the difference in Ni valence states between Ni^{2+} and Ni^{3+} but also the amount of Ni^{3+} that is able to shift to Ni^{4+} during discharge. Less Ni^{4+} is then available to shift to Ni^{2+}, resulting in less NiO and less degradation of the NMC cathode.

Too high a proportion of manganese will result in significant capacity loss as a high proportion of Mn^{3+} forms a spinel structure where Mn inhabits 16d octahedral sites and lithium inhabits 8a tetragonal sites [35]. While more stable only one lithium ion to every two manganese sites can delithiate resulting in poorer capacity compared to layered oxide structures.

NMC cathodes come in a range of ratios, including NMC111, NMC532, NMC622, and NMC811. With NMC cathodes the specific capacity increases with the proportion of nickel in the structure, Figure 4, at the cost of lower capacity retention. Though NMC cathodes are able to be cycled up to 4.5 V, any cycling above 4.3 V will also result in lower capacity retention due to decreases in structural stability caused by significant delithiation and decomposition of oxygen in the electrolyte due to reactions with Ni^{4+} ions [36]. NMC with higher proportions of nickel are also more attractive due to a smaller proportion on cobalt, an element some wish to phase out due to the ethics surrounding its mining that include child labour and environmental damage [25].

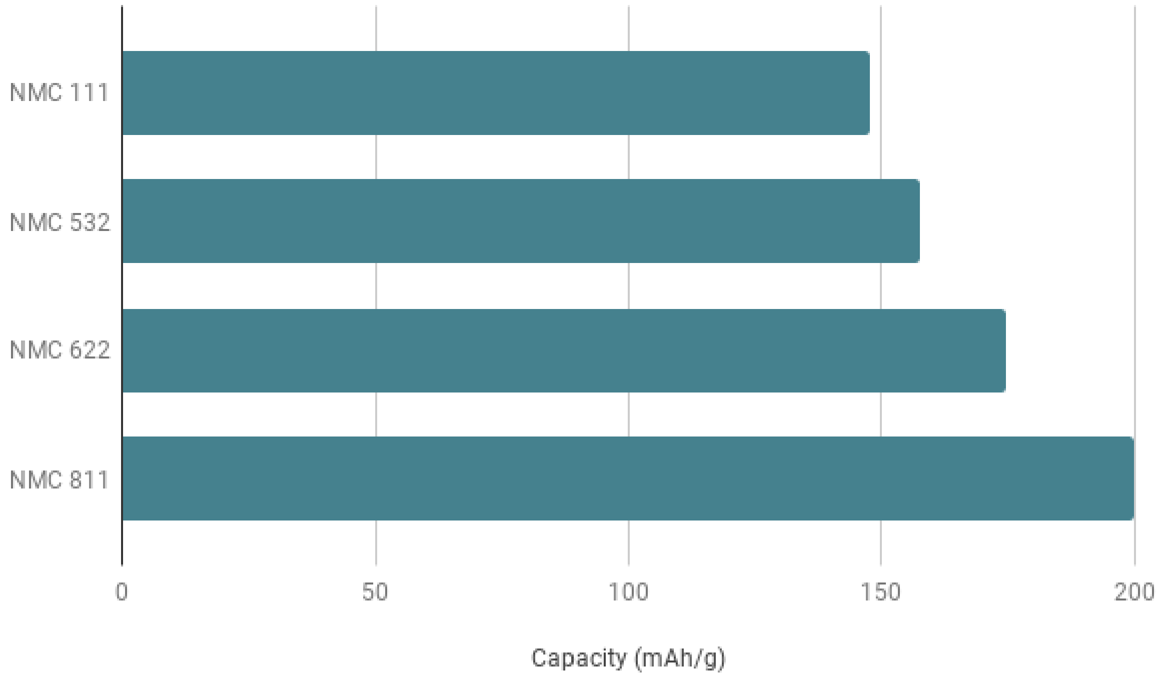

Figure 4 Specific capacities of NMC111, 532, 622, and 811 cathodes [37]

1.3.1.1 NMC811 cathode

NMC811 ($LiNi_{0.8}Mn_{0.1}Co_{0.1}O_2$) is a cathode where the proportion of Ni is much greater than that of Mn and Co combined and was developed to maximise the specific capacity of NMC cathodes [38]. NMC811 has high energy density and high reversible capacity of 175 to 190 mAh/g as a result of the high proportion of nickel as well as its low proportion of cobalt, while the small proportion of manganese was also seen as significant for improved structural stability. The cathode was also seen as having the most scope for improving cycling life and reducing cost while maintaining high energy density and capacity. Synthesis of high nickel NMC cathodes using solid state may prove difficult however, with mixing of Li and metal layers and poor stoichiometry control being compromised [31].

1.3.1.2 Alternative ratios of NMC cathodes

NMC111 is a cathode with equal proportions of Ni, Mn, and Co. NMC111 has the lowest specific discharge capacity of NMC cathodes at around 155 mAh/g and while still used in applications for devices that require lower capacities are being replaced with NMC cathodes with higher proportions of Ni such as NMC532 and NMC622 [36]. Mixing of cations and metals dissolving into the electrolyte leads to further cycling problems and compounds the relatively low specific capacity [39]. NMC532 represent the most equal compromise between specific capacity and structural stability when using NMC cathodes, exhibiting a specific discharge capacity of between 160 and 170 mAh/g and long lifetime stability [40]. Despite an improvement in energy density and rate capability over NMC111, NMC532 experienced greater capacity fade than NMC111 [41]. Commercial NMC532 is polycrystalline consisting of microscale secondary particles and agglomerated nanoscale primary particles with any commercial single crystal NMC532 consists of microscale primary particles. NMC622 represents the point where the proportion of Ni in NMC is greater than that of Mn and Co combined and is selected due to having both high specific capacity while still retaining structural stability [42]. The high discharge capacity of around 170 mAh/g [43] is due to the high ratio of Ni, however the high proportion of Ni also results in lower cycling stability as a result of Ni^{4+} ion mixing into Li sites during charging and parasite reactions with the electrolyte. The remaining proportion of Mn^{4+} ions improves structural stability, however the lower proportion results in less structural stability than NMC cathodes with higher proportions of Mn.

1.3.1.3 LNO cathode

Lithium nickel oxide (LNO) cathodes are the next step in the development of NMC cathodes. The cathodes is appealing to the battery industry due to the elimination of cobalt and this potential reduction in price [44]. The cathode also boasts very high specific discharge capacities of over 212 mAh/g with columbic efficiency of 93% [44]. LNO is a cathode still under development however with it exhibiting poor cycling stability, having a maximum capacity retention between 66 and 77% at 0.5 C after 50 cycles depending on the synthesis method used. Even when optimised to a specific discharge capacity of 240 mAh/g using a c-rate of C/10, capacity retention is no more than 80% after 100 cycles [45]. While LNO is a cathode that shows extreme promise and should be considered a viable high Ni cathode for the near future due to a high specific capacity and elimination of Co content, at its current development stage it is just short of the required cycling stability for use in lithium-ion cells.

1.3.2 Lithium Cobalt Aluminium Oxide (NCA)

Lithium Cobalt Aluminium Oxide, or NCA, is a more recently introduced cathode that uses cobalt and aluminium as an alternative way to improve stability in high nickel LNO and NMC cathodes [46]. NCA cathodes use Al as a way to reduce Li and Ni cation mixing and transition metal dissolution while improving thermal and cycling stability as a substitute for Mn, while Co is also used to reduce cation mixing and ensures high rate capability [47]. Co is also expensive however and is mined from the Democratic Republic of Congo (DRC) making it a poor cathode to pivot to from NMC cathodes. It is also noted that any amount of Al above 5% will begin to lead towards the production of a secondary phase, while NMC cathodes can contain up to 50% Mn before a spinel structure starts to form. NCA cathodes exhibit specific discharge capacities of 200 mAh/g with high thermodynamic stability. NCA cathodes still suffer from poor cyclability, low electronic conductivity, and structural instability at higher voltages. Thermal stability is disputed however with some research suggests the high Ni content of NCA results in significant thermal instability, with it also being stated that despite advancements in NCA technology the cathodes have significant capacity fade due to high Ni content and structural instability despite use in current Tesla vehicles [48].

1.3.3 Lithium Iron Phosphate (LFP)

Lithium Iron Phosphate, or LFP, is a stable cathode that boasts a high cycling life as well as a relatively low cost and high safety [28]. The disadvantages of LFP a low potential difference, energy density, specific capacity, and electrical conductivity when compared to other lithium-ion cathodes. Maximum energy density of LFP was recorded as 160 Wh/kg, with other lithium-ion cathodes showing significantly higher energy densities.

Previous research suggests the cathode cost could be reduced from 50% of the total cost of the cell when using LCO to 10% of the cell's total cost [49], however LFP cathodes have a lower theoretical specific discharge capacity of 170 mAh/g when compared to other Li-ion cathodes. Figure 5 highlights the olivine structure of the LFP which consists of one-dimensional pathways [50]. Such pathways result in a low electrical and ionic conductivity and are prone to blockages by impurities, which results in the theoretical capacity being difficult to reach. It has been observed that the ionic conductivity occurs along the (010) direction, with the structure having also been observed as having a semi-conducting nature due to the crystalline structure [51].

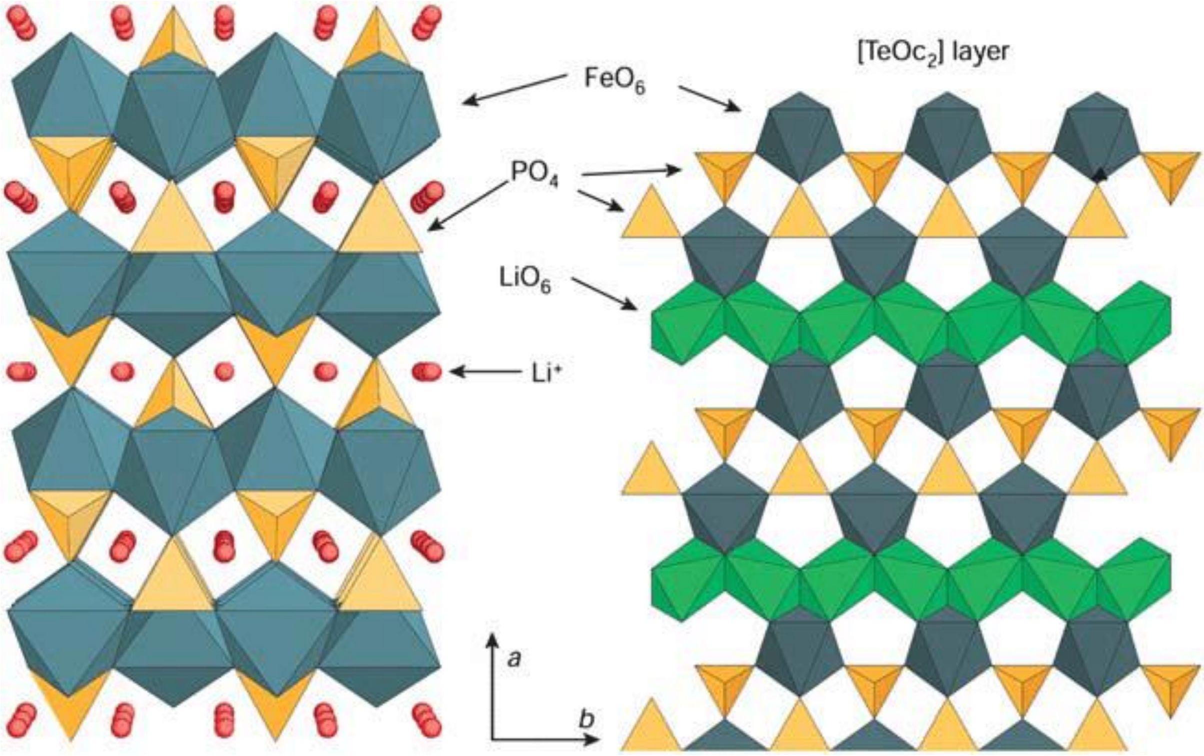

Figure 5 Olivine structure of LFP cathode [50]

LFP cathodes have previously been shown to be the only chemistry to pass all safety tests including nail penetration and short circuit tests [51]. Even without passing safety tests, LFP cathodes have been shown to be non-toxic and environmentally benign when compared to other lithium-ion chemistries, with some manufacturers including Tesla having started to produce electric vehicles with LFP cathodes as of December 2024 due to their relative safety and inexpensiveness [52].

1.3.4 Lithium Cobalt Oxide (LCO)

Lithium cobalt oxide (LCO) have moderate energy densities, higher than LFP but lower than NMC [49]. LCO exhibits high cycling stability but is prone to thermal instability and more expensive, with the cost of the LCO cathode potentially being as much as 50% of the total cost of the cell [49]. While previously being used in a wide range of consumer electronics due to being the first cathode able to operate above 4 V, Figure 7, it has quickly been overtaken by NMC cathodes due to nickel having a high potential and also in part due to the scarcity of cobalt inflating the price of the cathode [53]. While initially only being able to be cycled to 4.25, producing a specific discharge capacity of 135 mAh/g, LCO is now able to be cycled to 4.45 V albeit while requiring electrolytes that have higher stability at higher voltages. Despite this, the underlying chemistry has greater potential than chemistries such as LFP, with high theoretical specific capacities, cycling stability and cycle life, and high open circuit voltage in part due to 2D diffusion pathways for lithium ions [54], Figure 6, and while LCO cathodes are expensive the synthesis is relatively simple [55]. This is provided however that stoichiometric control can be kept as well as a reduction in the mixing of the layering of the Li and Co layers, which may falter during some synthesis methods such as solid state [31].

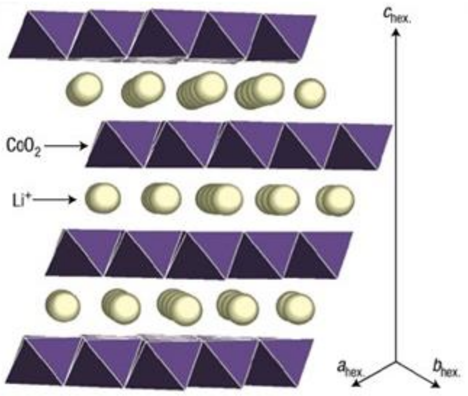

Figure 6 Layered structure of LCO cathode [56]

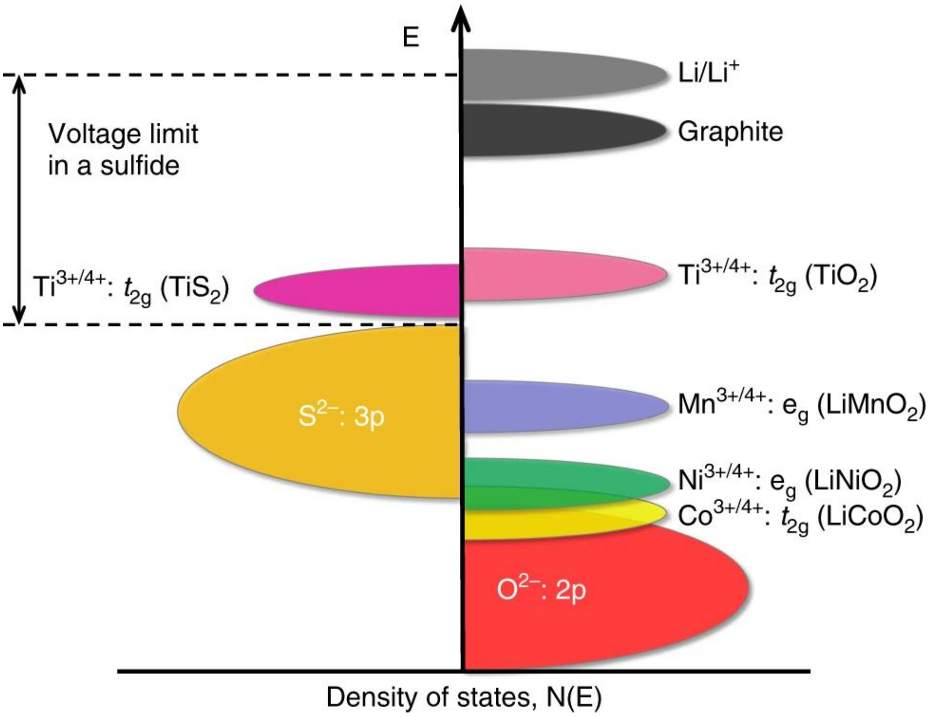

Figure 7 Potentials of charge carriers in lithium-ion electrodes [57]

1.3.5 Lithium Manganese Oxide (LMO)

Lithium manganese oxide (LMO) is the opposite, being less expensive and safer at the cost of a low cycling life [49]. LMO cathodes often take the form of $LiMn_2O_4$ in a spinel structure, Figure 8, which provides 3D diffusion pathways for lithium ions, with the cathode exhibiting high rate capability while being environmentally safer and easier to synthesise [58]. Despite this the cathode exhibits a relatively low theoretical capacity of 148 mAh/g with practical specific discharge capacities of 135 and 146 mAh/g being observed, with LMO cathodes exhibiting further poor performance due to poor lithium ion kinetics in bulk spinel LMO, structural destruction, and significant capacity fade [59].

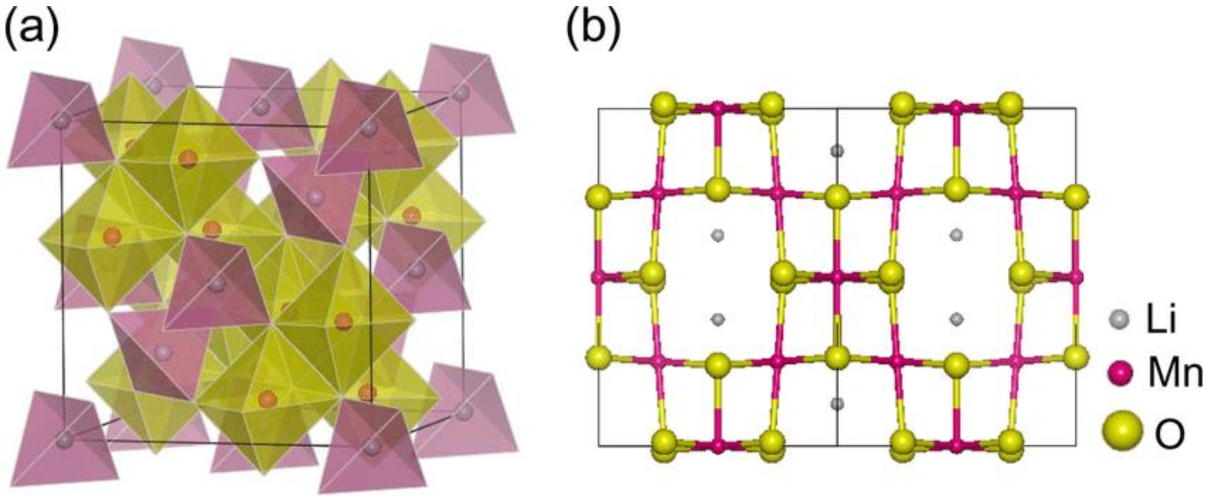

Figure 8 a) Spinel structure of LMO cathode and b) oxygen sub-lattice [60]

1.3.6 Comparison of NMC811 Cathode vs. Alternative Cathode Chemistries

When selecting a cathode to further optimise factors on which the cathode would be decided included a high specific capacity, high capacity retention, low cost, low environmental damage. This is in part based on consumer feedback which rate high charge life/range, cost, and effect on the environment [26], [27], with investment in net zero technologies being irrelevant if consumers do not buy in. As such, NMC811 was selected as the cathode to optimise. NMC811 has previously exhibited a reversible capacity of 190 mAh/g [38], with NMC622 only exhibiting a specific capacity of 170 mAh/g [43], LFP having a theoretical capacity of 170 mAh/g [49], LMO below 150 mAh/g, and LCO having a practical specific capacity of 135 mAh/g [53]. As such any cathode with the exception of NMC811 will not provide the charge life/range that is required from current lithium-ion cells.

NCA has a comparable specific capacity of 200 mAh/g but currently suffers from poor cyclability, a lower electrical conductivity, and poor structural stability, as well as containing a 15% ratio of cobalt compared to nickel (80%) and aluminium (5%) [47], [61]. With cobalt having significant environmental stigma attached to it due to poor mining practices in the DRC in addition to its increasing cost vs. even nickel [44], the trend of transitioning to low cobalt cathodes and the need to reduce cobalt mining effectively phases out any cathodes with a significant proportion of cobalt, including NCA, LCO, and high cobalt NMCs.

While NMC811 still has a ratio of 10% cobalt, NCA cathodes are unable to increase the proportion of aluminium in order to decrease the proportion of cobalt [47]. While there is scope to reduce cobalt further in NMCs by eliminating cobalt altogether through the development of lithium nickel oxide (LNO) cathodes [61], such cathodes are currently still too early in development to be used and despite specific discharge capacities upwards of 212 mAh/g exhibit poor cycling retention below 80% [44]. NMC811 can also suffer from poor cyclability and capacity retention, however as part of the optimisation of this cathode it is the aim that cyclability of NMC811 can be improved [38]. As such, NMC811 is selected as the cathode to be optimised due to its high reversible capacity and low proportion of cobalt. This is done with the aim that a higher charge life/range and more environmentally friendly cathode will increase the uptake in net zero technologies by consumers [26], [27]. While it is also hoped that further optimisation of NMC811 will further increase the scope for LNO to be developed in future such that nickel will be further increased to increase capacity while the proportion of cobalt will be decreased.

1.4 Synthesis

1.4.1 Dry Synthesis

1.4.1.1 Solid State

Synthesis of lithium-ion cathodes are predominantly synthesised using batch solid state synthesis. Solid state is a relatively simple method allowing for easy synthesis of cathodes usually requiring only one step and requiring no expensive or sophisticated equipment [62]. The method does require significant mechanical mixing and long synthesis times to ensure homogeneity and a complete reaction, with total synthesis times including heading, decarbonizing, heating, and annealing totalling 120 hours when synthesising lithium cobalt manganese oxide (LCMO) [63]. Failure to do this results in reaction boundaries that result in an inhomogeneous final product.

When used to synthesise LFP, a two-step heating process whereby a ground mixture of iron (ii) acetate or iron (ii) oxalate, lithium carbonate or lithium hydroxide, and ammonium phosphate is decomposed at between 300 °C and 400 °C, reground, and calcined at between 400 °C to 800 °C for 10 to 24 h under Ar or N_2 [49]. Partially as a result of the long calcination times uncontrollable particle growth and agglomeration are reported resulting in larger particle morphologies, with the purity of the LFP cathode also being dependent on particle growth parameters such as calcination time and temperature.

1.4.1.2 Solid State – Wet Chemical Synthesis Hybrid

A hybrid of solid-state and wet chemical synthesis can also be used to synthesise LCO and LNO cathodes with stoichiometric amounts of nickel acetate tetrahydrate, cobalt acetate tetrahydrate, and lithium acetate dihydrate being dissolved and mixed in 80 °C distilled water (where LCO uses only lithium and cobalt acetate hydrates and LNO uses only lithium and nickel acetate hydrates) [31]. The powders are then preheated in a tube furnace under O_2 for 10 h, with LCO being formed by preheating at 300 °C followed by sintering at 825 °C and LNO being preheated at 400 °C before being sintered at 775 °C. Sintering to the outlined temperatures produces layered structures of LCO and LNO, however reductions in sintering temperature leads to the synthesis of different phases. When heating LCO to 725 °C a spinel structure is formed, while heating LNO to 565 °C results in 50% of the structure consisting of rock salt nickel oxide. This highlights how synthesis of high nickel NMC and LCO cathodes using solid state may prove difficult, with mixing of Li and metal layers and poor stoichiometry control in addition to the synthesis of unwanted structures and intermediate phases being present dependent on synthesis temperature [31].

A similar hybrid of solid state and wet chemical synthesis can be employed in the synthesis of NMC622 [42]. Precursors dried overnight at 80 °C are ground with lithium nitrate at stoichiometric amounts, preheated at 450 °C for 5 h in air, ground, and calcined at 550 °C for 3 h, 700 °C for 3h, and 750 to 900 °C for 12 h under O_2, Figure 9. While solid-state is employed for the synthesis of NMC622, the precursors are formed using a wet chemical synthesis reaction, with nickel acetate tetrahydrate, manganese acetate tetrahydrate, and cobalt acetate tetrahydrate are dissolved in a 1:1 mixture of distilled water and ethylene glycol. While mixing continuously cetyltrimethyl ammonium bromide is added to the resulting solution followed by oxalic acid, before the solution was heated at 200 °C for 6 to 18 h in a Teflon-lined stainless steel precursor. Synthesis results in primary particles with no distinct morphology but nanoscale average particle size and crystallinity that increases as annealing temperature is increased, while the cathode exhibits initial specific discharge capacities of between 170 and 183 mAh/g at 0.2 C with 90% capacity retention.

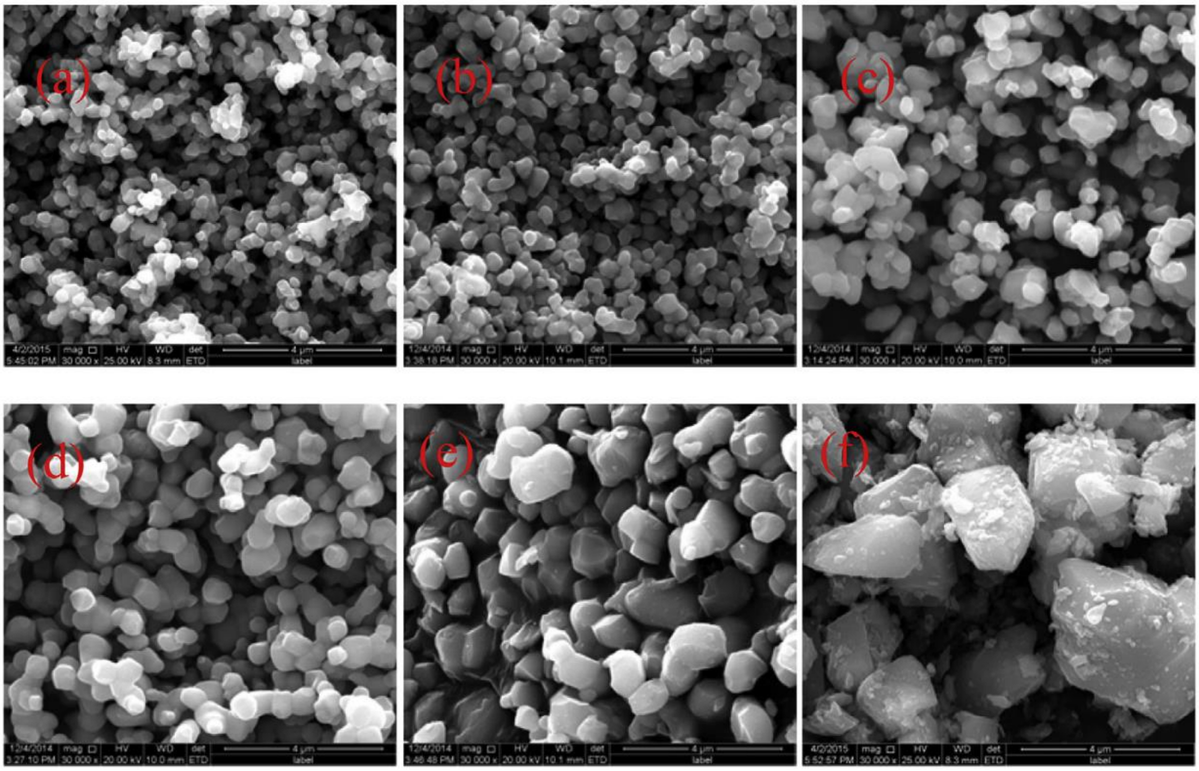

Figure 9 SEM of NMC622 calcined at a) 750 °C, b) 800 °C, c) 825 °C, d) 850 °C, e) 875 °C, and f) 900 °C

1.4.1.3 Solid State - Templating

A way of manipulating morphology using solid state synthesis is by use of a precursor that has undergone wet chemical synthesis to form a specific particle morphology on which the cathode particles are able to grow, i.e. a template.

Secondary particles with the morphology of hollow microspheres and consisting of agglomerated primary octahedral particles can be formed via the synthesis of spinel LMO using solid state synthesis [59]. This is achieved by the mixing of stoichiometric amounts of MnO_2 with lithium hydroxide monohydrate at 80 °C of which are calcined at 750 °C for 18 h. The resulting hollow microspheres exhibit an initial specific discharge capacity of 113 mAh/g when cycled at 0.5 C with capacity fade of 16.8% over 100 cycles. Despite this, the synthesis of the MnO_2 precursor requires significant preparation in order to form micro spherical morphologies, Figure 10 (left), requiring a precipitation reaction between manganese sulfate monohydrate and ammonium bicarbonate and multiple washing and filtering steps. Should this preparation not be done microspheres are not formed with only octahedral primary particles being synthesised.

A similar method is observed when synthesising LMO nanorods, Figure 10 (right). The reaction of a manganese precursor and lithium hydroxide monohydrate by dispersal in 3 ml anhydrous alcohol, grinding for several hours, drying at room temperature, and sintering at 700 °C for 10 h in a muffle furnace [64]. While showing an initial specific discharge capacity of 131 mAh/g at 0.1 C with minimal capacity fade of 93% of original capacity, the manganese precursor, in this case γ-MnOOH nanorods, again requires significant preparation this time using the hydrothermal process to produce distinct morphologies.

While reliable, the simplicity of the solid-state method allows for little fine tuning of the product without significant pre-preparation of reactants and requires long synthesis times to form homogenous products. Manipulation of particle morphologies often requires a second, often wet-synthesis process to produce the desires morphologies. As such these wet synthesis methods are investigated as stand-alone methods to evaluate their viability.

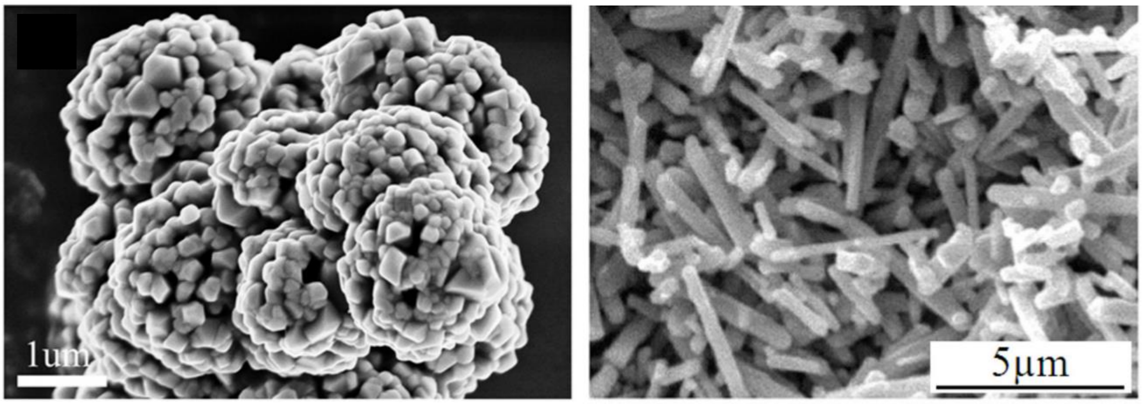

Figure 10 SEM of LMO hollow microspheres (left) and LMO nanorods (right) synthesised via the templating of LMO onto precursors synthesised using wet chemical synthesis, using solid state synthesis [59][64]

1.4.2 Wet Synthesis

1.4.2.1 Sol-gel

Wet chemical synthesis, divided into different synthesis techniques, is also used to produce NMC cathodes with varying degrees of success. Sol-gel synthesis is a method where a sol (solution) is produced by hydrolysis and condensation reactions, before the solution is reacted into a gel and heated [65]. When used to form LFP cathodes the sol-gel method results in cathodes of reversible specific capacity of 150 mAh/g at 0.2 C and 0.5 C with negligible capacity fade over the first 20 cycles, [66], and large "chess-like" structures of large, porous agglomerations of sub-microscale particles, Figure 11. Such cathodes are formed by mixing two separate solutions; Iron (iii) citrate dissolved in 60 °C water and a solution of equal parts lithium phosphate and phosphoric acid. Once mixed the solution is dried at 60 °C for 24 h, ground, and the resulting xerogel heated in argon at 700 °C for 10 h. While a relatively simple, there appears to be little control of particle morphology using this method.

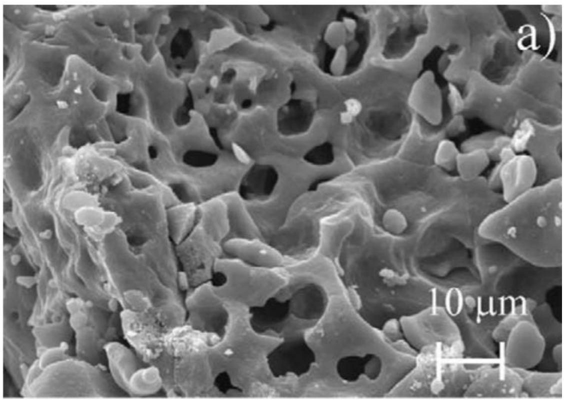

Figure 11 SEM of "Chess-like" structure of $LiFePO_4/C$ synthesised using sol-gel synthesis [66]

By dissolving stoichiometric amount of lithium acetate and manganese acetate in distilled water along with dissolving behenic acid separately in heated ethyl alcohol as a chelating agent, LMO can be synthesised using sol-gel synthesis [67]. The two solutions are mixed together and calcined at 850 °C for 6 h. This method results in uniform spherical grains of 500 nm average particle diameter, Figure 12 (left), with the cathode exhibiting a specific initial discharge capacity of 130 mAh/g and capacity retention of 88% over 10 cycles. A more cuboidal morphology, Figure 12 (right), can be formed by combining lithium acetate and manganese acetate dissolved in distilled water and combining with heated ethanol [68]. After mixing the two solutions 1M lauric acid is added dropwise as a chelation agent under heating and stirring with the solution being heated until a gel was obtained, at which point the gel is dried at 110 °C overnight and calcinated at 850 °C overnight. This results in an initial specific discharge capacity of 124 mAh/g with a capacity retention of 83% over 10 cycles, as well as microscale cubic morphologies.

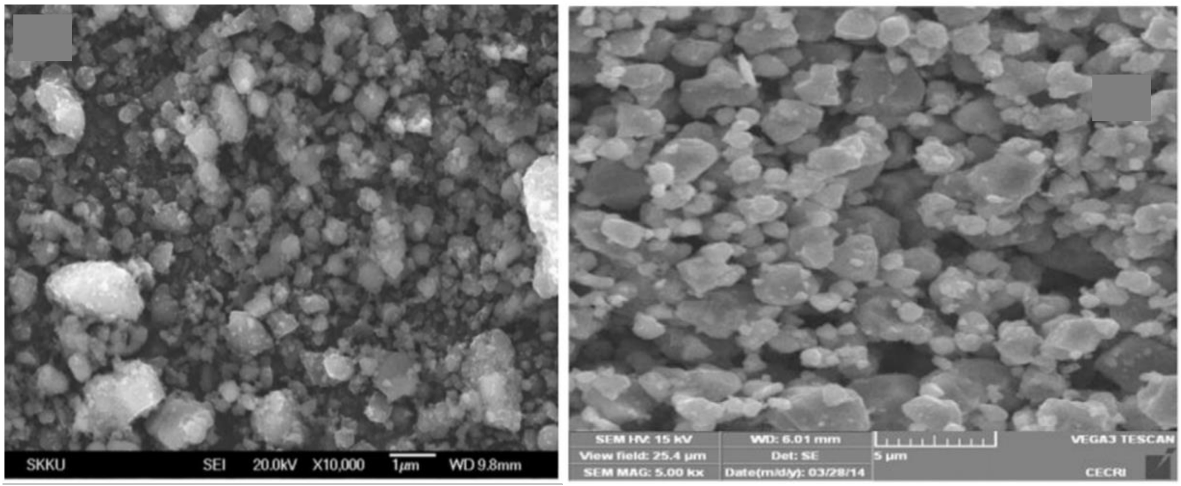

Figure 12 SEM images of uniform spherical primary particles (left) and cuboidal primary particles (right) LMO [67][68]

For the synthesis of NMC811 [69] lithium nitrate, nickel nitrate hexahydrate, manganese nitrate tetrahydrate, and cobalt nitrate hexahydrate are dissolved in distilled water and mixed with a separate solution of citric acid, also dissolved in distilled water. The sol is produced by mixing the two solutions together, with the pH maintained at 7.0 using ammonia. The gel is produced by stirring the sol and evaporating at 80 °C, before being dried, annealed at 480 °C for 5 h in air and calcined at 750 °C for 15 h. This method leads to the synthesis of nanoscale, agglomerated primary particles between 200 and 400 nm, Figure 13, with the cathodes exhibiting an initial specific discharge capacity of 200 mAh/g with 91% columbic efficiency when cycled at 0.1 C and a capacity retention of 89% after 50 cycles when cycled at 0.5 C.

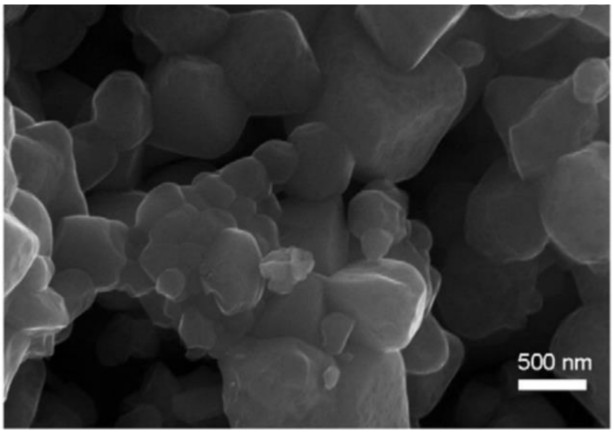

Figure 13 SEM image of nanoscale NMC811 primary particles synthesised using sol-gel [69]

Sol-gel is beneficial for ensuring good stoichiometry and high homogeneity in synthesised materials while required shorter synthesis times than solid-state. This method may face complexities when attempting to scale up however, with the gel drying non homogenously even under stirring.

1.4.2.2 Hydrothermal

Hydrothermal is an alternative wet chemical synthesis method involving reacting an aqueous solution in a closed reaction vessel and then heating under high pressure and temperature [70]. This method is useful for reacting substances that have poor solubility or are insoluble under atmospheric conditions, with the method also providing the conditions to grow a variety of different primary and secondary particle morphologies. LFP is able to be synthesised via the hydrothermal method by mixing iron, lithium, and phosphorus precursors in a 3:1:1 stoichiometric ratio (for this case Iron sulfate heptahydrate, lithium hydroxide, and phosphoric acid is used) [71]. Sugar and carbon nanotubes were added to the resulting gel to minimise oxidation and improve conductivity respectively, before the gel is sealed and heated at 150 to 220 °C for 5 h in an autoclave and dried under vacuum at 60 °C for 3 h. This method produced a cathode with initial specific discharge capacity of 160 mAh/g at 0.3 C with capacity retention being recorded at 86% over 50 cycles. The hydrothermal method was also found to produce primary particles with spherical morphologies and nanoscale diameters of between 60 and 320 nm, Figure 14, though depending on the synthesis conditions significant agglomeration of primary particles can occur [72].

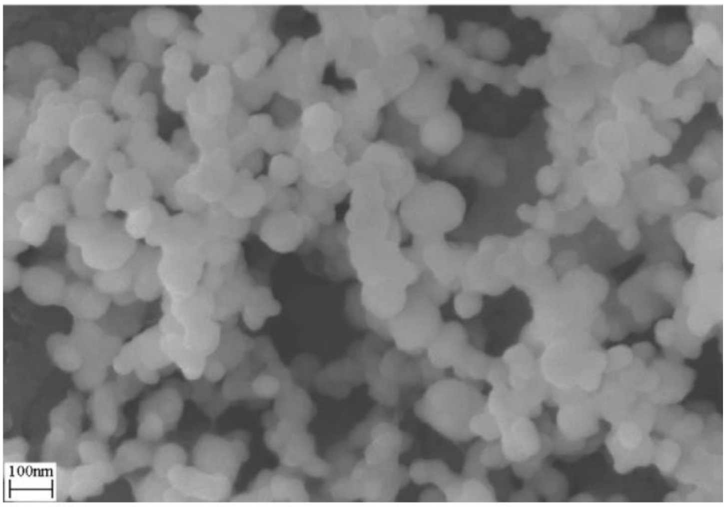

Figure 14 SEM image of spherical LFP primary nanoparticles synthesised using the hydrothermal method [72]

The hydrothermal method also allows for the synthesis of LCO from the synthesis of Co_3O_4, with morphological control allowing for the manipulation of both cubic and spherical morphologies. Cubic Co_3O_4 is formed by the dissolution of cobalt acetate, urea, and triethanolamine in deionised water followed by stirring for 1 h and then heating in a Teflon-lined stainless steel autoclave at 160 °C for 12 h [73]. The resulting powder is filtered and washed in deionised water and ethanol before being dried at 110 °C for 3 h and calcined in a muffle furnace at 600 °C for 10 h. Spherical Co_3O_4 is synthesised in much the same way with the exception of using cobalt chloride hexahydrate and urea dissolved and mixed in deionised water and glycerol and then heating in the same Teflon-lined stainless steel autoclave and heated at 120 °C for 12h [74]. All other heating processes are then identical. To form LCO, Co_3O_4 is ground with lithium carbonate and calcined in air at 850 °C for 12 h [75]. The two ways of synthesising LCO form microscale spherical and cubic secondary particles at both the Co_3O_4 and LCO stages, Figure 15, while primary particles are highly agglomerated with little distinct shapes. Initial specific discharge capacities for 0.7 C are shown to be 157 and 154 mAh/g for cubic and spherical morphology powders respectively relative to a theoretical capacity of 274 mAh/g [53], with capacity retention after 100 cycles of 92% and 90%. While this method exhibits high morphological control, it results in a cathode with poor specific discharge capacity relative to theoretical capacity.

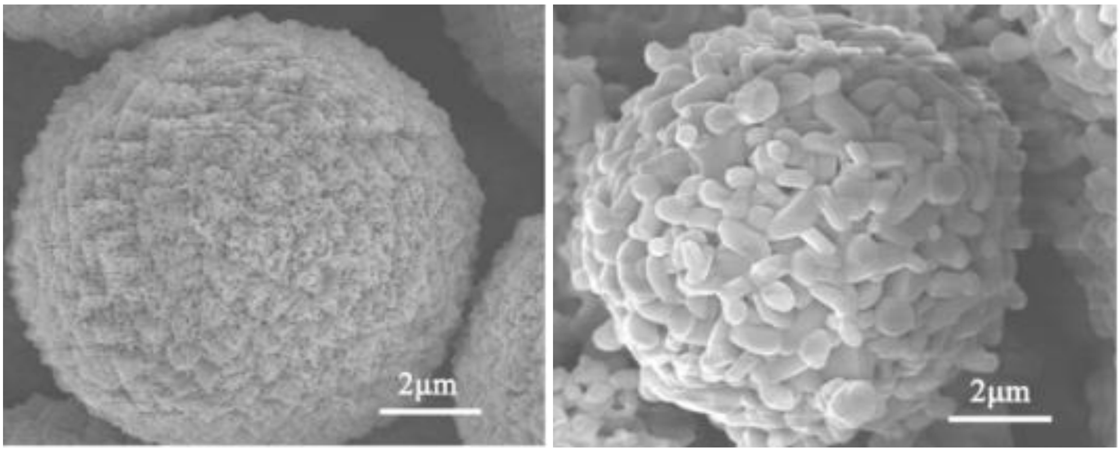

Figure 15 SEM images of Cubic LCO secondary particles formed from cubic Co_3O_4 (left) and spherical LCO secondary particles formed from spherical Co_3O_4 (right) synthesised using the hydrothermal method [75]

Hydrothermal reactions often result in better nucleation control of particles, a more uniform particle distribution, lower energy usage during synthesis, and higher purity compounds [58]. This is demonstrated when LMO is synthesised using one-step hydrothermal synthesis where lithium acetate dihydrate and manganese acetate tetrahydrate, are dissolved in solution with diammonium phosphate being added dropwise and then potassium manganate and then potassium hydroxide added under stirring [76]. The mixture is then added to a Teflon-lined autoclave where it is heated at 200 °C for 72 h and dried at 100 °C in air for 24 h. Primary particles are formed with octahedral nanoscale morphologies, Figure 16, 675 nm average particle diameter and a narrow size distribution, of which exhibit an initial specific discharge capacity of 116 mAh/g with only 2.3% capacity fade.

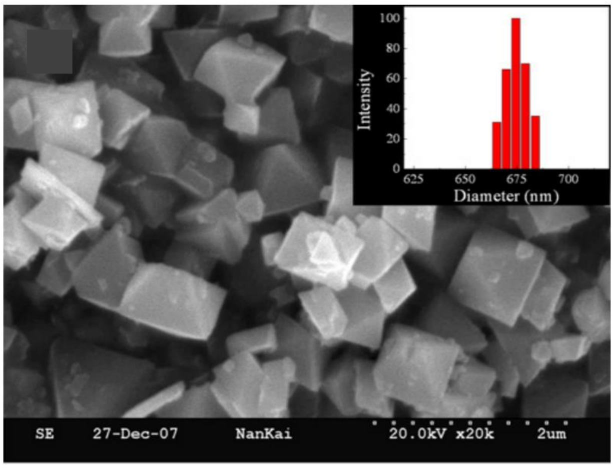

Figure 16 SEM image of octahedral LMO synthesised using the hydrothermal method [76]

This method, while allowing for control of particle morphology and having relatively quicker synthesis times, also requires specialist equipment in the form of a high pressure crucible which increases the cost of synthesis.

1.4.2.3 Co-precipitation

Co-precipitation [77] uses a mixing of reactant materials dissolved in solvent and a base added drop by drop in order to produce a precipitate. The precipitate is washed and dried before being annealed at high temperatures.

LFP may be formed using the co-precipitation method by the addition and stirring of aqueous solutions of stoichiometric amounts of lithium phosphate and iron (ii) phosphate while controlling the pH [78]. The resulting precipitate is filtered and washed in distilled water and dried under N_2 before being heated to between 650 and 800 °C under N_2 for 12 h. The morphology before the drying phase and after heating under N_2 consists of microscale flat, rhomboidal particles, Figure 17, while electrochemical testing when cycled at a c-rate of C/20 reveals a specific discharge capacity of 150 mAh/g with minimal capacity fade.

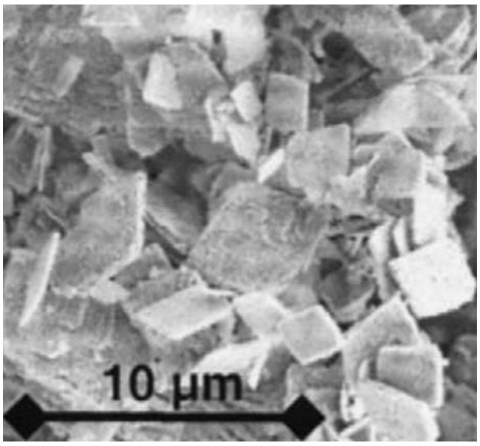

Figure 17 SEM image of LFP rhomboidal particles synthesised using co-precipitation [78]

The co-precipitation of LMO can be done by dissolving manganese acetate tetrahydrate and lithium hydroxide monohydrate separately in distilled water with PEG20000 dissolved in each solution as a surfactant [79]. The manganese solution undergoes ultrasonic irradiation for 0.5 h before dissolved sodium hydroxide is added dropwise and the solution is aged overnight, and suction filtration is undergone to obtain a precipitate. This is then added to the lithium solution, mixed under ultrasonic stirring for 0.5 h, evaporated at 85 °C in a water bath before being preheated at 500 °C for 6 h and calcined at 750 °C for 20 h in a muffle furnace. The resulting morphology is that of polyhedral primary particles, Figure 18, of which are agglomerated together, with the cathode exhibiting an initial specific discharge capacity of 95 mAh/g with a columbic efficiency of 84%.

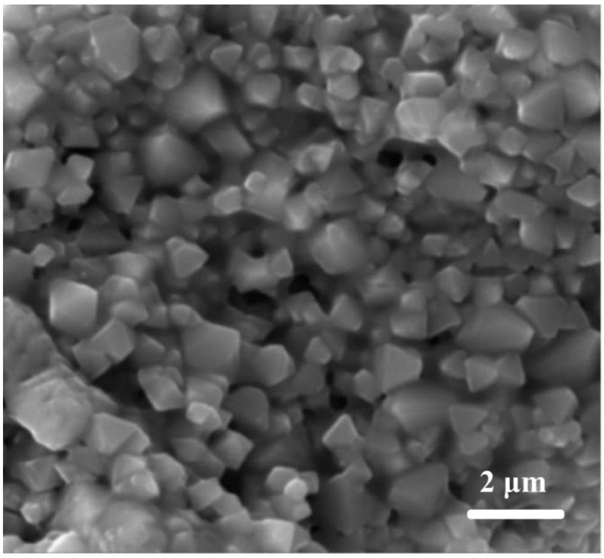

Figure 18 SEM image of polyhedral LMO primary particles synthesised using co-precipitation [79]

NMC811 can be synthesised using co-precipitation by dissolving a stoichiometric amount of nickel nitrate hexahydrate, manganese nitrate tetrahydrate, and cobalt nitrate hexahydrate in distilled water and added slowly into a reactor under stirring at 50 °C and 650 rpm with a separate solution of sodium carbonate dissolved in distilled water [69]. Ammonia solution was added to control the pH at 7.5 before aging for 12 h to produce nickel manganese cobalt carbonate ($Ni_{0.8}Mn_{0.1}Co_{0.1}CO_3$). The carbonate is filtered and washed, dried at 80 °C for 12 h under a vacuum, mixed with lithium nitrate in a pestle and mortar, annealed at 480 °C for 5 h in air and calcined at 750 °C under oxygen for 15 h. This results in nanoscale, agglomerated particles, Figure 19, between 200 and 400 nm in diameter. When cycled in a lithium-ion cell the cathode exhibits an initial specific discharge capacity of 195 mAh/g at 0.1 C with capacity retention of 85% at 0.5 C after 50 cycles. NMC532 can be synthesised using a similar method whereby nickel sulfate hexahydrate, manganese sulfate monohydrate, cobalt sulfate hexahydrate, sodium hydroxide, ammonium hydroxide are prepared in deionised water, dried, and ground with lithium carbonate before being heated between 930 and 1020 °C for 12 h in a box furnace [40]. This forms agglomerations of 600 nm average diameter primary particles with no distinct size and some unreacted lithium carbonate indicating inhomogeneity, with a maximum initial specific discharge capacity of 167 mAh/g and capacity fade of 12%.

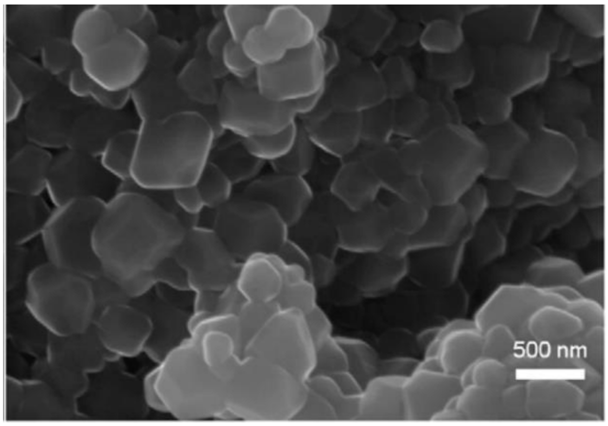

Figure 19 SEM image of NMC811 particles formed using co-precipitation [69]

A similar cathode to NMC, NCA cathodes can also be formed by co-precipitation by pumping a stoichiometric solution of nickel sulfate hexahydrate, cobalt sulfate heptahydrate, and aluminium sulfate octadecahydrate into a continuously stirred tank reactor [46]. The pH is kept at 11.4 by pumping in sodium hydroxide and ammonium hydroxide before the precipitate is filtered and washed in distilled water, dried under a vacuum at 120 °C for 12 h, mixed with lithium hydroxide monohydrate, preheated at 450 °C for 6 h, and calcined at 780 °C for 12 h. The resulting cathode powder consists of nanoscale, smooth, vaguely octahedral primary particles, Figure 20, with the cathode exhibiting an initial specific discharge capacity of 173 mAh/g with an 89% capacity retention after 110 cycles when cycled at 1C.

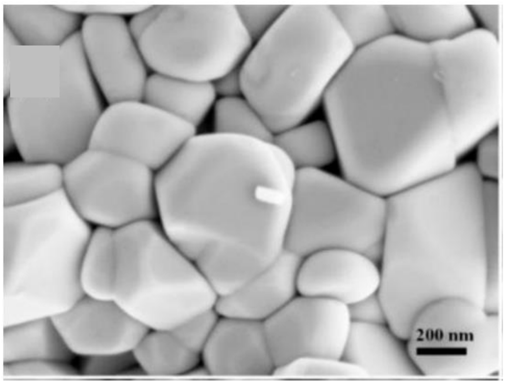

Figure 20 SEM image of NCA octahedral primary particles synthesised using co-precipitation [46]

Co-precipitation allows for significant control of the final product, including morphological control to produce nanoscale particles. The method however requires significant control over pH which requires additional bases above the reactants for the reaction to occur. The method also requires multiple steps include the drop-by-drop addition of reactants and the washing of the precipitate, as well as a synthesis time which, while less than solid-state, is still significant in length.

1.4.2.4 Pechini Method

The Pechini method is also a viable synthesis method for production of high nickel cathodes. The method works by using hydroxycarboxylic acid, normally citric acid, as a metal cation chelating agent [80]. Synthesis of NMC111 using lithium nitrate, manganese nitrate, nickel nitrate hexahydrate, and cobalt nitrate hexahydrate and dissolving the reactants in deionised water [81]. The solution is added dropwise to a solution of critic acid and ethylene glycol where the metal cations will chelate to the critic acid. The solution is then dried, ground, pressed into pellets, and heated at 400 °C for 4 h and calcined at between 700 and 1000 °C for 12 h with only the samples heated between 800 and 1000 °C producing NMC111. Uniform, nanoscale hexagonal particles are formed, Figure 21 (left), and as calcination temperature is increased particle diameter increases from 100 to 200 nm at 800 °C to 2000 to 3000 nm at 1000 °C. Specific initial discharge capacities range from 175 to 181 mAh/g when cycled at C/20 with capacity retentions above 90% when cycled at 1 C. Early attempts to synthesise LNO were also achieved using the Pechini method, whereby lithium nitrate and nickel nitrate were dissolved in deionised water, critic acid, and ethylene glycol, dried into a gel, and calcined between 400 and 800 °C under O_2 [82].

LMO spinels, $LiMn_2O_4$, have also been synthesised using the Pechini method [83]. A stoichiometric ratio of lithium nitrate and manganese nitrate hexahydrate was dissolved in a 1:4 ratio of critic acid and ethylene glycol and heated to 90 °C for 20 mins, underwent esterification at 140 °C, and then dried under vacuum at 180 °C before being calcined at 250 to 800 °C. This results in loosely agglomerated particles with no distinct morphology and particle diameters between 200 and 500 nm, Figure 21 (right), while initial specific discharge capacity is observed to be 140 mAh/g capacity fade of 11% after 10 cycles when calcined at 800 °C.

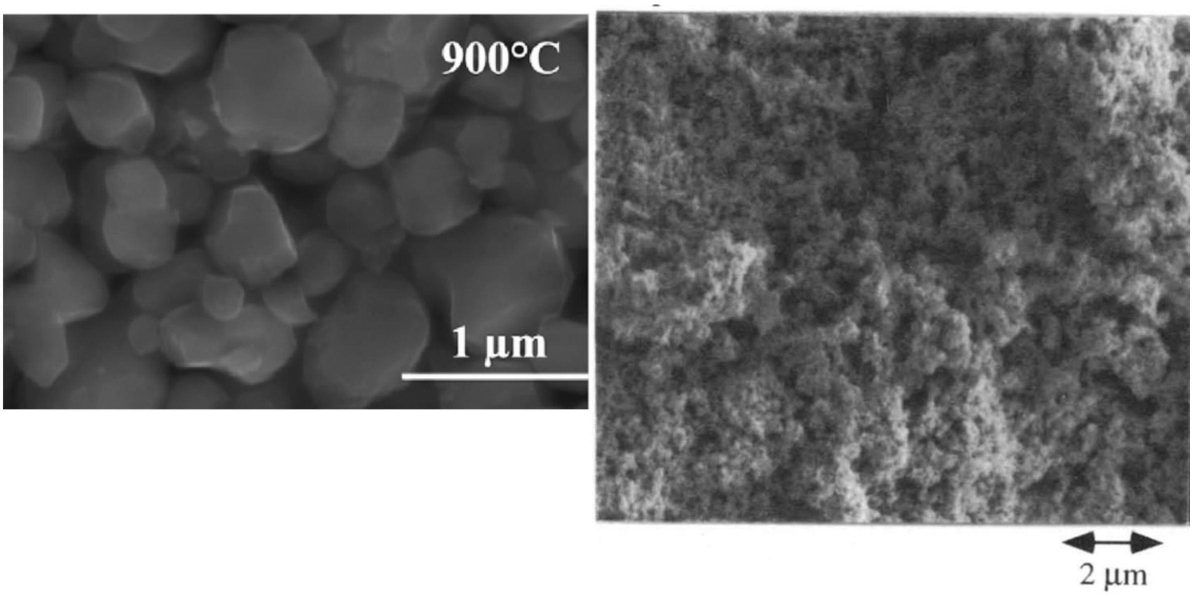

Figure 21 SEM images of NMC111 hexagonal primary particles (left) and LMO primary particles with no distinct shape (right) synthesised with the Pechini method [81] [83]

Use of the Pechini method allows for the synthesis of nanoscale morphologies and requires less heating time than solid-state. This method is however very time consuming in part due to adding the reactant solution dropwise which also produces scale-up issues.

1.4.2.5 Molten Salt Synthesis

Molten salt synthesis is a method whereby precursor salts, sometimes dissolved with a trace amount of distilled water, are mixed/ground and heated until melting before being washed and filtered [77]. NMC111 may be synthesised by this method, where sodium hydroxide is added dropwise to a solution of nickel sulfate hexahydrate, manganese sulfate monohydrate, and cobalt sulfate heptahydrate while stirring [84]. The precipitate is filtered and washed in distilled water, dried at 65 °C, mixed with lithium hydroxide monohydrate, and placed in an aluminium oxide crucible where it is heated to 1000 °C for 10 h and then reduced to 400 °C before being washed. From this synthesis method microscale octahedral primary particles with average particle diameters of 3.4 μm and no agglomeration are formed, Figure 22, of which exhibit a maximum initial specific discharge capacity of 160 mAh/g.

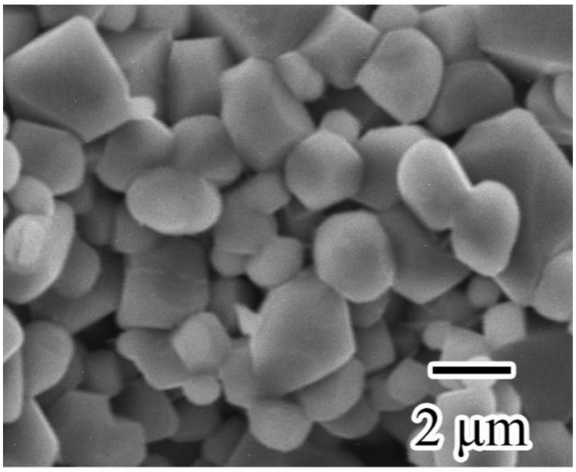

Figure 22 SEM image of octahedral NMC811 primary particles synthesised using molten-salt synthesis [84]

Such a method, similarly to solid-state, requires a large amount of grinding and/or a high maximum synthesis temperature that increases the cost of synthesis. The variation of heating conditions in addition to the ratio of reactants may be used to alter particle morphology and size, something not possible with solid state. As the name implies, this method also requires heating reactants beyond their melting point, making the reaction somewhat dependent on the reactants melting point and requiring reaction temperatures for salts with higher melting points.

1.4.2.6 Spray Pyrolysis

Spray pyrolysis is a method that may be employed for the control of particle size [85]. To synthesis NMC prepared aqueous solution of powder reactants, and critic acid and ethylene glycol to control morphology, are pumped through a nebulizer under a flow of oxygen. Droplets from the nebulizer were obtained using a device to collect charged particles in a 600 °C furnace, with a second heat treatment step at 800 °C for 20 h done separately.

When used to synthesise LFP cathode powder [86], stoichiometric amounts of lithium acetate monohydrate, iron (ii) chloride tetrahydrate, and phosphoric acid are dissolved in distilled water with hydrochloric acid to control pH. Critic acid may also be added to synthesise an LFP/C composite. The solution is atomised at a frequency of 1.7 MHz using an ultrasonic nebuliser and the spray droplets are carried under the flow of N_2 at a flow rate 1 dm^3/min to a reactor heated between 500 and 800 °C. Further sintering is then done at between 500 and 800 °C for 4 h in N_2 with 3% H_2. The morphology of the particles is observed to change during sintering from spherical morphologies formed pre-sintering to more irregular particles formed post sintering, Figure 23. Initial specific discharge capacities for LFP and LFP/C composite are 100 and 140 mAh/g with minimal capacity fade after 50 cycles when cycled at 0.5 C.

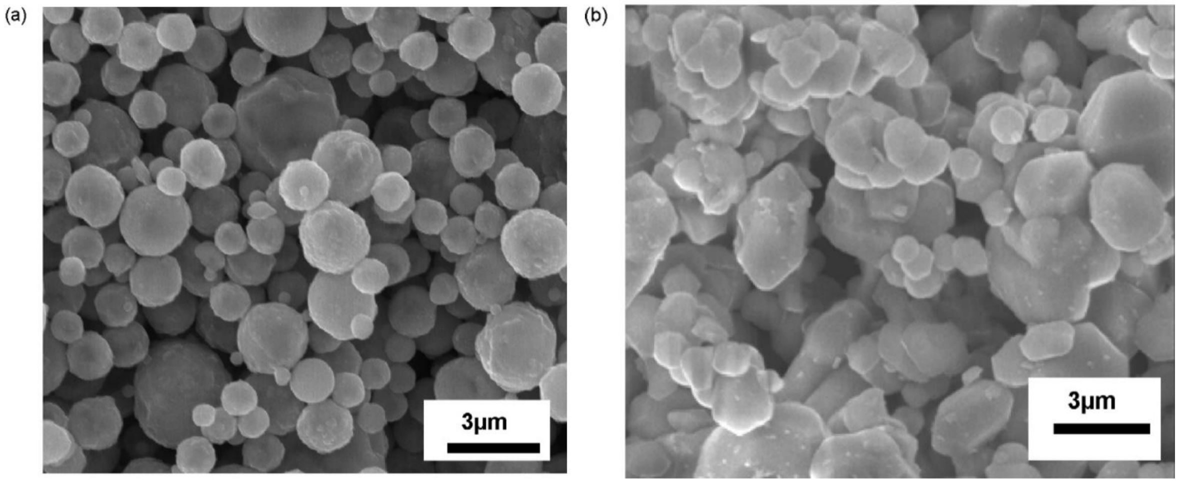

Figure 23 SEM images of LFP primary particles synthesised using spray pyrolysis a) pre- and b) post sintering [86]

Also being able to be used to synthesise LCO, cobalt nitrate hexahydrate and lithium nitrate, or cobalt acetate tetrahydrate and lithium acetate dihydrate, is dissolved in deionised water at stoichiometric ratios [87]. The precursor solution was atomised using a quartz nebuliser, before being vapourised at 400 °C under a flow of N_2 in a stainless steel preheating section. The resulting dried droplets are heating in a quartz tube furnace at between 600 and 1000 °C before being quenched under a 30 L/min air flow and further annealed under an air flow to manipulate particle morphology. LCO synthesised using nitrate precursors form microscale secondary particles while secondary particles formed using acetates have irregular shaping, Figure 24. Cathodes synthesised using nitrates exhibit initial specific discharge capacity of 178 mAh/g at 0.1 C with capacity fade of only 5% of initial specific capacity, while acetate synthesised particles exhibit specific initial discharge capacities of 135 and 136 mAh/g at 0.1 C.

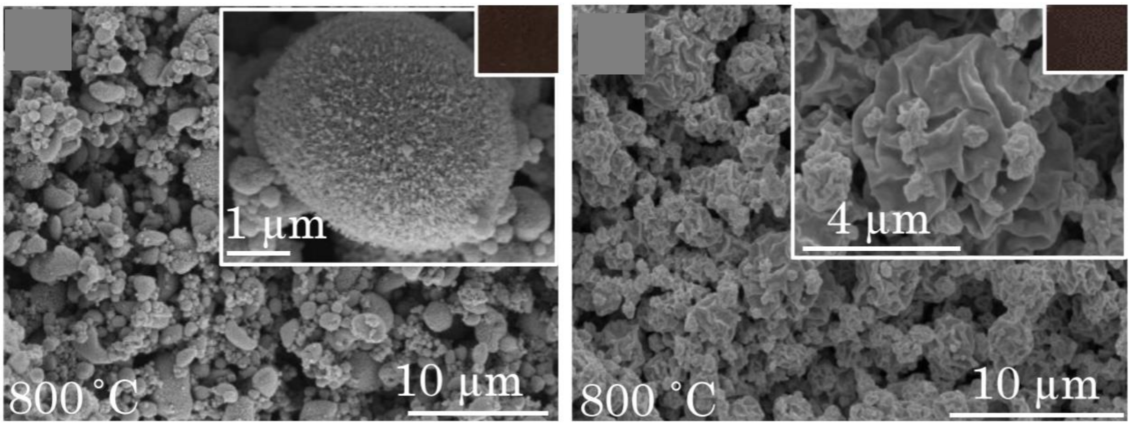

Figure 24 SEM images of LCO particles synthesised using spray pyrolysis using nitrate precursors (left) and acetate precursors (right) [87]

This technique, more so than other reviewed methods, allows for precise control of particle morphology down to the sub-micron level. To do this spray pyrolysis requires specific equipment and additional reactants to control the particle shape while also requiring long synthesis times for heat treatments. This amounts to this being a costly, if effective, method.

1.4.3 Novel Biotemplating Method

1.4.3.1 Method

Biotemplating is a relatively new and novel wet chemical synthesis method that uses long-chain organic molecules as chelating agent, similar to the role of citric acid in the Pechini method [88]. Dissolution of the biotemplate is done in tandem with the dissolution of the reactants and then combined under stirring before being dried and calcined. The dissolution, mixing, and drying of the reactants with the biotemplates produces a metal-ligand binding reaction where negatively charged chelation sites, or ligands, along the biotemplate chain are substituted for positive metal cations from the reactants, forming a coordinate bond and producing a chelate, an example of which is outlined in Figure 25. This chelate reduces reaction pathways between metal ions once the biotemplate is burned off during calcination, Figure 31, and reduces the possibility of recrystallisation of the reactants at lower synthesis temperatures.

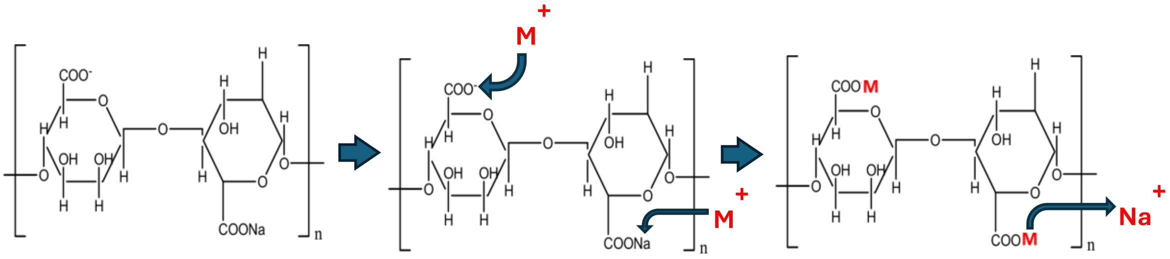

Figure 25 Chelation of Single Monomer of Sodium Alginate

Biotemplating ensures a homogenous reaction as a result of the mixing and dissolution of reactants, which reduces the effects of reaction boundaries and reduces the synthesis time required for calcination to occur. Different biotemplates are also observed to have different chelation methods, and so by controlling the type and mass of biotemplate as well as the synthesis conditions, fine tuning of the final product including morphological control can be done. Such control of particles may allow improvements in cathodes such as NMC811.

1.4.3.2 Dextran Biotemplating

The amount of biotemplates available for use in chelation is as varied as the amount of long-chain organic molecules that can be obtained in nature. One such biotemplate already widely used is dextran. Dextran, Figure 26, is a long-chain polysaccharide produced as a by-product of using bacteria to digest glucose. The organic molecule tends to be identifiable by 1:6 glucoside links, however it can come in many derivatives with pKa values of between 5.3 and 7.4 [89]. When dissolved alongside metal cations the chelation mechanism of the dextran results in dextran chains being tangled around each other, Figure 27, creating pockets in which metal ions fit and bond dextran chains together similarly to hydrogen bonding [90].

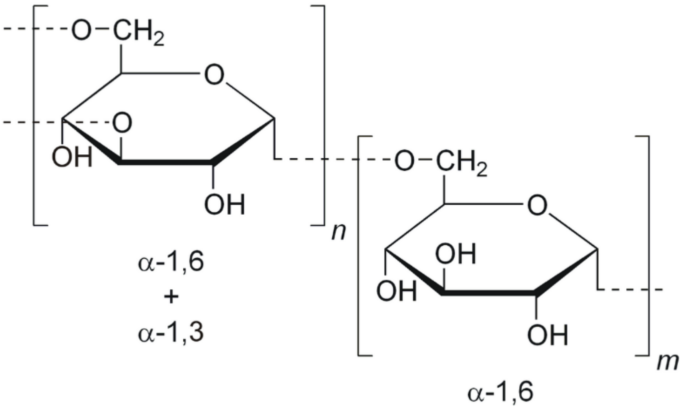

Figure 26 Dextran monomer structure

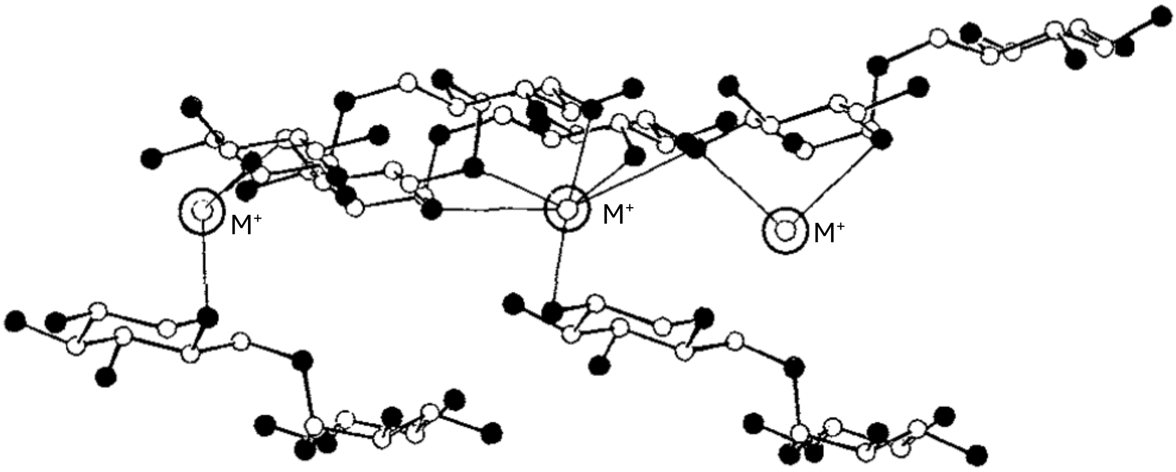

Figure 27 Chelation mechanism of dextran [90]

Initial research undertaken using dextran biotemplating to form macroporous metallic or metal oxide sponges, specifically copper-oxide containing silver sponges, proved that dextran could be used as a chelating agent to form sponge macroscale morphologies in metals and metal oxides [91]. When silver nitrate was dissolved in distilled water and mixed with dextran, before drying at room temperature and heating at 520 °C for 1 h a silver sponge was formed, Figure 28. Copper oxide could be added by adding copper nitrate hemipentahydrate to the silver sponge, drying for one day, and heating at 800 °C for 0.5 h. The resulting sponge was a macrostructure with an open framework of interconnecting silver and copper oxide rods synthesised using an inexpensive and relatively environmentally friendly method that has a wide scope for scale-up for industry. Following this successful application of dextran, it has been used to synthesise sodium nickel manganese (NNM) cathodes [92], LCMO cathodes [63], and yttrium barium copper oxide (YBCO) superconductors [93].

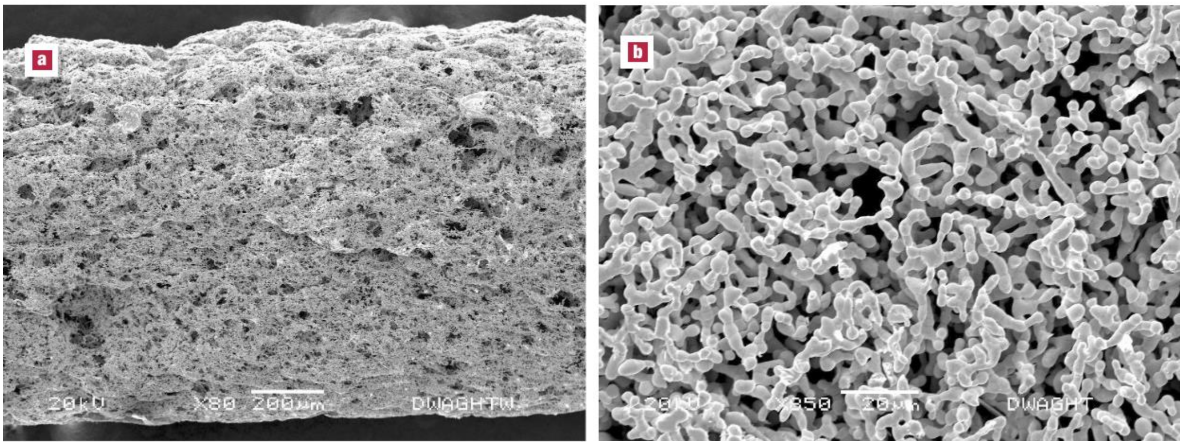

Figure 28 SEM images of silver sponge synthesised using dextran biotemplating at a) 200 μm scale and b) 20 μm scale [91]

NNM [92] formed using dextran was synthesised by mixing a stoichiometric solution of precursor salts and the biotemplate dissolved in water and nitric acid, drying at 90 °C, and calcining at either 550, 650, 750, or 850 °C for 2, 5, or 12 h. Using dextran biotemplating, particle size increased with an increase in calcination temperature and plate-like morphologies were formed when calcined at or above 750 °C. Average particle diameters using biotemplating never exceeded 600 nm regardless of synthesis conditions, whereas NNM synthesised using solid state at 850 °C for 12 h had an average particle size of 1740 nm. Particles formed using dextran at or above 750 °C were shown to have improved specific discharge capacities than those calcined below 750 °C despite having average larger particle widths due to the larger surface area of the plate morphology, Figure 29.

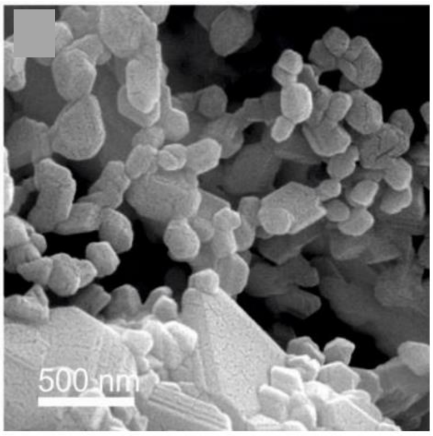

Figure 29 SEM image of NNM plate-shaped particles synthesised at 850 °C using dextran biotemplating [92]

LCMO [63] is formed in a similar way by dissolving and mixing stoichiometric masses of reactants and dextran in water, drying at 80 °C and calcining at 550 °C for 2 h. The method produced irregular spherical particles with an average diameter of 180 nm, Figure 30. No plate morphologies were formed using the 550 °C similarly to when forming NNM, highlighting the significance of calcination temperature for morphological control when using dextran.

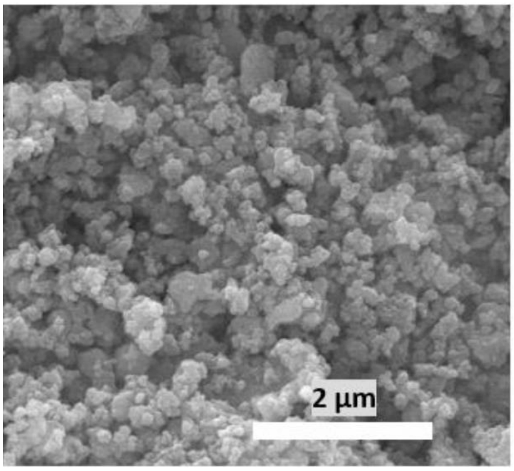

Figure 30 SEM image of LCMO particles synthesised using dextran biotemplating [63]

YBCO [93] formed using dextran is synthesised much in the same way by dissolving dextran with precursor salts in solution, drying at room temperature, and calcined at 920 °C for 2 h. By synthesising using dextran particles with average diameter of 500 nm, vs. 1000 to 5000 nm when synthesised using sol-gel, were formed with a range of morphologies. This comparison highlights how dextran may be used to control particle size and form nanoscale particles versus other synthesis methods.

1.4.3.3 Sodium Alginate Biotemplating

Sodium alginate is an organic polysaccharide extracted from brown algae. The sodium alginate polymer chain consists of polyguluronate $(\text{-G-})_n$ and polymannuronate $(\text{-M-})_n$ monomers, Figure 31, where the ratio of the number of G and M monomers is dependent on the seaweed the biotemplate is extracted from and effects the final morphology of the synthesised particles [94]. The ratio of G and M monomers also affects the pKa value, with the pKa of sodium alginate ranging from 3.3 to 3.6 depending on the ratio of monomers [95]. Use of a higher proportion of G monomers results in metal cations chelating according to the ‘egg-box’ model whereby ligands are substituted for metal cations along the biotemplate chains, with the biotemplate chains forming structures around the ions in an egg-box-like shape. This mechanism and proportion of G monomers may lead to the synthesis of nanowire morphologies as has been observed when synthesising YBCO [96] while a higher proportion of M monomers results in little control over particle morphology. Nanowire morphologies are beneficial due to having a high surface area vs volume for lithium intercalation, high amount of contact with the electrolyte, and high ionic conductivity of Li^+ ions along the length of the nanowires [97].

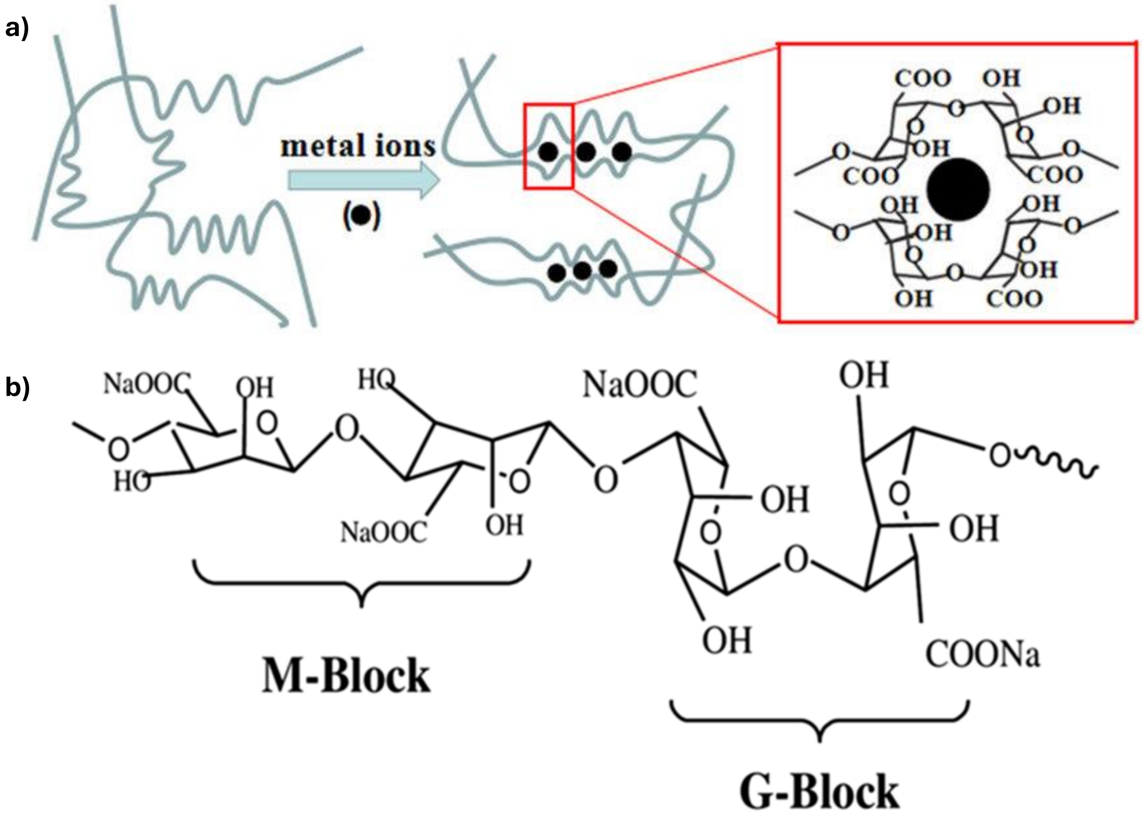

Figure 31 a) Sodium Alginate "Eggbox" model [98] and b) (-G-)n and (-M-)n monomer structurers [99]

Sodium alginate has previously been used to synthesise lanthanum strontium manganese oxide (LSMO) [94] and YBCO [96]. LSMO was synthesised by mixing La, Sr, and Mn nitrate precursor salts dissolved in deionized water and aqueous sodium alginate before drying at 40 °C for 24 h and calcining at 900 °C for 2 h. The resulting LSMO product had a nanowire morphology of uniform thickness that radiates out anisotropically from irregularly shaped central particles, Figure 32 (left). This central particle is significant to the synthesis of the nanowire as it is the nucleated “seed” from which the nanowire grows, with the irregular particle being a solid substrate on which a liquid or molten LSMO phase grows into a nanowire along a single dimension. When sodium is removed from the biotemplate and ammonium alginate used instead, nanoparticles are formed instead of nanowires, highlighting the importance of sodium in the synthesis of nanowires.

YBCO may be formed by mixing a preprepared solution of yttrium oxide, barium acetate, and copper acetate with a hot solution of sodium alginate before drying at 40 °C, calcining for 2 h at 500 °C and further heating for 2 h at 920 °C. As with LSMO biotemplated with sodium alginate, nanowire morphologies of 80 nm average diameter were formed that radiated out from a central particle and varied in length and diameter, Figure 32 (right). Bulbs at the end of the nanowires also shows the growth mechanism, with the nanowire growing via a liquid YBCO phase on the solid substrate (initially the solid “seed” particle and later the end of the solid nanowire).

Therefore, sodium alginate is an important biotemplate for manipulating particle morphology due to the synthesis of beneficial nanowires.

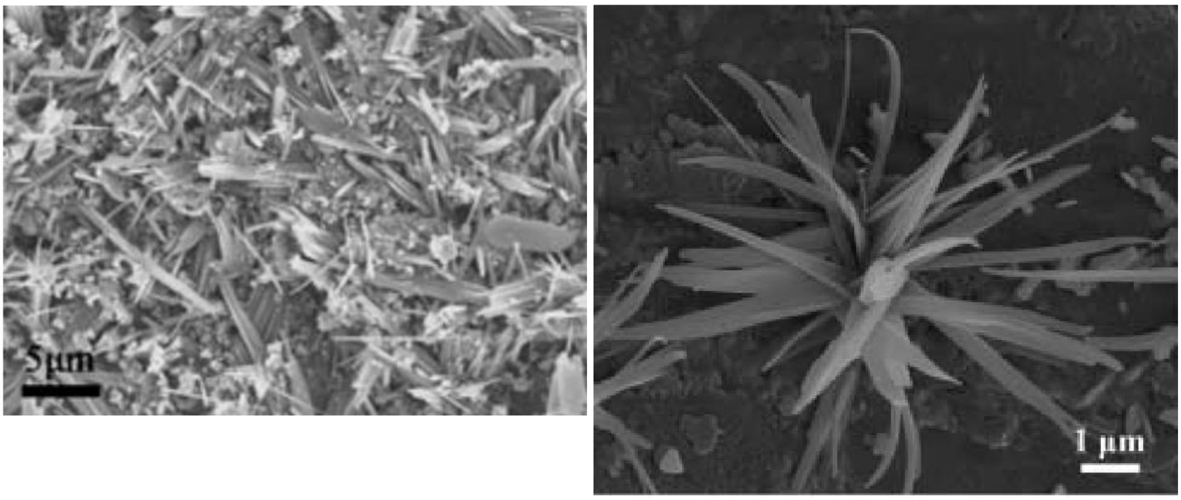

Figure 32 SEM images of nanowire morphologies formed from sodium alginate biotemplating for LSMO (left) and YBCO (right) [94] [96]

1.4.3.3.1 Sodium-doped lithium-ion cathodes

Previous evidence also exists for the Na-doping of high nickel lithium-ion cathodes. As such sodium alginate may be used as a mechanism to dope high nickel cathodes with sodium without the need for an additional dopant. Na-doped NMC532 cathodes using a sodium-to-lithium ratio of 3:97 have been synthesised and exhibited higher initial discharge capacities of 228.43 mAh/g at 0.2 C compared to ~190 mAh/g at 0.2 C for un-doped NMC532 [100]. Evidence given for this is a larger lithium layer spacing, a decrease in cation mixing, and a rapid diffusion of lithium ions after Na is substituted for Li. NMC603505 ($LiNi_{0.6}Mn_{0.35}Co_{0.05}O_2$) has also been doped using a 2:98 Na-to-Li ratio. The sodium-doped cathode has an improved initial discharge capacity and capacity retention of 121 mAh/g at 3 C and 93.3% after 100 cycles when compared to 93 mAh/g at 3 C and 83.2% after 100 cycles for the un-doped cathode [101]. Reasons for the improved electrochemical performance are cited as improved lithium diffusion kinetics, bulk layered structure stability, and thermal stability among other reasons.

In addition to NMC, NA-doped NCA cathodes were synthesised by calcining $Ni_{0.8}C0_{0.15}Al_{0.05}(OH)_2$ precursors with lithium carbonate and 1% by total mass of sodium chloride at 450 °C for 6 h and 850 °C for 12 h under O_2 [102]. While sodium doping with NaCl seems to have no effect on overall morphology, initial specific discharge capacity at 0.1 C is 199 mAh/g vs. 193 mAh/g for undoped NCA with a significantly improved capacity retention when cycled at 1 C of 81.6% for doped-NCA vs. 48.1% for undoped NCA.

Excessive sodium-doping is also examined using LNMO cathodes [103]. Co-precipitation of nickel sulfate hexahydrate and manganese sulfate hexahydrate was used to synthesise the nickel manganese hydroxide precursor, which is filtered and washed in distilled water, dried at 100 °C in air, mixed with lithium hydroxide and sodium hydroxide in a ball mill at 200 rpm for 1 h, and sintering at 800 °C for 20 h and 600 °C in air. The amount of sodium hydroxide is varied to produce 1%, 3%, 5%, and 10% Na-doped LMNO cathodes. Octahedral particle morphologies are produced with particle size being observed to decrease from 300 nm with an increase in sodium doping. Specific discharge capacity after 10 cycles at 1 C increases between un-doped and 3% doped LNMO and then decreases with 5% and 10% Na-doping, with specific discharge capacities of 113, 125, 124, and 107 mAh/g , respectively. Capacity retention is maintained at or above 90% for all doped LNMO with the exception of the 10% Na-doped cathode which exhibits 88% capacity retention.

Sodium alginate should therefore be investigated not just for its ability to exhibit morphological control on NMC particles, but also for its potential to sodium-dope high nickel cathodes.

1.4.3.4 K-carrageenan Biotemplating

K-carrageenan, Figure 34, is a biotemplate that shares similarities with sodium alginate. It is a long chain polysaccharide derived from red algae that contains sulphate as a functional group (OSO_3^-) to which metal ions chelate and has an effective pKa of 4.9 [104]. When κ-carrageenan is heated to 80 °C the polymer chains exist separately, Figure 35, with the chains electrostatically repulsing each other as metal ions chelate at the OSO_3^- chelation sites. When cooled post drying, the polymer chains form coil and helical structures which agglomerate together as the biotemplate is cooled further [105]. Once cooled the helical forms a 3D structure held together by intermolecular reactions and the metal cations.

YBCO may be formed using κ-carrageenan by dissolving yttrium, barium, and copper nitrate in deionized water before mixing with a separate solution of biotemplate dissolved in hot water, drying, and calcined at 920 °C for 2h [106]. Use of κ-carrageenan results in a blocky, reticulated morphology, Figure 33, however too high a ratio biotemplate may result in the synthesis of barium sulphate, an impurity phase that negative effects the performance of the YBCO. During synthesis barium sulphate does not melt, removing barium ions from the reaction and leading to different stoichiometries of YBCO.

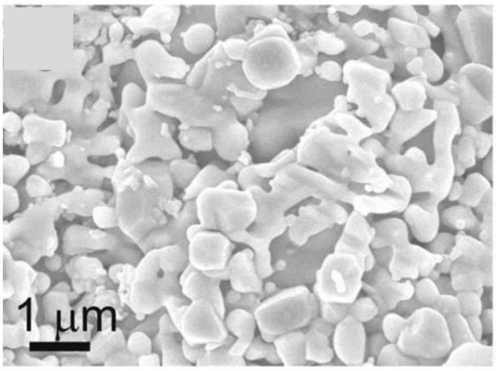

Figure 33 SEM image of blocky YBCO particles synthesised using κ-carrageenan biotemplating [106]

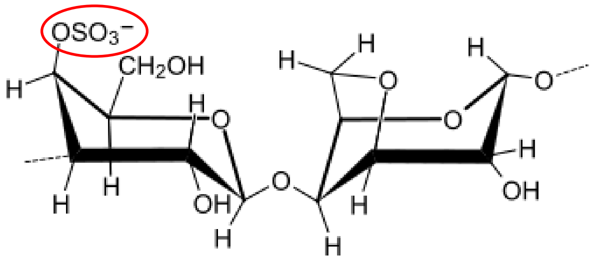

Figure 34 K-carrageenan monomer structure

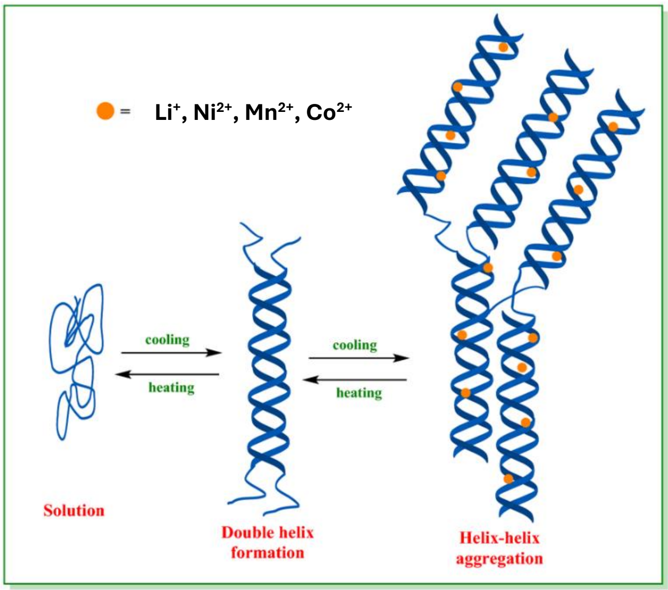

Figure 35 Chelation mechanism of κ-carrageenan, adapted from [107]

1.4.3.4.1 Sulfur-doped lithium-ion cathodes

A higher ratio of κ-carrageenan could be utilized to sulphur-dope lithium-ion cathodes. Sulphur-doped lithium nickel oxide, lithium nickel oxysulphide, is synthesised by mixing lithium and nickel acetate dissolved in deionized water with adipic acid and dried at 70 – 80 °C for 5 h [108]. The resulting gel is mixed with sulphur powers, ground, heated at 450 °C 10 h in air and under oxygen at 750 °C for 14 h. Rectangular particle morphologies between 500 and 1000 nm in diameter are produced. When used in a lithium-ion cell, cells exhibit a decreased initial discharge capacity vs. control lithium nickel oxide cells, 140 mAh/g vs. 160 mAh/g, but has a much greater capacity retention with 93% retention after 85 cycles vs. 81% after 45 cycles. As capacity retention is a significant problem with high nickel cathodes, sulphur doping may be beneficial to cathode performance.

High nickel NMC cathodes synthesised with sulfate phases have also been produced, with nickel, manganese, and cobalt sulfate hydrates and lithium hydroxide hydrate being used in a co-precipitation reaction with ammonia monohydrate and ammonium sulfate as a dopant to form NMC with a sulfate secondary phase [109]. The weight ratios of ammonium sulfate used were between 0.5 and 1.2%, with the resulting cathodes exhibiting nanoscale cuboidal morphologies that slightly decrease in size as ammonium sulfate is added. When cycled at 0.2

C, cathodes exhibit a maximum initial specific discharge capacities of 196 mAh/g with capacity retention as high as 81%, indicating improved cycling stability as the result of the sulfate phase.

Sulfate doping has also been attempted on LNO cathodes, with nickel nitrate hexahydrate, lithium carbonate or lithium hydroxide monohydrate, and ammonium sulfate used to produce the high Ni cathode with a sulfate secondary phase in either a solid state or co-precipitation reaction [110]. When analysed sulfur was both integrated into the LNO structure and formed a secondary lithium sulfate phase with solid state and co-precipitation synthesised cathodes exhibiting microscale irregular and nanoscale octahedral particles respectively. When solid-state synthesised LNO cathodes were cycled at 0.1 C LNO-sulfate cathodes exhibited an initial specific discharge capacity of 203 mAh/g vs. 176 mAh/g for undoped cathodes and a capacity retention of 84% vs. 74% after 100 cycles respectively. Co-precipitation synthesised cathodes exhibited initial specific discharge capacities for sulfate phase-containing and undoped LNO of 245 mAh/g and 223 mAh/g with 83% and 81% capacity retention after 100 cycles respectively.

1.4.3.5 Other Biotemplates

Other biotemplates were initially investigated but not pursued due to time constraints. Chitosan is a sugar derived from the shells of crustaceans that formed anisotropic crystallites, or micro-scale wires, Figure 36 (left), when used to synthesise YBCO [111]. Cellulose, aka. Avicel, was also used in the synthesis of YBCO forming cuboidal morphologies, Figure 36 (right), but required 1-ethyl-3-methylimidazolium acetate to be dissolved [112]. Other biotemplates such as cotton, wood, and pollen were investigated but mainly affected morphology at the macro scale when used to synthesise LCO [113].

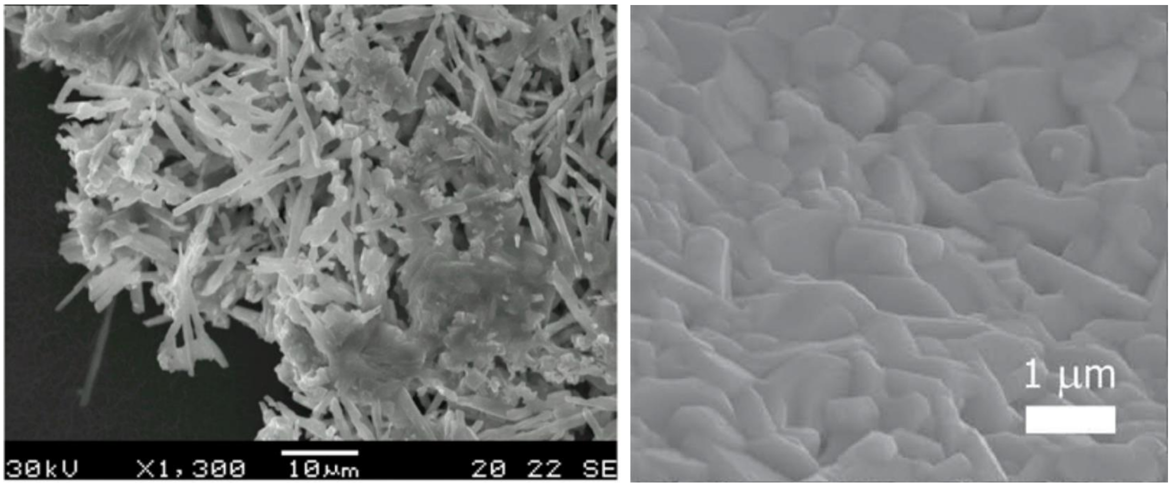

Figure 36 SEM images of YBCO particles synthesised using chitosan (left) and cellulose (right) biotemplating [111] [112]

1.4.4 Assessment of Biotemplating vs. Dry and Wet Synthesis Methods

When selecting a synthesis method, the method must be able to synthesise NMC811 in a way that is ideally inexpensive, scalable, repeatable, fast, allows for synthesis using relatively simple equipment and techniques, safe, and allows for the morphological control of particles. Solid state, while an industry standard for being highly scalable and inexpensive, requires long synthesis and grinding times to ensure homogeneity [49] [63] and exhibits little to no morphological control unless a wet chemical synthesis method is used to form precursors [59] [64].

When wet chemical synthesis methods are compared, spray pyrolysis allows for the synthesis of nanoscale particles but requires specific equipment in the form of a nebuliser, has a long synthesis time, and has difficulties with scalability [79]. While hydrothermal synthesis is faster and more scalable while also allowing for the control of different morphologies [73], it still requires specific equipment (an autoclave) and synthesis under higher pressures, increasing risk during the reaction phase. Molten salt synthesis, meanwhile, while also being able to manipulate particle morphologies and be scaled up, requires long grinding times and high synthesis temperatures similar to solid state synthesis which further increase synthesis costs [84]. The method is also somewhat dependent on the selected reactants and intermediate phases being able to melt.

Sol-gel also allows for the synthesis of a high stoichiometric and homogenous product as well as different particle morphologies [68] but often requires multiple steps for complete synthesis of the precursors to take place, with these steps potentially requiring synthesis times of 24 h [66] [69]. While scalable significant energy would be required to synthesise cathodes repeatedly for this length of time. Co-precipitation also allows for significant morphological control and control over the final product [78], but doing so requires significant control over pH, multiple synthesis steps, and either specific equipment such as continuously stirring tank reactors [46] or reactants added dropwise that make scalability difficult [79].

The Pechini method is a simple method that also allows for morphological control but relies on chelation to a hydroxycarboxylic acid which reduces the number of synthesis steps required [80]. The method is also able to be scaled up [83] and also allows for the morphological control of particles, albeit with limited results due critic acid being the main chelation mechanism [81]. It is also noted that a significant proportion of previous work in synthesising cathodes using the Pechini methods were done during or before the 2000s, with less research done using the Pechini method compared to other synthesis methods.

The novel biotemplating method meanwhile has all the benefits of the Pechini method. Biotemplating is also a simple but relatively new and novel method which allows for a greater variety of biopolymers/chelating agents to be used compared to the Pechini method, of which are sourced from organic sources such as algae which reduces the carbon footprint of the synthesis method. This method also allows for greater scale up and only requires short synthesis times of as low as 2 h which further reducing emissions produced during synthesis [92]. Morphological control of particles is also achieved with different biotemplates/chelating agents giving different morphologies due to different chelation mechanisms [94] [96]. As such, this relatively new and novel biotemplating method shall be employed to synthesise NMC811.

Of the biotemplate available, dextran is to be investigated due to its ability to form plates and spherical morphologies [63] [92], while sodium alginate and κ-carrageenan are able to be used to form nanowires and reticulated morphologies, respectively [94] [106]. Sodium alginate and κ-carrageenan may also be investigated for their sodium and sulfur content respectively, which may be used to improve the performance of lithium-ion cathodes via either doping or introduction of a secondary phase [102] [109]. While other biotemplates are available, such as chitosan, cotton, wood, and pollen [111] [113], dextran, sodium alginate, and κ-carrageenan will be the three biotemplates investigated such that the scope of the project does not exceed the time and resources allocated and each biotemplate can be given sufficient and appropriate time for investigation.

1.5 Aims and Objectives

With the cell and cathode chemistry and synthesis method outlined, the main aim of this thesis is to improve the performance of the NMC811 cathode via the use of the novel biotemplating synthesis method and the associated manipulation of particle morphologies. By using dextran, sodium alginate, and κ-carrageenan as biotemplates, each biotemplate will be investigated for their effectiveness in synthesising NMC811 and how they alter the particle morphology, with further optimisation of the synthesis method undertaken by changing precursors, synthesis times and temperatures with the goal of further improving the phase purity of the NMC811.

This optimisation will be done not only to attempt to optimise the synthesis of the NMC811, but also to manipulate particle morphology such that distinct morphologies such as plates or nanowires may be formed. This is so that it can be investigated whether the distinct morphologies may improve not only the already high specific capacity of the NMC811 but also the structural stability and cyclability of the cathode. Once NMC811 is synthesised, investigations into the scaling up of the novel biotemplating method will be done with the goal of producing lithium-ion cells containing the biotemplated cathodes, in order to study any potential improvements in performance either in specific capacity or cyclability.

Sodium alginate and κ-carrageenan will also be investigated as a potential dopant and in the synthesis of a sulfate secondary phase respectively, with each biotemplate containing sodium and sulfur respectively. It will be investigated as to whether sodium doped or sulfate phase-containing NMC811 cathodes are able to be synthesised using the respective biotemplate and whether such syntheses leads to any observed morphological changes or performance increases when cycling. All this is done with the aim that NMC811 will higher specific capacity and greater cyclability will be able to be produced using a simpler, quicker, cheaper, more efficient, and greener novel biotemplating method that will increase the uptake of green technologies such as EVs with the hope of reaching net zero.

2 Methodology

2.1 Powder Synthesis methodology

2.1.1 Results section 1 – Morphological control using dextran and sodium alginate biotemplates

To synthesise $LiNi_{0.8}Mn_{0.1}Co_{0.1}O_2$ the biotemplate method outlined in chapter 1 was used. The metal precursor salts used for the synthesis of the cathode powder are either acetate hydrates, nitrate hydrates, or sulfate hydrates, and with the exception of sodium nitrate, ($NaNO_3$, Sigma Aldrich, ≥99.0) used in an attempt to sodium dope NMC811, all metal precursor salts dissolved together will have the same anion group within the sample. Lithium, nickel, manganese, and cobalt precursor salts were weighed out into a 50 ml alumina crucible under atmospheric pressure and room temperature at a stoichiometric ratio of 10:8:1:1 or 2.5, 2, 0.25, and 0.25 mmol of Li, Ni, Mn, and Co precursor salt respectively. The precursor salts were then dissolved in a stated volume of room temperature distilled water and mixed until fully dissolved, with the ratio of the mass of precursors salts to volume of distilled water being selected based on the volume of distilled water required for the precursor salts to fully dissolve in the distilled water. The masses of each precursor salts when using acetate or nitrate precursors is outlined as such with the masses summarised in Table 2:

Acetate

- 0.2551 g lithium acetate dihydrate ($LiCH_3COO.2H_2O$, Sigma Aldrich, BioXtra), 0.4977 g nickel acetate tetrahydrate ($Ni(CH_3COO)_2.4H_2O$, Sigma Aldrich, ≥99.0%), 0.0613 g manganese acetate tetrahydrate ($Mn(CH_3COO)_2.4H_2O$, Thermofisher, Mn 22%), 0.0623 g cobalt acetate tetrahydrate ($Co(CH_3COO)_2.4H_2O$, Thermofisher, ≥98%), 10 ml distilled water at room temperature.

Nitrate

- 0.1724 g lithium nitrate ($LiNO_3$, Sigma Aldrich, Bioultra, ≥99.0%), 0.5816 g nickel nitrate hexahydrate ($Ni(NO_3)_2.6H_2O$, Sigma Aldrich, ≥99.999%), 0.0447 g manganese nitrate hydrate ($Mn(NO_3)_2.xH_2O$, Sigma Aldrich, ≥98.0%), 0.0727 g cobalt nitrate hexahydrate ($Co(NO_3)_2.6H_2O$, Sigma Aldrich, ≥98+%), 5 ml distilled water at room temperature.

	Acetate Hydrate	Nitrate Hydrate
Lithium (g)	0.2551	0.1724
Nickel (g)	0.4977	0.5816
Manganese (g)	0.0613	0.0447
Cobalt (g)	0.0623	0.0727
Distilled water (ml)	10	5

Table 2 Masses of acetate and nitrate precursors used

Acetate precursors are used due to being relatively inexpensive, safe, easy to handle, and require no special storage conditions. Their investigation is important to determine their viability as a safe and inexpensive option, especially when scaling up, when synthesising with biotemplates. Nitrates are more expensive and are more harmful, making them more unsafe to handle, and some require special storage conditions (Manganese nitrate hydrate will melt above 26 °C and so requires storage in a desiccator during summer). Previous literature [69][80] has proven their use for the synthesis of NMC cathodes and the production of nanoscale particles, however.

The biotemplate is dissolved in a separate 50 ml alumina crucible. Dextran (from Leuconostoc ssp. M_r = ~ 6,000, $(C_6H_{10}O_5)_n$, Sigma Aldrich) can be dissolved completely by stirring continuously in room-temperature distilled water at a ratio of 0.5 g of biotemplate to 10 ml of water. Sodium alginate $((C_6H_7O_7)_A(C_6H_7O_7)_BNa$, Thermofisher, alginic acid sodium salt, high viscosity powder) and κ-carrageenan (Sigma Aldrich, sulfated plant polysaccharide) are dissolved completely by stirring the biotemplate in 85 °C distilled water heated on a hot plate at a ratio of 0.1 g of biotemplate to 10 ml of distilled water. The ratios of mass of biotemplate to volume of distilled water were selected based on the volume of distilled water required to fully dissolve the weighed mass of biotemplate, and a summary of these methods is outlined in Table 3.

Biotemplate	**Solvent**	**Biotemplate to solvent ratio (g/ml)**
Dextran	Water, room temperature	0.5/10
Sodium Alginate	Water, 85 °C	0.1/10
K-carrageenan	Water, 85 °C	0.1/10

Table 3 Methods of and associated mass and volume ratios of dissolution for biotemplates

Once both the biotemplate and the metal precursor salts have been separately dissolved, the metal precursor salt solution is added to the biotemplate solution. 5 ml of excess room-temperature distilled water is added to the crucible previously containing the metal precursor salt solution to dissolve any remaining undissolved salts before being added to the biotemplate solution. The combined solution is mixed until fully combined before being placed into an 85 °C drying furnace for a minimum of 24 hours or until fully evaporated.

Once fully evaporated, powders synthesised with nitrate precursors are ground in an agate pestle and mortar in order to increase the surface area of the particles and reduce reaction boundaries during the preheat phase. Acetate precursors are unable to be ground at this stage as the resulting dried sample is too hard and is stuck to the crucible. Any attempts to remove it from the crucible require chipping it away which may damage the crucible and lead to loss of mass of the sample. Instead, the sample is ground after the preheat stage.

The powder is preheated at 300 °C in a box furnace in air with an increasing and decreasing ramp rate of 1 °C/min and a dwell time of 2 h. Maximum temperatures of 200, 400, 500, or 600 °C, as well as ramp rates of up to 10 °C/min and dwell times of 6 h may also be used to investigate variations in the cathode powder caused by the preheat phase. During the preheat phase the chelation of metal ions onto the biotemplate reduces the chance of recrystallisation into unwanted intermediate phases at lower temperatures until the biotemplate is burnt off, resulting in small particle sizes. Shorter reaction pathways are also formed as a result of the chelation of metal ions along the intertwined biotemplate chains that reduce temperature and dwell time requirements during the preheat phase.

Once removed from the box furnace, the powder is ground in an agate pestle and mortar (again if using nitrate precursors) to again ensure large particle surface area, increase homogeneity of the powder, and reduce reaction boundaries. The powder is then calcined in a tube furnace under oxygen at either 800 or 850 °C for samples synthesised with nitrate precursors and acetate precursors respectively. An increasing and decreasing ramp rate of 1 °C/min and 5 °C/min respectively, as well as a 2 h dwell time and an oxygen regulator pressure and flow rate of 1 bar (relative to atmosphere) and 1 l/min respectively are used. Ramp rates may again range up to 10 °C/min and dwell times up to 6 h depending on the sample being investigated.

2.1.2 Powder synthesis Methodology Issues

Nitrate precursor-produced samples are ground before the preheat stage, while samples produced with acetates are initially ground after the preheat phase. The reason for this is due to the dried sample produced using nitrates having soft, porous, particle agglomerations that can be easily ground, while samples made with acetates produce a hard surface upon drying that cannot be removed from the crucible until preheated.

The preheat phase is performed in a box furnace in air due to the large emission of gas observed at 160 °C. When preheating is done in a sealed tube furnace under oxygen, this emission of gas is large enough to either remove the inlet gas valve from the tube, or transport some of the powder sample into the outlet of the tube furnace. This gas is likely the synthesis of large amounts of carbon dioxide due to the large amounts of carbon present in the biotemplate, and in the case of where acetate salts are used, the precursor. Therefore, it is not viable to preheat the sample under a sealed atmosphere.

A similar, but more violent, gas emission can be observed during the preheat phase when using a box furnace in air, for a sample using the dextran biotemplate and nitrate precursors. The emission of gas when using this combination of biotemplate and precursors is large enough to cause the powder to exit the crucible such that the amount left in the alumina crucible is not enough to warrant continuing the synthesis, with only enough to do post-synthesis analysis (in this case XRD and SEM) remaining. This is likely due to the combination of smaller particle size when using nitrate precursors and large amount of carbon from the dextran biotemplate forming a large amount of carbon dioxide. Attempts to place a lid on the crucible have also failed with the lid deposited next to the crucible. As the amount of powder remaining is not enough to produce a cathode, cathode powders produced with dextran and nitrate precursors have not been formed into cells.

Post-synthesis, once removed from the tube furnace the powder is ground once more in an agate pestle and mortar such that it can be analysed using XRD or SEM or used to produce a cell. The sample is then stored in a sealed 5 ml glass vial in a desiccator maintained at room temperature and a humidity < 10%. If being used to produce a cell, the vial lid is replaced by perforated aluminium foil and stored in a vacuum oven under vacuum at 80 °C.

2.1.3 Results section 2 – Attempt to sodium dope NMC811 using sodium alginate biotemplating and the varying of Lithium-Sodium eutectics

In chapter 4, sodium alginate is primary used to investigate the possibility of sodium doping using biotemplating. In order to achieve this, the mass of sodium alginate is increased and the proportion of lithium precursors reduced accordingly such that Na = x and Li = (1 – x) whereby $Li_{(1-x)}Na_xNi_{0.8}Mn_{0.1}Co_{0.1}O_2$. The masses to attempt to synthesise Na-doped NMC811 are summarised in Table 4, showing the required changes in masses for lithium precursors and sodium alginate accordingly.

	Acetate Hydrate	Nitrate Hydrate
Lithium, x = 0.1 (g)	0.2296	0.1552
Lithium, x = 0.2 (g)	0.2041	0.1379
Sodium alginate, x = 0.1 (g)	0.1	0.1
Sodium alginate, x = 0.2 (g)	0.25	0.25
Nickel (g)	0.4977	0.5816
Manganese (g)	0.0613	0.0447
Cobalt (g)	0.0623	0.0727
Distilled water (ml)	10	5

Table 4 Masses of metal precursor salts used in the attempted synthesis of sodium-doped NMC811 via substitution of lithium ($Li_{(1-x)}Na_xNi_{0.8}Mn_{0.1}Co_{0.1}O_2$*) using sodium alginate*

As part of the investigation into sodium doping, a different sodium dopant will be compared against sodium alginate. Sodium nitrate will also be investigated as to whether it can be used alongside the sodium alginate biotemplate to effectively dope NMC811. The amount of sodium doping is maintained such that x = 0.2, with the cathode doped with 100% biotemplate and then a 50:50 ratio of sodium alginate and sodium nitrate, Table 5.

	X = 0.2, 1:0 Sodium alginate: sodium nitrate	X = 0.2, 0.5:0.5 Sodium alginate: sodium nitrate
Lithium acetate dihydrate/Lithium nitrate (g)	0.2041/0.1379	0.2041/0.1379
Sodium alginate (g)	0.25	0.1
Sodium nitrate (g)	0	0.0213

Table 5 Masses of metal precursor salts used in the attempted synthesis of Na-doped NMC811 via substitution of lithium ($Li_{(1-x)}Na_xNi_{0.8}Mn_{0.1}Co_{0.1}O_2$*) using sodium alginate and sodium nitrate*

In addition to doping when using sodium alginate as a biotemplate, Na-doping when biotemplating with dextran is also investigated. As no significant proportion of sodium is present within the dextran biotemplate, sodium nitrate is used as the primary dopant such that x = 0.1 and 0.2, Table 6. This is to compare any successfully sodium alginate biotemplated NMC811 against dextran biotemplated Na-doped NMC811 in order to discern if sodium being part of the sodium alginate biotemplate has a significant effect vs. dextran biotemplating and sodium nitrate doping.

	X = 0.1	X = 0.2
Lithium acetate dihydrate/Lithium nitrate (g)	0.2296/0.1552	0.2041/0.1379
Dextran (g)	0.25	0.25
Sodium nitrate (g)	0.0213	0.0425

Table 6 Masses of metal precursor salts used in the attempted synthesis of Na-doped NMC811 via substitution of lithium ($Li_{(1-x)}Na_xNi_{0.8}Mn_{0.1}Co_{0.1}O_2$*) when using dextran as a biotemplate and using sodium nitrate*

The final experiments into the sodium-doping of NMC811 will involve adding sodium to a full NMC811, such that Na = x and Li = 1 ($Li_1Na_xNi_{0.8}Mn_{0.1}Co_{0.1}O_2$) instead of substituting lithium for sodium. This is to deduce whether NMC811 can still be effectively doped with sodium without the removal of lithium in order to maintain the full amount of lithium for lithiation to occur while still gaining any benefits from sodium doping. The same investigations, doping with sodium alginate, doping with sodium alginate and sodium nitrate, and doping with sodium nitrate when using dextran are undertaken using the addition of sodium without the removal of lithium instead of substituting lithium for sodium with the masses of biotemplate, precursors, and dopants, outlined in Table 7 to Table 9, being similar with the exception of the mass of lithium precursor used.

	Acetate Hydrate	Nitrate Hydrate
Lithium (g)	0.2551	0.1724
Nickel (g)	0.4977	0.5816
Manganese (g)	0.0613	0.0447
Cobalt (g)	0.0623	0.0727
Sodium alginate, x = 0.1 (g)	0.1	0.1
Sodium alginate, x = 0.2 (g)	0.25	0.25
Distilled water (ml)	10	5

Table 7 Masses of metal precursor salts used in the attempted synthesis of Na-doped NMC811 via addition of sodium ($Li_1Na_xNi_{0.8}Mn_{0.1}Co_{0.1}O_2$) using sodium alginate and sodium nitrate

	X = 0.1	X = 0.2	X = 0.3
Sodium alginate (g)	0.1	0.1	0.1
Sodium nitrate (g)	0	0.0213	0.0425

Table 8 Masses of metal precursor salts used in the attempted synthesis of Na-doped NMC811 via addition of sodium ($Li_{(}Na_xNi_{0.8}Mn_{0.1}Co_{0.1}O_2$) using sodium alginate and sodium nitrate

	X = 0.1	X = 0.2
Dextran (g)	0.25	0.25
Sodium nitrate (g)	0.0213	0.0425

Table 9 Masses of metal precursor salts used in the attempted synthesis of Na-doped NMC811 via addition of sodium ($Li_{(}Na_xNi_{0.8}Mn_{0.1}Co_{0.1}O_2$) when using dextran as a biotemplate and using sodium nitrate as a dopant

2.1.4 Results section 3 - Synthesis and morphological control of NMC811 with sulfate secondary phase using sulfur-based κ-carrageenan

When using κ-carrageenan as a biotemplate the masses of precursors used, Table 10, differ from when using other biotemplates. When using κ-carrageenan the ratio of masses between the metal precursor salts and biotemplate is derived from work using κ-carrageenan to synthesise YBCO [106], and as such the masses of the metal precursor salts are varied relative to 0.1 g of biotemplate such that the same ratio of metal precursors to biotemplate is applied as when synthesising YBCO using the higher mass of biotemplate.

	Acetate Hydrate	Nitrate Hydrate
Lithium (g)	0.2551	0.1158
Nickel (g)	0.04977	0.3722
Manganese (g)	0.0613	0.0286
Cobalt (g)	0.0623	0.0466
κ-carrageenan (g)	0.1	0.1
Distilled water (ml)	10	5

Table 10 Reactant masses for synthesising NMC811 using acetate or nitrate precursors and κ-carrageenan

When synthesising YBCO using a high ratio of κ-carrageenan to precursor salts Barium sulfate, $BaSO_4$, is formed as an impurity phase. It is theorised when κ-carrageenan is used in the synthesis of NMC811 sulfur in the biotemplate will either be integrated into the NMC811 structure or that a similar process to that when synthesising YBCO will occur and lithium sulfate, Li_2SO_4, will be formed as an impurity phase. By using κ-carrageenan and controlling the ratio between the biotemplate and metal precursor salts, it is the aim to be able to control the amount of Li_2SO_4 being produced such that NMC811 is synthesised with a secondary sulfate phase that improves capacity retention of the cathode during cycling.

In addition to the use of κ-carrageenan, sulfate precursors are investigated as an alternative way of forming sulfate secondary phases in NMC811. The masses of sulfate precursors used, summarised in Table 11, are 0.3199 g lithium sulfate monohydrate ($Li_2SO_4.H_2O$, Sigma Aldrich, ≥99.0%), 0.5257 g nickel sulfate heptahydrate ($NiSO_4.7H_2O$, Sigma Aldrich, ≥99.0%), 0.0424 g manganese sulfate hydrate ($MnSO_4.xH_2O$, Sigma Aldrich, ≥99.0%), 0.0703 g cobalt sulfate heptahydrate ($CoSO_4.7H_2O$, Sigma Aldrich, ≥99%) being dissolved in 10 ml distilled water at room temperature. Sodium alginate using a mass of 0.1 g is selected as the biotemplate due to its similarities to κ-carrageenan.

Reactant	Mass /Volume
Lithium Sulfate monohydrate (g)	0.3199
Nickel Sulfate heptahydrate (g)	0.5257
Manganese Sulfate hydrate (g)	0.0423
Cobalt Sulfate heptahydrate (g)	0.0703
Sodium Alginate (g)	0.1
Distilled water (ml)	10

Table 11 Reactant masses for synthesising NMC811 using sulfate precursors and sodium alginate

2.2 Cathode analysis

2.2.1 X-ray Diffraction

X-ray Diffraction (XRD) is a non-destructive analytical technique that for the purposes of this project is used to analyse the phases, crystal structure, and crystal orientation of powder samples. The XRD instrument used in the analysis of samples in this project is primarily the Panalytical Aeris, with some analysis also being done using the Panalytical XPert and Bruker D2. XRD employs the use of X-rays emitted by a source, Figure 37, in this case a copper source, which is diffracted from the surface of the powder and received by a detector. X-rays are produced by firing free electrons from an electron gun and accelerating them across a potential difference. 1s electrons within the copper source are excited by an interaction with the accelerated free electrons are emitted from the electron shell. 2p electrons are then de-excited to the 1s energy shell and emit the excess energy in the form of X-rays, Figure 38. Such X-rays are of wavelengths unique to the electronic transitions, with wavelengths of 1.5406 Å and 1.5444 Å for copper Kα1 and Kα2 emissions respectively. 3p electrons may also deexcite to the 1s shell and emit Kβ radiation with wavelength 1.392 Å.

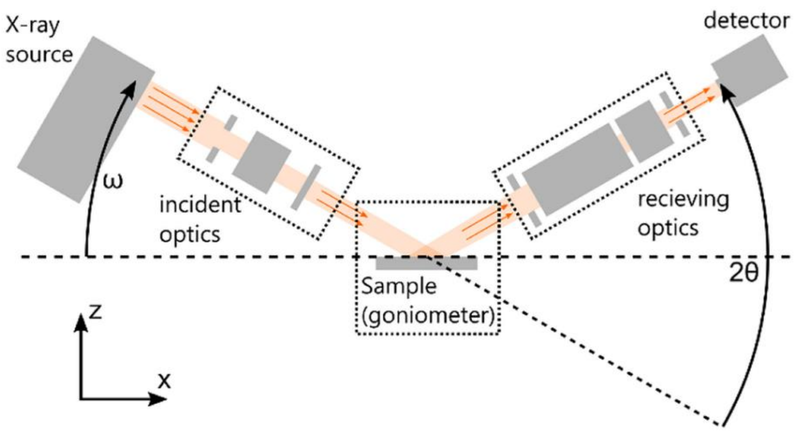

Figure 37 Diagram of X-Ray Diffraction [114]

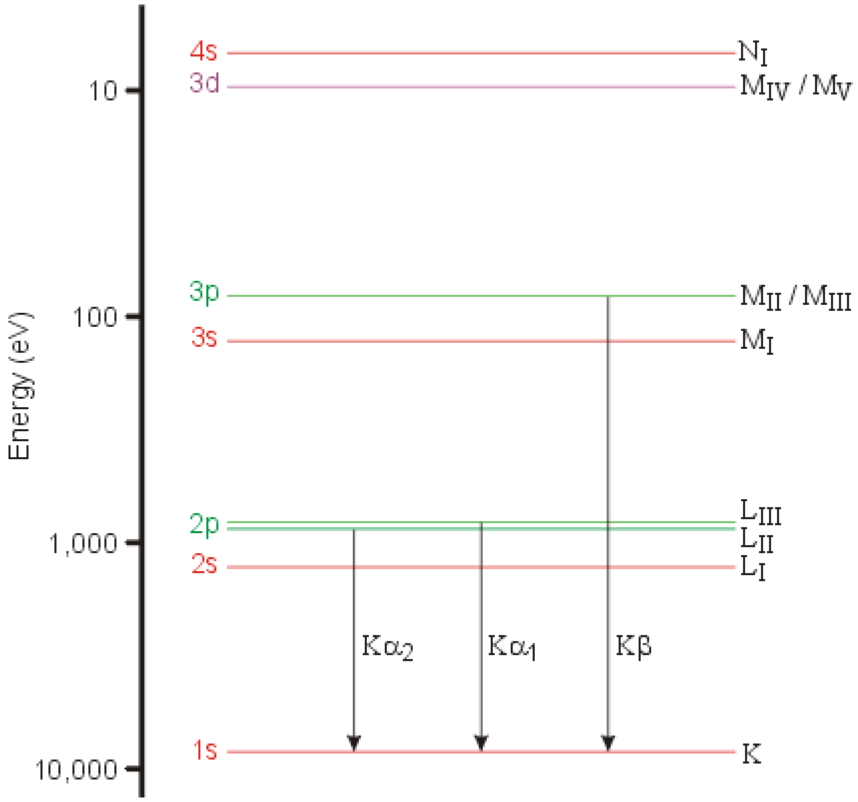

Figure 38 Diagram showing emission of characteristic X-Rays of copper [7]

Produced X-rays are directed towards the sample being analysed at an angle of incidence, Θ. Upon the X-rays interacting with the sample, the X-rays are either absorbed by the sample or reflected, with the reflected X-rays being reflected at an angle equal to the angle of incidence, Figure 39. X-rays will travel different distances depending on which plane they interact with and are reflected off of. Diffraction occurs when two or more X-rays which have travelled different distances and interacted with different planes interact with each other. Diffracted X-rays may undergo constructive or destructive interference depending on the distance between the planes and the distances the X-rays have travelled, (Eq. 1), with such interference being defined by Bragg's law:

$$n\lambda = 2dsin\Theta$$

(Eq. 1)

Figure 39 shows this relationship between visually, where n is a positive integer, λ is the wavelength of the X-rays, d is the spacing between the atomic planes, and Θ is the angle of incidence/reflection of the X-ray to the sample.

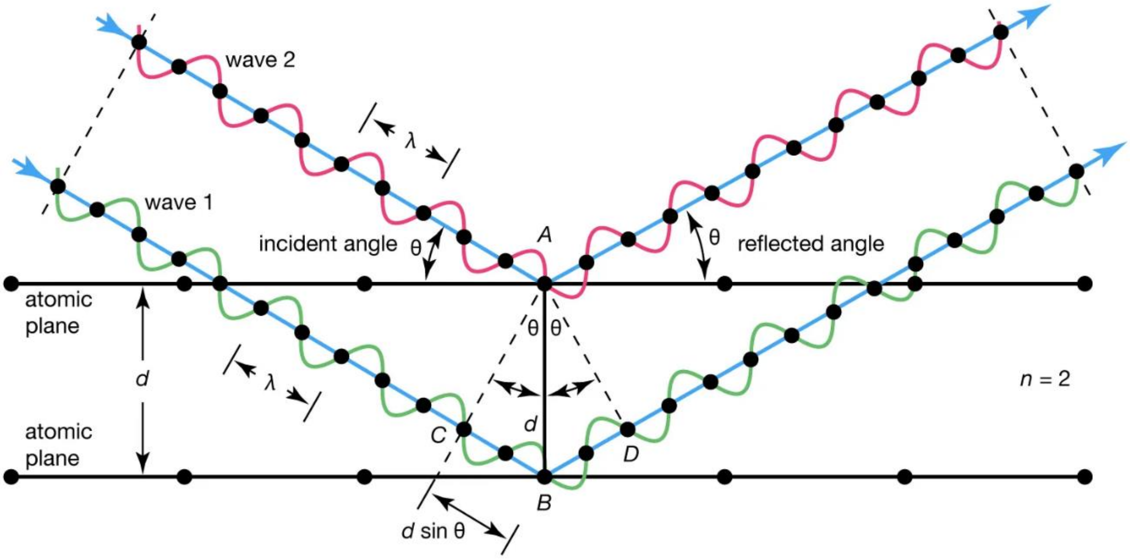

Figure 39 Visual Illustration of Bragg's Law [115]

Constructive interference between two or more X-rays occurs where the extra distance travelled by the addition X-rays upholds Bragg's Law, where the distance *CB* + *BD* is equal to *2dsinΘ* and so an integer of the wavelength, $n\lambda$. When this relationship is upheld X-rays may interact with the detector. Should the extra distance travelled by the X-ray, *CB* + *BD*, not be equal to *2dsinΘ*, destructive interference will occur due to the X-rays being out of phase and X-rays will cancel each other out. The resulting X-rays detected as a result of the constructive interference will form an XRD pattern with 2Θ plotted against intensity of X-rays detected. Each individual peak on the XRD pattern represents a different crystallographic plane denoted by different Miller indices, or *hkl* coordinates, provided the intensity of detected X-rays is high enough. Provided it is not amorphous (does not have a crystalline structure) each crystal structure has a distinct pattern of peaks of varying intensities and angles of incidence, which can be compared against existing data to determine the phases of the analysed sample.

If this intensity is not high enough, peaks may be lost in background noise or merge into larger peaks. A nickel filter may be employed when using a Cu source to reduce the appearance of twin peaks, or peak splitting, occurring during XRD. Twin peaks are the result of a) Kα and Kβ radiation or b) Kα1 and Kα2 radiation. Twin peaks as a result of Kα and Kβ may be removed by using a Ni filter to block Kβ radiation.

When analysing samples with nickel, manganese or cobalt in, elements used widely within this project, a low fluorescent mode must also be used to reduce the effect of fluorescence. Fluorescence is the emission of characteristic X-rays by the sample being analysed, in addition to the X-rays being reflected, and due to Ni, Mn, and Co being similar in size to Cu the emitted characteristic X-rays are similar in energy to the characteristic X-rays of the Cu source. This results in further background peaks and requires a low fluorescence mode in order to reduce the intensity of background radiation by increasing the minimum threshold at which energy may be detected. By using low fluorescence mode, characteristic Ni, Mn, and Co X-rays do not meet the minimum intensity to be detected and so this reduces the noise of the background radiation.

When analysing NMC811 using XRD, certain characteristic peaks help denote whether the NMC811 is layered and organised, or disorganised. Layered, organised NMC811 has altering layers of lithium and transition metal atoms and is highlighted by a large intensity ratio between the (003) and (104) reflections, and strong, distinct twin peaks at (006)/(012) and (018)/(110) reflections. Disorganised NMC811 will have mixing of lithium and transition metal atoms between the layers and the greater the disorganisation the greater the mix of atoms between the layers. Increased disorganisation is denoted by a lower intensity ratio between (003) and (104) reflections, and less distinct twin peaks at (006)/(012) and (018)/(110) reflections.

How distinct the twin peaks are at the (006)/(012) and (018)/(110) reflections can be calculated quantitatively by determining the resolution of separation of the twin peaks [116]. The resolution of separation, R_s, is primarily used in chromatography however can be also used to determine how well separated twin peaks are in XRD patterns. Resolution of separation can be calculated by taking the difference in the 2Θ values of the two peaks, $t_{R2} - t_{R1}$, Figure 40a, and dividing by the average of the width of the two peaks, $(w_1 + w_2)/2$, Figure 40b, as per (Eq. 2). This will result in a value of between 0 and 1.5, where 0 is a single peak and 1.5 is two separate twin peaks with almost no overlap.

$$R_s = \frac{t_{R2} - t_{R1}}{(w_1 + w_2)/2}$$

(Eq. 2)

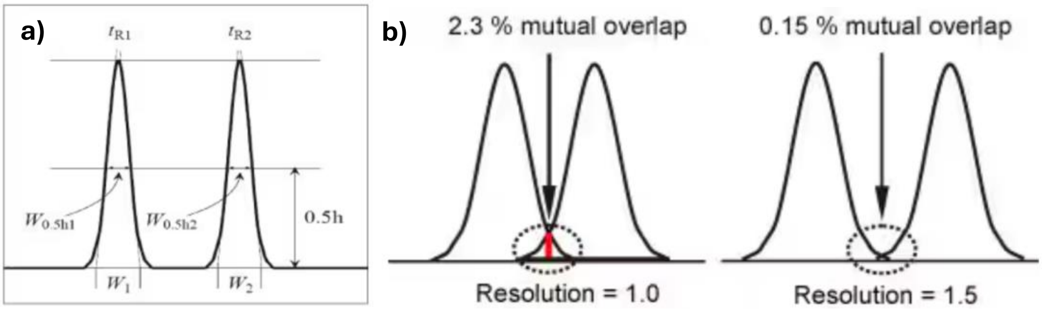

Figure 40 Images showing method for determining resolution of separation in twin peaks and a) the variables used to calculate R_s and b) how R_s relates to peak overlap [117]

2.2.1.1 Rietveld Analysis

Rietveld analysis may be employed post XRD in order to refine the crystal structure of the analysed sample to determine variation in structure between the sample and the known referenced material patterns. This technique is useful when comparing structures with different proportions of atoms, additional phases, or different structural orientations, and can show variations in characteristics such as unit cell dimensions, distribution of elements, and atomic spacing. Rietveld analysis can be undertaken using a number of programs, including General Structure Analysis System, GSAS, or Malvern Panalytical's Highscore. For this project GSAS-ll is primarily used due to the program still being supported with updates and due to expertise from staff in the University of Sheffield including Lewis Owen.

Rietveld is undertaken by attempting to fit phase data, recorded crystallography data file, or CIF file, obtained from the Crystallography Open Database [118] to powder XRD data from the sample, in this case NMC811 powder data from the Panalytical Aeris, Phase data for this study is the crystallography CIF file for high nickel NMC811 with minimal mixing of the lithium and transition metal layers (COD ID **1520789** [119]). When importing phase data, additional data from the phase data must be added manually and includes the space group, unit cell dimensions, cell volume, and the initial atom data, outlined in Table 12. Due to the similarities between NI, Mn, and Co, it is assumed when using NMC phase data that Mn and Co are Ni.

- Space Group: R-3m (a=b≠c, α=β≠γ)
- a = b = 2.8645 Å
- c = 14.161 Å
- α = β = 90 °
- γ = 120 °
- Cell Volume = 100.629 Å^3

Atom	Element	X coordinate	Y coordinate	Z coordinate	Fraction	Site Symmetry	Multiple	Thermal Parameters, U_{iso}
Li1	Li	0	0	0	1.0	-3m	3	0.01
Li2	Li	0	0	0.5	0	-3m	3	0.01
Ni1	Ni	0	0	0	0	-3m	3	0.01
Ni2	Ni	0	0	0.5	1.0	-3m	3	0.01
O	O	0	0	0.25	1.0	3m	6	0.01

*Table 12 NMC811 (CID ID **1520789**) Atomic Data for Rietveld Analysis [119]*

Powder data, NMC811 data obtained from the Panalytical Aeris which the phase data will be fitted against, and the instrument parameter file, for this case the parameter file for the Panalytical Aeris, is also uploaded. The background function is also set to Chebyschev-1 with 6 degrees of freedom which gives a compromise between the accuracy and computational power required of the refinement. When the refinement process is begun the initial refinement will often be a poor fit between the powder and phase data. When refining peaks, background function, instrument parameters and sample parameters, and phase parameters. These parameters may be used to refine peak intensity, shape, and position.

- The background may be refined by first refining the background function to attempt to refine the background noise.

- Sample parameters, such as histogram scale factor, sample displacement, and sample transparency may be refined if there is significant differences in scale between powder data and phase data. This would be the case if one data set was analysed using a greater count/second resulting in a pattern with a greater overall intensity.

- Instrument parameters may be broadly split into gaussian and Lorentzian parameters and are used to refine peak shape. While both are used in tandem to describe peak shape, they are defined by different equations. Gaussian peaks tend to be sharper and narrower with a higher intensity and are defined as where *A* is the peak scaling function, *b* is peak position, and *c* relates to the peak width, (Eq. 3).

$$G(x) = Aexp(-\frac{(x-b)}{2c^2})$$

(Eq. 3)

  Lorentzian peaks tend towards wider peaks with a lower intensity and are defined as where x_0 is the peak position and γ is the full width at half maximum, (Eq. 4), and as such, peak shape may be refined by refining gaussian (U, V, and W parameters) and Lorentzian (X, Y, and Z parameters) parameters.

$$L(x) = \frac{1}{\pi}\frac{\frac{1}{2}\gamma}{(x-x_0)^2 + (\frac{1}{2}\gamma)^2}$$

(Eq. 4)

- Unit cell parameters may be refined in order to refine peak positions of the phase data. Peak position is related to the unit cell constants (a, b, c, α, β, γ) and so be refining the unit cell constants peak positions may be accurately defined.

- Finally peak intensity may be refined by refining the atomic positions, site fractions, and thermal parameters defined in Table 12. By refining for different atoms in the structure, relative peak intensities may be refined. This is important for phase identification of the NMC where the ratio between peak intensities is an important identifier of the ratio of different elements within the crystal structure.

Such refinements must be done with the understanding that the GSAS II software may generate numbers during refinement that are not possible in the real world. Therefore, after each refinement a check must be done to ensure all values are still realistic. The patterns may be considered to be refined when both patterns visually line up. The χ^2 value may be used as a shorthand for a good fit, with the fit being considered better as the value approaches 0 but may still produce a structure that is not physically possible or does not fit as well as the value suggests. Once fitted, the refined parameters, such as unit cell values, site fractions, and atomic positions may be used gain insight into the crystalline structure and makeup of the powder data. This is therefore a valuable tool when analysing crystalline powders.

2.2.2 Scanning Electron Microscopy

Scanning electron microscopy, SEM, is an analytical method for imaging samples, with it differing from traditional light-based microscopy by using electrons as an imaging source instead of light. This allows SEM to produced high quality images with higher levels of magnification than traditional light-based microscopy due to electrons having a significantly smaller wavelength than visible light (~10^{-10} m vs. 10^{-7} m), with the downside being that images must be taken under a vacuum to ensure electrons have sufficient mean free path length to reach the sample surface. Samples are placed on a carbon disc (Agar Scientific, 12.5mm) on a metal stub, and the microscope primarily used to take images in this project is the FEI Inspect F. Electrons are generated using an electron gun, Figure 41a, where a source of either tungsten or solid state lanthanum hexaboride is excited and deexcited by an applied voltage across the source, emitting free, or primary, electrons that are accelerated across a potential difference. A field emission gun may also be employed, whereby tungsten cooled using liquid nitrogen emits primary electrons in a column from a single point. This allows higher resolution images to be taken a much lower scales, including nanoscale.

Once accelerated the primary electrons are focused through a condenser lens, Figure 41b, which defines the size of the electron beam and then focused through an objective lens. Modifying the condenser lens will affect the resolution of the final image while altering the objective lens allows for the magnification and focus of the final image to be varied. Primary electrons then interact with the sample and exhibit different behaviours depending on the type of interaction occurring, Figure 41. Secondary electrons are the result of interactions between the primary electrons and outer shell electrons. When primary electrons interact with atoms at or near the surface of the sample, they may excite outer shell electrons during an inelastic collision. The outer shell electron may gain enough energy to leave the surface. Secondary electrons may be picked up by a detector and their detection is used to produce an image of the surface of the sample. Should a secondary electron be emitted from a lower energy level, an outer shell electron will de-excite and emit characteristic X-rays.

Back scattered electrons are the product of elastic scattering between primary electrons and the atomic nuclei. Instead of colliding with an electron in the energy shell, the primary electron will travel close to the nuclei before being reflected out of the atom. Back scattered electrons are able to be detected by a separate detector, made of a silicon superconductor, which allows for an image to be produced that composition of the sample.

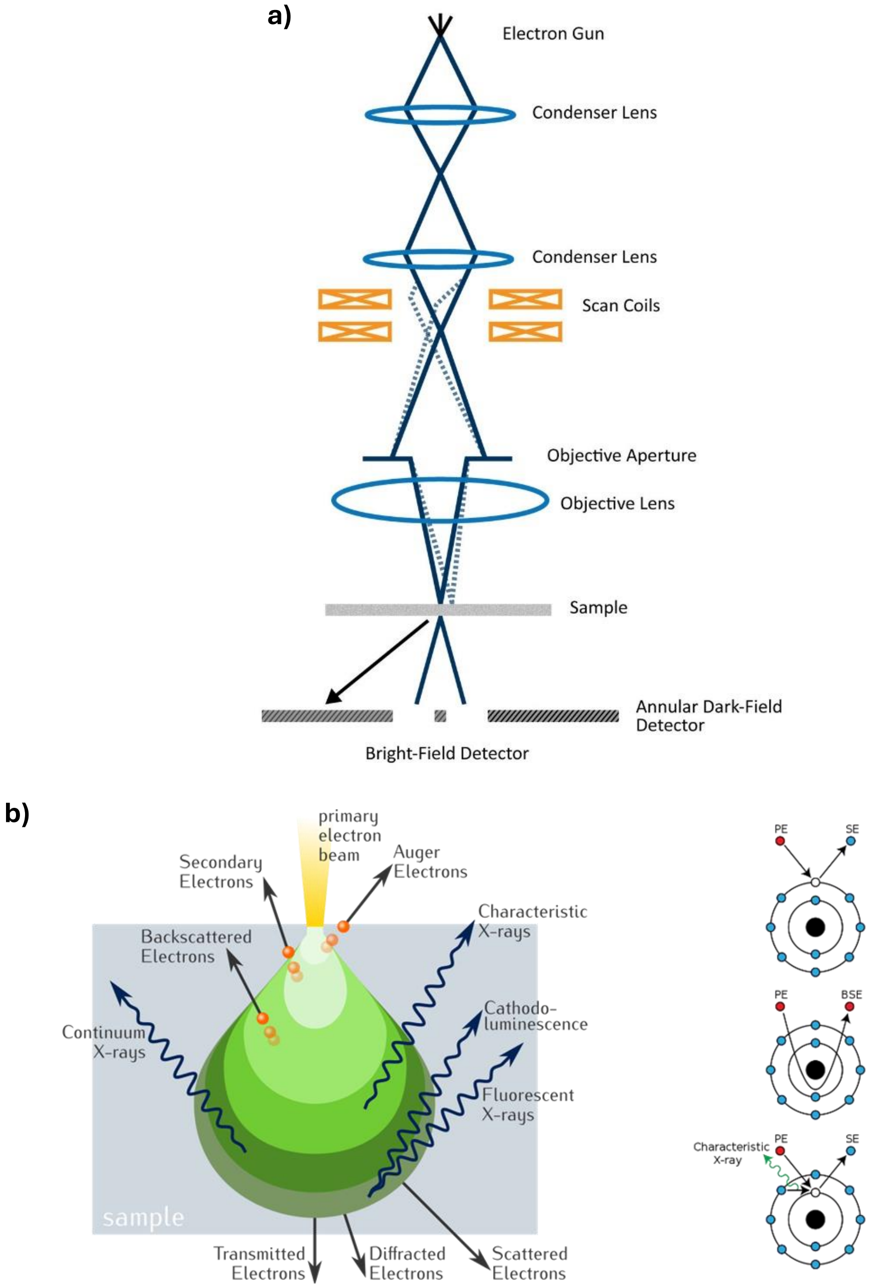

Figure 41 Scanning Electron Microscopy a) Schematic [120] and b) Types of Interactions [121]

Individual particles were measured using ImageJ, a program that allows for the analysis of SEM images. Using ImageJ, an average particle size can be calculated by taking an average of the diameters of a range of particles in the SEM image. A reference scale of 0.055 pixels/nm is set by drawing a line of equal length to the scale bar, and then assigning the line a distance value equal to the distance stated on the scale. Using this scale, any new lines drawn with be assigned a length value relative to this scale. The average particle diameter of a range of particles is determined by drawing lines across the widths of the particles and recording the values before taking the average. Such diameters can be recorded to the nearest whole nanometre ensuring an error value of +/- 1 nm. While drawing distance lines be hand is a slower method this is more accurate using ImageJ's inbuilt particle analyser, as this program is reliant on the contrast of the image to determine what is a particle. The images obtained using SEM of NMC811 in this project consists of particles grouped together in too high a density to be analysed computationally and so must be done by hand. Human error however may lead this error value to become greater. This may lead to the program misidentifying particles, identifying blank space as particles, or taking measurements incorrectly.

2.2.2.1 Energy dispersive X-ray analysis

Energy dispersive X-ray analysis, or EDAX, may also be employed as an analysis method when using SEM. EDAX is mainly used to determine the composition and concentration of different elements of a sample, and works by the excitation of lower shell electrons results in the emission of a secondary electron. A higher shell electron will then de-excite to fill the gap, resulting in the emission of a characteristic X-ray. The energy of the emitted X-ray is unique to the element and transition from which it was emitted, and along with the intensity of X-rays can be collected by a detector to determine the composition and the concentration of different elements of a sample. This is provided that the energy of the electrons emitted from the SEM source is sufficient to produce characteristic X-rays from the sample atoms. For NMC811, an accelerating voltage of 20 kV is required to fully map the range of characteristic X-rays emitted.

2.2.3 Differential Scanning Calorimetry/Thermogravimetric Analysis

Differential Scanning Calorimetry (DSC) and Thermogravimetric Analysis (TGA) are analytical techniques for measuring the energy flow and mass change respectively of a sample over time as it is heated or cooled. For this project this analysis is done using a TA Instruments Waters Discovery SDT 650. A maximum of 200 mg of preheated sample is weighed out into a crucible and placed into the SDT against an empty control crucible. The sample is preheated due to high amounts of gas emissions at 150 [122] or 212 °C [123] which may cause damage to the SDT. In order to replicate the synthesis conditions, the SDT is able to be connected to gas, where in this case the SDT is connected to oxygen to simulate the environmental conditions of the tube furnace when using O_2.

DSC/TGA was done by heating the sample under oxygen and to a maximum temperature of 850 °C at a 10 °C/min ramp, with a dwell time of 1 h before being ramped down at 10 °C/min to room temperature. The ramp up, dwell time, and ramp down are denoted by blue, green, and red lines respectively.

During heating normalised heat flow, W/g, and relative mass (when compared to the initial mass at the beginning of heating),%, are plotted against the program temperature, °C. Normalised heat flow and relative mass are indicated using solid and dashed lines respectively. Normalised heat flow, (Eq. 2), may either be positive, representing an exothermic reaction, or negative, denoting an endothermic reaction, and is calculated using the sample heat capacity, C_p, heating rate in °C per min, dT/dt, and the calibration constant, K:

$$\frac{dH}{dt} = C_P \frac{dT}{dt} \times K$$

(Eq. 5)

This allows for the analysis of the heat flow of the sample, either exothermic or endothermic, while relative mass is simple recorded by weighing the mass of the sample. Normalised heat flow can be used to identify different phases or materials during the reaction [124] by identifying the temperature points of phase transition, while TGA can provide information on thermal stability and when combined with DSC can provide further evidence of phase transitions using increases or decreases in the rate of relative mass.

The advantages of using DSC and TGA is that both only require a small mass of sample for analysis to take place and requires minimal preparation, there also being precise temperature control. When doing DSC, normalised heat flow can give accurate measurements of phase transitions and heat capacities while also being sensitive enough to record small or weak phase transitions. When using TGA both qualitative and quantitative analysis is available with detection of multiple events where mass is loss from both physical and chemical changes in material possible. Disadvantages of both analysis techniques is that they are destructive techniques, with any sample being unable to be used after analysis, while disadvantages for DSC are that the mass of the sample has to remain constant, meaning any reactions containing evaporation or sublimation phases are not accurate, and that accurate data is not able to be obtained when a reaction event, such as decomposition, occurs at the same temperature as a phase change such as melting.

2.3 Cell Manufacture

Powders produced by calcination under oxygen were able to be synthesised into cathodes for use in lithium-ion coin cells in line with National Physics Laboratory (NPL) methodology [125]. The powder, or active material, is weighed out on a balance separately Carbon Black (MTI Corp, Timical super C65) powder and polyvinylidene difluoride, or PVDF (CH_2F_2, MTI Corp, HSV900, ≥99.5) at a ratio of 90:5:5. The active material and carbon black are combined together in a glass vial and the PVDF is transferred into a planetary mixer (Thinky Mixer) pot. All are transferred into a glovebox under argon, where the active material and carbon black are ground in an agate pestle and mortar for 15 minutes. In parallel, 1-methyl-2-Pyrrolidinone, or NMP (C_5H_9NO, Sigma Aldrich, 99.5%) is added to the PVDF using a syringe at a ratio of 0.5 ml of NMP per 0.4 g of combined active material, carbon black, and PVDF. The NMP/PVDF mixture is premixed in the planetary Thinky mixture at 5 repetitions of 2 minutes of mixing at 2000 rpm and 30 seconds of defoaming at 2200 rpm. The active material/carbon black mixture is then combined into the Thinky pot with the premixed NMP/PVDF under argon along with an additional 0.5 ml NMP per 0.4 g of active material/carbon black/PVDF. The sealed Thinky pot is then mixed again, this time for 2 repetitions of 5 minutes at 1000rpm, 5 minutes at 1500rpm, and 10 minutes at 2000 rpm, before defoaming at 2200rpm for 20 minutes.

The slurry is then coated onto carbon-covered aluminium foil at a thickness of 0.2 mm using a drawdown table and a doctor blade inside a fume hood, in line with NPL protocol [125]. The drawdown table is connected to a pump, allowing the foil to be sucked to the drawdown table during the drawdown, and a heating element allowing the slurry to be dried without removing from the drawdown table or the fume hood. The slurry is dried on the drawdown table for a minimum of 2 hours (provided thickness is 0.2mm) at 120 °C before being wrapped in aluminium foil and stored in a vacuum oven at 80 °C.

After being dried overnight in the drying oven the cathode is calendared. The cathode is covered by 0.2mm thick “Whatman” cellulose filter paper and the thickness of the cathode and Whatman paper before calendaring is recorded by measuring at three different points using a micrometer. After the average of the measurements is taken, the cathode and Whatman paper is sandwiched between two sheets – either aluminium, laminate, or plastic sheet – and calendared at intervals of 0.02 mm , beginning at the collective thickness of the sheets. For each thickness interval the cathode is passed through three times before being flipped over and being passed through a further three times. Calendaring stops when either 80% of the pre-calendaring thickness is reached, the cathode has been calendared by a thickness of 0.1 mm

+/- 0.02 mm, or when the cathode surface begins to become dull. Calendaring beyond this will result in the cathode being shiny, bumpy, and tearing, irreparably damaging the cathode.

Cathode discs are then punched at a diameter of 12.5mm using an electrode punch and being covered by 0.2mm thick Whatman paper. Each cathode disc is weighed to determine the mass of the active material, m_{act}, where m_{act} is a function of the mass of the cathode, m_{cath}, the mass of the aluminium foil, m_{foil}, and ratio of the mass active material to the mass of the slurry, (Eq. 3). Unless stated otherwise m_{cath} is recorded by weighing the cathode disc on an electronic balance post being removed from the electrode punch. m_{foil} is 0.005 g, calculated by weighing aluminium foil of 0.2 mm thick and 12.5 mm in diameter. The ratio of the mass active material to the mass of the slurry unless stated otherwise is 0.9 (90:5:5 active material to PVDF to carbon black), in line with NPL protocol [125].

$$m_{act} = ratio\ of\ active\ material * (m_{cath} - m_{foil})$$

(Eq. 6)

The cathode discs are then transferred into an argon filled glovebox and assembled into lithium-ion CR2032 coin cells. The coin cell is assembled in the following order:

- Aluminium CR2032 coin cell bottom casing
- Aluminium coin cell spring
- Aluminium coin cell spacer
- 12.5 mm diameter lithium metal disc (Li, Pi-Kem, 99.9%) both sides brushed with toothbrush to remove oxidation layer.
- Fibreglass separator
- 100 µL Hexafluorophosphate solution ($LiPF_6$ in 1.0 M 1:1 DMC:EC, Sigma Aldrich) applied using 100 µL Gilson pipette.
- NMC811 cathode disc, slurry side facing down
- Aluminium CR2032 coin cell top casing

The resulting cell is crimped under 4 bar relative pressure for a minimum of 6 seconds before being removed from the glovebox.

2.4 Electrochemical Testing

Cells were transferred onto a Neware BTS-4000 Series battery tester situated in a custom FDM climatic chamber set to 25 °C. The cell is placed in a crocodile clip connector, is wrapped in electric tape to inhibit short circuiting, and wrapped in a labelled plastic bag to allow easy identification of the cell being analysed, provide further protecting against short circuiting, and catch any leaking electrolyte under the extremely unlikely scenario the cell is damaged.

Electrochemical testing of the cell is achieved by the battery tester applying a current across the cell during ‘cycling’. While the cell is connected to the battery tester a signal feeds back cell information, such as potential difference, at a set frequency which is able to be recorded by an accompanying program. The cell undergoes an initial 4 h rest period, allowing the cell to rest before cycling such that there is full dispersion of the electrolyte through the fibreglass separator. The cell is then cycled using constant current – constant voltage (CCCV) charging where the cell is initially charged under a stated constant current until a stated voltage is reached [126]. When the stated voltage is reached the charging changes to constant voltage in order to prevent overcharging, where the stated voltage is applied across the cell while the current decreases until a set time or current limit is reached. The cell is allowed a 5 h rest before undergoing a constant current (CC) discharge where the cell is discharged at a set current down to a stated voltage. Following this, the cell is rested again for 5 h before the cell undergoes CCCV again with the cycle repeating until the cell has either cycled for a given number of cycles or the cell has failed.

Required parameters for the cell analysis are the mass of active material, m_{act}, (Eq. 3) and specific capacity, Q, in mAhg^{-1} (Eq. 4), where Q is a function of the valance state of the charge carrier of the lithium ion cell, n, where in this case the valance state of Li$^+$ is +1, the Faraday constant in Cmol^{-1}, F, the molar mass of active material in gmol^{-1}, M_r, calculated from the ratio and atomic masses of Li, Ni, Mn, Co, O, and any other electrochemically active dopant atoms within the active material, and 3600, being equal to the number of seconds in an hour. Both m_{act} and Q are input as variables before the cell begins cycling.

$$Q = \frac{nF}{M_r * 3600} * 1000 = \frac{1 * 96485.3329}{M_r * 3600} * 1000$$

(Eq. 7)

Cells are cycled for 50 cycles, discharging at 0.1 C between either 4.5 V and 2.8 V or 4.2V and 3 V, and charging at 0.1 C between either 2.8 V and 4.5 V or 3 V and 4.2 V, depending on the cycling program selected. The range 4.2 V to 3 V was selected due to representing the standard working voltage range under which most Li-ion cells will be operated, while the range 4.5 V to 2.8 V is the maximum and minimum safe voltages under which it is possible for the Li-ion cells to operate. The voltage range between 4.2 V and 4.5 V is especially important to test as it is where the lithium cathode structure is mostly likely to break down due to the phase transition of H2 to H3 when charging and H3 to H2 when discharging [127]. This phase change is responsible for structural instability in high nickel lithium-ion cathodes, and as such it is important to test cells in this higher voltage range to investigate to the fullest extent how biotemplating may impact cycling stability. Cycling analysis is done to obtain following data:

- Specific discharge capacity, mAh/g
- Specific charge capacity, mAh/g
- Cycling efficiency,%
- Differential capacity, mAh/g/V

2.4.1 Electrochemical Testing Data Analysis

Cell cycling data may be saved as either an NDAX or Excel file. For ease of analysis, Python 3 code written by George J. Wilson in Jupyter is used to format cycling data from Excel files into Python Code so that the raw data may be used to generate plots that can be analysed. Plots are generated by first transferring the Excel file into Python code by converting it to the “String” data format. The following columns of data are then converted into arrays so they may be plotted against each other:

- Cycle Number
- Step (denotes whether the cell is being charged or discharged)
- Voltage, V
- Charge Specific Capacity, mAh/g

- Discharge Specific Capacity, mAh/g
- Specific Differential Capacity, mAh/g/V

The first plot, Figure 42 (left), is a potential different against capacity plot, which allows for the analysis of charge and discharge capacities for the total number of cycles, as well as capacity retention during cycling, and any potential phases changes or structural transformations the cathode undergoes. From further analyses of the plot, plateaus in the curve indicate different phase transitions in the electrode while sloped sections allows for the inference of the kinetics and resistivity of the reaction [128].

The second plot, Figure 42 (right) to be produced is a differential capacity plot, where differential capacity is plotted against potential difference for the total number of cycles.

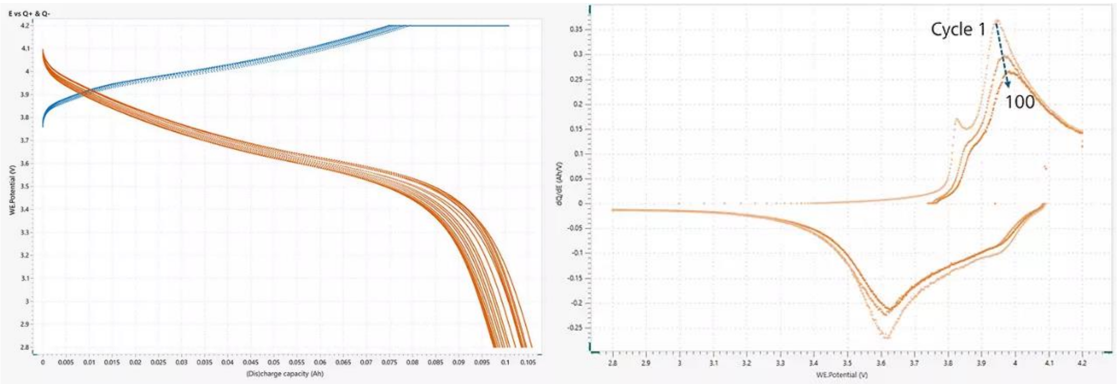

Figure 42 Example plots of potential difference vs. capacity (left) and differential capacity vs. potential difference curve (right) [128]

Analysing this plot helps to identify phase changes during cycles, as well as the efficiency of the reversibility of the charge/discharge cycle and any signs of cathode degradation. This plot can be analysed in tandem to the potential difference vs. capacity plot, with the peaks in the differential capacity plot indicating phase transitions that appear as plateaus in the potential difference vs. capacity plot [128]. Shifts in the peaks cycle-by-cycle can also be analysed in order to determine potential degradation.

3 Results section 1 – Morphological control using dextran and sodium alginate biotemplates

3.1 Aims for the synthesis of NMC811 biotemplating

The primary aim of results chapter 1 is to determine the viability of using biotemplating to produce NMC811 and to determine what benefits there may be for using the biotemplate technique in the synthesis of high nickel lithium-ion cathodes. It is also to investigate the potential in using biotemplating to manipulate the particle morphology of NMC811, what particle shapes may be formed, and how beneficial they may be when NMC811 is used as a cathode. Dextran and sodium alginate are selected as the biotemplates due to previous evidence of forming plate and nanowire morphologies respectively, as well as previous research suggesting using these biotemplates to form a variety of different chemistries has largely been successful. Secondary aims include determining what conditions such as preheat and calcination maximum temperature, synthesis atmosphere, and relative masses of biotemplate to precursor metal salts are most optimal. This is in addition to evaluating the possibility of scale-up and synthesis of lithium-ion cells using the biotemplating technique, with the ultimate goal of biotemplating being used as a substitute for solid-state synthesis.

3.2 Synthesis of NMC811 using biotemplating

3.2.1 Analysis of control NMC811

Before synthesising biotemplated NMC811, commercial NMC811 ($LiNi_{0.8}Mn_{0.1}Co_{0.1}O_2$, Pi-Kem) is analysed to determine a control. When analysed using XRD, Figure 43, telltale signs of layered, organised NMC811 are observed. Good peak splitting at peaks (006)/(012) and (018)/(110) indicate a well layered structure [129], while a peak intensity ratio between peaks at (003) and (104) of 1.68 highlights low mixing of Li^+ and Ni^{2+} cations across Ni and Li sites (where <1.2 is considered a high level of cation mixing [130]). When analysed using SEM spherical microscale secondary particles, Figure 44a, consisting of irregular nanoscale primary particles, Figure 44b, of average particle diameter of 400 nm are observed. This provides a baseline to which biotemplated NMC811 can be analysed.

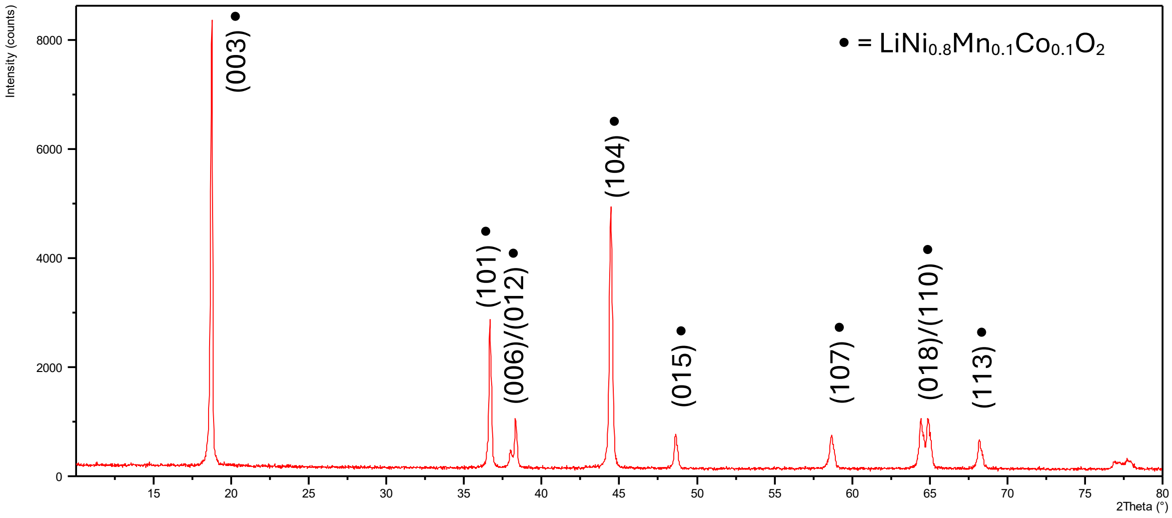

Figure 43 XRD of control NMC811 powder

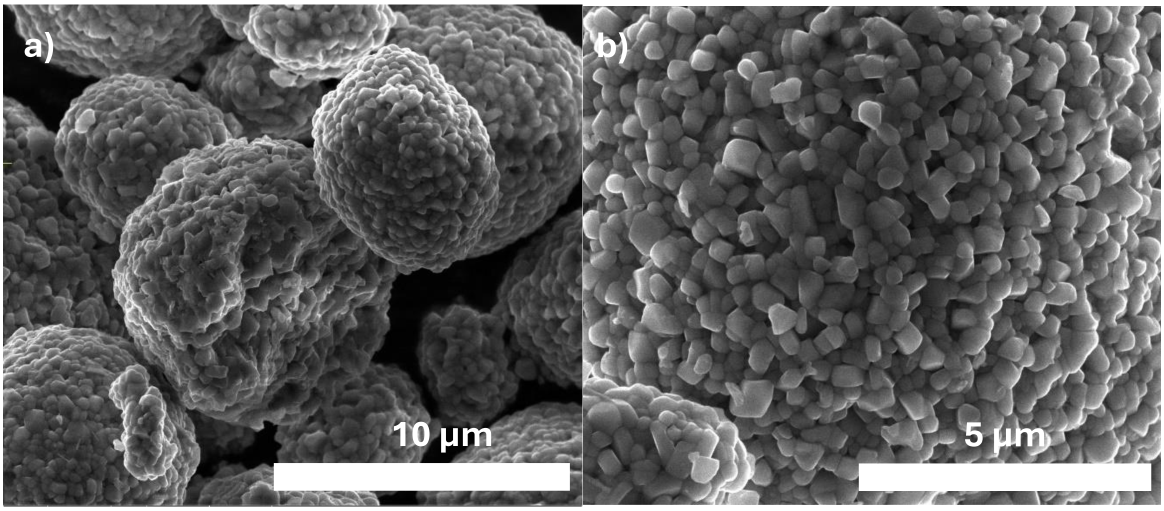

Figure 44 SEM of control NMC811 a) secondary spherical particles and b) primary irregularly particles

3.2.2 Synthesis of NMC811 using Dextran

The first stage of investigating whether NMC811 is able to be synthesised using biotemplating is to determine the minimum calcination temperature for each biotemplate and precursor (acetate or nitrate) combination. Dextran, as mentioned in 1.4.3.2 a polysaccharide derived from glucose. was investigated first using acetate precursors and the masses established in the methods, Table 3. A calcination temperature of 850 °C was selected based on the calcination temperature used for solid state synthesis, with a 500 °C preheat temperature (a parameter that will be refined later in the chapter). The calcination temperature was the reduced incrementally until evidence suggested organised NMC811 was no longer being synthesised.

3.2.2.1 Variation of calcination temperature using dextran and acetate precursors

Figure 45 highlights how variation of the maximum calcination temperature can greatly affect the final product when synthesising NMC811, even when adjusted by increments as small as 50 °C. When using dextran with acetate precursors and calcining at 800 °C and 850 °C, the ratio between the peak intensities at (003) and (104) reflections is 1.54 and 1.55 respectively.

However, when comparing the peaks at (006)/(012) and (018)/(110) reflections, twin peaks, or peak splitting, are shown to be slightly more pronounced when calcined at 850 °C, especially at (006)/(012). This shows that there is slightly more disorganisation in the NMC811 calcined at 800 °C, and so calcination at 850 °C is better for producing organised NMC811. The more pronounced peak splitting at 850 °C is an indicator of better defined layering of the structure [129], with a layered structure allowing for more sites for lithium to intercalate as well as providing pathways for lithium ions to conduct through the cathode. The slightly higher peak intensity ratio is significant as it gives an indication of the amount of nickel in lithium sites and vice versa [130], with a value of less than 1.2 is considered a high level of mixing. The higher ratio when calcining at 850 °C shows there is less mixing of the lithium and nickel sites, which is further evidence of better defined layers in the 850 °C sample. However, there is still disorganisation in NMC811 calcined at both temperatures due to the ratio between (003) and (104) peaks being below 1.6, where any value below 1.6 is an indicator of mixing of Li and Ni sites, and the weak peak splitting when calcined at both temperatures.

One possible reason for this is the high amount of carbon present in both the dextran and acetate precursors. During preheat, is it observed that between 150 °C and 200 °C a large volume of gas is emitted from the crucible. This is observed when attempting to preheat the sample in a sealed tube furnace as opposed to a box furnace, where during this temperature range a large enough volume of gas is produced to forcibly remove the jubilee clips keeping the tube sealed or expel powder towards the inlet or outlet. This is in line with evidence that states the first stage of thermal decomposition of bound dextran occurs at 150 °C [122]. This thermal decomposition of bound dextran results in carbon from the bound dextran being freed up reacting with oxygen in the atmosphere to form carbon dioxide. The synthesis of CO_2 and the subsequent reduction of oxygen to synthesise the carbon dioxide and later the NMC811 results in a reducing atmosphere not dissimilar to the conditions for incomplete combustion. This reduces the amount of oxygen available for the synthesis of the intermediate metal oxide, in this case a high nickel lithium NMC, resulting in less oxygen in the final NMC811 product and a poorer and more disorganised crystalline structure.

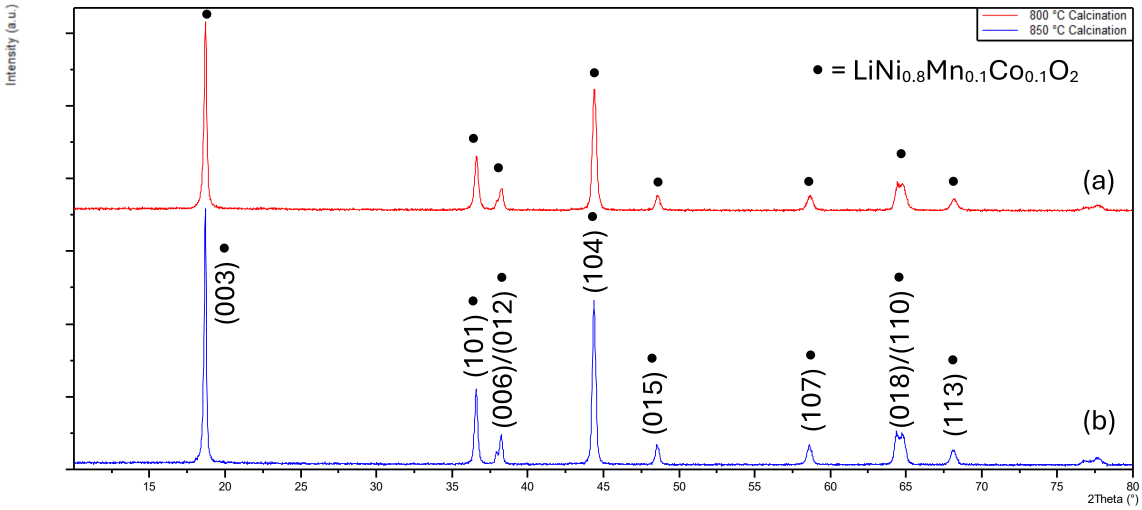

Figure 45 Calcination of NMC811 using dextran and acetate precursors at a) 800 °C and b) 850 °C

3.2.2.2 Variation of calcination temperature using dextran and nitrate precursors

A precursor with a lower carbon content than acetates may be required to reduce the effects of CO_2 on the synthesis of NMC811. Nitrate precursors, while more harmful than acetate precursors, may be a suitable alternative. NMC811 is calcined at 800 and 850 °C with a 500 °C as a direct against when NMC811 is synthesised with acetates.

Figure 46 shows the XRD patterns for synthesis of NMC811 using dextran and nitrate precursors, calcined at 800 °C and 850 °C respectively. The peak intensity ratios between (003) and (104) reflections is 1.57 and 1.84 respectively, and both patterns show distinct twin peaks at reflections of (006)/(012) and (018)/(110) with the sample calcined at 850 °C having significantly more distinct twin peaks and a higher (003)/(104) peak intensity ratio than NMC811 synthesised using acetate precursors. When comparing NMC811 samples produced using both acetate and nitrate precursors with the dextran biotemplate, a sample calcined at 800 °C using nitrates has a comparable pattern, and so comparable organisation, to a sample calcined at 850 °C using acetates. Meanwhile a sample calcined at 850 °C using nitrates is significantly more organised than any acetate sample synthesised thus far.

A higher calcination temperature is required to produce the same level of organisation in the crystalline structure when using acetates vs. when using nitrates. A higher calcination is required for acetates due to the higher amount of carbon present in the reactants when using a combination of dextran and acetates than when using dextran and nitrates, which results in the thermal decomposition of a greater amount of the biotemplate and precursor into a reducing CO_2 atmosphere. This occurs as the biotemplate and precursor decompose to free up carbon which reacts with the oxygen atmosphere. This leaves less oxygen available to be incorporated into the NMC structure when using acetates compared to using nitrates at the same temperature. As CO_2 begins to thermal decompose around 700 °C [131], a higher calcination temperature is therefore required to extract oxygen from CO_2 and incorporate it into the NMC structure when using acetates, hence the 850 °C calcination temperature. This highlights the significance of the effect of carbon content in the reaction and how much carbon can affect the organisation of the final NMC811 product.

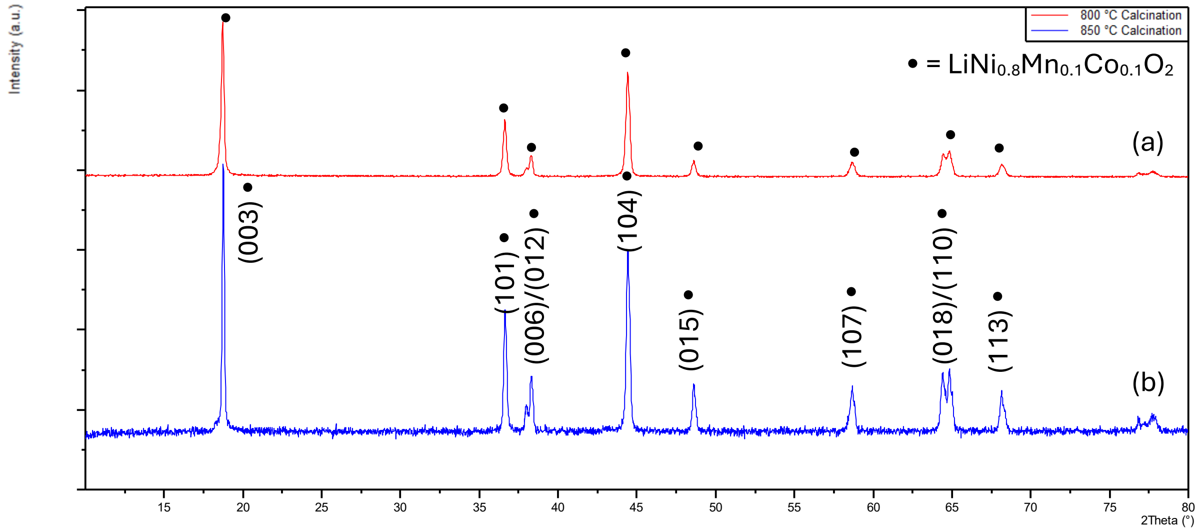

Figure 46 Calcination of NMC811 using dextran and nitrate precursors at a) 800 °C and b) 850 °C

3.2.2.3 Morphology of NMC811 produced using dextran and acetate precursors

The morphologies on the NMC811 samples calcined at 800 °C and 850 °C while similar in shape have significant size differences. Individual particles were measured using ImageJ, where a reference scale of 0.055 pixels/nm is produced by assigning the image scale to a line of length equal to the scale bar. Using this scale, the average particle diameter is determined by recording the diameters of a range of particles from the image. Such diameters can be recorded to the nearest whole nanometre ensuring an error value of +/- 1 nm. When comparing particle morphologies in Figure 47 (a) and (c), morphologies calcined at the different temperatures show similar, irregular morphologies, however particles calcined at 800 °C have a smaller primary particle size, averaging roughly 300 nm in diameter, than those synthesised at 850 °C, which average roughly 600 nm in diameter. This increase in the particle diameter at higher calcination temperatures is due to the higher temperature itself and increase in time to ramp to the maximum temperature allows for more energy and time for the particles to grow [92]. As such a lower calcination temperature is beneficial to maintain a smaller particle size.

Novel morphologies can also be observed when NMC811 is calcined at 800 °C. Plate morphologies, shown in Figure 47 (b), are found in isolated clusters in few instances in the NMC811. This highlights some inhomogeneity in the NMC811. Such a morphology may be beneficially if it can be replicated due to a large surface area and high conductivity across the cross-section of the plate but is unlikely to be replicated at mass scale in layered NMC811. Initial results show layered NMC811, specifically when using dextran and acetates, requires a minimum calcination temperature of 850 °C to form an organised, layered structure, whereas the synthesis of plate morphologies appears to occur at or below 800 °C where the layering of NMC811 is not fully formed. Furthermore, the presence of a small number of plates and not widespread plate morphologies across the entire sample is proof of inhomogeneity across the sample. As such it appears the synthesis of plate morphologies is not compatible with the synthesis of layered NMC811.

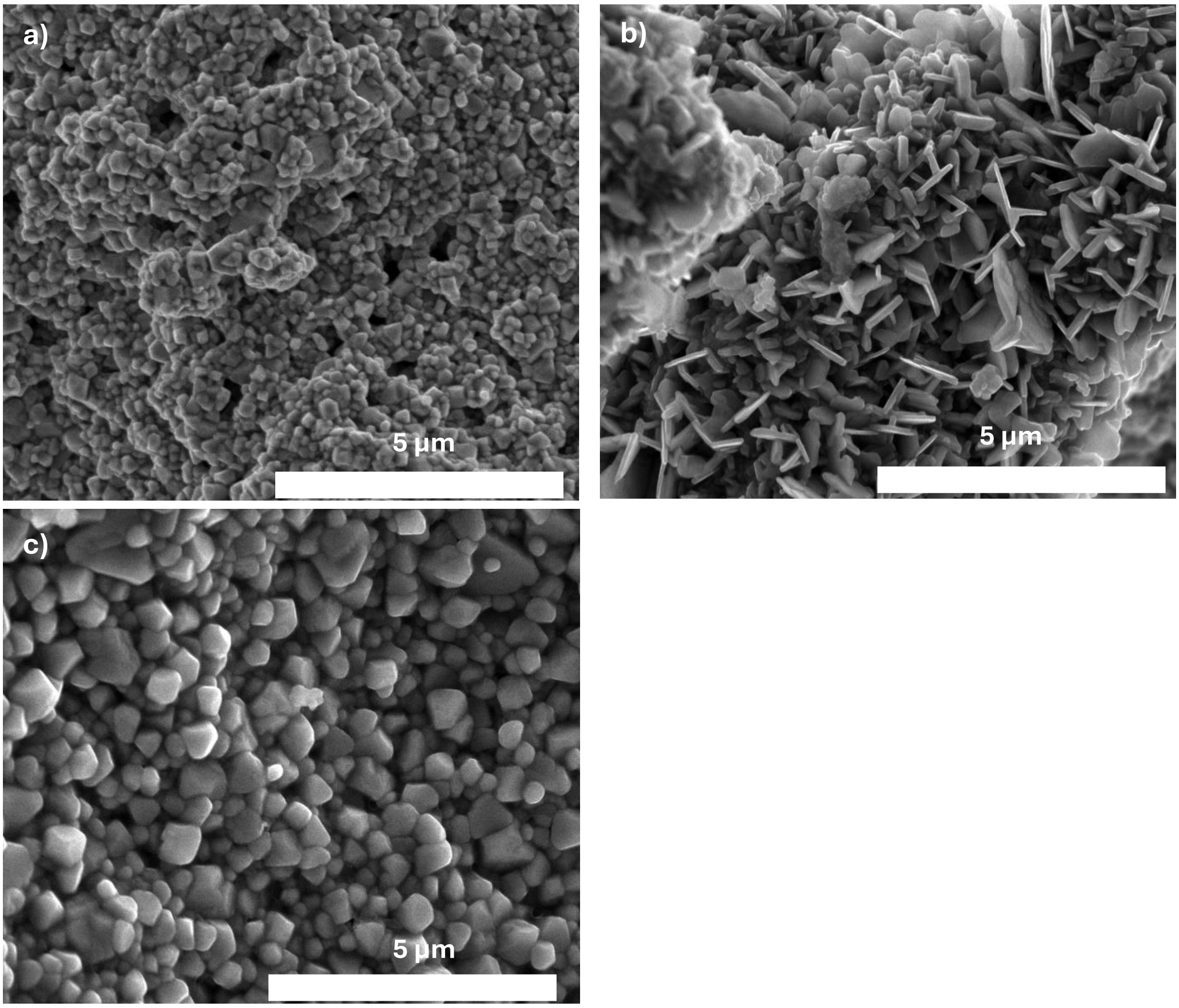

Figure 47 SEM of NMC811 particles synthesised with dextran and acetate precursors, calcined at a) and b) 800 °C, and c) 850 °C, with a) exhibiting irregular particle morphologies, b) exhibiting plate morphologies, and c) also exhibiting irregular particle morphologies

3.2.2.4 Variation of crucible size on the synthesis of NMC811 using dextran and acetate precursors

The effect of the CO_2 atmosphere does not seem to be affected by crucible size either. Figure 48 shows the XRD patterns for NMC811 synthesised using dextran and acetate precursors at 850 °C with 10% Na. Despite being preheated in a tall and shallow crucible respectively, there is little difference between the XRD patterns, with a peak intensity ratio between (003) and (104) reflections of 1.06 and 1.15 respectively and no distinct twin peaks at (006)/(012) and (018)/(110) reflections when synthesised in either crucible. This hints that the CO_2 atmosphere has a significant effect on the synthesis of NMC811 regardless of the depth of the crucible being used. The reason for this is that a) CO_2 is denser than air and b) hints that the amount of CO_2 produced by the dextran and acetate precursors is such that the sample is heated in carbon dioxide regardless of the surface area or volume of the crucible, essentially creating the same reaction conditions.

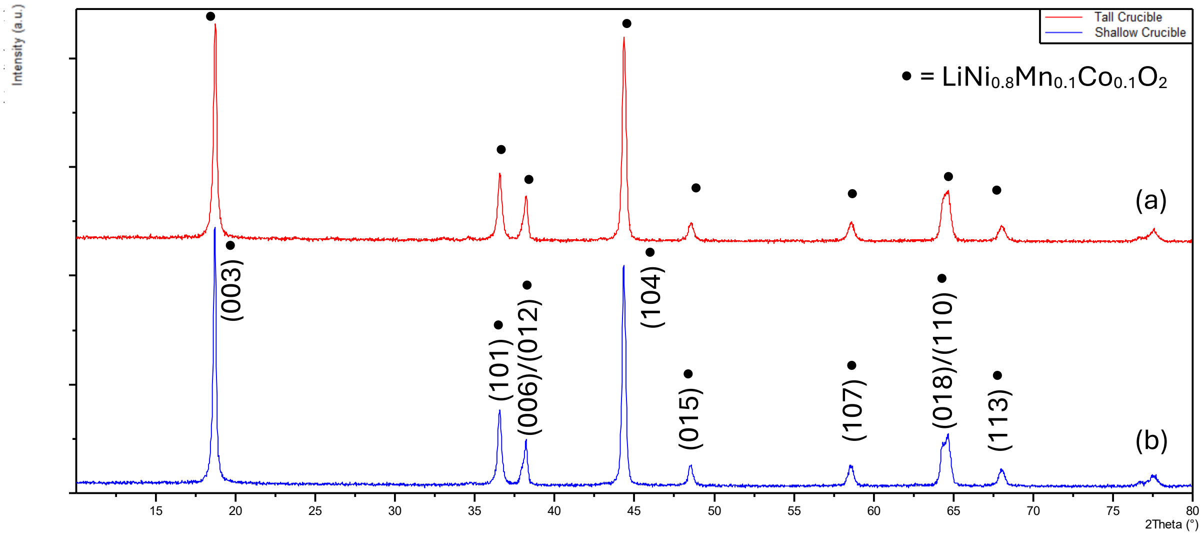

Figure 48 Calcination of NMC811 using dextran, acetate precursor, and 10% Na at 850 °C in a) Tall Crucible and b) Shallow Crucible

3.2.2.5 Morphology of NMC811 produced using dextran and nitrate precursors

Such as when using acetate precursors, NMC811 produced using nitrate precursors show similar particle morphologies but different particle sizes between samples calcined at 800 °C and 850 °C respectively. While still irregular, particles produced using nitrate precursors are observed to be less rounded than their acetate produced counterparts, as well as slightly larger in diameter. Average particle diameter is obtained using the same analytical technique in ImageJ as when using acetates, Figure 47. Average particle diameters when calcined at 800 °C and 850 °C, Figure 49 a) and b) respectively, are 700 nm and 1200 nm. Particles calcined at 800 °C are still observed to have smaller diameter particles calcined at 850 °C with evidence suggesting that regardless of the precursor used particle size is greater when synthesising at higher temperatures [92]. Reasons for this are a) the particles have more energy to grow and b) particles have a longer overall synthesis time when using the same ramp rate but a higher synthesis temperature as more time is required to reach the maximum temperature, allowing for more time at high temperatures for the particles to grow.

Larger average particle diameters are detrimental to the performance of the cathode as it reduces the overall surface area of the cathode, allowing less area for the lithium to intercalate. Previous evidence has shown that for NMC811 cathodes a larger particle size leads to a lower specific discharge capacity [132]. NMC811 should therefore be synthesised at the lowest possible temperature (i.e. 800 °C nitrates instead of 850 °C) to minimise particle diameter and increase particle surface area and possible specific discharge capacity, while still synthesised layered NMC811.

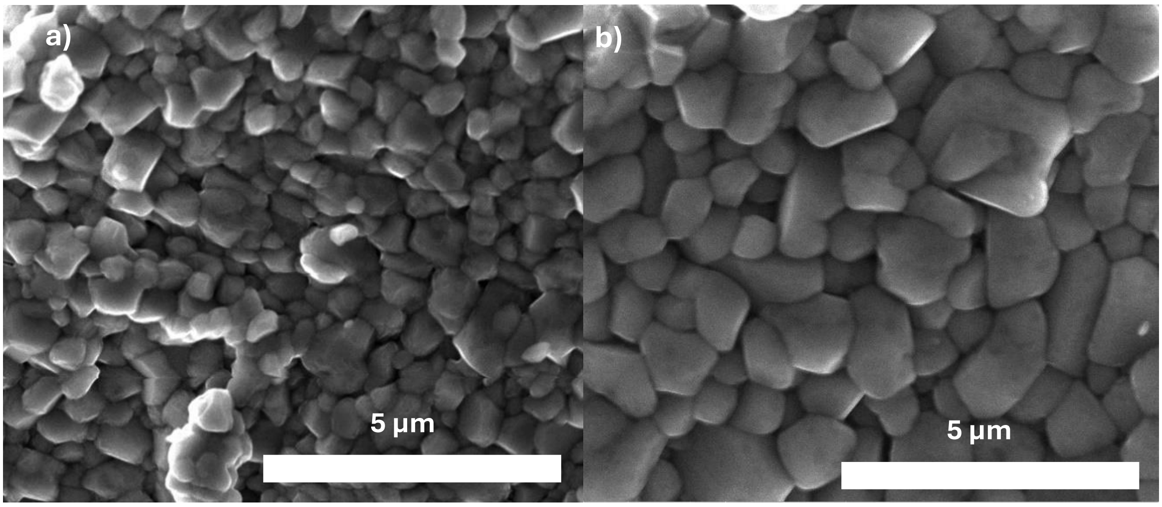

Figure 49 SEM of NMC811 irregular primary particles synthesised with dextran and nitrate precursors, calcined at a) 800 °C and b) 850 °C

3.2.3 Synthesis of NMC811 using sodium alginate

Sodium alginate is investigated as an alternative biotemplate to dextran. Being derived from a different source (algae instead of sugar) and that it is known to aid in the synthesis of different morphologies than those produced by dextran (nanowires instead of plates) [94] make sodium alginate an ideal alternative for dextran. As with investigating dextran, the minimum calcination temperature for forming NMC811 using both acetates and nitrates is first established by calcining at 850 °C using sodium alginate and reducing the calcination temperature incrementally until NMC811 is no longer formed. Masses used are those in 2.1.1 from the methods chapter with a preheat temperature of 500 °C.

3.2.3.1 Variation of calcination temperature using sodium alginate and acetate precursors

XRD shows how when calcined at 750 °C, 800 °C, and 850 °C, Figure 50a, b, and c respectively, NMC811 synthesised using sodium alginate and acetate precursors will show significant disorganisation when calcined at 750 °C, some disorganisation when calcined 800 °C, and little disorganisation when calcined at 850°C. The ratio between peaks at (003) and (104) reflections are 1.2, 1.3, and 1.5 for 750 °C, 800 °C, and 850 °C calcination respectively (summarised in Table 13, where < 1.2 is considered to be a high level of Li/Ni site mixing [130]). Peak splitting at (006)/(012) and (018)/(110) reflections respectively have a resolution of separation value, R_s, of 0.44 and 0.22 for 750 °C calcination, 0.5 and 0.37 at 800 °C calcination, and 0.69 and 0.80 at 850 °C calcination as calculated using (Eq. 2) in 2.2.1 indicating disorganisation of the layers when calcining at 750/800 °C but organised layers at 850 °C as the R_s value approaches 1. The requirement for an 850 °C calcination temperature for an organised layered NMC811 structure is again due to the high amount of carbon present in acetate precursors and, to some extent, sodium alginate. As with when using dextran, the sodium alginate chain thermal decomposes, this time at 212 °C [123] and along with the decomposition of the acetate precursors results in the formation of a reducing CO_2 atmosphere due to the biotemplate and precursor decomposing and freeing up carbon to react with the oxygen atmosphere, which uses up the available oxygen, allowing less O_2 for the synthesis of the NMC811 structure. As such the 850 °C is required to decompose the CO_2 to free up more oxygen for synthesis of the NMC811 structure.

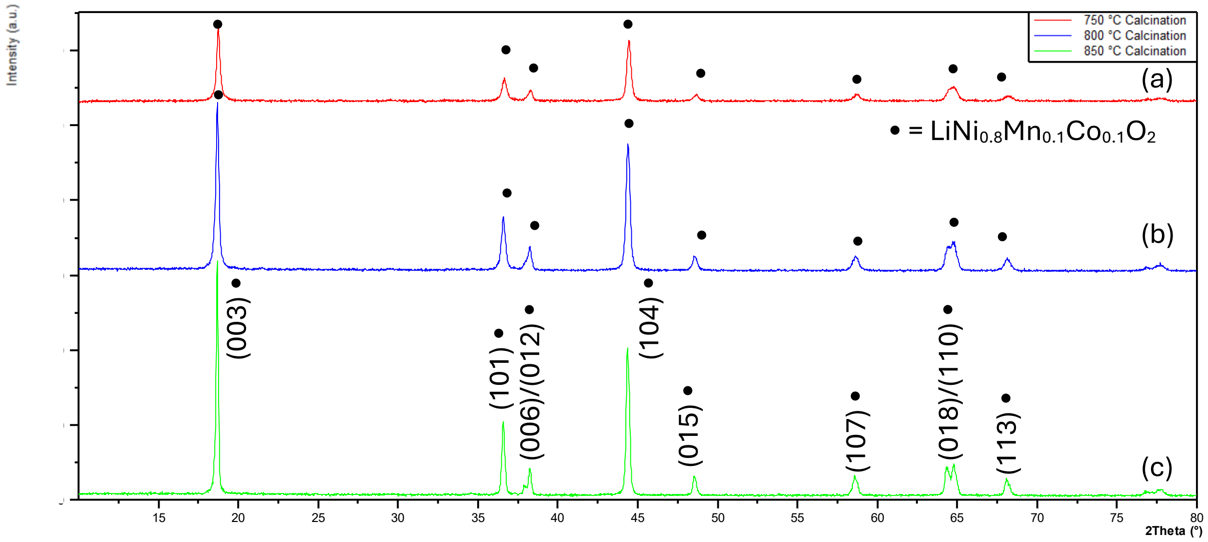

Figure 50 Calcination of NMC811 using sodium alginate and acetate precursors at a) 750 °C b) 800 °C and c) 850 °C

Temperature, °C	(003)/(104) Intensity ratio ($I_{(003)/(104)}$), abs units	Resolution of (006)/(012) reflections, R_s	Resolution of (018)/(110) reflections, R_s
750	1.2	0.44	0.22
800	1.3	0.60	0.37
850	1.5	0.69	0.80

Table 13 Comparison of organisation of layered NMC811 when synthesising with sodium alginate and acetate precursors

3.2.3.1.1 Morphology of NMC811 produced using sodium alginate and acetate precursors

When observed using SEM, particles produced using sodium alginate in these samples with acetate precursors are observed to have a larger size distribution than when using dextran and consist of irregular, octahedral-shaped particles. As with when using the dextran biotemplate, particle size increases with calcination temperature, with an average diameter of 400 nm for calcination at 750 °C, Figure 51 a), 200 nm for smaller particles and 600 nm for larger particles when calcined at 800 °C, Figure 51 b), and for particles calcined at 850 °C, Figure 51 c), an average diameter greater than 1 μm.

The octahedral morphologies are a result of the use of sodium alginate in the synthesis of NMC811, with octahedral particles not being synthesised when using dextran. As with dextran however, the increase in particle diameter as calcination temperature is increased is due to the particles having more energy and more time to grow due to the higher calcination temperature and the increase in ramp time required to reach the maximum calcination temperature [92]. The increase in particle size distribution points to an increase in inhomogeneity when using sodium alginate as the calcination temperature is increased.

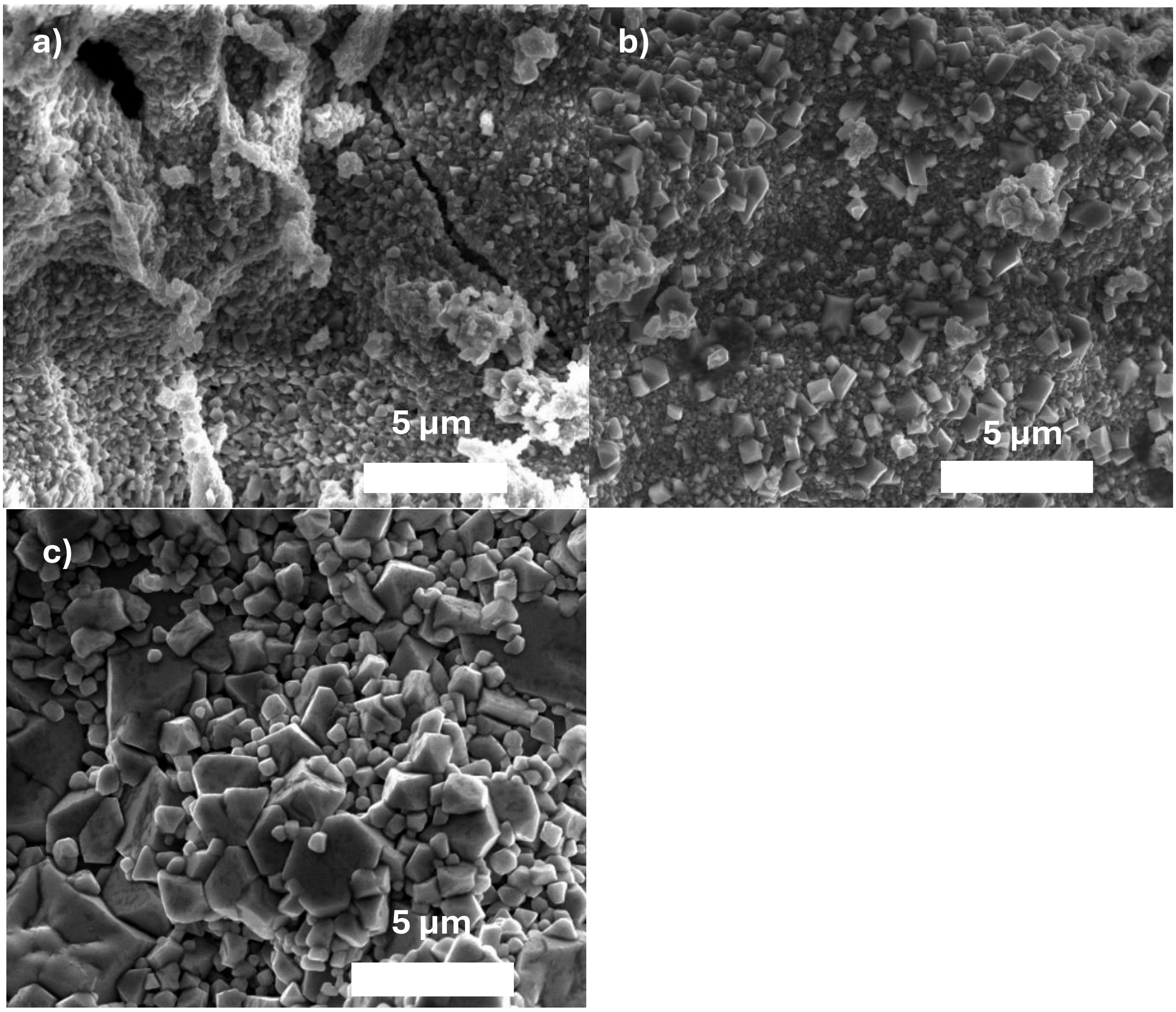

Figure 51 SEM of NMC811 particles synthesised with sodium alginate and acetate precursors, calcined at a) 750 °C, b) 800 °C, and c) 850 °C

3.2.3.2 Variation of calcination temperature using sodium alginate and nitrate precursors

When synthesising NMC811 with sodium alginate and nitrate precursors, the calcination temperature can again be reduced, as shown by Figure 52. Peak intensity ratios, summarised in 2.2.1, for (003) and (104) reflections show 1.55, 1.68, and 1.5 for 750 °C, 800 °C, and 850 °C calcination, Table 14, with all samples showing twin peaks at (006)/(012) and (018)/(110) reflections, but with the sample calcined at 750 °C having R_s values of 0.56 and 0.62, 800 °C having R_s values of 0.71 and 0.92, and 850 °C having R_s values of 0.94 and 0.66. As such the samples calcined at 800 and 850 °C have the most defined twin peaks/peak splitting with R_s values approaching 1, and the sample calcined at 750 °C has the least defined twin peaks. The reduction in required calcination temperature is again due to the reduction in carbon in the nitrate precursors and reduction in the synthesis of CO_2 due to only the decomposition of the biotemplate freeing up carbon. This means there is less carbon to react with the oxygen atmosphere resulting in less carbon dioxide and so a less reducing atmosphere. This frees up more oxygen for the synthesis of NMC811 resulting in greater organisation at the aforementioned lower calcination temperature. The increased disorganisation in the 850 °C calcined sample may also be due to the deterioration of the sample at higher temperatures as the particle morphology begins to break down. Regardless, while peak intensity ratios between

(003) and (104) >1.2 show improvements in the mixing of Li and Ni sites, a higher ratio of 1.68 vs. 1.5 and high levels of peak splitting at 800 °C shows there is no need to heat to 850 °C when 800 °C is sufficient to produce organised layered NMC811.

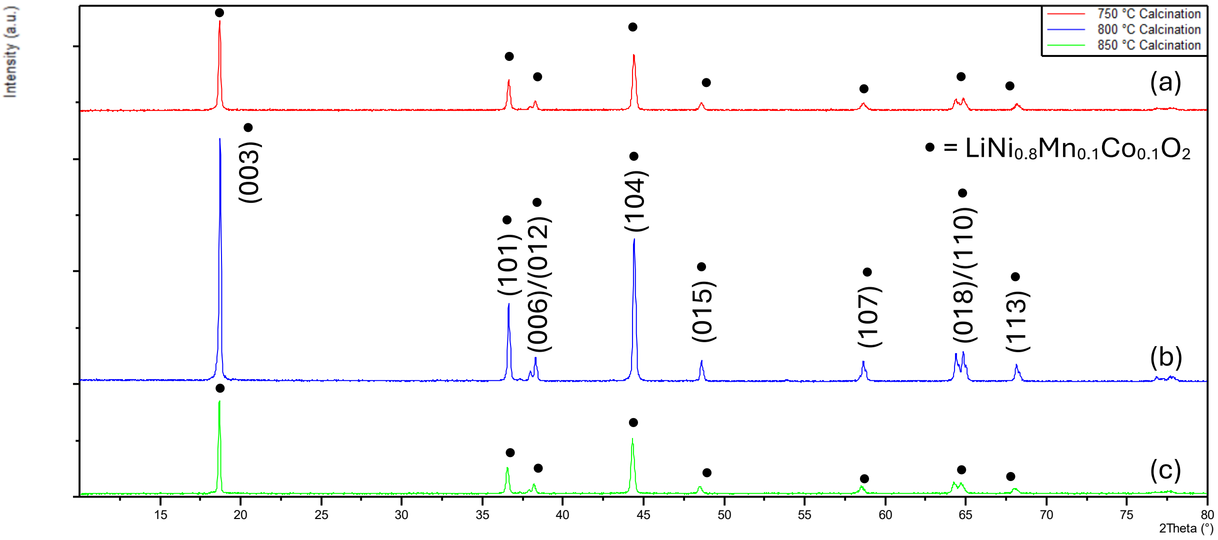

Figure 52 Calcination of NMC811 using sodium alginate and nitrate precursors at a) 750 °C b) 800 °C and c) 850 °C

Temperature, °C	(003)/(104) Intensity ratio ($I_{(003)/(104)}$), abs units	Resolution of (006)/(012) reflections, R_s	Resolution of (018)/(110) reflections, R_s
750	1.55	0.56	0.62
800	1.68	0.71	0.92
850	1.5	0.94	0.66

Table 14 Comparison of organisation of layered NMC811 when synthesising with sodium alginate and nitrate precursors

Across NMC811 synthesised with both dextran and sodium alginate, it is apparent that due to the increased carbon content and production of carbon dioxide, NMC811 produced with acetate precursors need to be calcined at 850 °C, while NMC811 produced with nitrate precursors need only be calcined at 800 °C to product a structure with similar levels of organisation of the crystal structure. This is in part due to the formation of a reducing carbon dioxide atmosphere formed when the biotemplate undergoes decomposition during heating and the resulting carbon reacts with oxygen in the atmosphere to form CO_2. The formation of this reducing atmosphere means less oxygen is available for the synthesis of NMC811 and leads to a more disorganised structure containing less oxygen. When using acetate precursors, a greater calcination temperature is required to decompose the carbon dioxide, of which begins to thermally decompose at 700 °C [131], in order to free up oxygen for the synthesis of more organised, layered NMC811.

3.2.3.2.1 Morphology of NMC811 produced using sodium alginate and nitrate precursors

When using nitrate precursors with the sodium alginate biotemplate the range of particle diameter varies with calcination temperature with a mix of octahedral and smooth, round particles being synthesised, as observed in Figure 53. At 750 °C calcination temperature, Figure 53 a), an average particle diameter of 450 nm is estimated with small handful of outlier particles present where particle diameter exceeds 1000 nm. At 800 °C and 850 °C calcination temperature, Figure 53 b) and c) respectively, there are particles with diameters of 900 nm and 1000 nm respectively. This observation highlights how the increase in particle diameter with calcination temperature is smaller when using nitrate precursors vs. acetate precursors in the presence of a sodium alginate biotemplate. This is supported by previous evidence suggesting chemistries synthesised using biotemplates such as dextran and nitrate precursors will often synthesise nanoscale particles [93], [133].

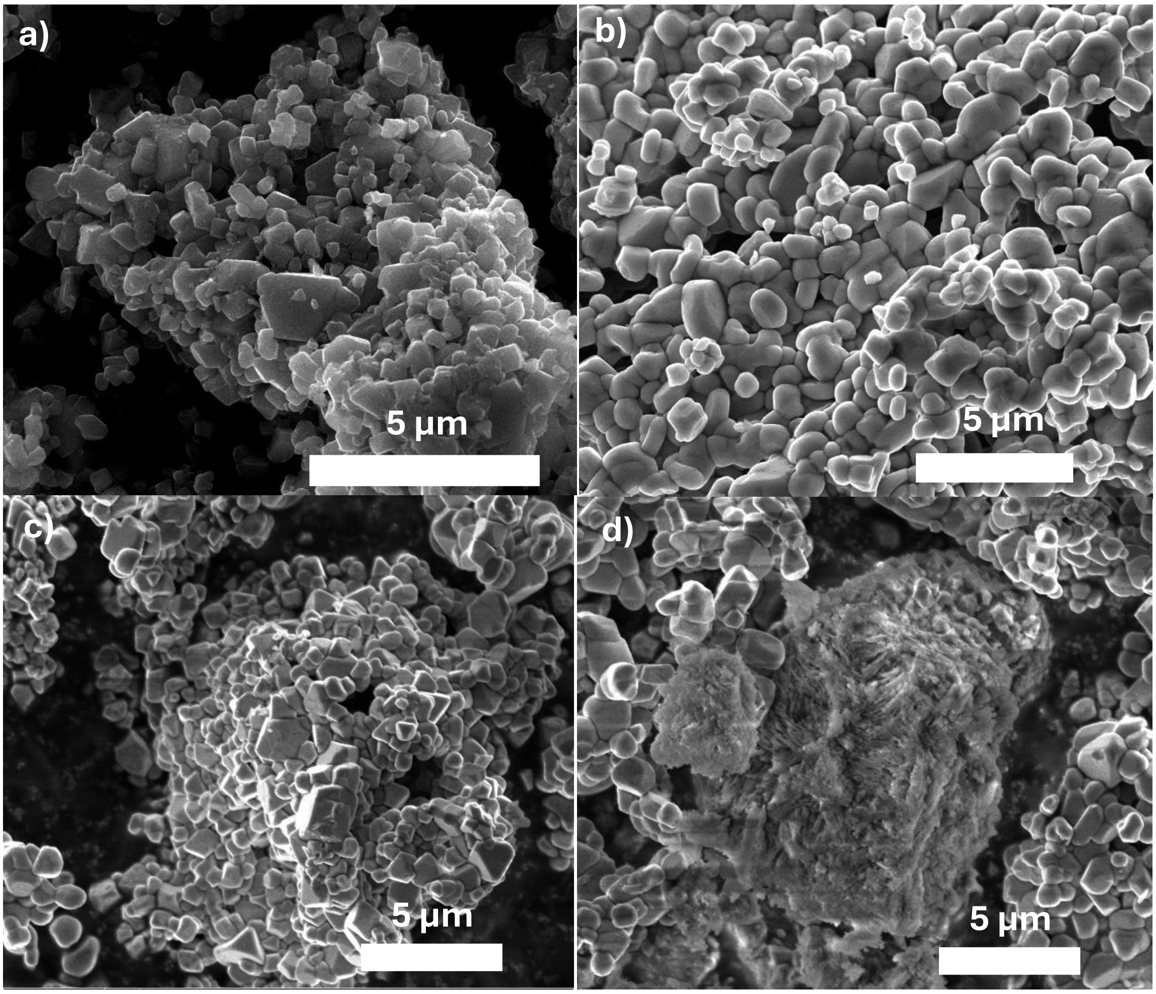

Figure 53 SEM of NMC811 particles synthesised with sodium alginate and nitrate precursors, calcined at a) 750 °C, b) 800 °C, and c-d) 850 °C, with a-c) consisting of smooth/octahedral primary particles and d) exhibiting nanowire morphologies

Also observed when using a calcination temperature of 850 °C is the synthesis of long, thin nanowire particles radiating outwards from a single agglomeration of particles, Figure 54a. This is a higher magnification image of nanowires shown in Figure 53c. While nanowire morphologies may be a beneficially morphology to be present in NMC811 due to its high ionic conductivity, high surface area for lithium intercalation, and improved structural stability, this morphology is only observed in isolated areas and are possibly formed of lithium carbonate impurities. This is supported by Figure 54b, which shows fuzzy wire-like morphologies forming on the surface of the particles 9 days after nanowires in Figure 54a were observed. As lithium in the cathode powder reacts with CO_2 in the atmosphere, lithium carbonate is known to form on the surface of NMC cathodes, with this reaction being observed the most on NMC811 cathodes [134]. This occurs even when the sample is stored in a desiccator and so cannot be attributed to humidity. We can therefore assume that the nanowire formed within the NMC811, Figure 54a, sample may also be formed of lithium carbonate impurities.

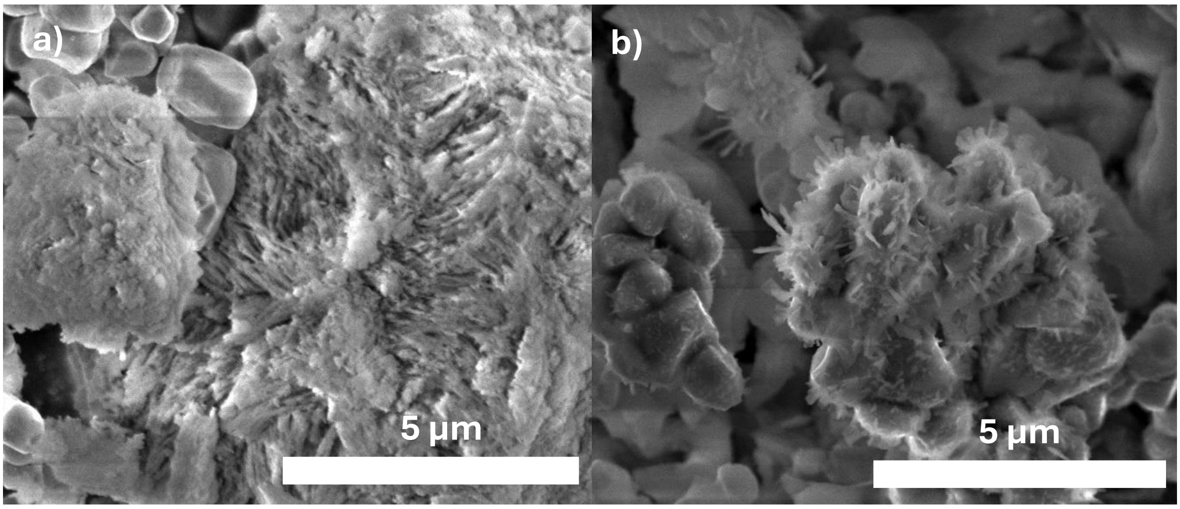

Figure 54 SEM of NMC811 particles synthesised with sodium alginate and nitrate precursors at 850 °C showing a) nanowires 1 day after calcination and b) surface impurities 10 days after calcination

3.2.4 Discussion on synthesising NMC811 using biotemplating

Initial investigations into biotemplating with dextran and sodium alginate has shown that synthesis of layered NMC811 is viable using the biotemplating technique. NMC811 is able to be synthesised using either dextran or sodium alginate by calcining at 800 °C when using nitrates and 850 °C using acetates. Lower calcination temperatures results in a more disorganised NMC811 due to the mixing of lithium and transition metal layers and due to Li^+ and Ni^{2+} mixing in Ni and Li sites respectively. Evidence of novel morphology formations are also observed, though have not been able to be reproduced. Plates morphologies are observed by calcining using dextran and acetate precursors at 800 °C with nanowires being formed using sodium alginate and nitrates at 850 °C. Particles with octahedral morphologies are formed using sodium alginate however, with dextran forming irregular but rounded particles. All combinations of biotemplate and precursors are able to synthesise nanoscale particles, with particles formed using acetates being smaller than those synthesised with nitrates and particle diameter increasing with calcination temperature. As such, precursor is observed to affect particle size more and biotemplate has a greater effect on particle shape, with a lower calcination temperature resulting in smaller primary particles.

3.3 Synthesis of NMC811 under air vs. oxygen

As referenced in 3.2, the atmosphere under which layered NMC811 Is an important variable to control. If an increase in carbon dioxide during the preheat stage leads to a more disorganised structure, as oxygen required for the synthesis of an organised NMC811 reacts with carbon freed up from the decomposition of the biotemplate to form a reducing atmosphere, it would stand to reason that synthesising NMC811 under a different gas would also vary the organisation of the layered structure. Previous evidence supports that a more oxidising atmosphere is recommended for the calcination of layered NMC [133] This is to prevent the mixing of Ni^{2+} ions to Li sites and Li^{+} ions to Ni sites but also provides more oxygen to be available for the synthesis of the NMC structure. A comparison on calcining NMC811 under air and oxygen after the preheat stage was performed using a tube furnace with both dextran and sodium alginate biotemplates, heated to 800 °C when using nitrate precursors and to 850 °C when using acetate precursors. This was only done post preheat due to pressure produced by the decomposition of bonded dextran and sodium alginate into carbon dioxide at 150 and 212 °C respectively leading to potential damage on sealed tube furnaces and so being not feasible with the equipment available. This has already been seen when using dextran and nitrate precursors, where the emission of carbon dioxide has been enough to remove the lid from the crucible.

3.3.1 Synthesis of NMC811 in air and oxygen using dextran

When calcined under air and oxygen using the same precursors, biotemplates, and calcination temperature, NMC811 synthesised under oxygen has a more organised structure when using dextran as a biotemplate. This is denoted in Figure 55 by a peak intensity ratio between reflections (003) and (104) of 1.44 when synthesised in air vs. 1.53 under oxygen, where > 1.2 is the minimum required value for reduced mixing of the Li and Ni sites, and greater peak splitting at (006)/(012) and (018)/(110) when calcined under oxygen vs. being calcined in air. The reduced organisation of the air synthesised NMC811 is likely due to reducing effect of the carbon dioxide atmosphere, of which is formed by the breaking down of the biotemplate and the resulting carbon reacting with oxygen in the air. Such a reducing carbon dioxide environment would be formed from in the air oxygen required for the synthesis of NMC811, with less oxygen in the NMC811 structure resulting in greater disorganisation. The NMC811 synthesised under oxygen was calcined in an oxidising atmosphere. The more oxidising atmosphere therefore frees up more oxygen for the synthesis of the NMC811 structure and reducing the mixing of Ni^{2+} and Li^{+} into Li and Ni sites respectively.

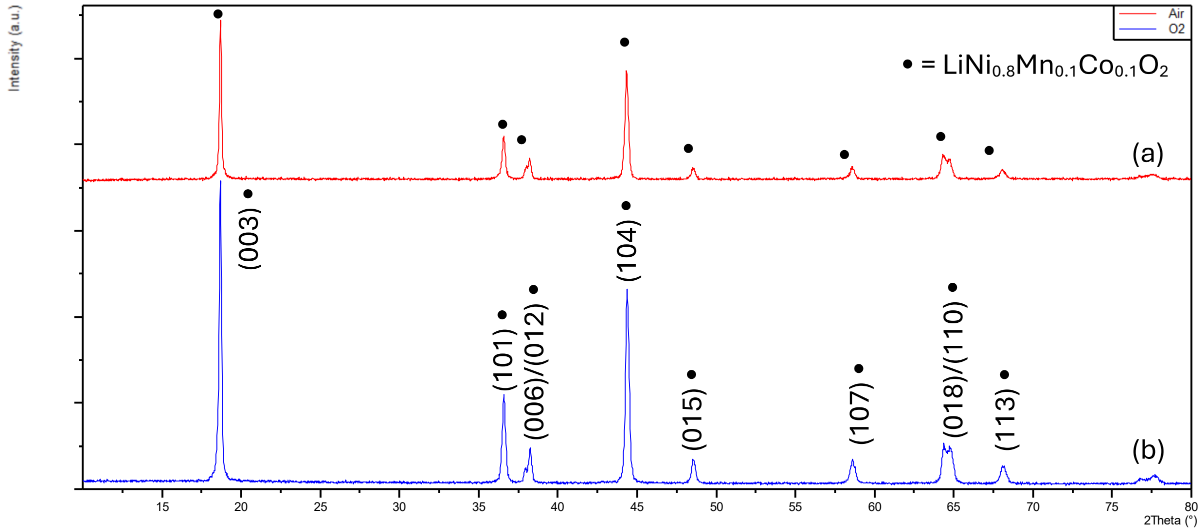

Figure 55 Calcination of NMC811 using dextran, acetate precursor, at 850 °C in a) air and b) under oxygen

3.3.2 Synthesis of NMC811 in air and oxygen using sodium alginate

The effect of atmosphere on the synthesising of NMC811 when using sodium alginate is more significant, however. The XRD pattern for NMC811 synthesised using sodium alginate and acetate precursors, and calcined at 850 °C in air, shown in Figure 56, shows little evidence of peak splitting at (006)/(012) and (018)/(110) reflections and a peak intensity ratio between reflections (003) and 1.04 of only 1.03, where < 1.2 indicates significant mixing of the Li and Ni sites. This highlights significant disorganisation within the NMC811 whereby instead of a layered structure the structure of the NMC811 begins to form a disorganised rock salt structure. Meanwhile, the XRD pattern for NMC811 calcined under oxygen shows strong twin peaks at (006)/(012) and (018)/(110) reflections and a peak intensity ratio between (003) and (104) reflections of 1.5.

This highlights an organised, layered structure when calcined under oxygen vs. air and reinforces the significance of calcination under an oxidising atmosphere instead of a reducing air or carbon dioxide atmosphere. A carbon dioxide atmosphere is formed by the breakdown of the biotemplate and the resulting reaction of carbon from the biotemplate with the oxygen in the atmosphere. When carbon dioxide forms when using air, a reducing atmosphere as oxygen is removed from the atmosphere to form carbon dioxide leaving less oxygen to synthesise into NMC811, resulting in a more disorganised structure. When using an oxygen atmosphere this formation of carbon dioxide will not necessarily lead to a reducing atmosphere due to the greater amount of oxygen present, leaving enough oxygen present such that there is sufficient oxygen for the synthesis of an organised NMC811 structure. As such, the oxidising atmosphere is important for the freeing up of oxygen to be available for the synthesis of NMC811 and to reduce the mixing of Li^+ and Ni^{2+} into Ni and Li sites respectively.

The significant differences between the organisation of the structure when biotemplating with sodium alginate and dextran may not be accounted for just by calcination atmosphere but by other variables. Preheat temperature or relative mass of the biotemplate to the mass of precursor materials may also alter the synthesis of NMC811, which are covered in sections 3.4 and 3.5 respectively.

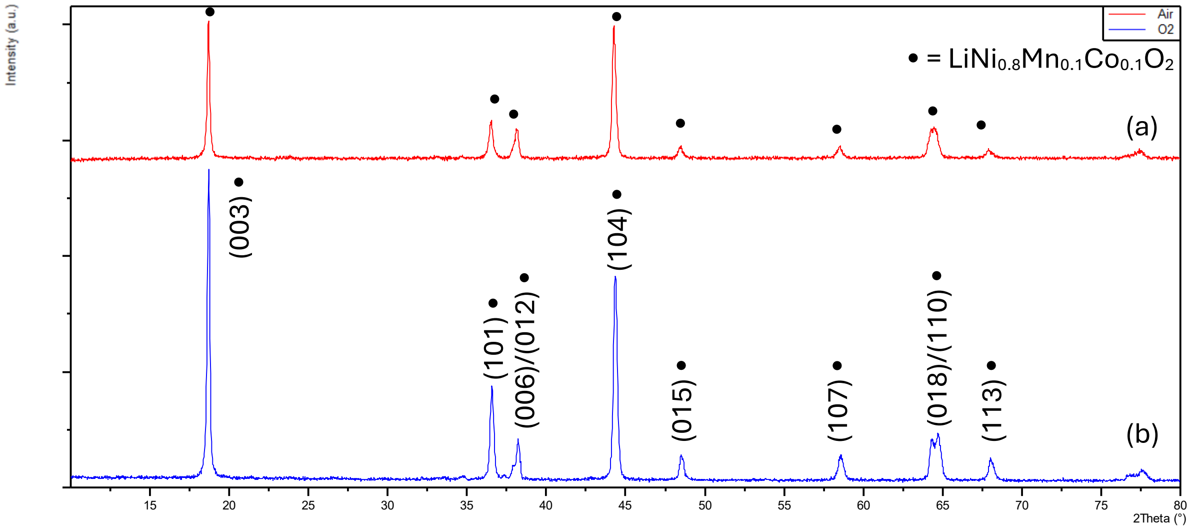

Figure 56 Calcination of NMC811 using sodium alginate, acetate precursor, at 850 °C in a) air and b) under oxygen

3.3.3 Discussion of synthesis of NMC811 in air and oxygen

In summary, calcination under an oxygen atmosphere is a requirement for the synthesis of layered NMC811 regardless of whether dextran or sodium alginate is used. [133]. A more oxidising atmosphere is required to limit the mixing of Li^+ and Ni^{2+} ions into Ni and Li sites respectively and improve layering of the final NMC811 product. Use of air only will result in NMC811 being synthesised in a more reducing atmosphere which will cause significant mixing of Li and Ni sites as well as poor layering of NMC811.

3.4 Variation in preheat temperature in the synthesis of NMC811

Varying the preheat temperature during synthesis is a significant variable in the synthesis of biotemplated NMC811. The compound, which is formed during the preheat stage, and so the compound at which calcination is done on, can affect the organisation of the NMC811 structure post calcination. For the manipulation of particle morphology, the intermediate phases formed during the preheat stage can greatly affect what particle is formed when calcined into NMC811. For example, nanowire synthesis is dependent on the synthesis of a seed crystal formed of an intermediate compound during the preheat stage. During calcination this seed will form a molten salt, which when formed on a solid substrate phase will grow nanowires [135]. While still highly dependent on calcination conditions, the controlling of the preheat phase is vital for the synthesis of the final NMC811 product and the manipulation of particle morphology.

3.4.1 Why Preheat in air?

NMC811 is preheated in air primarily due to safety reasons. When heated under a gas the samples are placed in a tube with inlet and outlets clamped with jubilee clips for optimum gas flow and to reduce the leakage of the gas occurs. When heated to between 150 and 212 °C where bonded dextran and sodium alginate decompose respectively, the sample produces a large amount of carbon dioxide due to the presence of high carbon content biotemplates and, in the case of acetates, high carbon precursors. This expansion of gas may damage the inlet and outlet on the tube furnace or lead to the sample being ejected into through the outlet. As such, samples are preheated in a box furnace in air to reduce the risk of damage to equipment and ensure the safety of lab users.

3.4.2 Variation of preheat temperature when synthesising NMC811 using dextran

3.4.2.1 Variation of preheat temperature when synthesising NMC811 using dextran and acetate precursors

NMC811 is calcined at 850 °C using dextran and acetate precursors, with the preheat temperature being varied in 100 °C intervals from 200 °C to 500 °C, . When analysing the XRD patterns in Figure 57 the peak intensity ratios between reflections of (003) and (104), summarised in Table 15, are 1.55, 1.51, 1.38, and 1.7 for 200 to 500 °C respectively, Figure 58a. This indicates that the mixing of Li^+ and Ni^{2+} into Ni and Li sites respectively increases as preheat temperature increased until 500 °C where the mixing becomes significantly less. While a 500 °C preheat has the largest peak intensity ratio, the lack of strong peak splitting at reflections (006)/(012) and (018)/(110), Figure 58b and c, as indicated by R_s values of 0.48 and 0.35 when using a 500 °C preheat indicate a disorganised NMC811 structure with poor layering. Therefore, either a 200 or 300 °C preheat, with R_s values of 0.71 and 0.52 when using a 200 °C preheat and 0.55 and 0.48 with a 300 °C preheat, are the optimum preheat temperature as both exhibit XRD patterns with better peak separation while also having a peak intensity ratio > 1.2 between (003) and (104).

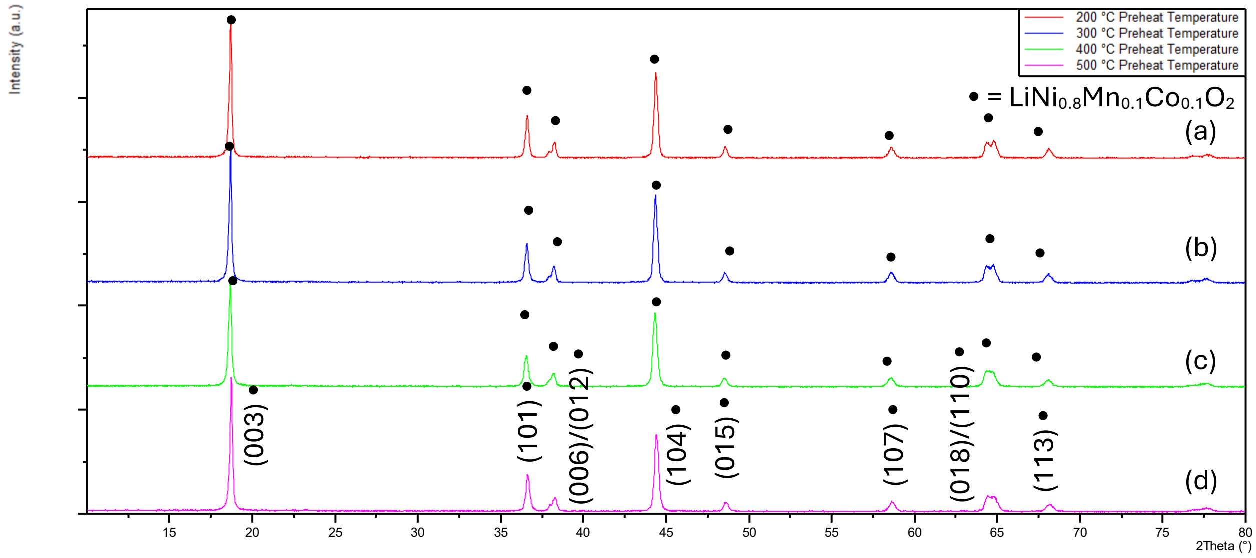

Figure 57 Calcination of NMC811 using dextran and acetate precursors at 850 °C calcination and a) 200 °C, b) 300 °C, c) 400 °C, and d) 500 °C preheat temperature

Preheat Temperature, °C	(003)/(104) Intensity ratio ($I_{(003)/(104)}$), abs units	Resolution of (006)/(012) reflections, R_s	Resolution of (018)/(110) reflections, R_s
200	1.55	0.71	0.52
300	1.51	0.55	0.48
400	1.38	0.37	0.21
500	1.7	0.48	0.35

Table 15 Comparison of organisation of layered NMC811 when preheat temperatures using dextran and acetate precursors

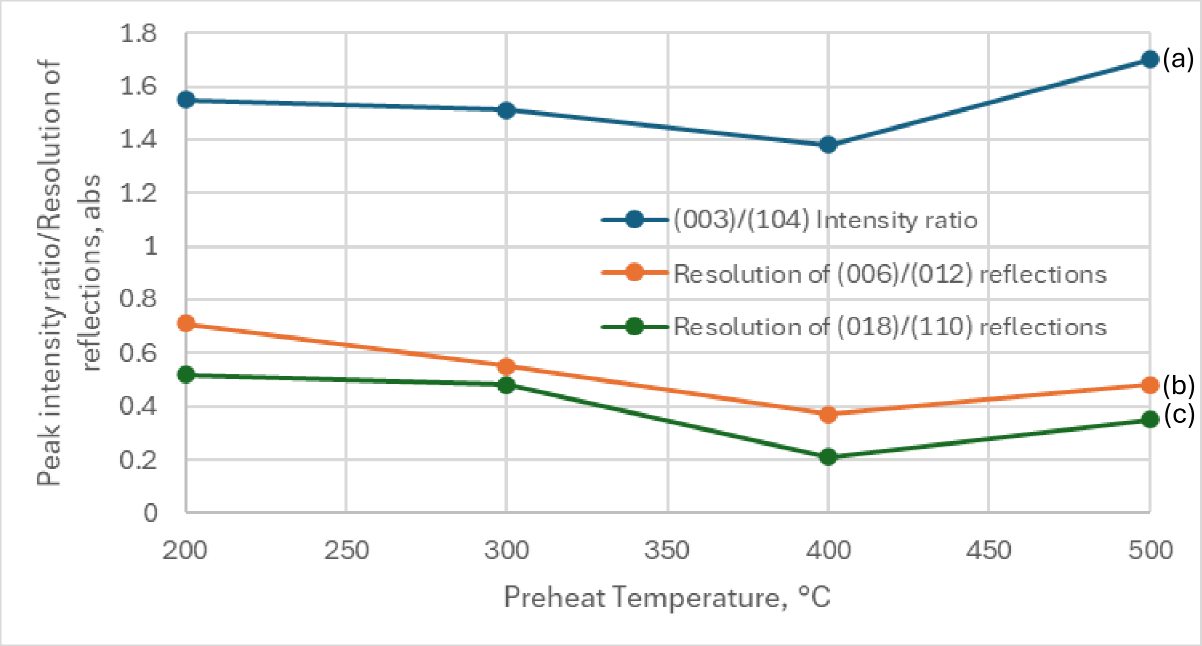

Figure 58 a) Peak Intensity ratios for (003)/(104) reflections and Resolution of Reflections for b) (006)/(012) and c) (018)/(110) reflections vs. Preheat Temperature using dextran and acetate precursors

The reason for the increase in disorganisation as preheat temperature is increased from 300 to 400 °C is due to intermediate phases being synthesised in air instead of an oxidising atmosphere. It is theorised that once the biotemplate is burned off between 150 and 212 °C a hydroxide intermediate phase, $LiNiMnCo(OH)_2$ is formed. Previous work suggests pure $Ni(OH)_2$ decomposes between 200 and 300 °C where it forms nickel oxide, NiO [136]. As such when synthesising a high Ni NMC cathode, the intermediate hydroxide phase is likely to decompose and form a disorganised NMC oxide intermediate phase at around 300 °C. Therefore, NMC811 synthesised with a preheat temperature of 200 or 300 °C will synthesise the NMC hydroxide intermediate phase, possibly due to the decomposition of the biotemplate and the theorised reaction between the metal ions and hydroxide functional groups, but the hydroxide phase will decompose into NMC oxide during the calcination phase in an oxidising environment. When using a 400 or 500 °C preheat however, the hydroxide phase is both formed and decomposes in air, leading to an increase in the disorganisation of the layers in the final NMC811 product. As such preheating at either 200 or 300 °C will produce an organised layered structure Preheating at 200 °C is optimum however as it will have a lower synthesis time and less energy usage during synthesis.

3.4.2.1.1 Differential Scanning Calorimetry (DSC) and Thermogravimetric Analysis (TGA) of NMC811 calcined with dextran and acetate precursors

Differential scanning calorimetry (DSC) and Thermogravimetric Analysis (TGA) was performed on a sample preheated in air to 300 °C, Figure 59. The blue, green, and red solid lines show the normalised heat flow during ramp up, dwell, and ramp down respectively while the dashed blue, green, and red lines represent the percentage weight of the sample during ramp up, dwell, and ramp down. The plot can be differentiated into three main sections [137], where between 20 and roughly 300 °C an exothermic reaction occurs whereby water is released from the surface of the sample as the calcination temperature is ramped up and the sample is dried after being exposed to atmospheric humidity, with the water likely being evaporated off as the percentage sample weight decreases from 100 to 90%.

Between 300 and 500 °C an exothermic oxidation reaction occurs, and a large amount of thermal energy is emitted resulting in a heat flow peak of 15 W/g. At this stage the NMC hydroxide intermediate phase is oxidised into a disorganised NMC oxide phase, releasing hydrogen as it is emitted during the oxidation reaction. This results in a percentage weight loss from 90 to 75%. The final stage from 500 to 850 °C is an endothermic reaction in which a small amount of oxygen is released from the sample, resulting in a final weight of 65% of the initial weight before the reaction. As the temperature is reduced, a small increase in weight is recorded as the sample absorbs oxygen from the atmosphere.

It is observed that with the exception of the release of water up to 300 °C and the release of oxygen between 500 and 850 °C, there is one major reaction and phase change which is the oxidation of NMC hydroxide into the disorganised NMC oxide. It can therefore be assumed that a) the NMC hydroxide intermediate phase was formed during the preheat stage and that b) there is no secondary reaction after the oxidation of the hydroxide phase.

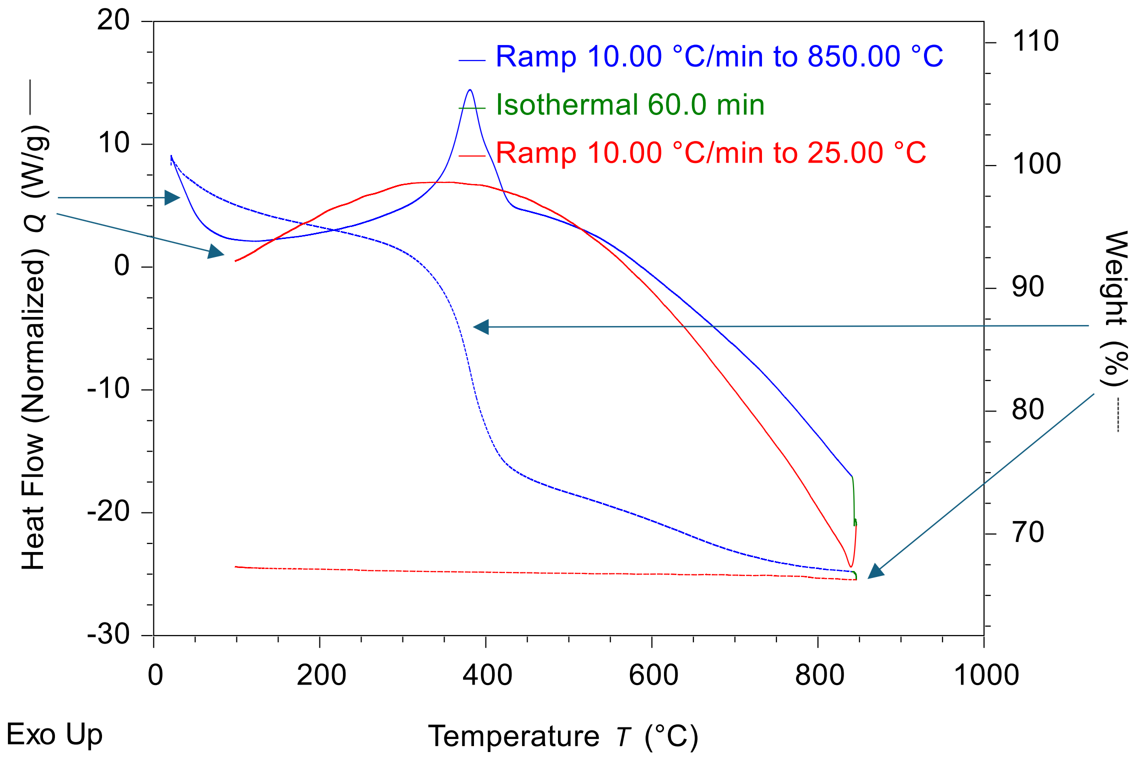

Figure 59 DSC/TGA for NMC811 calcined to 850 °C in O_2 using dextran and acetate precursors and a preheat temperature of 300 °C.

3.4.2.1.2 High temperature study of NMC811 synthesised with dextran and acetate precursors

The intermediate phases of the calcination of NMC811 in air shows the transformation of the precursor and biotemplating solution from being majority amorphous at 200 °C, Figure 60a, to disorganised NMC811 at 800 °C, Figure 60g. (disorganised due to the calcination in air as opposed to an oxidising atmosphere for this study). Peaks at 13° and 18° at 200 °C highlight some crystallisation in the overall amorphous material, likely the recrystallisation of unchelated metal ions. The initial synthesis of an NMC hydroxide intermediate phase can be observed when heated to 300 °C, Figure 60b, as the biotemplate is broken down and the metal ions are theorised to synthesise with the hydroxide functional groups. At 300 °C peaks denoting disorganised NMC oxide can be observed as the NMC hydroxide begins to oxidise [136] as well as the synthesis of lithium carbonate as a secondary phase [134]. At 400 °C Figure 60c the entire NMC hydroxide phase has oxidised to disorganised NMC oxide. As the temperature increases to 700 °C, Figure 60f, the lithium carbonate and any CO_2 decomposes, with the newly available lithium being incorporated into the disorganised NMC phase.

The High temperature study highlights the significance of the NMC hydroxide and oxide intermediate phases as well as lithium carbonate impurity phases within the biotemplating process, with the synthesis of these phases being significant to the synthesis of NMC811 and particle morphologies. Such morphologies require both molten lithium carbonate, which degrades at 723 °C, and the solid NMC oxide to act as a substrate. Without these two phases, nanoscale NMC811 and any novel morphologies seen within the structure could not be achieved. The reason why preheating is selected at between 200 and 300 °C is in part due to the synthesis of the intermediate hydroxide and carbonate phases, which are essential to the synthesis of organised NMC811 when the NMC oxide phase is calcined under oxygen.

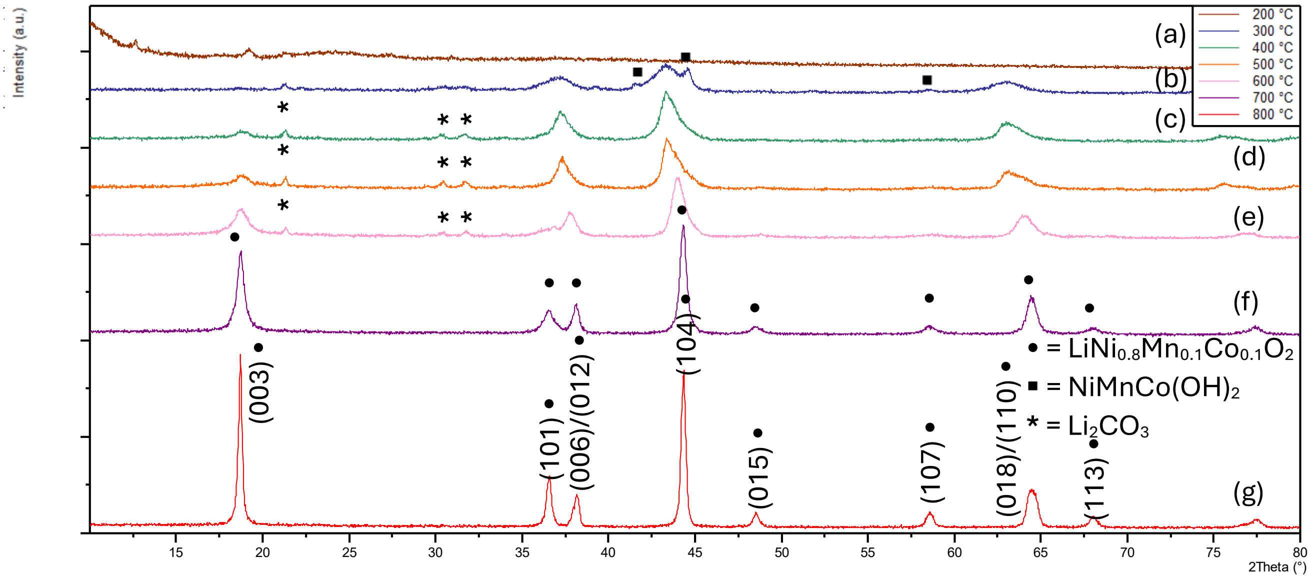

Figure 60 Calcination of NMC811 using dextran and acetate precursors in air at a) 200 °C, b) 300 °C, c) 400 °C, d) 500 °C, e) 600 °C, f) 700 °C, and g) 800 °C

3.4.2.1.3 Post-drying Analysis of dissolved dextran and acetate precursors

The sample is also analysed between the drying and preheat stages. While mostly amorphous, Figure 61 shows three peaks at 12, 14, and 19 °, with some low intensity wide peaks at 25, 40, and 60 °. These peaks represent nickel hydroxide, and are theorised to be synthesised from the reaction between nickel ions and hydroxide functional groups upon the breakdown of the dextran biotemplate under heating, from unchelated Ni ions and highlights inhomogeneity within the sample as early as the drying phase, with full chelation of the biotemplate and precursors not occurring. Any attempt to increase the amount of biotemplate to ensure full chelation would result in excess carbon, which would cause an increase in the amount of CO_2 as the biotemplate breaks down and frees up carbon to react with the oxygen atmosphere. This as a result would mean less oxygen to react with metal ions to form NMC811 and would result in greater disorganisation as a result of poor stoichiometry of the cathode. Section 1.4.3 covers more in depth how the variation of biotemplate mass affects the organisation of the final

NMC811 product but generally, as previous discussed, this would not only create a more reducing atmosphere leading to greater mixing of Li^+ and Ni^{2+} ions into Ni and Li sites respectively but would also use up oxygen previously available for the synthesis of layered NMC811. As such an increase in the relative mass of biotemplate leads to greater disorganisation in the final NMC811 product and increase an in lithium carbonate impurities.

Fixing this would require a significant increase in synthesis temperature to rectify due to the higher carbon content. However, given organised NMC811 can already be synthesised at 850 °C, highlighted previously in Figure 45, and due to the hydroxide phase degrading at 300 °C with the synthesis of nickel oxide, it would not be practical to increase the mass of reactants or synthesis temperature.

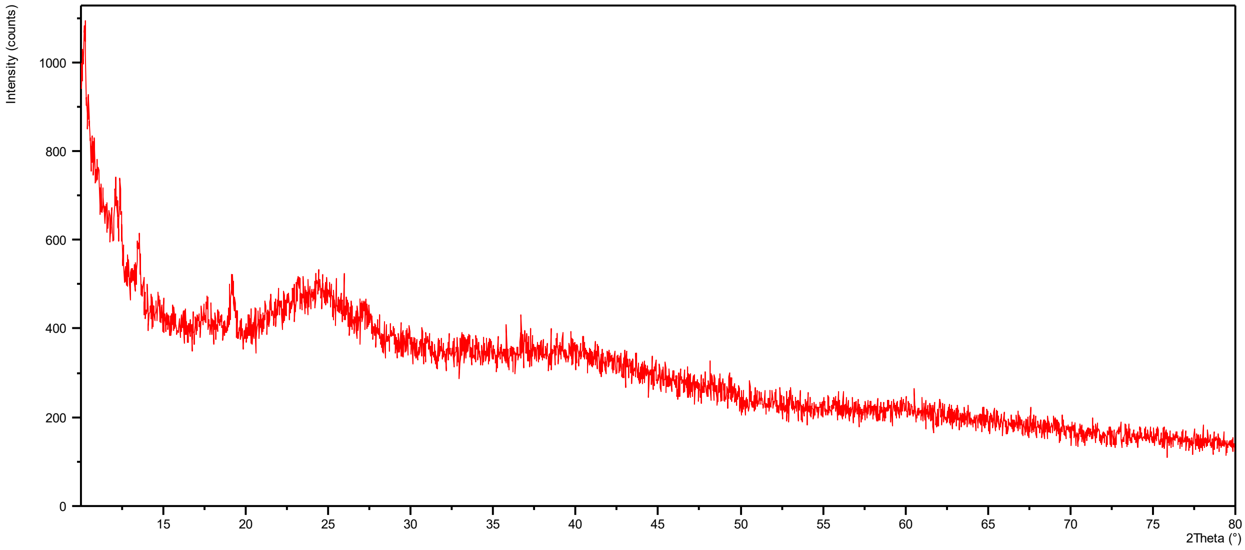

Figure 61 Dextran and acetate precursor solution post-drying

3.4.2.1.4 Morphology of NMC811 preheated using a range of preheat temperatures using dextran and acetate precursors

Figure 62 indicates how preheat temperature may vary particle morphology in addition to crystalline structure. As preheat temperature is increased from 200 to 500 °C average particle diameter decreases from 400 nm at 200 °C, to 300 nm at 300 °C, before increasing to 400 nm at 500 °C. Given that decomposition of the biotemplate only begins at 150 °C, the larger particle diameters at 200 °C can be inferred to be due to biotemplated metal ions that have not yet decomposed. The reason for the increase in particle size as the preheat temperature approaches 500 °C is due to a longer synthesis time and higher preheat temperature, allowing the particles of the intermediate phases more energy and time to grow [92]. Particles at 200 °C are irregularly shaped with a mix of smaller rounded and larger octahedral particle shapes, while as preheat temperature is increased particle morphology tends to a more rounded particle shape. At a preheat of 300 °C or above, there is little variation in particle morphology once the particles have undergone calcination at 850 °C, with all of the particles being agglomerated, roughly rounded in shape, with a 300 to 400 nm average diameter. With the exception of the 200 °C preheat, there is little benefit in varying the preheat temperature to alter particle morphology for the combination of acetates and dextran.

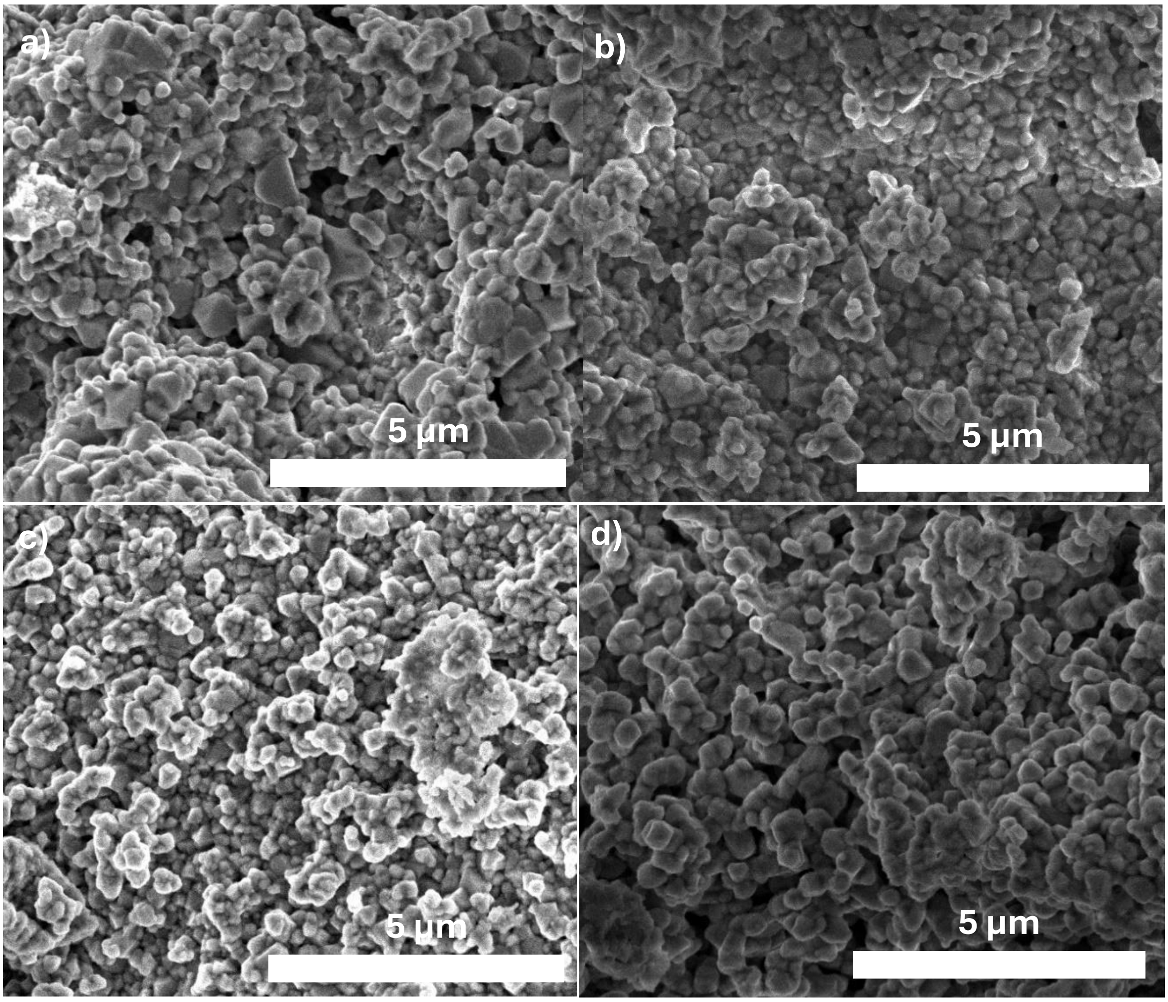

Figure 62 Morphology of NMC811 calcined using dextran and acetate precursors at 850 °C calcination and a) 200 °C, b) 300 °C, c) 400 °C, and d) 500 °C preheat temperature

3.4.2.2 Variation of preheat temperature when synthesising NMC811 using dextran and nitrate precursors

When using nitrate precursors instead of acetate precursors organised NMC811 can be achieved using a higher preheat. This is indicated in Figure 63a to Figure 63d, and summarised in Table 16, by the peak intensity ratio between reflections (003) and (104) of 1.6, 1.56, 1.62, and 1.47, for 200 to 500 °C respectively, where < 1.2 is a sign of significant mixing of Li and Ni sites. This shows little pattern in how preheat temperature affects the mixing of sites other than significantly more mixing when using a 500 °C preheat, Figure 64a. XRD patterns with preheats up to and including 400 °C show stronger peaking splitting at (006)/(012) and (018)/(110), Figure 64b and c, reflections with R_s values of 0.58 and 0.51 with a 200 °C preheat, 0.56 and 0.44 with a 300 °C preheat and 0.56 and 0.53 with a 400 °C preheat, while peaks with a 500 °C preheat have R_s values of 0.45 and 0.41 indicating poorer peak splitting.

When using nitrates instead of acetates less carbon is present in the precursors, and less carbon dioxide is emitted during the preheat stage resulting in a less reducing atmosphere. Such an atmosphere is formed as only the decomposition of the biotemplate, and not the precursor salt, results in less carbon being freed up to react with oxygen in the air to form less CO_2 than when also using acetate precursors. While this reaction still results in less oxygen available for the synthesis of NMC811, having less carbon available to react with oxygen not only frees up oxygen for the synthesis of NMC811 but reduces the mixing of Li and Ni sites as more oxygen is available to become part of the NMC811 structure and ensure greater structural organisation. As such while 200 and 300 °C are viable preheat temperatures, 400 °C is more viable as a preheat temperature when using nitrates than when using acetates. The reason for this difference between using nitrates and acetates may stem from the less reducing atmosphere altering temperature at which the NMC hydroxide phase decomposed into NMC oxide.

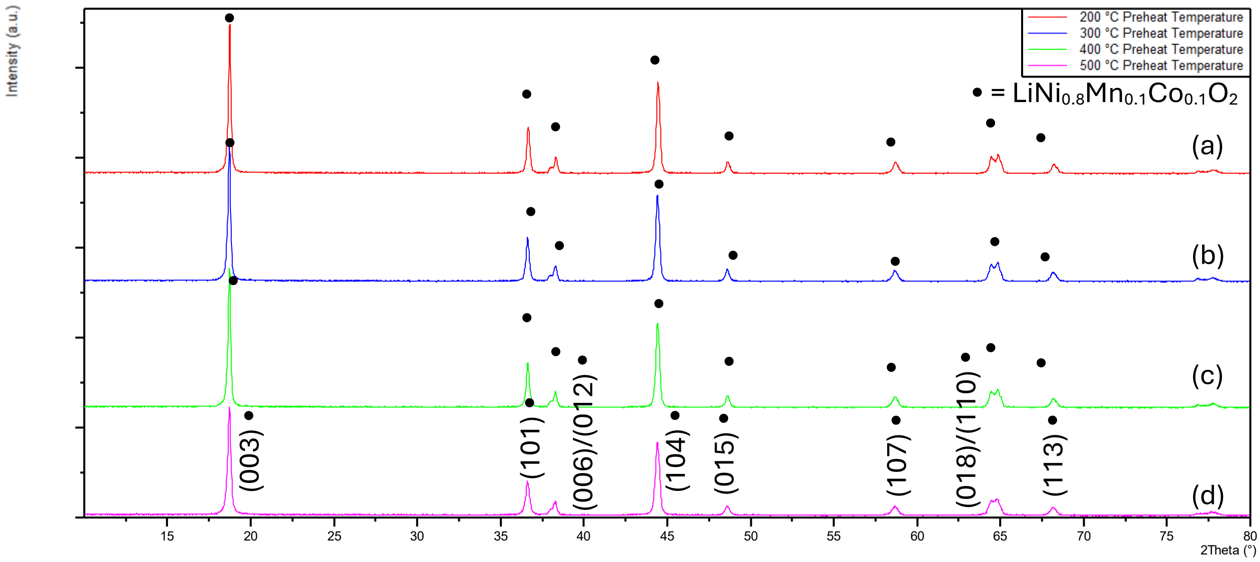

Figure 63 Calcination of NMC811 using dextran and nitrate precursors at 800 °C calcination and a) 200 °C, b) 300 °C, c) 400 °C, and d) 500 °C preheat temperature

Preheat Temperature, °C	(003)/(104) Intensity ratio ($I_{(003)/(104)}$), abs units	Resolution of (006)/(012) reflections, R_s	Resolution of (018)/(110) reflections, R_s
200	1.6	0.58	0.51
300	1.56	0.56	0.44
400	1.62	0.56	0.53
500	1.47	0.45	0.41

Table 16 Comparison of organisation of layered NMC811 when preheat temperatures using dextran and nitrate precursors

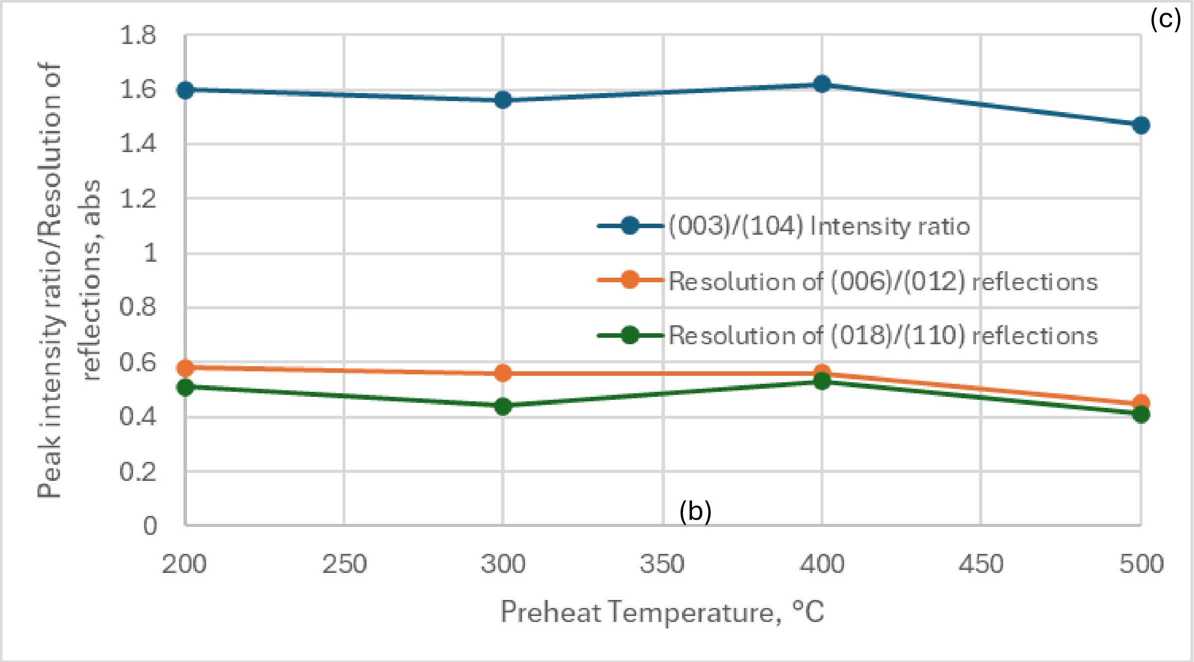

Figure 64 a) Peak Intensity ratios for (003)/(104) reflections and Resolution of Reflections for b) (006)/(012) and c) (018)/(110) reflections vs. Preheat Temperature using dextran and acetate precursors

3.4.2.2.1 Differential Scanning Calorimetry (DSC) and Thermogravimetric Analysis (TGA) of NMC811 calcined with dextran and nitrate precursors

When a nitrate precursor sample preheated at 300 °C is analysed using DSC/TGA, it can be observed that there is no significant exothermic reaction taking place during calcination, Figure 65. There are two distinct sections, the first being as the calcination temperature is increased to 350 °C, an exothermic reaction occurs as water is evaporated off the surface of the sample resulting in an increase in an increase in the normalised heat flow I the exothermic direction and a decrease in percentage weight of the sample from 100 to 90%. The second stage of the reaction occurs above 350 °C and is an endothermic reaction as oxygen is slowly reacted out of the sample which results in a relative weight loss of 90 to 80%. Unlike when using acetate precursors, Figure 59, there is no exothermic peak at 400 °C. When using acetates this denotes the oxidation of NMC hydroxides to a disorganised NMC oxide [137]. This reaction does not seem present during calcination when using nitrate precursors and is likely not present due to the reaction taking place below 300 °C during the preheat stage, with this being possible as high nickel NMC hydroxide can decompose at temperatures as low as 200 °C [136]. This would be possible due to the less reducing atmosphere produced by the nitrate precursors compared to when the acetate precursors. Less CO_2 is produced upon the decomposition of nitrate precursors vs acetate precursors as less carbon is freed up and so less oxygen is required for the reaction to form CO_2 which frees up more oxygen for the synthesis of a stoichiometric NMC811, resulting in greater structural organisation. This highlights the importance of the atmosphere where the reaction is taking place not only during calcination but also during preheat.

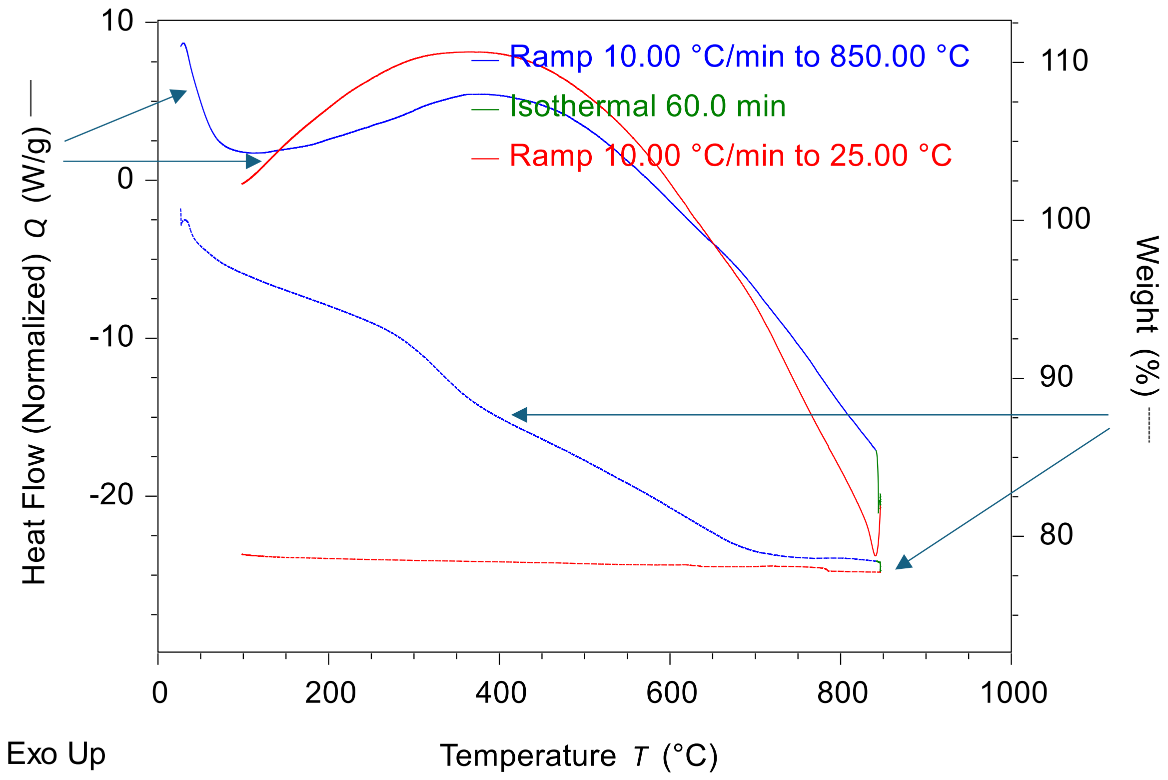

Figure 65 DSC/TGA for NMC811 calcined to 850 °C in O_2 using dextran and nitrate precursors and a preheat temperature of 300 °C.

3.4.2.2.2 High temperature study of NMC811 synthesised with dextran and nitrate precursors

As with acetate precursors, a high temperature study highlights the synthesis of nickel oxide and lithium carbonate intermediate phases at between 300 and 400 °C, Figure 66 b and c. There is however only the single peak between 40 and 45 ° at 300 °C compared to three peaks at 300 °C in Figure 60b. This denotes that there is no NMC hydroxide phase present at 300 °C, and the presence of no peaks between 40 and 45 ° at 200 °C, Figure 66a, gives further evidence that the synthesis of NMC hydroxide from transition metal ions and hydroxide functional groups as the biotemplate was broken down and its oxidation to disorganised NMC oxide took place during preheat between 200 and 300 °C. This is a result of the less reducing atmosphere with only the dextran biotemplate and not the nitrate precursor freeing up carbon upon decomposition. This results in less carbon available to result with the oxygen atmosphere and less carbon dioxide. As such there is more oxygen available for the synthesis of the NMC811 structure ensuring a more stoichiometric ratio of metal ions to oxygen and a more organised structure.

At 200 °C the sample is mostly amorphous, with only a single peak indicating very little crystalline phase present, likely due to the unchelated metal ions recrystalising. At 700 °C peaks for lithium carbonate and disorganised NMC oxide are again no longer present as layered NMC is beginning to be formed. The High temperature study shows again how synthesis of intermediate nickel oxide and lithium carbonate phases at 300 °C is essential for the synthesis of organised NMC811 and particle morphology, while also showing how conditions in the preheat phase can affect the synthesis and oxidation of the NMC hydroxide intermediate phase.

(a)

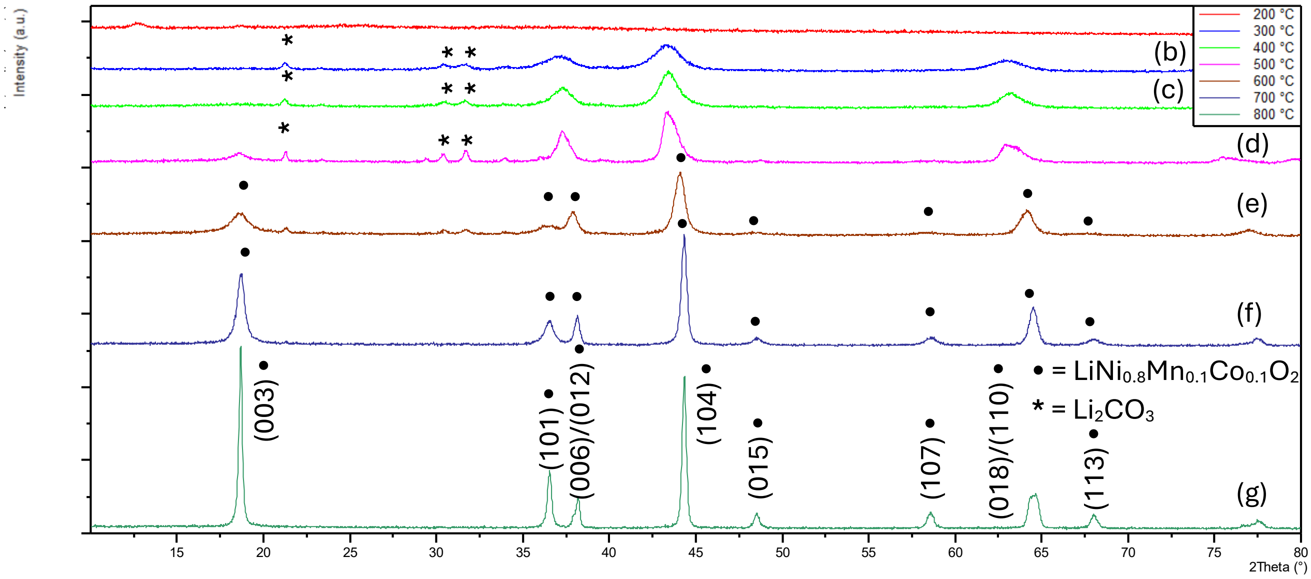

Figure 66 Calcination of NMC811 using dextran and nitrate precursors in air at a) 200 °C, b) 300 °C, c) 400 °C, d) 500 °C, e) 600 °C, e) 700 °C, and g) 800 °C

3.4.2.2.3 Post-drying Analysis of dissolved dextran and nitrate precursors

During the drying phase, full chelation of the solution does again not occur, with metal ions recrystalising as indicated by peaks between 10 and 25 ° in Figure 67. This again shows that an increase in the biotemplate would be required for full chelation, but such an increase would require a higher calcination temperature to in order to provide enough energy to decompose the excess CO_2. When using nitrates, the phases formed during the drying process are broken down before being preheated to 200 °C, with significantly less peaks shown in Figure 66a. This reduced chelation does not appear to hinder the synthesis of intermediate phases during the preheat phase, and still results in organised NMC811 at as low as 800 °C.

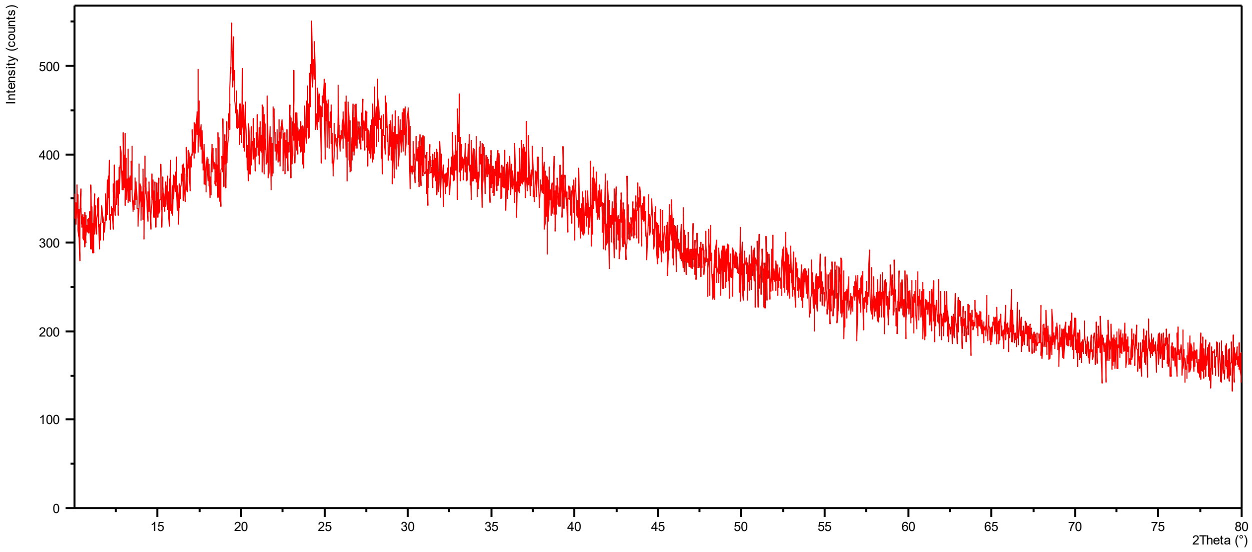

Figure 67 Dextran and nitrate precursor solution post-drying

3.4.2.2.4 Morphology of NMC811 preheated using a range of preheat temperatures using dextran and nitrate precursors

Similarly to when using acetate precursors, Figure 62, NMC811 preheated using nitrate precursors contains highly agglomerated particles with both rounded and more irregular, angular particles, this time regardless of preheat temperature used. Average particle diameter increases from 300 nm to 400 nm between 200 and 300 °C, Figure 68 a and b, and decreases to 200 nm when using a 500 °C preheat Figure 68d.

When using nitrates, it appears varying the preheat does little to alter particle morphology, with the exception of a slight increase in particle diameter as the preheat temperature is increased from 200 and 400 °C due to the increased preheat temperature and associated ramp time. There is also little difference in morphology between acetate and nitrate-formed NMC811 when using above a 300 °C preheat and dextran, with both consisting of a mix of rounded and irregularly shaped particles.

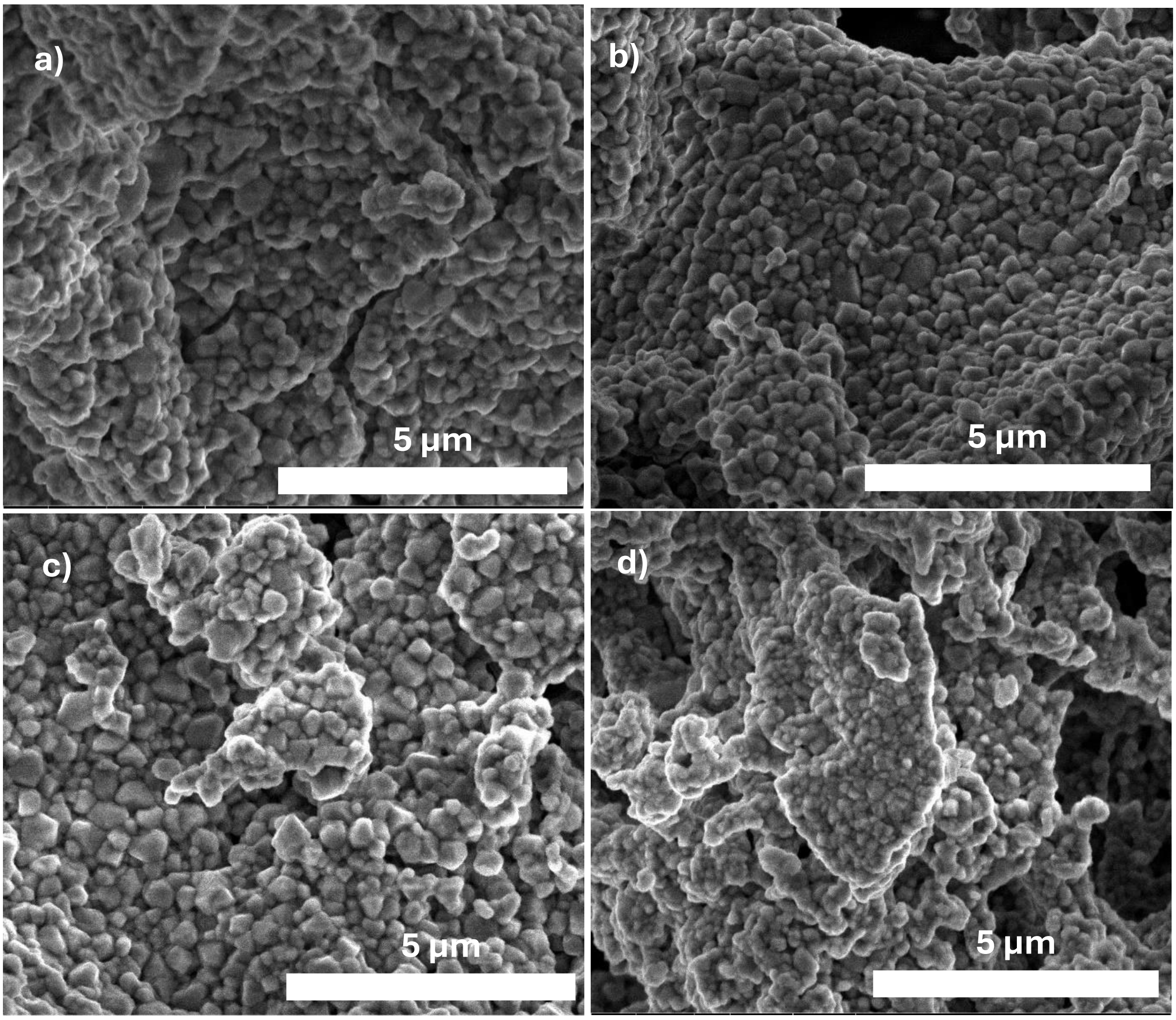

Figure 68 Morphology of NMC811 calcined using dextran and nitrate precursors at 800 °C calcination and a) 200 °C, b) 300 °C, c) 400 °C, and d) 500 °C preheat temperature

3.4.3 Variation of preheat temperature when synthesising NMC811 using sodium alginate

3.4.3.1 Variation of preheat temperature when synthesising NMC811 using sodium alginate and acetate precursors

For the combination of sodium alginate and acetate precursors, the required preheat temperature is not as straight forward as with dextran. When XRD patterns for samples calcined at 850 °C for preheat temperatures between 200 and 500 °C are compared, peak intensity ratios between reflections (003) and (104), Figure 70a, summarised in Table 17, are 1.41, 1.5, 1.53, and 1.57 respectively. Furthermore, peak splitting shown at reflections (006)/(012) and (018)/(110) are not very strong with a 200 °C preheat, Figure 70b and c, as indicated by R_s values of 0.56 and 0.36 but grow stronger with a 300 °C and 400 °C preheat, Figure 69b and c, as indicated by R_s values of 0.69 and 0.55 for a 300 °C preheat and 0.62 and 0.49 for a 400 °C preheat. Peak splitting then becomes weaker at a preheat of 500 °C, Figure 69d. which has R_s values of 0.6 and 0.39. A more organised layered NMC811 structure is therefore produced when synthesising with either 300 or 400 °C preheat as the R_s values are closer to 1, with 200 and 500 °C preheats leading to greater disorganisation of the NMC811 layers.

When peak intensity ratios between (003) and (104) are plotted against preheat temperature, Figure 70a, a clear positive correlation is observed. While all peak intensity ratios are greater than lower 1.2, with the lowest value being 1.41 at 200 °C, which ensures less mixing of Li^+ and Ni^{2+} ions into Ni and Li sites, NMC811 preheated at 500 °C presents the least amount of mixing between sites. In part this is due to the decreased carbon content of the sodium alginate vs. the dextran biotemplate decomposing into carbon dioxide and results in a less reducing atmosphere. Production of less carbon dioxide results in more oxygen being freed up for the synthesis of NMC811 resulting in a more organised structure, as less oxygen has reacted with the reduced amount of carbon freed up by the decomposition of the biotemplate. This is in line with previous evidence suggesting that a more oxidising environment results in less mixing of Li and Ni sites [133]. This less reducing environment allows for the synthesis of NMC hydroxide, theorised to be from the reaction between transition metal ions and hydroxide functional groups as the biotemplate undergoes decomposition, and its oxidation into disorganised NMC oxide to occur at lower temperatures. While site mixing of the final NMC structure increases with preheat temperature, poor peak splitting at 500 °C denotes poor layering of the NMC811 structure and so 300 °C and 400 °C are the optimum preheat temperatures. 300 °C is selected due to the synthesis of an organised structure, of which is formed with a 300 °C preheat, and the reduced energy and time required to preheat at lower temperatures.

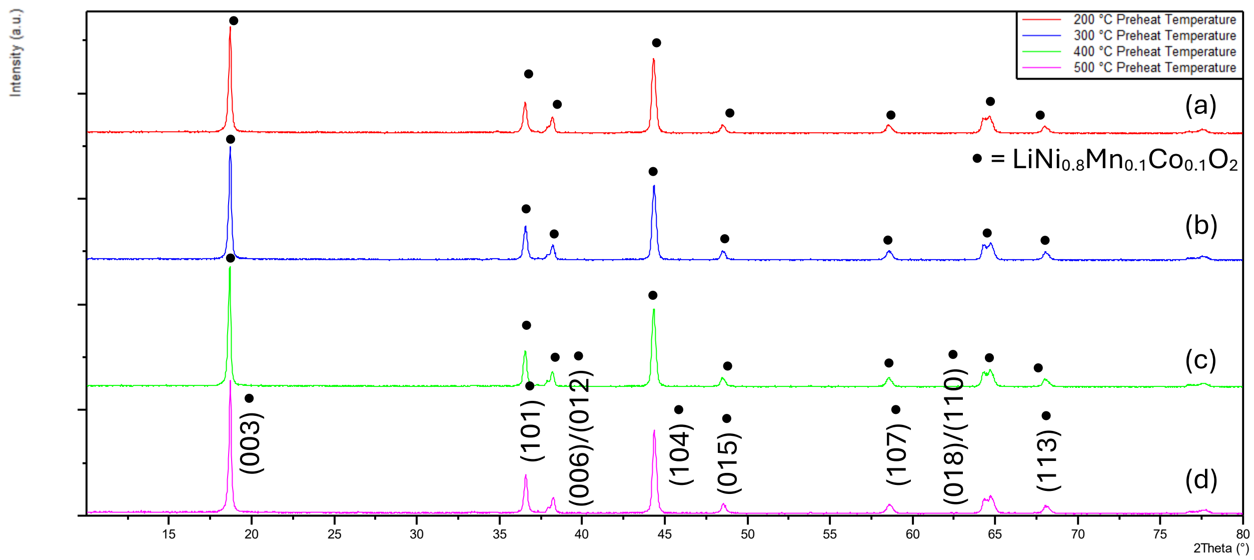

Figure 69 Calcination of NMC811 using sodium alginate and acetate precursors at 850 °C calcination and a) 200 °C, b) 300 °C, c) 400 °C, and d) 500 °C preheat temperature

Preheat Temperature, °C	(003)/(104) Intensity ratio ($I_{(003)/(104)}$), abs units	Resolution of (006)/(012) reflections, R_s	Resolution of (018)/(110) reflections, R_s
200	1.41	0.56	0.36
300	1.5	0.69	0.55
400	1.53	0.62	0.49
500	1.57	0.60	0.39

Table 17 Comparison of organisation of layered NMC811 when preheat temperatures using sodium alginate and acetate precursors

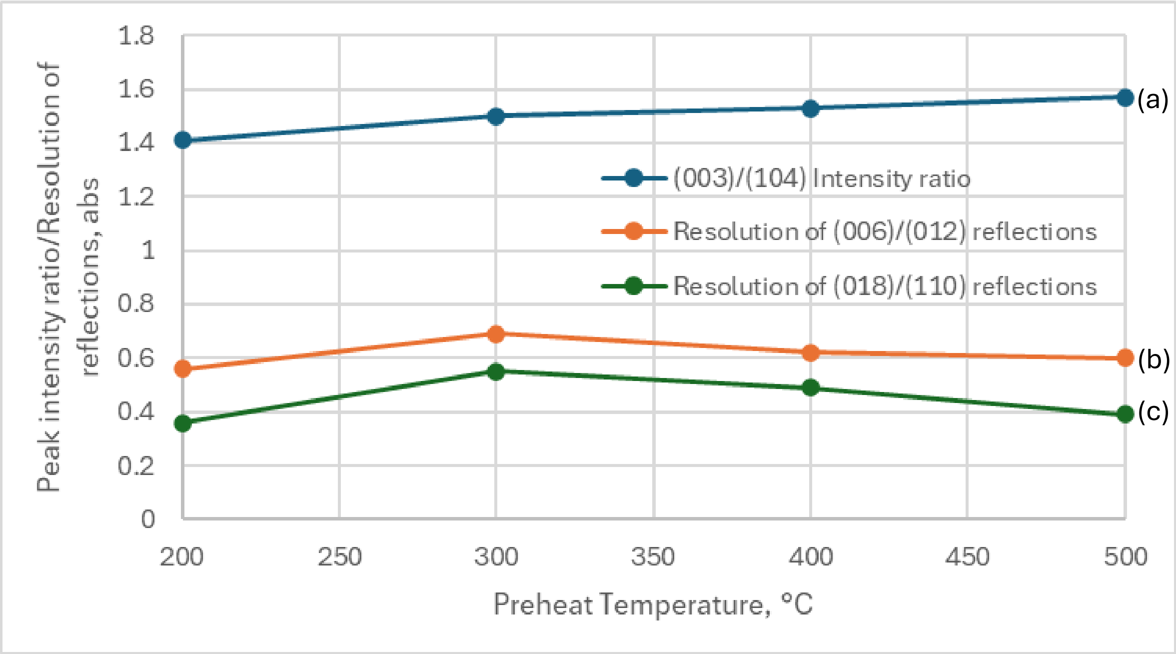

Figure 70 a) Peak Intensity ratios for (003)/(104) reflections and Resolution of Reflections for b) (006)/(012) and c) (018)/(110) reflections vs. Preheat Temperature using dextran and acetate precursors

3.4.3.1.1 Differential Scanning Calorimetry (DSC) and Thermogravimetric Analysis (TGA) of NMC811 calcined with sodium alginate and acetate precursors

When the 300 °C preheated sample is analysed using DSC/TGA it is apparent that, similarly to when using acetates with dextran Figure 59, oxidation of the NMC has not taken place during the preheat phase. The heating of the sample may be split into three separate stages Figure 71. The ramp up to 250 °C shows an exothermic reaction of up to 2 W/g resulting in a percentage weight loss of 100 to 92% as water is evaporated from the surface as the sample is dried in the initial stages of the reaction. During the second stage between 250 and 500 °C NMC hydroxide is oxidised to disorganised NMC oxide and hydrogen [137] is released in an exothermic reaction with a maximum normalised heat flow of 9 W/g. This is represented by three separate peaks This result in a percentage weight loss of 92 to 70% of the initial mass. The final section is between 500 and 850 °C and is an endothermic reaction extracting oxygen from the final NMC811 product resulting in a final percentage weight of 62% of the initial mass.

When preheated at 300 °C NMC hydroxide is theorised to be formed during the preheat phase as the biotemplate breaks down and transition metal ions and hydroxide functional groups react, and oxidised into disorganised NMC oxide during the calcination phase. It is possible this oxidation reaction may at least partly take place during the preheat stage when preheating at either 400 or 500 °C, and if this is the case the atmosphere produced when preheating sodium alginate and acetate precursors is oxidising enough to oxidise NMC hydroxide below 400 or 500 °C and still produced layered NMC811 during calcination. This is due to less carbon in the sodium alginate biotemplate vs. dextran, which results the freeing up of less carbon upon the composition of the biotemplate and so requires less oxygen for the synthesis of the reducing carbon dioxide atmosphere. As such there is oxygen available for the oxidation reaction, further highlights the importance of carbon content and an oxidising atmosphere during preheating.

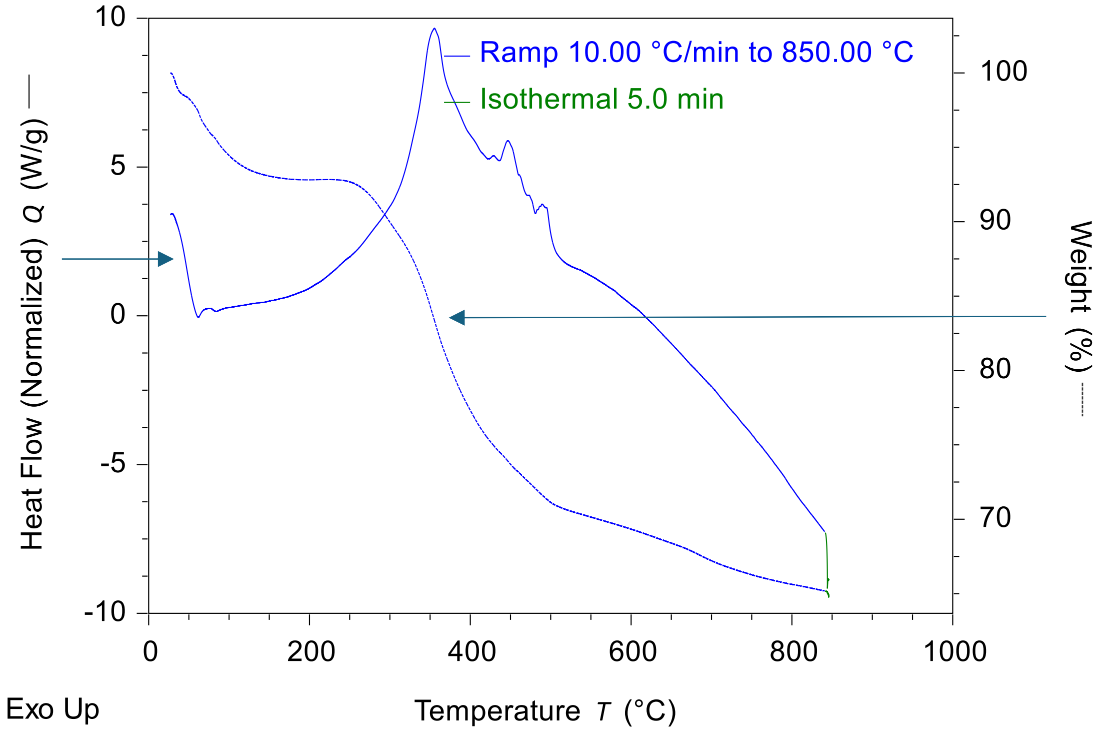

Figure 71 DSC/TGA for NMC811 calcined to 850 °C in O_2 using sodium alginate and acetate precursors and a preheat temperature of 300 °C.

3.4.3.1.2 High temperature study of NMC811 synthesised with sodium alginate and acetate precursors

A high temperature study of the calcination of NMC811 using sodium alginate in combination with acetates further reinforces evidence found doing DSC/TGA. The structure at 200 °C, Figure 72a, is not amorphous, with strong peaks at 12, 21, and 24 ° indicating recrystallisation of unchelated metal ions. This is possibly due to a too low mass of biotemplate compared to the precursors. This phase is however not present at 300 °C, Figure 72b, where it is likely the chelated biotemplate breaks down to form NMC hydroxide, possible formed from the theorised reaction between transition metal ions and hydroxide functional groups. The hydroxide oxidises to disorganised NMC oxide at 400 °C, Figure 72c, with lithium carbonate being formed as an intermediate phase, which at 700 °C, Figure 72f, decomposes when the NMC811 is formed. The NMC hydroxide intermediate phase is theorised to therefore form between 200 and 300 °C, with oxidation to disorganised NMC oxide beginning between 300 and 400 °C. Oxidation of NMC hydroxide to disorganised NMC oxide would therefore take place if NMC is preheated to 400 or 500 °C while synthesis of NMC hydroxide likely occurs if preheated to 300 °C. A preheat temperature of 300 °C should therefore be used so that NMC hydroxide is formed during preheat but oxidation to disorganised NMC oxide occurs during calcination.

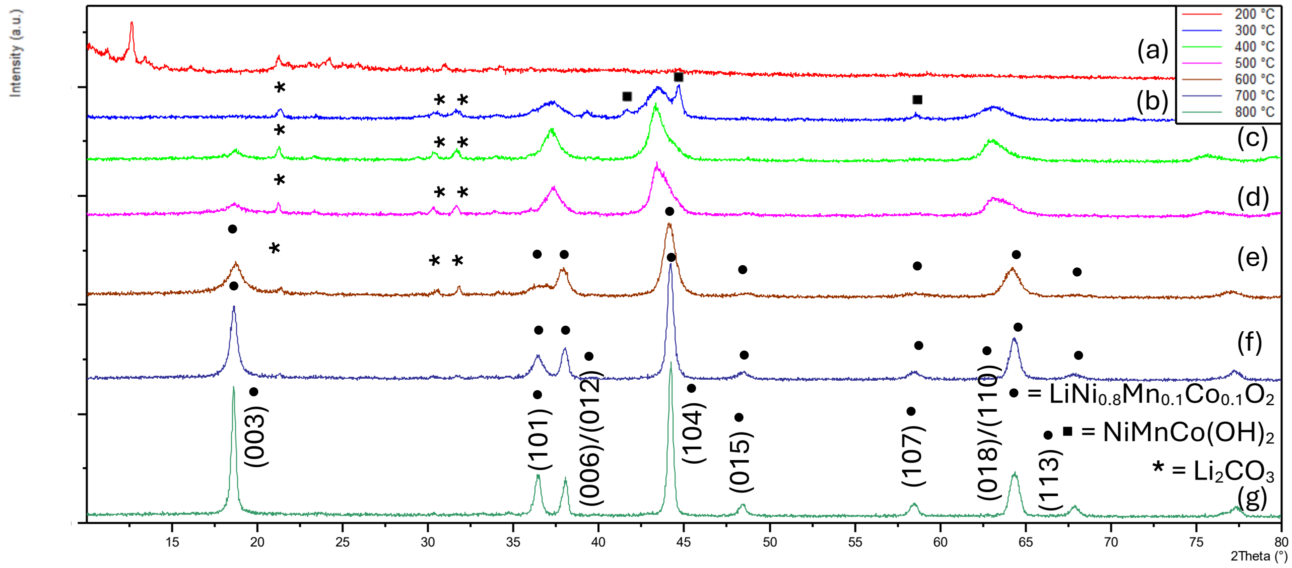

Figure 72 Calcination of NMC811 using sodium alginate and acetate precursors in air at a) 200 °C, b) 300 °C, c) 400 °C, d) 500 °C, e) 600 °C, f) 700 °C, and g) 800 °C

3.4.3.1.3 Post-drying Analysis of dissolved sodium alginate and acetate precursors

Post-drying, the solution formed of sodium alginate and acetate precursors forms a mostly amorphous phase, Figure 73. Only two peaks with small intensities are present between 20 and 25 °, highlighting minimal crystalline phases in the solution and so minimal recrystallisation of metal ions during the drying phase. Minimal recrystallisation of metal ions is due to the eggbox method [94] which ensures that the multivalent metal cations are bonded to multiple sodium alginate chains, whereas when using a biotemplate such as dextran multivalent metal ions may only formed a bond with a single dextran chain. This increased chelation is what allows for a relatively high level of structural organisation of the NMC811 regardless of preheat temperature used, Figure 69. When compared against the phase at 200 °C, Figure 72a, higher intensity peaks are present in the phase formed during preheating at 12, 21, 23, and 30 °, further indicating how the sample has formed a crystalline structure at 200 °C from an amorphous sample post drying rather than formed a large amount of crystalline phase during the drying phase.

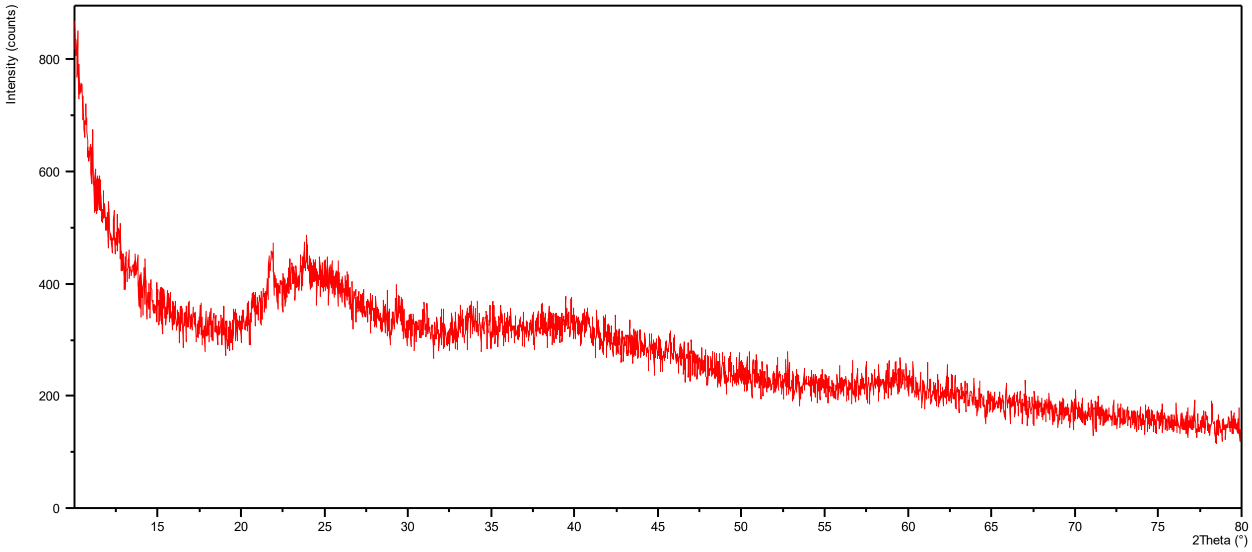

Figure 73 Sodium alginate and acetate precursor solution post-drying

3.4.3.1.4 Morphology of NMC811 preheated using a range of preheat temperatures using sodium alginate and acetate precursors

Particles synthesised using acetate precursors and the sodium alginate biotemplate show a significantly higher average particle diameter, in comparison to particles synthesised using dextran. When preheated at 200, 400 and 500 °C, Figure 74a, b, and d, and then calcined at 850 °C, particles have an average diameter of 600, 700, and 500 nm, respectively. Using a preheat of 300 °C produces a significantly smaller average particle diameter of 400 nm. A smaller average particle diameter using a 300 °C preheat produces a large surface area for lithium intercalation and a higher capacity, in addition to shorter ionic conduction pathways [138]. This is beneficial as not only is a 300 °C preheat theorised to allow for the synthesis of NMC hydroxide from the breaking down of the biotemplate and reaction between transition metal ions and hydroxide functional groups during the preheating, and then the oxidation of disorganised NMC oxide in the calcination stage to form organised, layered NMC811, but also this preheat temperature also produces the smallest average morphology.

For particles produced using all preheat temperatures, particle shapes range from smaller, roughly shaped particles to larger octahedral particles and larger agglomerations. Such agglomerations are formed by melted intermediate phases forming together during calcination, whereas the larger octahedral particles are a product of the combination of the acetate with the sodium alginate biotemplate.

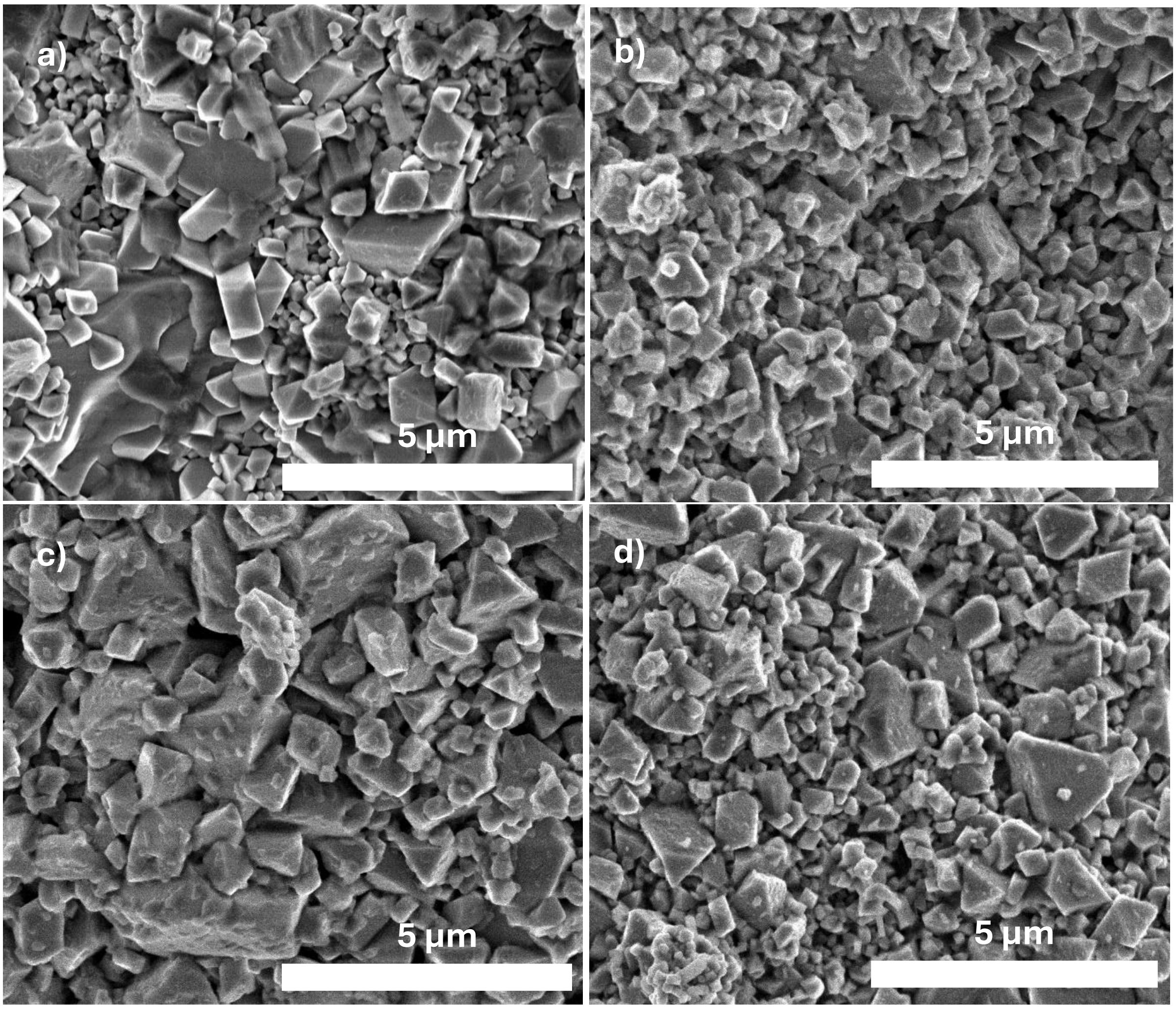

Figure 74 Morphology of NMC811 calcined using sodium alginate and acetate precursors at 850 °C calcination and a) 200 °C, b) 300 °C, c) 400 °C, and d) 500 °C preheat temperature

3.4.3.2 Variation of preheat temperature when synthesising NMC811 using sodium alginate and nitrate precursors

When using nitrates, a similar pattern of disorganisation due to preheat temperature can be observed in XRD patterns in Figure 75. (003) and (104) hkl peak intensity ratios, Figure 76a and summarised in Table 18, show as 1.7, 1.93, 1.84, and 1.47 for preheat temperatures from 200 to 500 °C respectively. Peak splitting at (006)/(012) and (018)/(110) reflections meanwhile, Figure 76b and c, are most prominent with a preheat of 200 or 300 °C, indicated by R_s values of 0.69 and 0.62 at a preheat of 200 °C and 0.91 and 0.72 when using a preheat of 300 °C, but is poor at 500 °C where the R_s values are 0.44 and 0.35. When comparing peak intensity ratios and the definition of twin peaks, 300 °C is the optimum preheat temperature when using sodium alginate and nitrates both for minimal mixing of Li^+ and Ni^{2+} ions in Ni and Li sites [133] due to having the highest peak intensity ratio between (003) and (104), Figure 76a, and organisation of the NMC811 layers as highlighted by the R_s values at (006)/(012) and (018)/(110) reflections approach 1, but also for synthesis energy use due to a lower maximum preheat temperature and ramp time when using 300 °C. The significantly lower carbon content of the combination of sodium alginate and nitrate precursors results in a more oxidising environment during preheat relative to when using acetates or dextran as less carbon dioxide is produced due to the decomposition of the precursor and biotemplate. This decomposition would result in the freeing up of carbon to react with oxygen in the atmosphere, of which would reduce the oxygen available for the synthesis of the NMC811 structure of which would cause increased disorganisation. The relatively more oxidising environment results in less mixing of Li and Ni sites and frees up more oxygen during preheat for the theorised reaction of the NMC hydroxide and disorganised oxide intermediates.

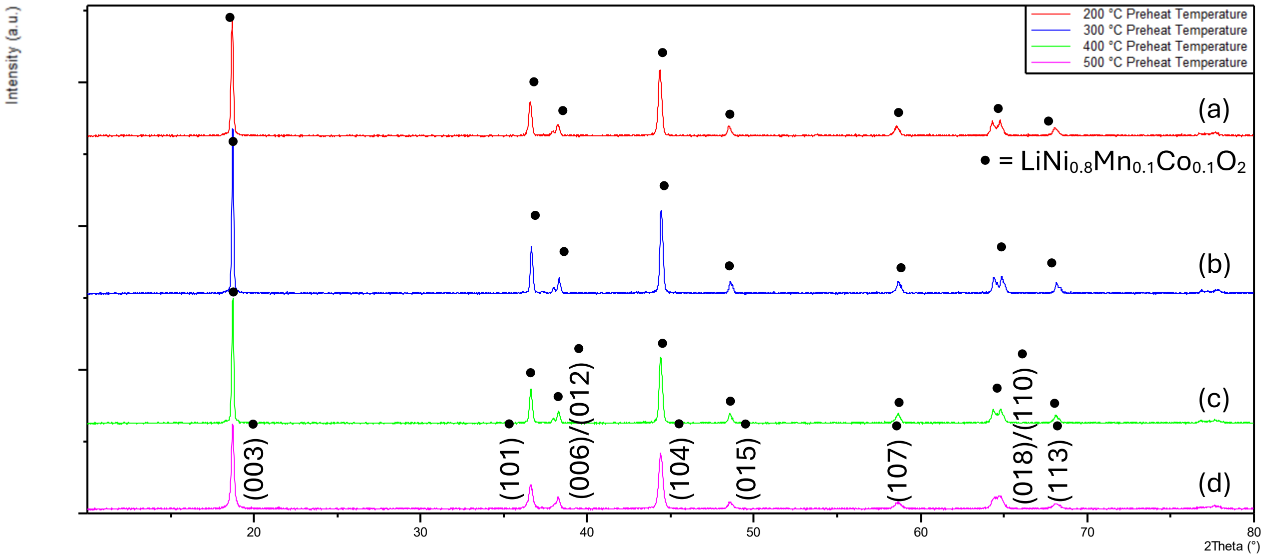

Figure 75 Calcination of NMC811 using sodium alginate and nitrate precursors at 800 °C calcination and a) 200 °C, b) 300 °C, c) 400 °C, and d) 500 °C preheat temperature

Preheat Temperature, °C	(003)/(104) Intensity ratio ($I_{(003)/(104)}$), abs units	Resolution of (006)/(012) reflections, R_s	Resolution of (018)/(110) reflections, R_s
200	1.7	0.69	0.62
300	1.93	0.91	0.75
400	1.84	0.71	0.63
500	1.47	0.44	0.35

Table 18 Comparison of organisation of layered NMC811 when preheat temperatures using sodium alginate and nitrate precursors

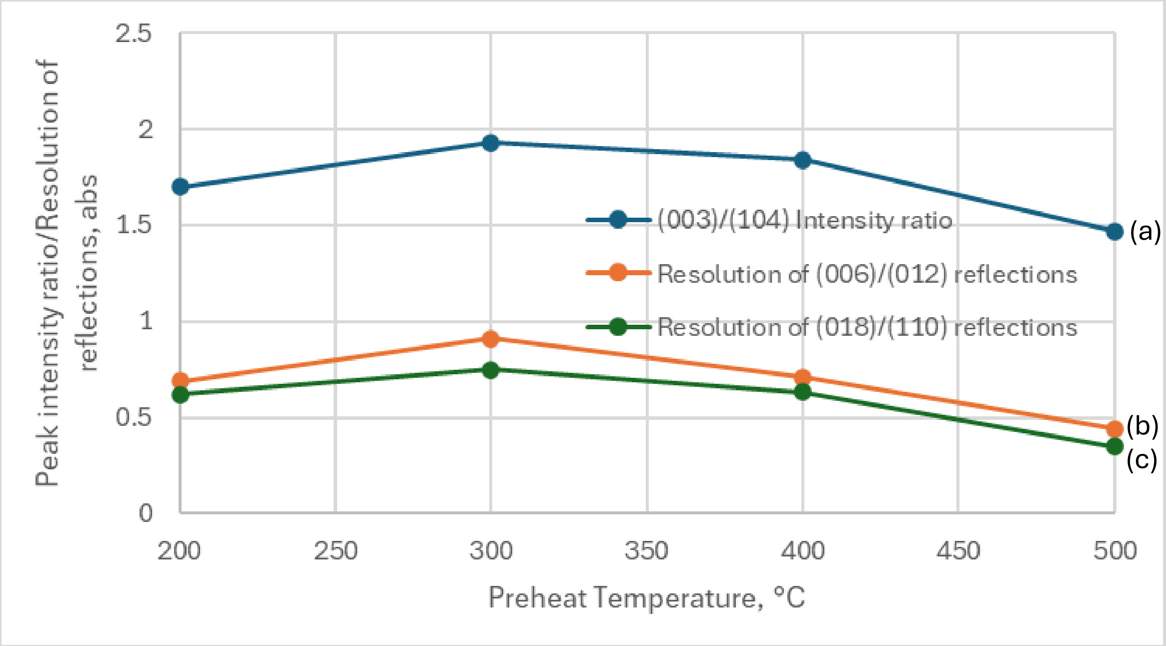

Figure 76 a) Peak Intensity ratios for (003)/(104) reflections and Resolution of Reflections for b) (006)/(012) and c) (018)/(110) reflections vs. Preheat Temperature using dextran and acetate precursors

3.4.3.2.1 Differential Scanning Calorimetry (DSC) and Thermogravimetric Analysis (TGA) of NMC811 calcined with sodium alginate and nitrate precursors

DSC/TGA analysis further highlights the benefits of this more oxidising environment during the preheat phase. When calcined to 850 °C in oxygen following a 300 °C preheat there are three main phases to the reaction. During preheat the synthesis of NMC hydroxide from transition metal ions and hydroxide functional groups after the breaking down of the biotemplate has already occurred. The first phase occurs up to 400 °C and is the evaporation of water from the surface of the NMC hydroxide phase in an exothermic reaction, resulting in a percentage weight loss from 100 to 85% due to a normalised heat flow of between 0 and 3 W/g. The initial drop in percentage weight from 100 to 90% below 100 °C likely occurs due to the sample being wetter or being exposed to a higher humidity before being analysed. Between 400 °C and 700 °C a significant percentage weight loss from 85 to 60% of initial weight occurs as oxidation of the remaining NMC hydroxide oxidises to disorganised NMC oxide in an exothermic reaction. This stage begins at 400 °C, even though oxidation can occur from 300 °C [137], due to the less reducing environment of the preheat phase where some of the NMC hydroxide may have begun oxidising. Above 700 °C an endothermic reaction where oxygen is released from the NMC structure occurs. The loss in percentage weight is minimal due to little oxygen being released at this stage due to a ramp of only 150 °C occurring. Analysis shows oxidation of the NMC hydroxide and release of oxygen from the NMC structure occurs at a higher temperature than when using dextran or acetates due to the less reducing atmosphere during preheat caused by synthesis of less CO_2. Such a reducing CO_2 atmosphere is formed by the breaking down of the sodium alginate, which frees up carbon to react with the oxygen atmosphere. A reduction in the amount of this reducing atmosphere that is synthesised results in less oxygen being removed from the reaction in the final phase of calcination and frees up more oxygen for the synthesis of stoichiometric NMC811, and so results in a greater structural organisation of the final NMC811 product.

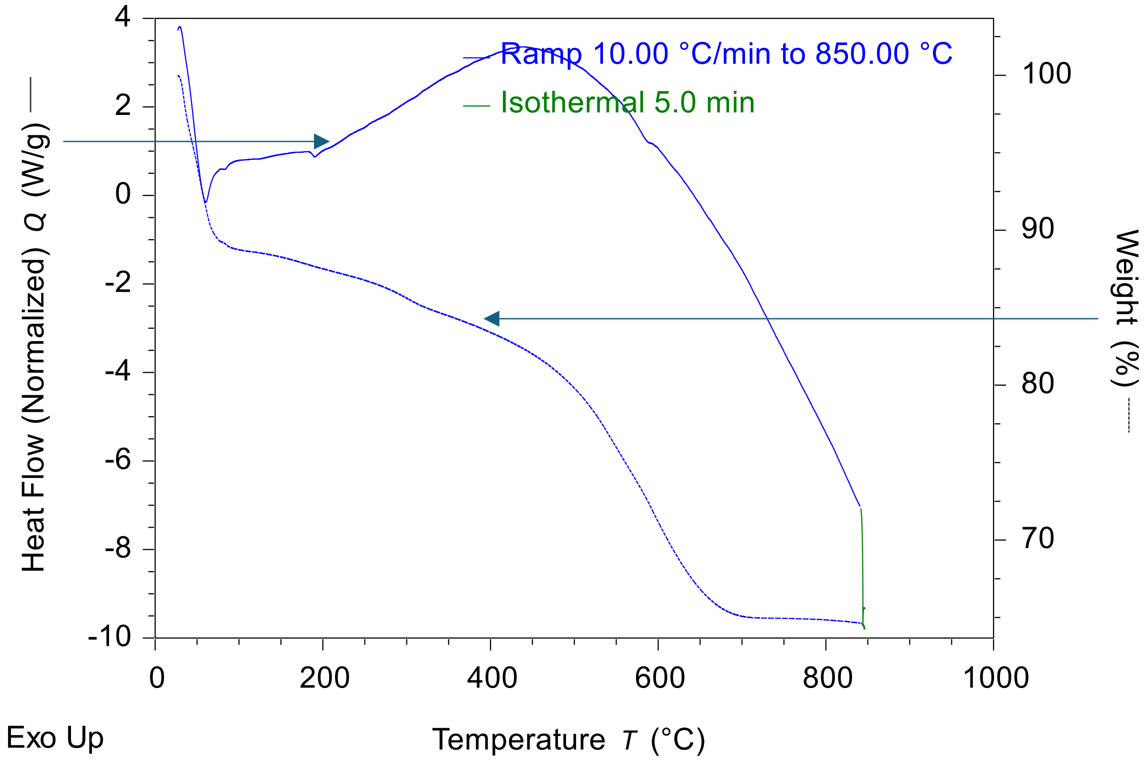

Figure 77 DSC/TGA for NMC811 calcined to 850 °C in O_2 using sodium alginate and nitrate precursors and a preheat temperature of 300 °C.

3.4.3.2.2 High temperature study of NMC811 synthesised with sodium alginate and nitrate precursors

When investigated through a high temperature study the delayed oxidation of the NMC hydroxide can be observed. At 200 °C, Figure 78a, crystalline phases are already present due to the recrystallisation of metal ions that were not chelated but also the possible synthesis of NMC hydroxide from transition metal ions and hydroxide functional groups after the decomposition of the biotemplate. At between 400 and 500 °C, Figure 78c and d, NMC hydroxide begins to oxidise into disorganised NMC oxide intermediate phase and lithium carbonate phase. The lithium carbonate is observed as breaking down at 600 °C, Figure 78e, with layered NMC811 beginning to be formed at 700 °C, Figure 78f.

The high temperature study reinforces that NMC hydroxide is formed before 200 °C and only begins oxidising after 400 °C. Despite this the lower carbon content and reduced decomposition into carbon dioxide, due to less carbon being freed up from the decomposition of the biotemplate and precursor and so less oxygen reacting with the carbon to form a reducing carbon dioxide atmosphere, provides a more oxidising environment due to the amount of oxygen remaining of which did not react to form carbon dioxide. This results in layered NMC811 beginning to form between 600 and 700 °C, with the oxygen in the oxidising atmosphere being sufficient to produce NMC811 with the correct proportion of oxygen and a more organised structure. Due to the highly structured nature of the layered NMC811, a delayed oxidation of the NMC hydroxide phase therefore may be beneficial for the synthesis of a more organised crystalline structure.

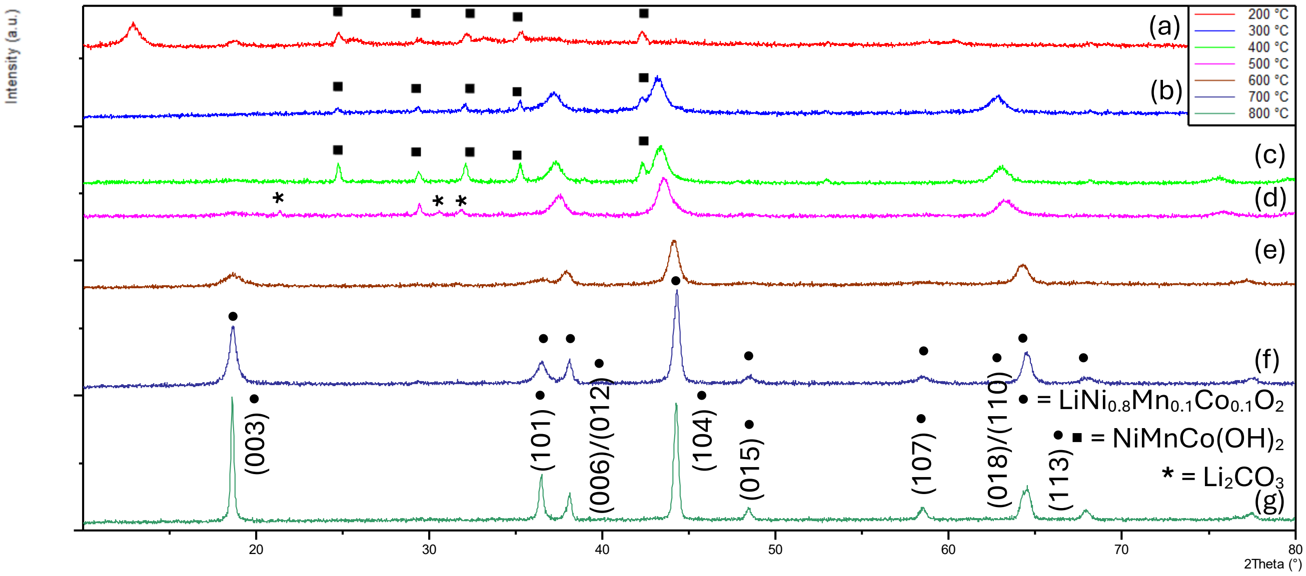

Figure 78 Calcination of NMC811 using sodium alginate and nitrate precursors in air at a) 200 °C, b) 300 °C, c) 400 °C, d) 500 °C, e) 600 °C, f) 700 °C, and g) 800 °C

3.4.3.2.3 Post-drying Analysis dissolved in sodium alginate and nitrate precursors

The presence of a crystalline phase is also present after the solution has been dried at 85 °C, with Figure 79 highlighting how full chelation of metal precursor ions to the biotemplate has not occurred. While full chelation has not occurred, potential synthesis of NMC hydroxide from hydroxide functional groups and transition metal ions as a result of the decomposition of the biotemplating beginning during the drying phase and not at 200 °C, Figure 78a. Despite this, organised NMC811 is still synthesised without full chelation and the early synthesis of NMC hydroxide.

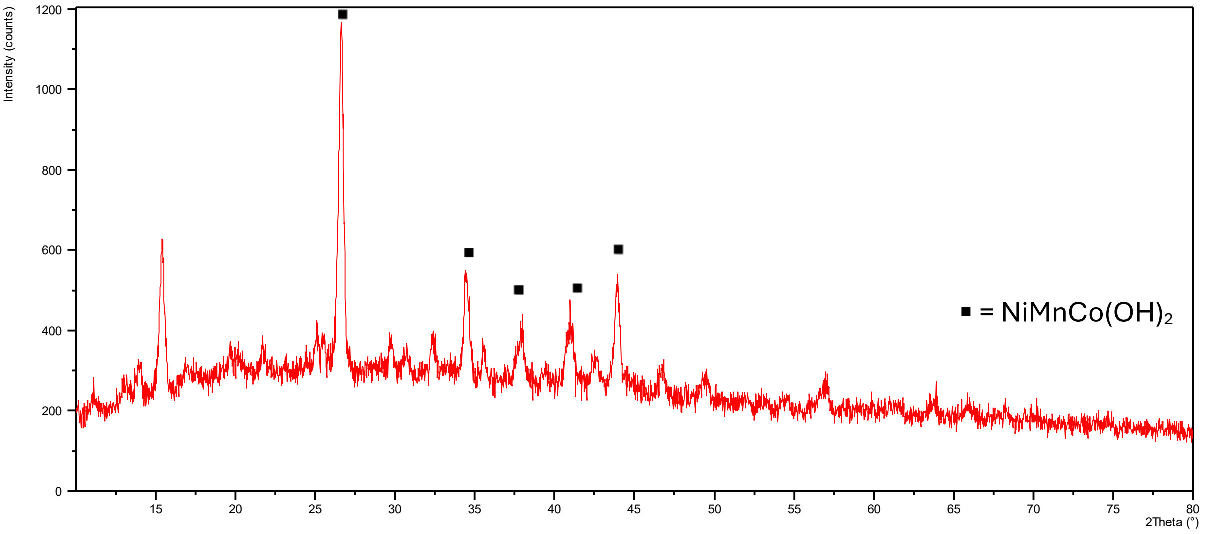

Figure 79 Sodium alginate and nitrate precursor solution post-drying

3.4.3.2.4 Morphology of NMC811 preheated using a range of preheat temperatures using sodium alginate and nitrate precursors

When the particle morphology of NMC811 calcined at 800 °C using sodium alginate and nitrates is observed, particles appear to increase in diameter the greater the organisation of the

NMC811. Particles preheated at 300 °C, consisting of organised NMC811 have the largest average particle diameter at 900 nm, shown in Figure 80b, while more disorganised NMC811 preheated at 200 and 500 °C, Figure 80a and d, have average particle diameters of 700 and 500 nm respectively. Calcination using sodium alginate and nitrates forms round, rounded, irregular particle morphologies, with little different in shape between particles synthesised using a 200 to 400 °C, Figure 80c, preheat with the exception of a small number of octahedral particles observed at with a 400 °C. When NMC811 is preheated at 500 °C however, particles have octahedral morphologies similar to those found when using acetates and sodium alginate.

For the combination of sodium alginate and nitrates, NMC811 synthesised using preheats that produced a more organised structure, 200 and 300 °C, produce larger particles. Particles synthesised with a 300 °C preheat have the largest average diameter, limiting lithium sites for intercalation and reducing capacity. Particles synthesised using 200 and 500 °C meanwhile have smaller average particle diameters which have larger surface areas and increase the number of possible lithiation sites, yet use of these preheat temperatures results in greater disorganisation of the NMC811 structure. The particle diameters, particularly at 300 °C, may be attributed to the synthesis of the NMC hydroxide phase, potential from the reaction between transition metal ions and hydroxide functional groups after the biotemplate is broken down under heating, with the NMC hydroxide particles being formed before 200 °C and then growing up to 400 °C. During calcination, NMC hydroxide oxidises into disorganised NMC oxide and is able to grow as the temperature is ramped up to 800 °C. When the average particle size is decreased to a 500 °C preheat it may be attributed to the disorganised NMC oxide particles being formed during the preheat as NMC hydroxide is decomposed around 400 °C, giving the NMC oxide little time to grow during the preheat phase. As such the NMC oxide particles begin the calcination stage much smaller than the NMC hydroxide particles formed when using preheats from 200 to 400 °C, which results in a small particle size when calcined to 800 °C. The removal of the oxidation step from the calcination reaction also appears to increase the number of octahedral morphologies present. Such morphologies are not present when calcination is undertaken using NMC hydroxide and as such the synthesis of octahedral morphologies may be linked to the synthesis of NMC oxide occurring during the preheat phase.

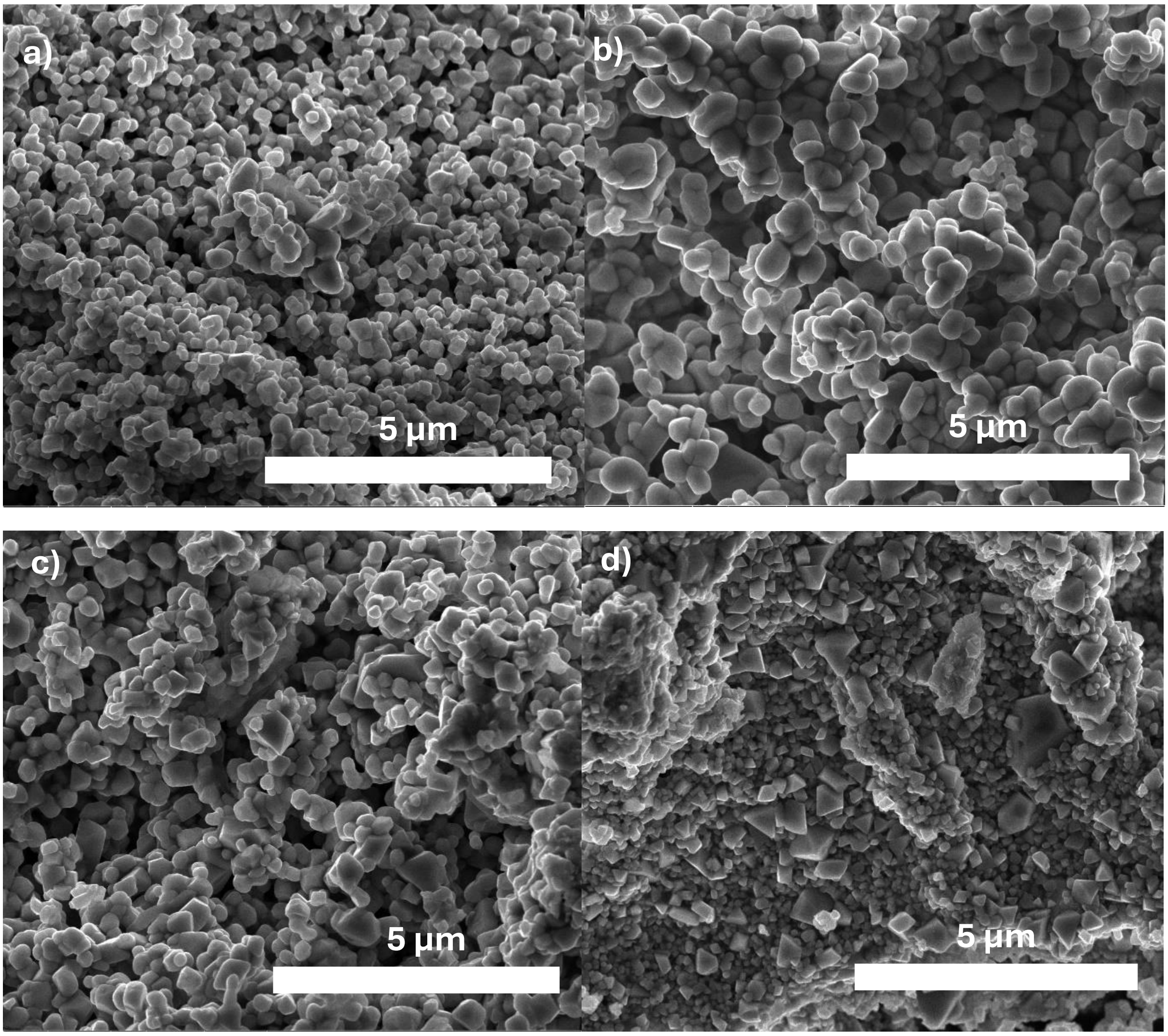

Figure 80 Morphology of NMC811 calcined using sodium alginate and nitrate precursors at 800 °C calcination and a) 200 °C, b) 300 °C, c) 400 °C, and d) 500 °C preheat temperature

3.4.4 Discussion on when varying preheat temperature in the synthesis of NMC811

By varying and analysing the preheat temperature using all combinations of acetates, nitrates, dextran, and sodium alginate, 300 °C is determined to be the optimum preheat temperature across all combinations while 500 °C and above is the poorest choice. It is theorised that NMC hydroxide is formed from the reaction between transition metal ions and hydroxide functional groups following the decomposition of the biotemplate during the preheat stage, but that the oxidation into disorganised NMC oxide intermediate phase must occur during calcination for the best conditions to form organised and layered NMC811. Bar certain situations where NMC hydroxide was formed before 200 °C or oxidised after 500 °C, NMC hydroxide was formed before 300 °C and oxidised at or after 400 °C, making a 300 °C the ideal preheat temperature. A 300 °C preheat often leads to a slight increase in average particle diameter of 100 to 200 nm when compared to other preheat temperatures such as 200 or 500 °C. Octahedral morphologies formed using sodium alginate are also only observed when using 400 or 500 °C preheat temperatures, while particles synthesised at 300 °C have irregular but rounded morphologies. A decrease in average particle diameter of 200 nm and octahedral morphology is however not sufficient enough reason when the decreased organisation of the layered NMC811 formed using a 200 or 500 °C preheat is taken into consideration. Variation in the morphology or size of particles by varying preheat temperatures are also minimal when compared to the variations caused by altering calcination temperatures, and as such changes in particle morphology caused by preheat temperatures are unlikely to be significant when compared to changes caused by calcination temperatures.

3.5 Varying the biotemplate mass in the synthesis of NMC811

Discussions in previous sections have highlighted the significance of both carbon content and chelation in the synthesis of layered NMC811. Previous analysis has shown the production of a reducing atmosphere caused by a high content of carbon within the biotemplate chain and recrystallisation of metal ions during the drying phase negatively effecting synthesis. Both variables can be altered by varying the mass of biotemplate used relative to the mass of metal precursors. By varying the mass of biotemplate relative to the precursors it can be investigated how an increase or decrease in relative mass affects the final NMC811 product and the feasibility of altering the mass of the biotemplate.

3.5.1 Varying the biotemplate mass in the synthesis of NMC811 using dextran

Variation of the mass of the biotemplate used is required to ensure the optimum ratio of biotemplate to precursor metal ions is used with greater ratio of biotemplate to precursors will result in a greater number of chelation sites for metal ions. When synthesising samples using dextran 0.25 g of dextran has been used as the standard mass of biotemplate, with 0.5 g being double the relative mass of biotemplate relative to precursors used in a standard sample.

3.5.1.1 Varying the biotemplate mass in the synthesis of NMC811 dextran and using acetate precursors

When 0.5 g and 0.25 g respectively of dextran are used, Figure 81a and b, greater disorganisation of the NMC811 structure occurs when using a greater relative mass of dextran. The peak intensities for reflections (003) and (104) have a ratio of 1.43 when using 0.5 g and 1.5 when using 0.25 g indicating less mixing of Li^+ and Ni^{2+} to Ni and Li sites respectively when using the lesser relative mass of biotemplate. A significantly greater peak splitting at (006)/(012) and (018)/(110) when using 0.25 g of dextran versus when using 0.5 g is also observed indicating greater organisation of the layers in the final NMC811 structure when using less biotemplate.

Despite the theoretical increase in chelation sites from an increase in the mass of the biotemplate, a smaller mass of biotemplate leads to greater organisation of the layered structure. While there are more chelation sites when using more dextran, there is also more carbon present in the dextran chain. The increased amount of mass of biotemplate frees up more carbon when the biotemplate decomposes and results in a greater volume of CO_2 during synthesis when than when using the low mass of biotemplate which results in more oxygen being required for the synthesis of the greater volume of CO_2 making the atmosphere more reducing. Less oxygen is therefore available up for the synthesis of stoichiometric NMC811 resulting in a more disorganised structure but also increases Li^+ and Ni^{2+} mixing in Ni and Li sites [133], increasing disorganisation of the NMC811 structure.

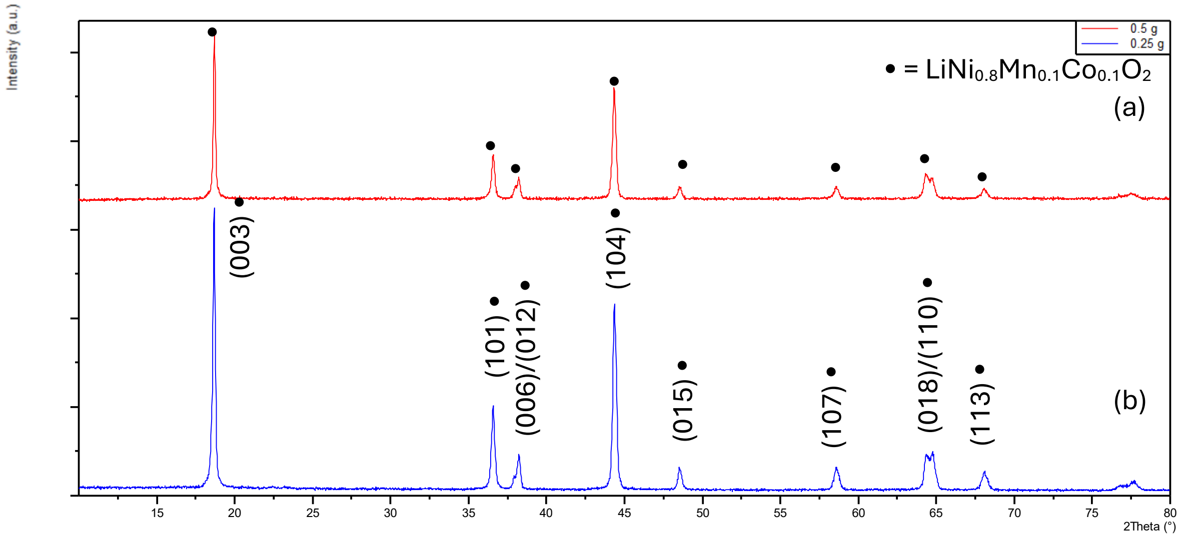

Figure 81 Calcination of NMC811 at 850 °C in oxygen with 300 °C preheat in air using acetate precursors and a) 0.5g and b) 0.25g dextran biotemplate

3.5.1.2 Varying the biotemplate mass in the synthesis of NMC811 using dextran and nitrate precursors

When acetate precursors are swapped for nitrate precursors doubling the relative mass of dextran biotemplate still results in a more disorganised structure, though not as significantly more disorganised as when using acetates. When comparing peak intensity ratios between (003) and (104) reflections, Figure 82a and b, 0.5 g of dextran has a ratio of 1.78 and 0.25 g a ratio of 1.90 where, < 1.2 is considered high mixing of Li and Ni sites [130]. NMC811 synthesised with both 0.25 g and 0.5 g dextran have equally strong peak splitting at (006)/(012) and (018)/(110) reflections.

While the number of chelation sites increases with the mass of dextran so does the amount of carbon content in the biotemplate chain. Use of nitrates instead of acetates reduces the overall carbon content of the reaction, however the dextran chain still decomposes allowing freed up carbon to react with the oxygen atmosphere to form CO_2 and leading to the synthesis of a reducing atmosphere. When more biotemplate is used and more of the reducing CO_2 atmosphere is produced, less oxygen is available for the synthesis of NMC811 which results in greater structural disorganised as all oxygen sites are not filled. This more reducing atmosphere is what results in the increased mixing of Ni^{2+} and Li^+ ions into Li and Ni sites respectively, [133], when a greater mass of biotemplate is used, where the peak intensity ratio between (003) to (104) is greater when using 0.25g vs. 0.5 g dextran (1.9 > 1.78). While both masses of dextran are viable due to similar layering of the NMC811, the reduced mixing of cations ensures a lower mass of biotemplate is more optimal.

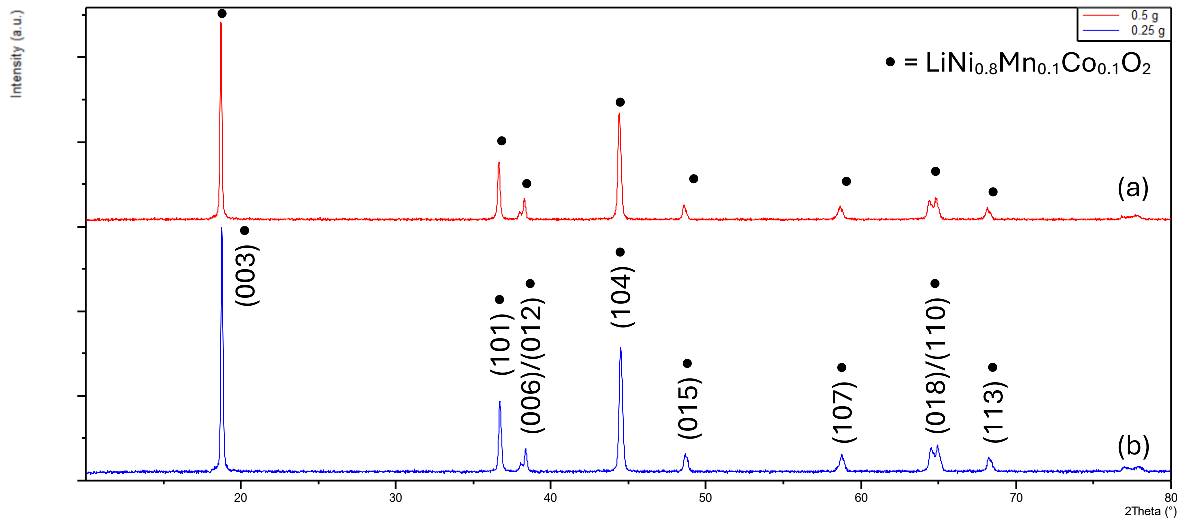

Figure 82 Calcination of NMC811 at 800 °C in oxygen with 300 °C preheat in air using nitrate precursors and a) 0.5g and b) 0.25g dextran biotemplate

3.5.2 Varying the biotemplate mass in the synthesis of NMC811 using sodium Alginate

3.5.2.1 Varying the biotemplate mass in the synthesis of NMC811 using sodium alginate acetate precursors

By varying the mass of sodium alginate, significant differences in the NMC811 structure is observed. The masses of sodium alginate biotemplate used are the standard mass established in the method, 0.1 g, as well as a third and 2.5x the relative mass of biotemplate, 0.03 and 0.25 g respectively.

Peak intensity ratios between peaks with reflections (003) and (104) when using 0.03 g, 0.1g, and 0.25 g of sodium alginate, Figure 83a - c, are 1.27, 1.49, and 1.32, respectively, where < 1.2 denotes NMC811 with a high level of Ni and Li site mixing. It can also be seen that there is strong peak splitting between (006)/(012) and (018)/(110) reflections when using 0.03 g and 0.1 g sodium alginate, but when using 0.25 g of sodium alginate little to no peak splitting occurs. Significant amounts of sodium secondary phases are also present in the form of sodium peroxide (Na_2O_2) when using 0.25 g sodium alginate.

An increase in the biotemplate mass increase the number of chelation points for metal ions. Using 0.03 g of sodium alginate results in NMC811 with highly organised layers as denoted by the strong peak splitting between (006)/(012) and (018)/(110) peaks, but the low (003)/(104) peak intensity ratio of 1.27 highlights significant mixing of Li^+ and Ni^{2+} ions into Ni and Li sites. Use of 0.1 g sodium alginate results in less mixing of metal cations into Li and Ni sites indicated by a ratio of 1.49, as well as an organised layering of the NMC811 structure as shown by good peak splitting. When 0.25 g biotemplate is used a (003)/(104) peak ratio of 1.32 and minimal peak splitting indicates an NMC811 product with high cation mixing and disorganisation of the layers. The incorporation of a Na_2O_2 secondary phase due to a high content of sodium within the sodium alginate and the sodium not being released from the structure during calcination also leads to further disorganisation of the NMC811. It may be possible for this sodium phase to be beneficial however, which will be investigated in chapter 4. For the variation of biotemplate mass however 0.1 g sodium alginate is the optimum choice for both minimising the mixing of both cation sites and crystalline layers.

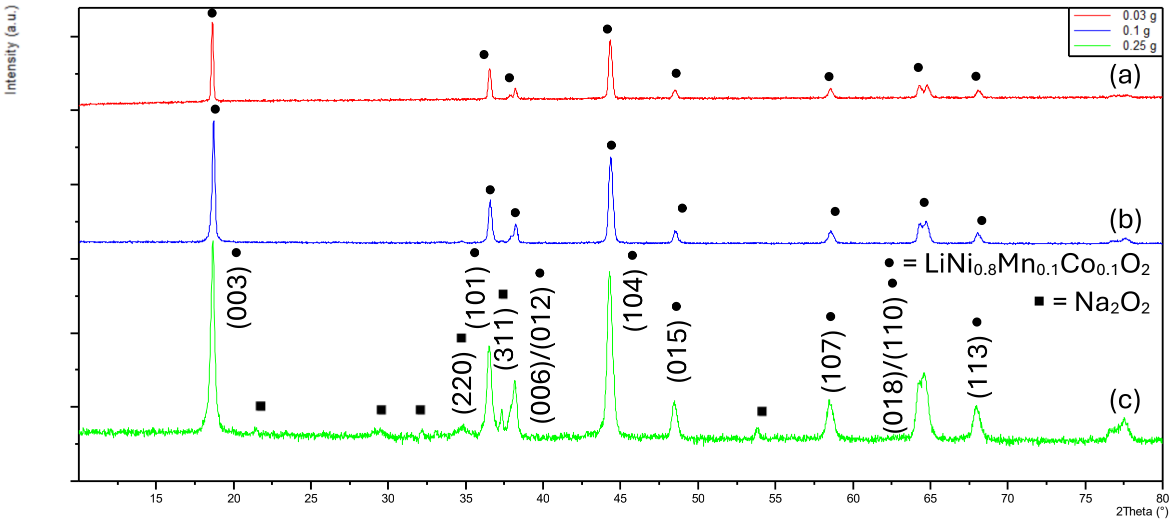

Figure 83 Calcination of NMC811 at 850 °C in oxygen with 300 °C preheat in air using acetate precursors and a) 0.03 g, b) 0.1 g, and c) 0.25g sodium alginate biotemplate

3.5.2.2 Varying the biotemplate mass in the synthesis of NMC811 using sodium alginate and nitrate precursors

Use of nitrate precursors with sodium alginate results in greater organisation of NMC811 compared to when using acetates, regardless of mass of biotemplate used. Masses of biotemplate used are 0.1 g, 0.25 g, and 0.5 g equating to x1, x2.5, and x5 the biotemplate mass outlined in the method. When peak intensity ratios between (003) and (104) reflections are compared, 0.1 g, 0.25 g, and 0.5 g of sodium alginate, Figure 84a – c, are shown to have ratios of 2.09, 1.74, and 1.56, respectively, with peaks at (006)/(012) and (018)/(110) reflections showing well defined peak splitting for all masses of biotemplate used, Strong peaks for Na_2O_2 secondary phases are also present for masses of 0.25 g and 0.5 g of biotemplate.

Low mixing of Li^+ and Ni^{2+} in Ni and Li sites, [133] and organised layering of the NMC811, denoted by a high (003)/(104) peak intensity ratio and strong peak splitting at (006)/(012) and (018)/(110) respectively, show how organised layered NMC811 is formed using all masses of sodium alginate. There is relatively little carbon available upon the decomposition of the biotemplate when using this combination of biotemplate and precursor, so little CO_2 is formed when the carbon reacted with the oxygen atmosphere, resulting in a very low reducing environment. As such it leaves a large volume of oxygen available for the synthesis of NMC811 and allows for greater structural organisation as more oxygen sites are filled. Despite being the lowest mass and so having the least amount of chelation sites, a mass of 0.1 g of biotemplate is optimal for the synthesis of NMC811 due to having the highest peak intensity ratio of 2.09 and the best peak splitting. Additionally, 0.25 g and 0.5 g masses should not be used as they synthesise Na_2O_2 intermediate phases that further negatively effects the homogeneity and organisation of the NMC811.

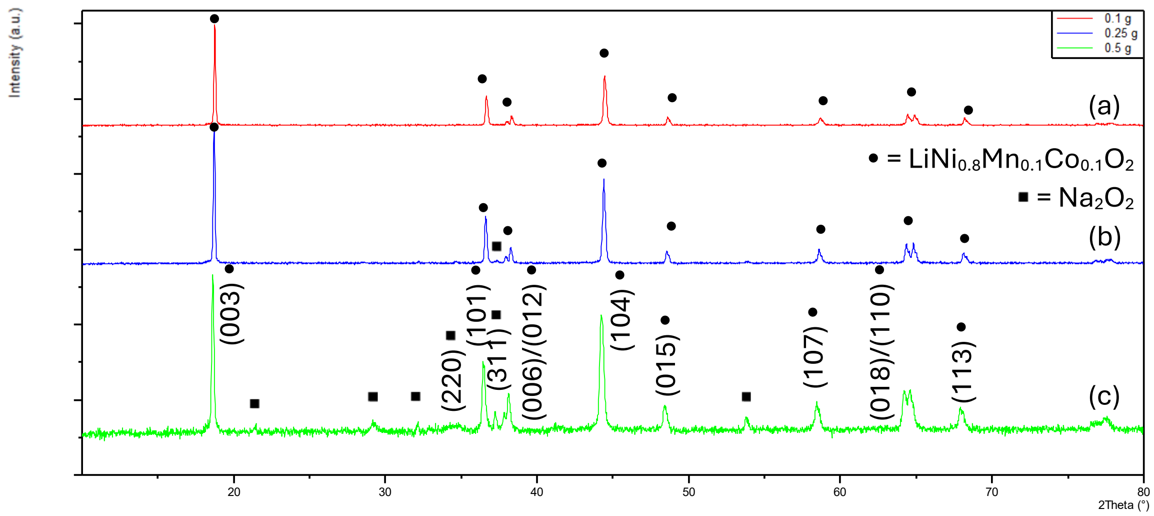

Figure 84 Calcination of NMC811 at 800 °C in oxygen with 300 °C preheat in air using nitrate precursors and a) 0.1 g, b) 0.25 g, and c) 0.5g sodium alginate biotemplate

3.5.3 Discussion when varying the biotemplate mass in the synthesis of NMC811

As such 0.25 g of dextran and 0.1 g of sodium alginate should be used when synthesising NMC811 with either precursor salts to ensure a high level of structural organisation of the NMC811. Despite an increase in the mass of the biotemplate allowing for an increased amount of chelation sites, the increased carbon content of the biotemplate caused by the mass increase appears to negatively affect the organisation of the final NMC811 more than an increase in chelation sites benefit it.

3.6 Scale up of reactants materials in the synthesis of NMC811

While increasing the mass of the biotemplate may be unnecessary, scaling up the biotemplating method by increasing the biotemplate and metal precursor salt mass is a significant step in testing both whether this method is commercially viable, but also to produce sufficient NMC811 cathode powder (active material) for the production and testing of CR2032 coin cells. In order to produce cathodes for the coin cells, a scale up of double the mass of cathode powder outlined in the method, between 0.4 and 0.5 g minimum, is required. This minimum mass is to ensure that an appropriately thick and even slurry is able to be produced from the mass of NMC811 powder synthesised such that the slurry is not inhomogeneous and uneven. The scale up of NMC811 powder needs to be investigated due to the effect an increase in the amount of carbon content in the biotemplate and precursor salt and the effect of increasing the volume of reactants relative to the size of the crucible may have on the final NMC811 product. For this investigation the same sized 50 ml crucible is used for all samples and the masses of all biotemplates and precursors, and the volume of distilled water is scaled up equally

3.6.1 Scale up of reactant materials in the synthesis of NMC811 using dextran

3.6.1.1 *Scale up of reactant materials in the synthesis of NMC811 using dextran and acetate precursors*

When scaled up, organised layered NMC811 formed using acetate precursors and dextran appears to form more readily at a higher mass than at a lower mass. The XRD patterns, Figure 85a and b, show that the scaled up NMC811 is more organised than that formed at the original mass. This is indicated in by a peak intensity ratio between 0.03 and (104) reflections of 1.60 vs. 1.54 for scaled up masses vs. masses outlined in the method respectively, as well as sharper peaks at (006)/(012) and (018)/(110) reflections for the scaled up mass. The scaled up cathode power therefore has more organised layering and less mixing of Li^+ and Ni^{2+} ions into Ni and Li sites [133].

This is in contrast to section 3.5 where an increase in the mass of the biotemplate would lead to a greater amount of carbon content in the reactants. This larger carbon content would be as a result of the decomposition of a larger mass of biotemplate, reacting with more oxygen in the O_2 atmosphere to form into a large volume of CO_2. This would produce a reducing environment that would synthesise a less organised NMC811 structure due to their being less oxygen available to fill the oxygen sites. For this combination of precursor and biotemplate, the opposite appears true, with scale up of synthesis of NMC811 possible without increased disorganisation or synthesis of additional impurities. The reason for this is due to exothermic oxidation reaction of NMC hydroxide to disorganised NMC oxide. When calcination of the masses of dextran and acetates outlined in the methods is calcined, Figure 85b, a normalised heat flow of 15 W/g occurs as heat is emitted during the reaction, Figure 59. When the mass of biotemplate and precursors is scaled up, a larger amount of heat will be emitted during the exothermic oxidation reaction as NMC hydroxide is oxidised into disorganised NMC oxide [137]. This greater amount of heat provides more energy for the decomposition of CO_2 in the atmosphere, freeing up oxygen and producing a more oxidising environment such that there is more oxygen to fill the oxygen sites during the synthesis of NMC811. This and the reduction in the mixing of Li and Ni sites leads to the synthesis of a more organised layered NMC811 structure.

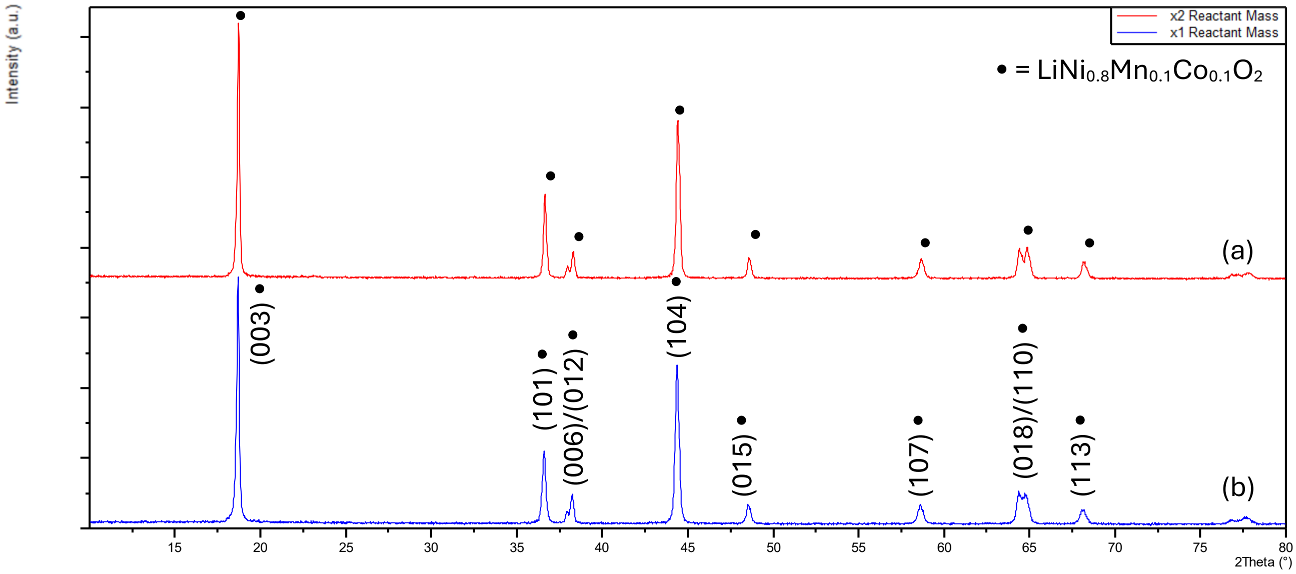

Figure 85 Calcination of NMC811 using dextran and acetate precursors 300 °C preheat and 850 °C calcination using a) x2 and b) x1 precursor and biotemplate mass relative to masses outlined in the method

3.6.1.1.1 Morphology of scaled up NMC811 synthesised with dextran and acetate precursors

When analysed using SEM scaled up NMC811 synthesised using dextran and acetate precursors, Figure 86a, consists of particles with an average diameter of 600 nm, double that of the 300 nm average diameter of particles synthesised using the masses outlined in the method, Figure 86b. The larger particles synthesised when scaled up are a further indication of a large emission of heat during the calcination process, with the particles from the scaled up mass able to grow larger and faster due to a larger amount of energy present in the reaction. The larger particle sizes however will result in less surface area for intercalation, potentially reducing cathode capacity and effecting the performance of the final produced cells. The particle morphology for the scaled up mass also differs from the sample made from the lower mass outlined in the methods, with the scaled up NMC811 consisting of individual primary particles of irregular octahedral morphologies. NMC811 synthesised from the mass of reactants outlined in the methods meanwhile consists of agglomerated primary particles of highly irregular morphologies. Despite being larger in diameter and so consists of less surface for lithium intercalation, scaled up particles may prove more effective when used as an active material in cells.

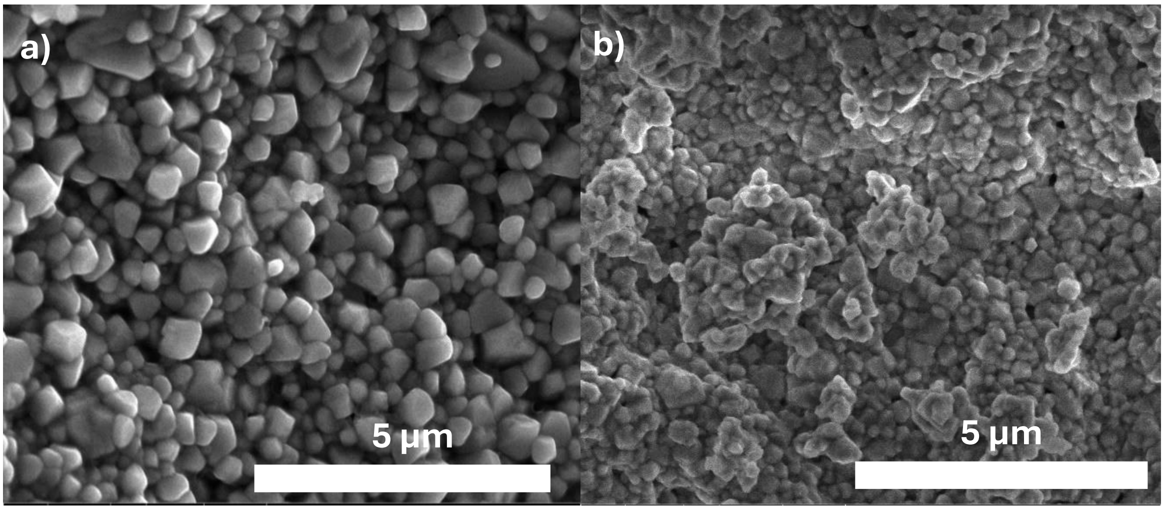

Figure 86 Morphology of NMC811 calcined using dextran and acetate precursors, 300 °C preheat, and 850 °C calcination using a) x2 and b) x1 precursor and biotemplate mass relative to masses outlined in the method

3.6.2 Scale up of reactant materials in the synthesis of NMC811 using nitrate precursors

NMC811 synthesised using dextran and nitrates was not able to be produced in large enough quantities to analysed. During preheat a significant amount of the sample is ejected from the crucible at around 150 °C as a large volume of gas is produced. The use of a lid for the crucible did not prevent the ejection of the sample, with the lid also being deposited next to the crucible. Scale up of NMC811 using nitrates and dextran can therefore not be safely done with the equipment and techniques used in this thesis.

3.6.3 Scale up of reactant materials in the synthesis of NMC811 using sodium alginate

3.6.3.1 Scale up of reactant materials in the synthesis of NMC811 using sodium alginate and acetate precursors

The scaling up of NMC811 synthesised with sodium alginate and acetate precursors results in the synthesis of layered, organised NMC811 as with using dextran and acetate precursors, Figure 85. When XRD patterns for the scaled up NMC811 and NMC811 using the mass outlined in the methods are compared, Figure 87a - b, peak intensity ratios for (003)/(104) reflections are 1.73 and 1.49 respectively with peaks at (006)/(012) and (018)/(110) reflections having strong and moderate peak splitting.

When NMC811 synthesised with the lower mass outlined in the method is calcined, a large, normalised heat flow of 10 W/g occurs when NMC hydroxide is oxidised to disorganised NMC oxide between 250 and 500 °C, Figure 71. When the mass is scaled up, the heat emitted given out from this exothermic reaction is much greater which provides the reaction with more energy. CO_2 in the environment, itself formed from the reaction between carbon freed up from the decomposed acetates and sodium alginate and the oxygen atmosphere, decomposes and frees up oxygen while also producing a more oxidising reaction that reduces the mixing of metal cations into Li and Ni site [133]. This leads to greater layering of the NMC811 and a more organised crystalline structure.

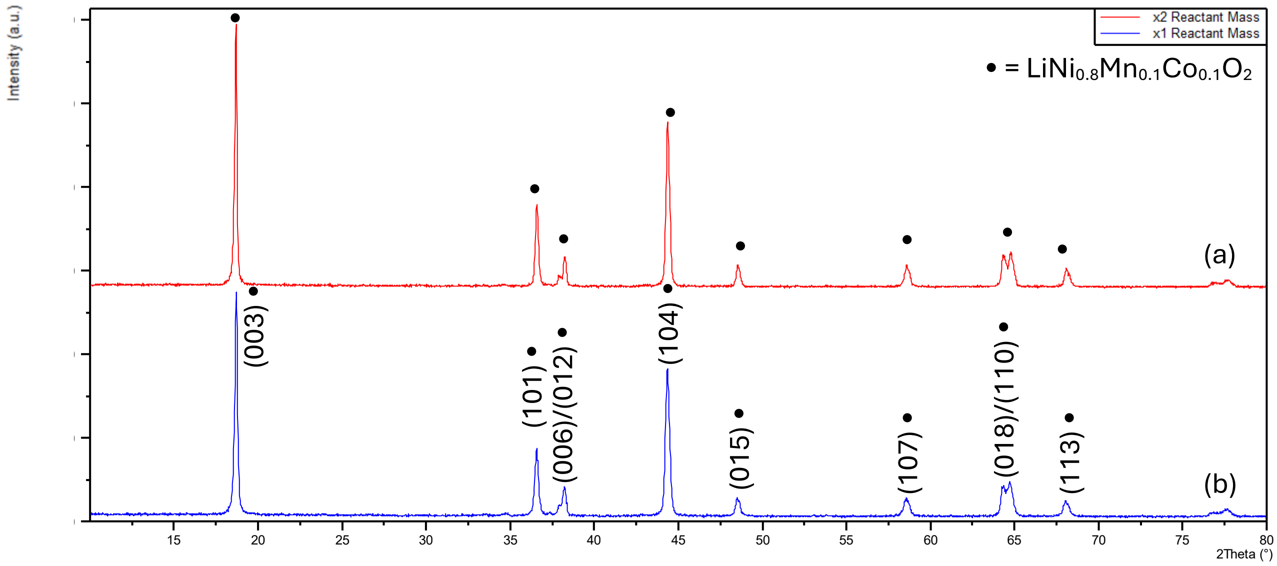

Figure 87 Calcination of NMC811 using sodium alginate and acetate precursors 300 °C preheat and 850 °C calcination using a) x2 and b) x1 precursor and biotemplate mass relative to masses outlined in the method

3.6.3.1.1 Morphology of scaled up NMC811 synthesised with sodium alginate and acetate precursors

Particle size increases with the scaling up of the mass of the sodium alginate biotemplate and acetate precursors. NMC811 with an average diameter of 400 nm is synthesised using the smaller masses stated in the methods, with the average diameter increasing to greater than 1000 nm when the mass is scaled up, Figure 88a - b. The increase in average particle diameter as the mass is scaled up is due to the larger emission of heat during the exothermic oxidation of NMC hydroxide, Figure 71, which provides the particles with energy to grow larger and quicker.

When comparing using average diameter alone, particles synthesised when scaled up are detrimental for use as cathodes in lithium ion cells, as the larger average particle size results in less surface area for intercalation to occur and a lower overall capacity. This is however a compromise with the greater organisation of the layered NMC811 structure (Figure 87a), which will increase capacity and by increasing structural stability, increase capacity retention. When the morphology of the scaled up sample is compared with that of the sample synthesised with the masses outlined in the methods, both samples consist of primary particles with irregular octahedral morphologies with the only difference being the sample synthesised with the original masses contains small agglomerations of secondary particles on the surfaces of the primary particles.

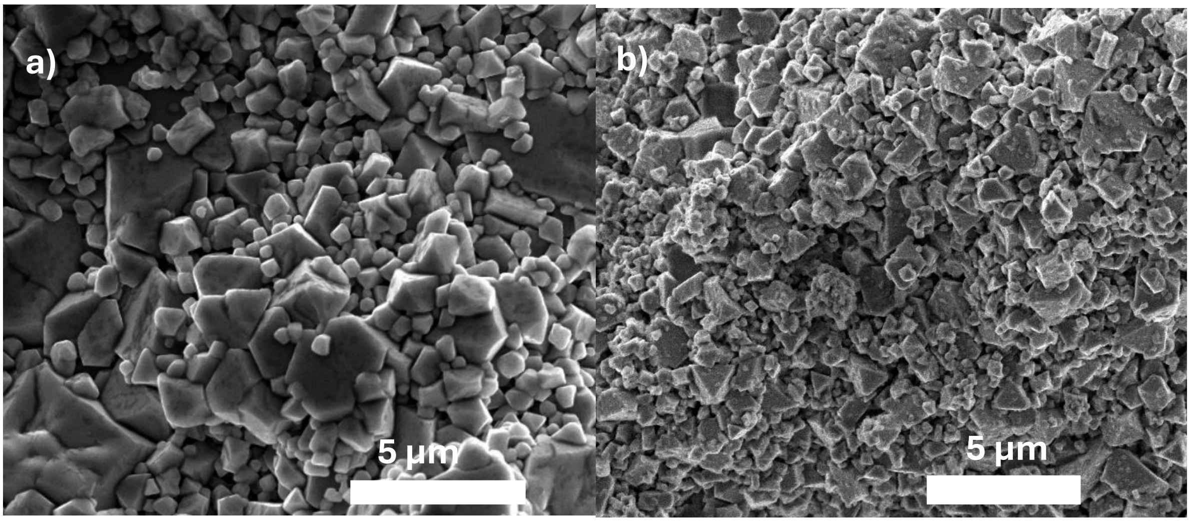

Figure 88 Morphology of NMC811 calcined using sodium alginate and acetate precursors, 300 °C preheat, and 850 °C calcination using a) x2 and b) x1 precursor and biotemplate mass

3.6.3.2 Scale up of reactant materials in the synthesis of NMC811 using nitrate precursors

For the combination of sodium alginate and nitrate precursors, scaling up the precursors and biotemplate may be detrimental to the organisation of the final NMC811 product. Peak intensity ratios between reflections (003) and (104) for NMC811 synthesised with the scaled up mass and mass of reactants as outlined in the method are 1.53 and 1.92 respectively, Figure 89a-b, while the peak splitting of the twin peaks at (006)/102 and (018)/(110) appear to be strong for both masses of precursors and biotemplate. Good layering of the NMC811 structure is present in both samples, however the scaled up sample has greater mixing of Li^+ and Ni^{2+} cations in Ni and Li sites as indicated by a lower (003)/(104) peak intensity ratio [133].

This is in line with existing evidence that an increase in precursor and biotemplate mass would result in an increase in the content of carbon in the reactants, which would decompose into a greater volume of carbon dioxide and produce a more reducing atmosphere. Such carbon would be obtained from the decomposition of the biotemplate and acetate precursors and would result in a more reducing atmosphere as the amount of oxygen is reduced as the carbon reacts with the oxygen in the atmosphere to produce carbon dioxide. When the exothermic oxidation of NMC hydroxide occurs, the reaction takes place slower over a longer temperature range, exhibiting a maximum normalised heat flow of only 3 W/g, Figure 77. There isn't therefore a large amount of energy released to decompose the CO_2 in the environment and so a reducing atmosphere is maintained. The resulting reducing atmosphere would then result in greater mixing of cation of the final NMC811 product as less oxygen is available for the synthesis of stoichiometric NMC811 and fill up the oxygen sites. The organisation of the scaled up NMC811 is still however sufficient for the production of NMC811 cathodes, though is not as organised as NMC811 synthesised under the original masses.

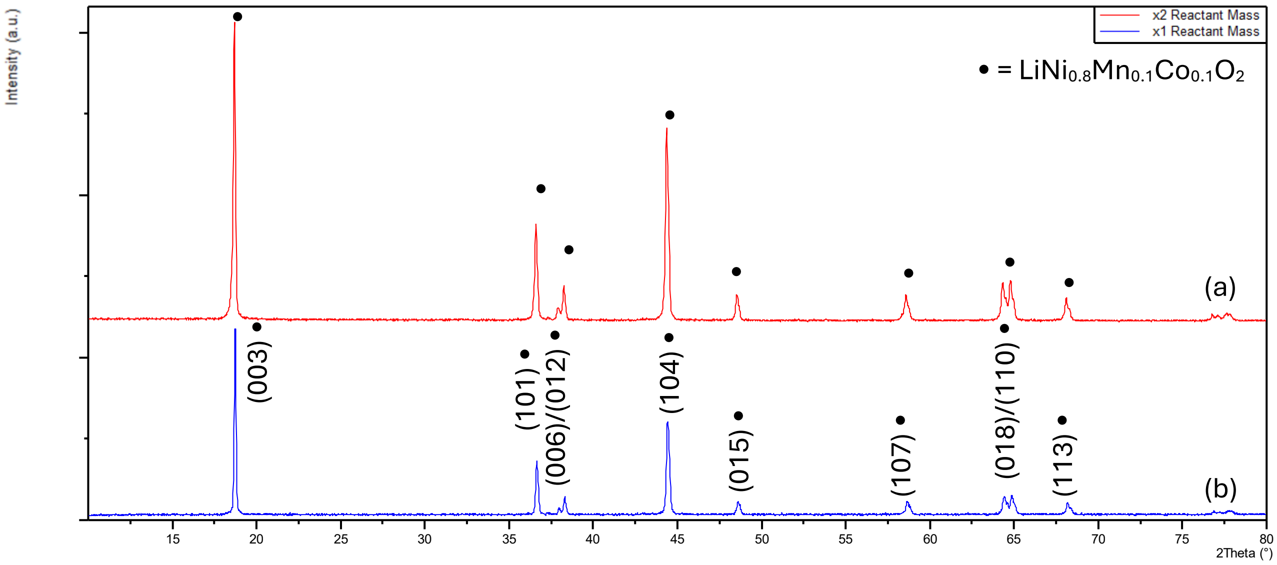

Figure 89 Calcination of NMC811 using sodium alginate and nitrate precursors 300 °C preheat and 800 °C calcination using a) x2 and b) x1 precursor and biotemplate mass

3.6.3.2.1 Morphology of scaled up NMC811 synthesised with dextran and acetate precursors

When examined under SEM particles synthesised when scale up have a smaller average diameter of 600 nm, Figure 90a, with those synthesised using the base mass outlined in the method of reactants having an average particle diameter of 900 nm, Figure 90b. This highlights how the synthesis conditions for the scaled up sample were such that particles were not provided sufficient energy able to grow as much as the sample synthesised with the base mass. It is reiterated that due to a longer oxidation process that gives out less energy, particles in the scaled up sample were not subject to a large increase in heat that led to the growth of the particles. The smaller particle sizes are beneficial by providing a greater surface area for lithiation of the cathode, which will increase specific discharge capacity, while particles of both samples exhibit irregular rounded morphologies with no obvious difference in shape between them other than size. As the organisation of scaled up NMC811 is still sufficient with only minor mixing of cation sites, scale up of sodium alginate and nitrate-based cathodes is viable.

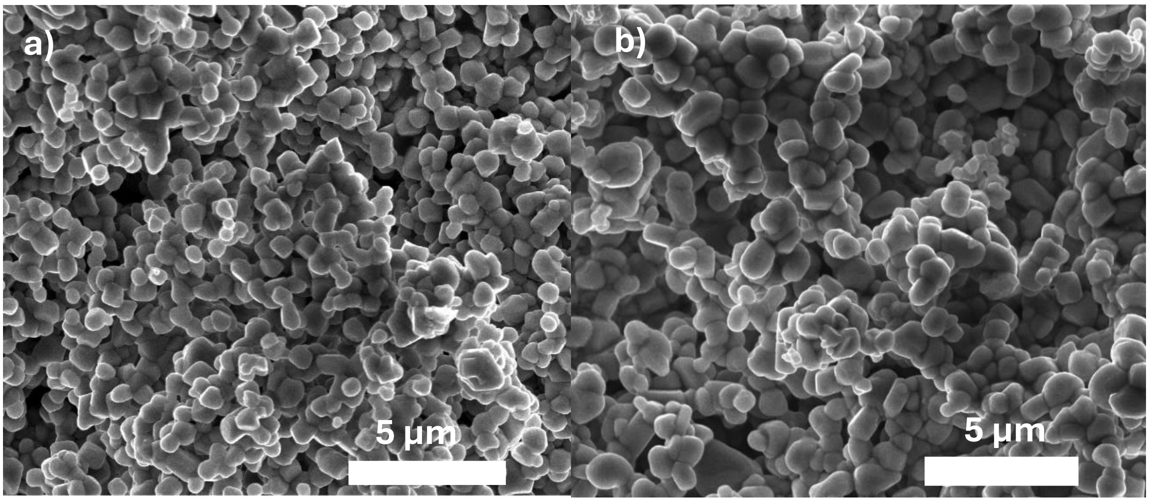

Figure 90 Morphology of NMC811 calcined using sodium alginate and nitrate precursors, 300 °C preheat, and 850 °C calcination using a) x2 and b) x1 precursor and biotemplate mass relative to masses outlined in the method

3.6.4 Discussion when scaling up reactant materials in the synthesis of NMC811

Scale up of the biotemplating process when using dextran and sodium alginate is not only viable but may also benefit the overall structure of the cathode powder. When using acetates in association with dextran or sodium alginate the scaling up of the cathode powder leads to a more organised layered NMC811 structure with smaller scale particles with octahedral and octagonal morphologies due to the exothermic oxidation of NMC hydroxide giving out the energy required to decompose CO_2 in the atmosphere and produce a more oxidising environment as oxygen is freed up from the decomposition of the CO_2. As such scale up using acetates is very much viable. When using nitrates with sodium alginate the opposite is true, and a scale up in mass will lead to greater mixing of cation sites and larger particles as the exothermic reaction takes place over a larger temperature range. This scale up is still viable however, unlike the combination of dextran and nitrates which were not investigated due to safety issues and significant loss of the sample during the preheat stage due to a sudden ejection of the sample from the crucible.

3.7 Cell cycling for lithium-ion cells using biotemplated NMC811 cathodes

Having refined and scaled up the synthesis of the NMC811 cathodes using the biotemplating method, the cathode powders using each combination of biotemplate and precursors can now be used to make lithium-ion coin cells as per the method outlined in 2.3, with the exception of the combination of dextran and nitrates which was unable to be scaled up due to safety reasons. Cells were tested in order to determine a) if initial discharge capacity was maintained or improved when compared against standard NMC811 cells [139] and b) if capacity retention is improved when compared against standard NMC811 cells. Cells are also cycled between 4.2 V and 3 V, and 4.5 V and 2.8 V respectively, in order to investigate the effect of biotemplating on structural stability when high nickel lithium ion cells are subject to the H2 to H3 phase change above 4.2 , with this phase change often being referenced as a significant reason for capacity fade in NMC cathode [127].

3.7.1 Cycling of Li-ion cells using commercial NMC811 cathode powder between 4.5 V to 2.8 V

Commercial NMC811 active material purchased from Pi-KEM, analysed in 3.2.1, is used to make lithium-ion coin cells. With the exception of the source of the active material, the method used for making lithium-ion coin cells from biotemplated NMC811 is identical to that outlined in the method. When cycled for 50 cycles at 0.1 C between 4.5 and 2.8 V, a high initial capacity of between 175 and (110) mAh/g is achieved across all three lithium-ion cells, Figure 91b, e, and h, before a significant drop off in capacity which decreases with each cycle as the overall capacity decreases. This is characteristic of a lithium-ion cell cycled to 4.5 V, where the structure of standard NMC811 cathodes will begin to break down when charged above 4.2 V due to overcharging and too much de-intercalation of lithium within the cathode. This in turn causes the cathode structure to collapse upon overcharging, resulting in less area for lithium intercalation and a smaller capacity with each cycle.

This is highlighted in Figure 91a, whereby the second discharge cycle is shown to have an erratic increase in capacity. This is indicative of a significant change in the cathode structure as an excessive amount of lithium de-intercalates from the cathode. Further evidence of degradation in the cathode structure is seen in the differential capacity curves, Figure 91c, f, and I, which highlight 4 main peaks. Differential capacity is a good indicator of state of health (SoH) and so investigating it will provide evidence on the stability of the NMC811 cathode. During the first cycle, peaks during charging at 3.7 and 3.8 V indicate oxidation of Mn^{3+} to Mn^{4+} and Ni^{2+} to Ni^{3+} and Ni^{4+}, respectively, which represents phase changes of H1 to M (hexagonal 1 to monoclinic) and M to H2 (monoclinic to hexagonal 2), while the peak at 4.2V represents the phase change H2 to H3 (hexagonal 2 to hexagonal 3). During discharge the peak at 4.2 V indicates a phase change from H3 to H2, the peak between 3.7 and 3.9 V (depending on the cell being cycled) is a phase change from H2 to M and a reduction of Ni^{4+} to Ni^{2+} and Co^{4+} to Co^{2+}, while the reduction of Mn^{4+} to Mn^{3+} and the phase change from M to H1 occurs at 3.55 V.

In subsequent cycles, voltage and capacity fade of the cathode occurs whereby peaks during charging occurs at higher voltages and during discharge peaks occur at a lower voltage. Within the first cycles, voltage is no longer high enough for the H2 to H3 phase change due to deterioration of the structure, leading to a reduction in capacity [140]. As the cell is continued to be cycled, the voltage at which the M to H2 and then H1 to M phases occur at too high a voltage, which as the cell approaches 50 cycles results in no phase change during cycles and cell failure.

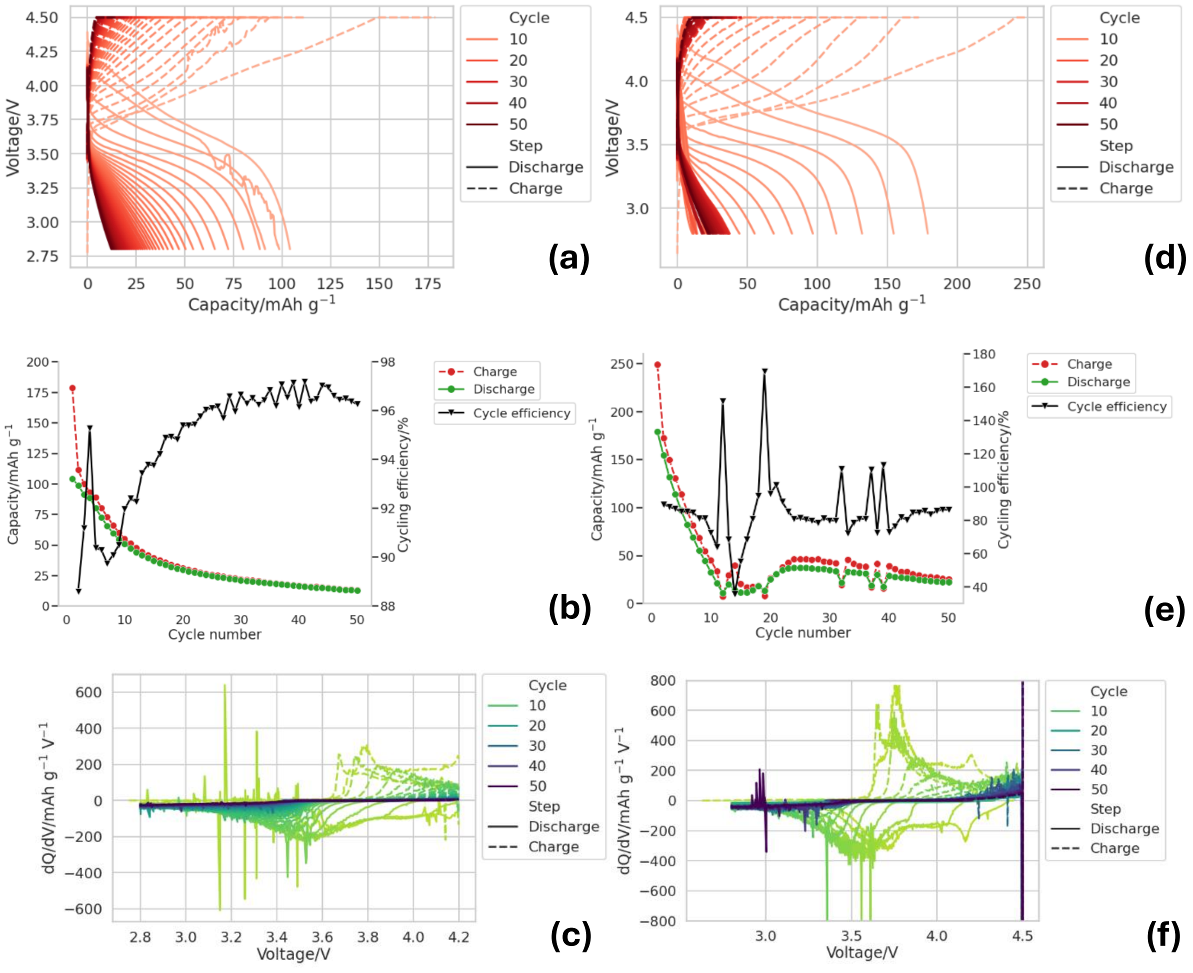

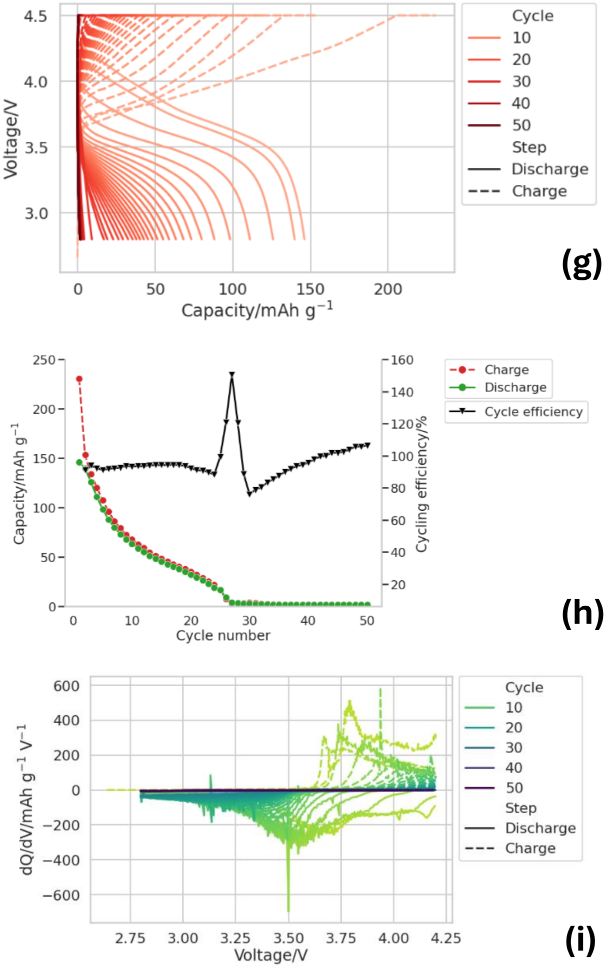

Figure 91 Charge-discharge cycling (a, d, g), Cycling efficiency and charge-discharge capacities (b, e, h), and Differential capacity vs. voltage curve (c, f, i), for Li-ion coin cells 1-3 with commercial NMC811 Cathode cycled between 4.5 and 2.8 V for 50 cycles

3.7.2 Cycling of Li-ion cells using dextran biotemplated NMC811 cathode powder

3.7.2.1 Cycling of Li-ion cells using acetate precursors synthesised NMC811 cathode power

3.7.2.1.1 Cycling of Li-ion cells synthesised with dextran and acetate precursors between 4.2 V – 3 V

Li-ion coin cells using NMC811 cathodes synthesised with acetate precursors and dextran biotemplating shows high cycling retention but a relatively lower overall capacity in comparison to control NMC811 cathodes, Figure 91, when cycled between 4.2 and 3 V for 50 cycles. Discharge capacity at the first cycle for both cells, Figure 92b and e, is shown to be between 150 and 160 mAh/g, decreasing at an average rate of 0.2 mAh/g over 50 cycles to between 140 and 150 mAh/g. NMC811 biotemplated with dextran produces a cathode that is structurally very stable and does not collapse upon deintercalation of lithium. Peaks during charging at 3.7 and 3.8 V, Figure 92c shows the cathode undergoes phase changes from H1 to M and M to H2, with during discharge at 3.9 and 3.7 V, Figure 92 f show the cathode undergoes the phase transitions H2 to M and M to H1, respectively. As the cell is only being cycled to 4.2 V, there is no H2 to H3 phase change normally associated with the cycling of high nickel cathodes [127]. With the exception of some high differential capacity peaks during the first charge and discharge cycle, the peaks in the differential capacity curves occur at the same voltages at each cycle indicating little voltage or capacity fade. This is highly beneficial to NMC811 which are known to be unstable during cycling. This is at the cost of overall capacity however, with a reduction of at least 50 mAh/g when compared to current NMC811 cathodes [139]. The relative lack of capacity is due to reduction in lithiation sites compared to other NMC811 cathodes, with an average particle size of 600 nm, Figure 85, having a lower surface area resulting in a lower capacity.

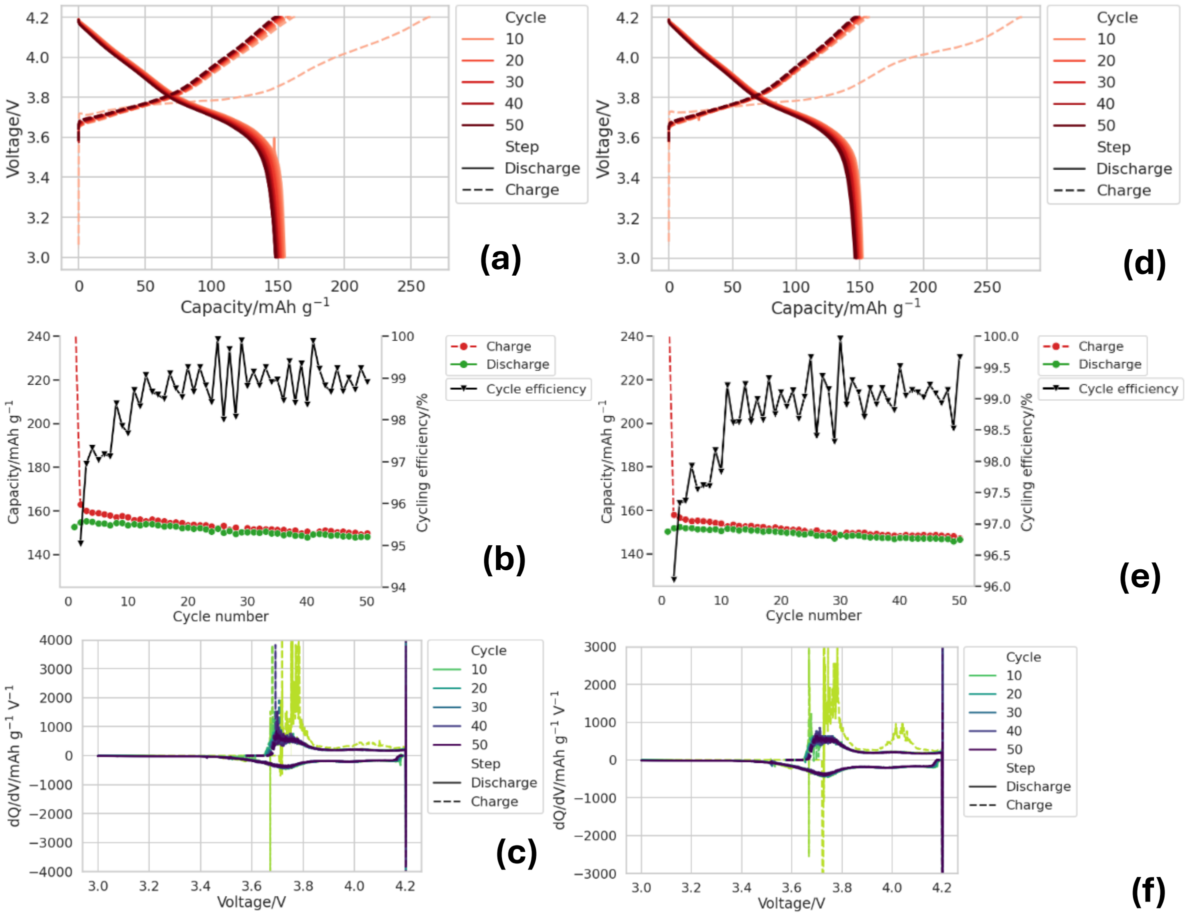

Figure 92 Charge-discharge cycling (a, d), Cycling efficiency and charge-discharge capacities (b, e), and Differential capacity vs. voltage curve (c, f), for Li-ion coin cells 1 and 2 with acetate and dextran synthesised cathodes between 4.2 and 3.0 V for 50 cycles

3.7.2.1.2 Cycling of Li-ion cells synthesised with dextran and acetate precursors between 4.5 V – 2.8 V

When cycled between 4.5 and 2.8 V, cells produced with the same dextran and acetate-synthesised cathodes have a higher initial capacity, between 160 and 200 mAh/g, Figure 93 b, e, h, than both control Pi-Kem cells cycled at 4.5 to 2.8 V, (110) to 180 mAh/g, Figure 91, and dextran and acetate synthesised cells cycled between 4.2 and 3 V, 150 to 160 mAh/g, Figure 92, respectively. Capacity retention meanwhile is very poor, dropping to between 50 and 0 mAh/g after 50 cycles. This is comparable to Pi-Kem cells cycled between 4.5 and 2.8 V but is significantly worse than the 10 mAh/g capacity drop over 50 cycles when the same dextran-acetate synthesised cathodes are cycles between 4.2 and 3 V. The differential capacity curves, Figure 93 c, f, i, show H1 to M, M to H2, and H2 to H3 phase transitions at 3.7, 3.8 and 4.2 V during charging and phase transitions from H3 to H2, H2 to M, and M to H1 at 4.1, 3.7, and 3.5 V during discharge. Transition from the H2 to H3 phase leads to structure instability with the required voltage for the phase change increasing [127]. Approaching 20 cycles, the voltage required for the M to H2 phase transition increases beyond 4.5 V, with the voltage for the H1 to M phase transition shifting above 4.2 V at 50 cycles. After 50 cycles, as the cathode can only phase transition between H1 and M phases up to 4.5 V, specific discharge capacity is 50 mAh/g.

This highlights how there is sufficient particle area in the dextran-biotemplated NMC811 structure for lithium intercalation to occur such that an initial discharge capacity during the first cycle can reach 200 mAh/g, and that for at least the initial cycle deintercalation of all this lithium is able to occur due to the structure being stable enough to maintain ionic conductivity pathways. However, biotemplating with dextran still results in an unstable NMC811 structure whereby if the cell is cycled above 4.2 V the H2 to H3 phase change will result in significant capacity fade.

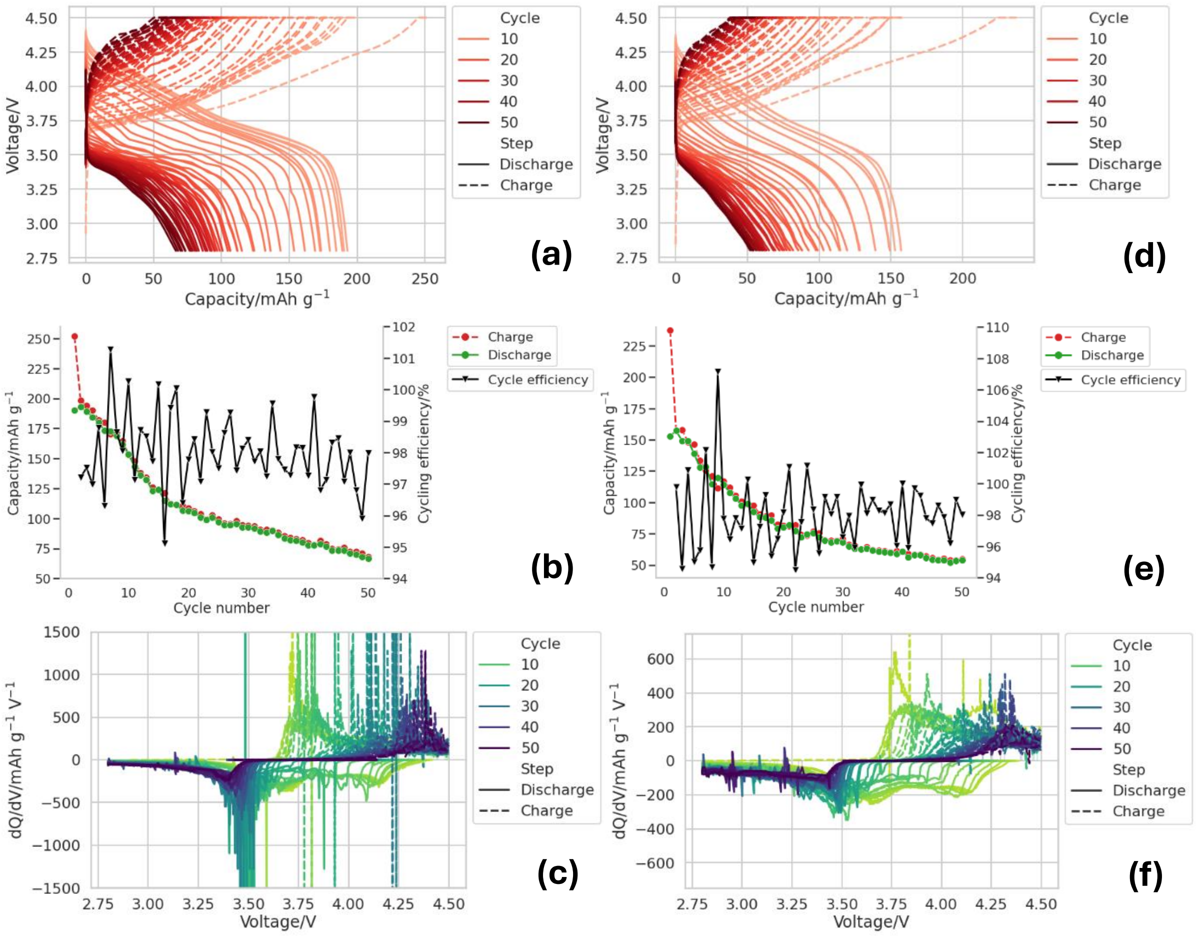
Voltage/V
Capacity/mAh g^{-1}
Cycle
10
20
30
40
50
Step
Discharge
Charge
(a)
(d)
Capacity/mAh g^{-1}
Cycling efficiency/%
Cycle number
Charge
Discharge
Cycle efficiency
(b)
(e)
dQ/dV/mAh g^{-1} V^{-1}
Voltage/V
(c)
(f)

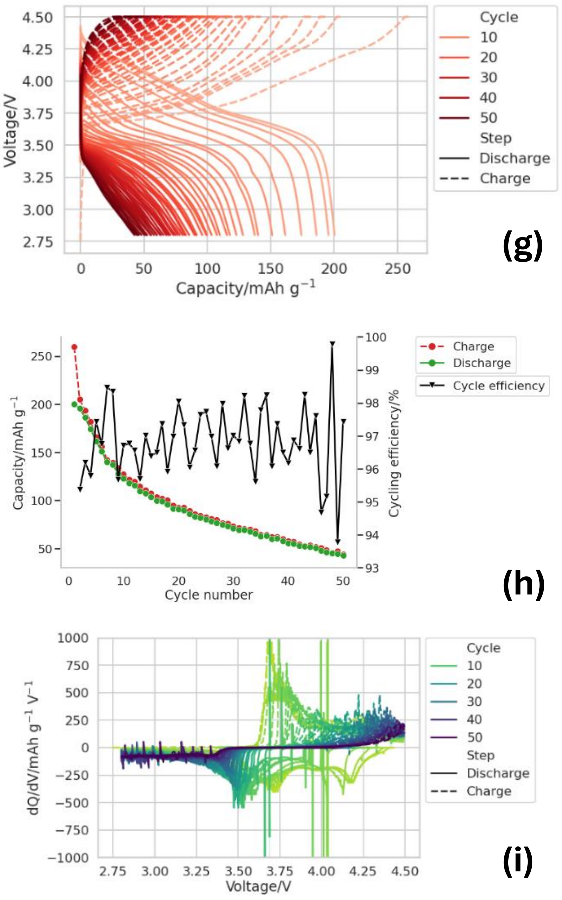

Figure 93 Charge-discharge cycling (a, d, g), Cycling efficiency and charge-discharge capacities (b, e ,h), and Differential capacity vs. voltage curve (c, f, I), for Li-ion coin cells 1-4 with acetate and dextran synthesised cathodes between 4.5 and 2.8 V for 50 cycles

3.7.3 Cycling of Li-ion cells using sodium alginate biotemplated NMC811 cathode powder

3.7.3.1 Cycling of Li-ion cells using acetate precursors synthesised NMC811 cathode power

3.7.3.1.1 Cycling of Li-ion cells synthesised with sodium alginate and acetate precursors between 4.2 V – 3 V

When lithium-ion cells are made using acetate precursors with sodium alginate biotemplate, the initial discharge capacity when cycled between 4.2 and 3 V, Figure 94b, is 140 mAh/g, lower than the initial discharge capacity of 150 to 160 mAh/g when the cathode is synthesised using acetate precursors but with dextran and cycled at the same voltage range, Figure 92. The lower initial discharge capacity can be attributed to an average particle size of > 1 µm, Figure 88a, compared to 600 nm when using dextran with acetate precursors, Figure 86a. Larger particle diameters will result in less particle surface area, allowing less lithium to intercalate in the cathode and reducing the initial discharge capacity.

Capacity retention is comparable to using dextran and acetates however, with a 10 mAh/g reduction in discharge capacity over 50 cycles. The differential capacity curve, Figure 94c, shows there is a significant structural change when charging during the first cycle at 3.8 V as the phase transitions from the M to H2 phase, as well as a high differential capacity peak signifying a large structural change at 3.7 V when the H1 phase transitions to M during subsequent cycles. As the cell is only cycled to 4.2 V there is no H2 to H3 phase change, and so phase changes during charging at 3.7 and 3.8 V from H1 to M and M to H2 respectively, and H2 to M and M to H1 phase changes at 3.9 and 3.7 V during discharge [140] show little to no voltage fade after the first cycle. As such there is minimal capacity drop across the 50 cycles. Like when using dextran, biotemplating using sodium alginate produces a highly stable structure that resists reorganisation upon de-lithiation to the cathode, highlighted by the high capacity retention.

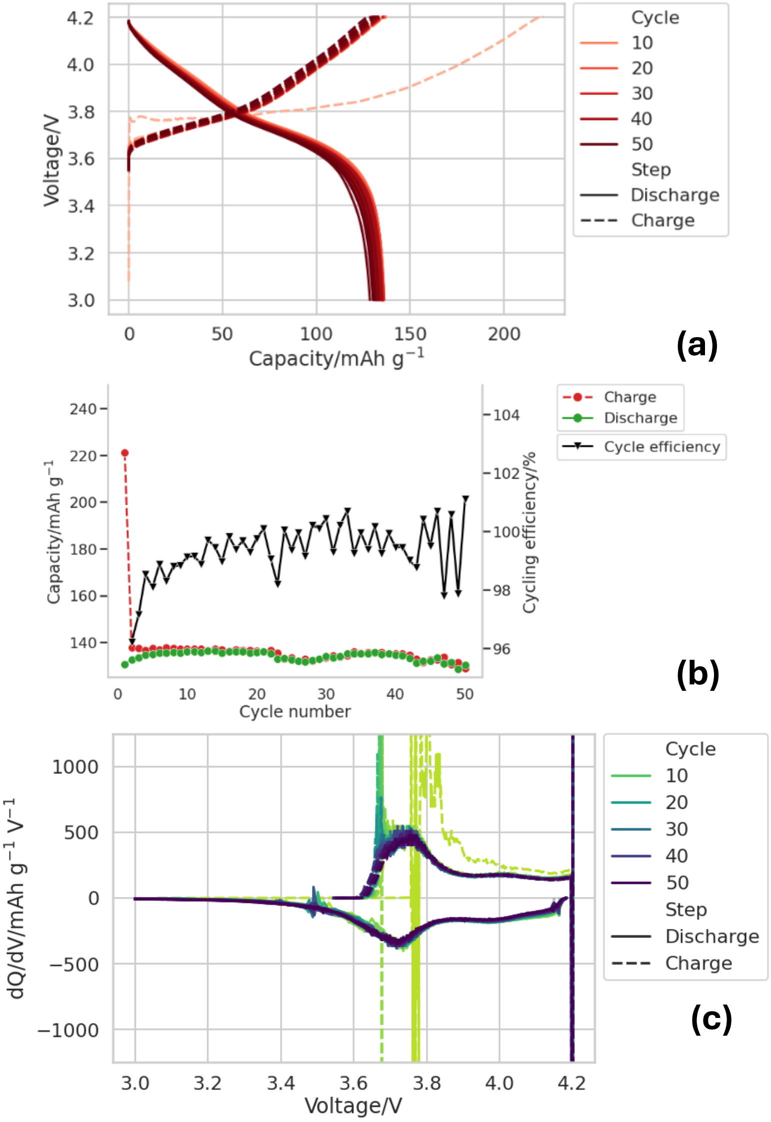

Figure 94 Charge-discharge cycling (a), Cycling efficiency and charge-discharge capacities (b), and Differential capacity vs. voltage curve (c) for Li-ion coin cell with acetate and sodium alginate synthesised cathode between 4.2 and 3.0 V for 50 cycles

3.7.3.1.2 Cycling of Li-ion cells synthesised with sodium alginate and acetate precursors between 4.5 V – 2.8 V

When cycled between 4.5 and 2.8 V, initial discharge capacities for the three tested cells range between 150 and 180 mAh/g, Figure 95 b, e, h. This is slightly below the 160 to 200 mAh/g when dextran and acetate synthesised cathodes are cycled at the state voltage range, Figure 93, due to a larger particle diameter of at least 400 nm which restricts possible lithiation sites and capacities, Figure 86a and Figure 88a. An increase of between 10 and 40 mAh/g when compared to the same cathode cycled at 4.2 to 3 V, Figure 94, indicates full di-lithiation of the cathode occurs at the cost of structural instability.

When cycled between 4.5 and 2.8 V capacity retention is very poor, with a discharge capacity of between 0 and 20 mAh/g for all cells after 50 cycles. The poor capacity retention is again in part due to the structural rearrangement of NMC811 when full de-lithiation of the cathode takes place above 4.2 V. When the cell is charged, the phase transitions of H1 to M at 3.7, M to H2 at 3.9 V, and H2 to H3 at 4.2 V occurs with phase changes during discharge of H3 to H2 at 4.2 V, H2 to M at 3.7 V, and M to H1 at 3.6 V. An initial large structural change can be observed during the first cycle during the H1 to M phase change, and Due to the H2 to H3 phase change large structural instability occurs above 4.2 V which increases the required voltage of each phase change as the number of cycles increases. This leads to severe capacity retention as the structure becomes such that the phase change of H1 to M phases requires a voltage greater than 4.2 V.

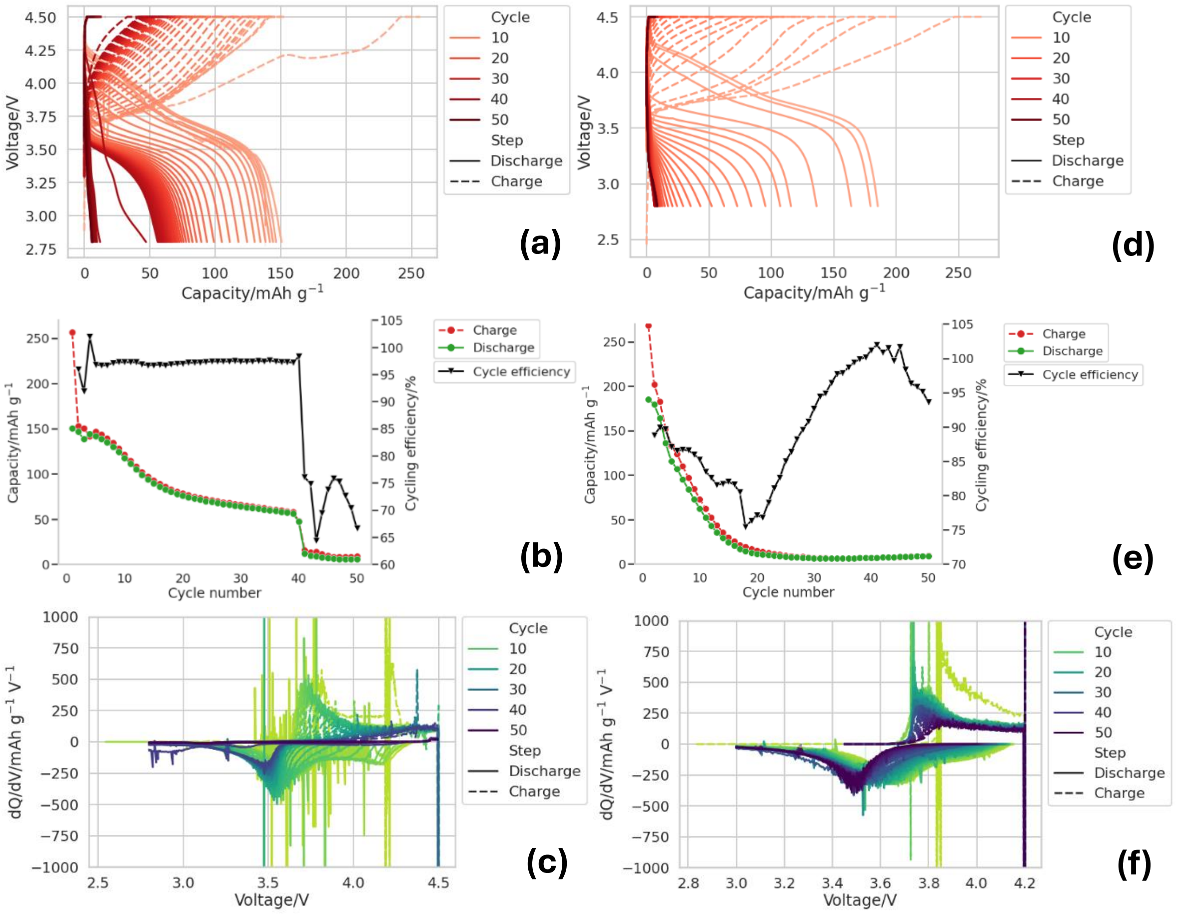

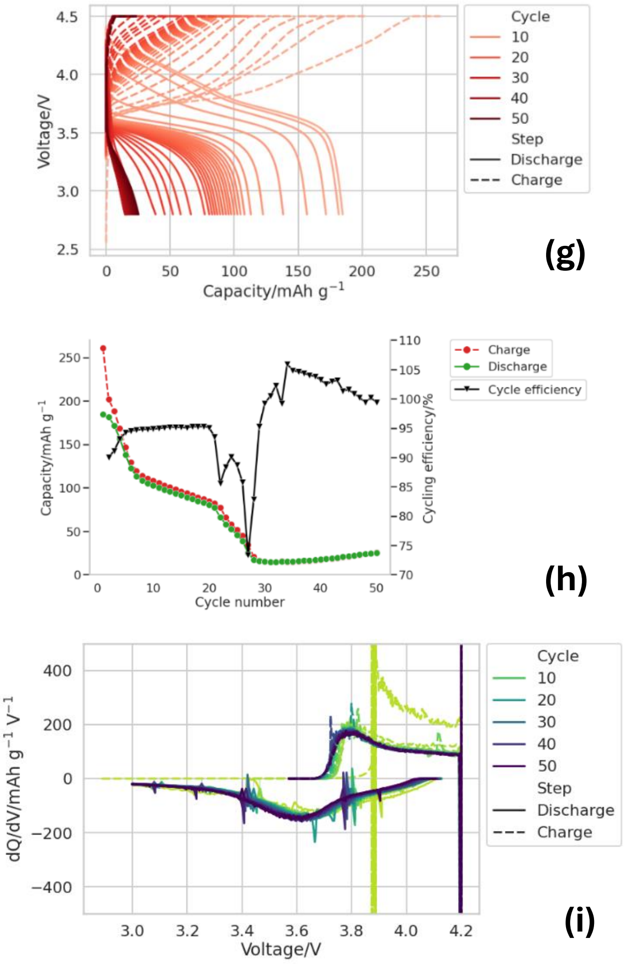

Figure 95 Charge-discharge cycling (a, d, g), Cycling efficiency and charge-discharge capacities (b, e, h), and Differential capacity vs. voltage curve (c, f, i), for Li-ion coin cells 1-3 with acetate and sodium alginate synthesised cathodes between 4.5 and 2.8 V for 50 cycles

3.7.3.2 Cycling of Li-ion cells using nitrate precursors synthesised NMC811 cathode power

3.7.3.2.1 Cycling of Li-ion cells synthesised with sodium alginate and nitrate precursors between 4.2 V – 3 V

The combination of sodium alginate and nitrates produces NMC811 cathodes with the largest initial discharge capacity. When cycled between 4.2 and 3 V, an initial discharge capacity of 240 mAh/g, Figure 96b, 40 mAh/g higher than the capacity of other biotemplated cathodes. An average particle diameter of 600 nm, Figure 90a, gives a high surface area, large number of lithiation sites, and so a high discharge capacity.

A capacity retention of 30 mAh/g loss over 50 cycles, Figure 96b, when cycled between 4.2 and 3 V shows the high capacity come at the cost of increased capacity fade. As the maximum cycling voltage is 4.2 V, the cell does not undergo a phase change of H2 to H3, however it does undergo a phase change of H1 to M at 3.6 V and M to H2 at 4 V when charging. During discharge, phase changes of H2 to M and M to H1 occurs at 4 V and 3.7 V, respectively. A significant peak at 3.6 V shows a large structural change during the first cycle during the H1 to M phase change. While there is little voltage fade from the phase changes, a decrease in the differential capacity during phase changes denotes small structural changes during cycling that leads to the small amount of capacity fade of 30 mAh/g over 50 cycles.

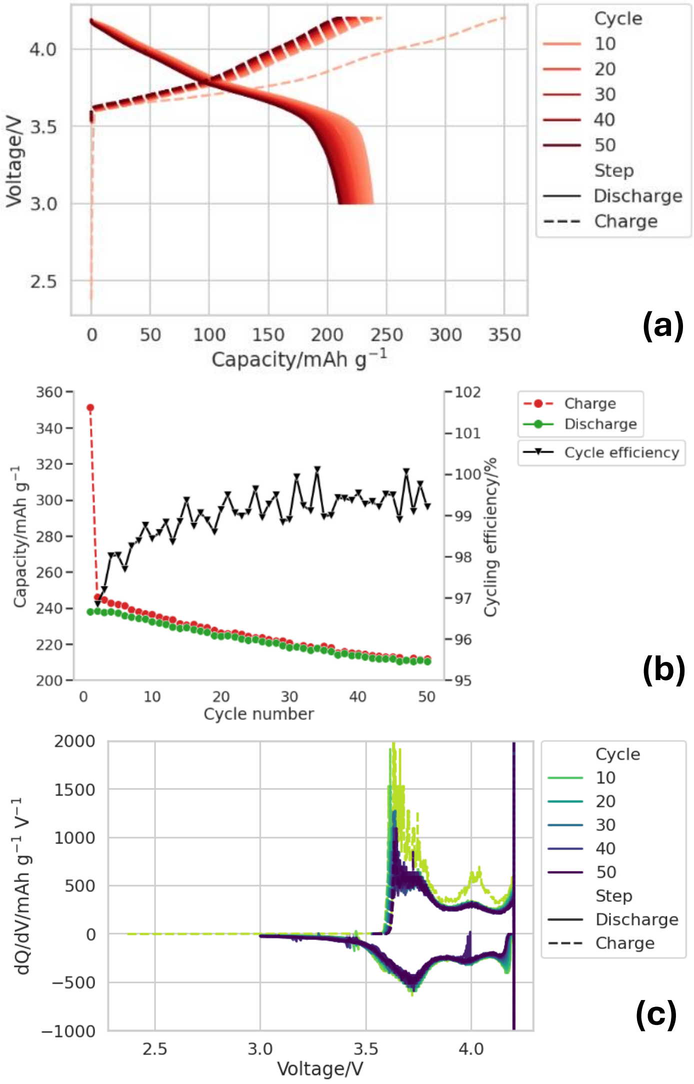

Figure 96 Charge-discharge cycling (a), Cycling efficiency and charge-discharge capacities (b), and Differential capacity vs. voltage curve (c) for Li-ion coin cell with nitrates and sodium alginate synthesised cathode between 4.2 and 3.0 V for 50 cycles

3.7.3.2.2 Cycling of Li-ion cells synthesised with sodium alginate and nitrate precursors between 4.5 V – 2.8 V

When cycled at 4.5 to 2.8 V, cells with cathodes made of the same biotemplate and precursors have a lower initial discharge capacity of 170 to 200 mAh/g, Figure 97b, e, h, and a worse capacity retention of a 90 to 180 mAh/g decrease over 50 cycles compared to the same cathode cycled at 4.2 to 3V, Figure 96. The low capacity retention when cycled between 4.5 and 2.8 V indicates low structural stability as de-lithiation occurs and the cathode rearranges. Differential capacity curves, Figure 97c, f, I, indicate phase changes during the initial charge cycle of H1 to M at 3.7 V, M to H2 at 3.8 V, and H2 to H3 at 4.2 V, with phase transitions of discharge cycling of H3 to H2 at 4.1 V, H2 to M at 3.7 V, and M to H1 at 3.5 V. Significant differential capacity peaks are also present during the initial cycle and subsequent cycles, representing structural changes due to high instability.

For cells 1 and 2, Figure 97c and f, the instability caused by the H2 to H3 phase transition [127] resulting in a large increase in the required voltage for all phase changes during the charge cycle as the number of cycles completed increased. This eventually results in cell failure as the H1 to

M phase change requires a voltage greater than 4.2 V. For cell 3, Figure 97i, despite a significant differential capacity peak at 3.7 V during charge, and the increase in the required voltage for the H2 to H3 phase change, the change in the required voltage for the H1 to M and M to H2 phase transitions after 50 cycles is 3.7 and 4 V respectively for both charge and discharge cycles. A discharge capacity of 150 mAh/g is therefore possible after 50 cycles despite the H2 to H3 transition being outside the 4.5 V upper voltage limit. The decrease in initial discharge capacity when cycling at a larger voltage range shows how the combination of sodium alginate and nitrates is not able to produce a structure whereby full de-lithiation is able to occur. The structural instability caused by cycling at a voltage greater than 4.2 V is such that less lithium is able to be extracted from the cathode than when the same cathode is cycled between 4.2 and 3 V, indicating a highly unstable structure above 4.2 V.

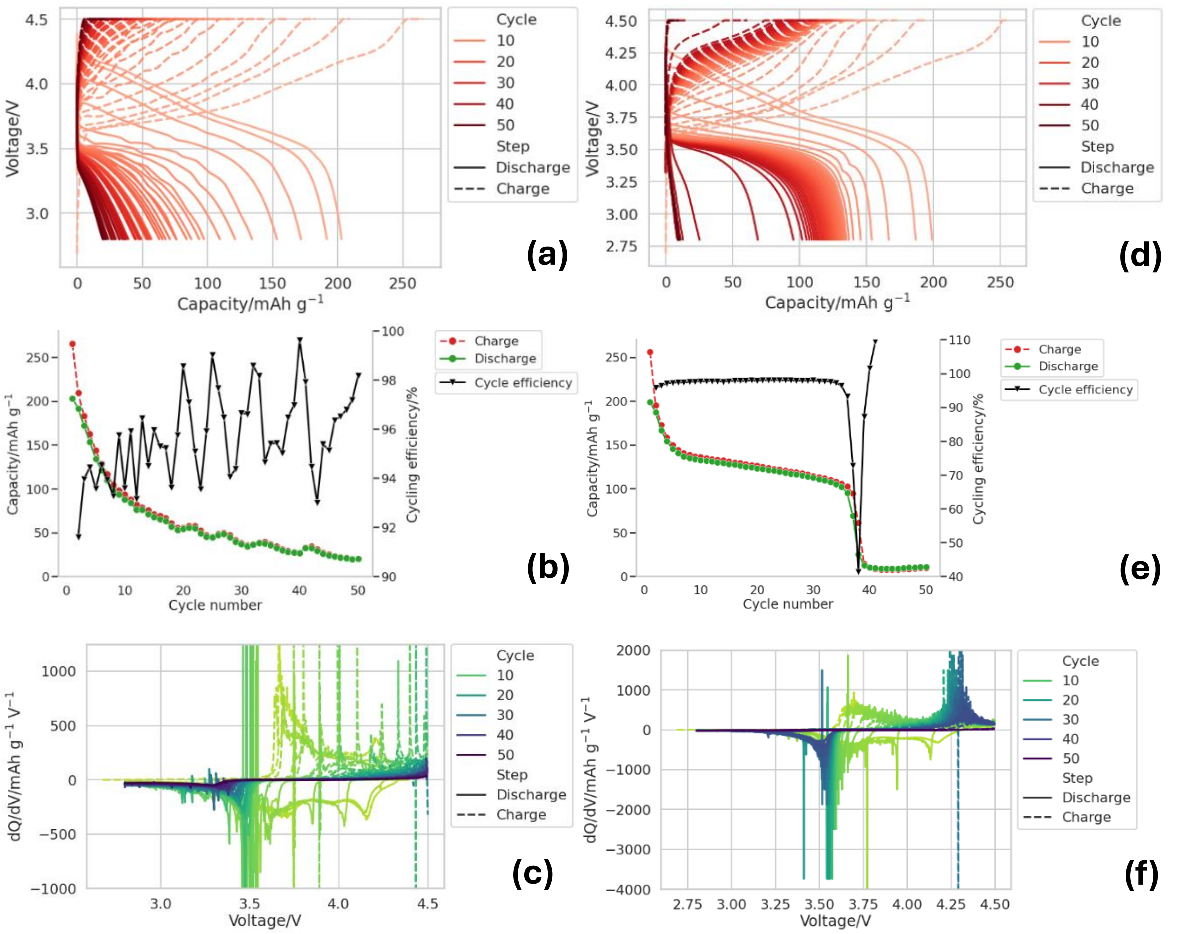

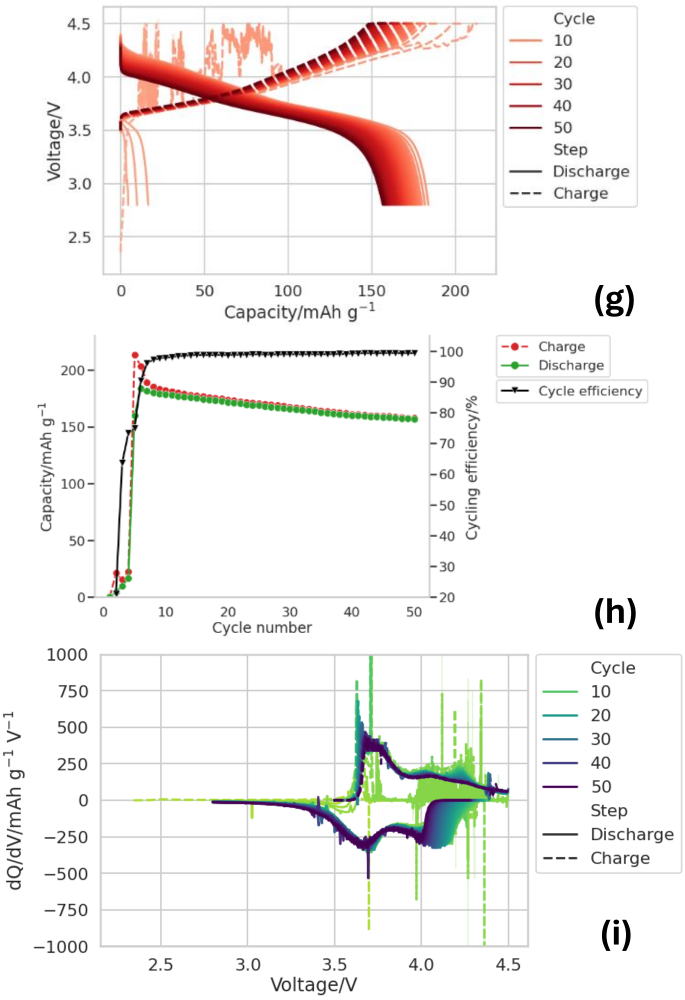

Figure 97 Charge-discharge cycling (a, d, g), Cycling efficiency and charge-discharge capacities (b, e , h), and Differential capacity vs. voltage curve (c, f, I), for Li-ion coin cells 1-3 with nitrate and sodium alginate synthesised cathodes between 4.5 and 2.8 V for 50 cycles

3.7.4 Effects of cell manufacture on cell performance

While the changes in the NMC811 structure as the cathode underwent lithiation and delithiation may have contributed to poor capacity and/or cycling stability, further variables related to the manufacturing process of the lithium-ion cells may also have contributed to the poor performance of some cells. Such variables may also have contributed to the differences in performance between cells manufactured using the same cathodes, despite attempts to use the same process to manufacture each cell outlined in 2.3.

One issue may have been the quality of the lithium metal used in the cell. Lithium chips of diameter 12.5 mm were used which due to supply issues were often stored for lengths of time of upwards of a year before use. While stored in a glovebox under argon, oxidisation of the chips as well as bending of the chips often occurred, and while attempts were made to brush off the oxidation and flatten the chips before use the oxidation, bending, and cleaning of the chips could lead to damage. This damage could include introduction of an oxide into the coin cell or the removal of too much lithium from the chip while removing the oxide which in serious cases could lead to holes in the chips, both of which would be detrimental to the cell's performance and reduce the cathode capacity.

In a similar case, the electrolyte was also stored for upwards of a year in the glovebox. As such the electrolyte could have deteriorated or may have contained traces of water during its storage, leading to further poor performance. Furthermore, due to the time constraints of the project only one electrolyte was use; $LiPF_6$ in 1.0 M 1:1 DMC:EC from Sigma Aldrich. There was therefore no electrolyte to which the performance could be compared and as such it is not known whether use of a different electrolyte or the same electrolyte from a different source would have been beneficial to the cell performance, or whether the electrolyte used was actually beneficial or detrimental to the cell performance.

The manufacturing process of the cathode itself is also susceptible to many variables and while the aim was to refine the process, issues could still occur. The mixing process could still lead to inhomogeneity despite attempts to refine the mixing and defoaming speeds, times, and number of cycles to ensure the cathode slurry was mixed until homogenous. The uniformity of the thickness of the slurry during drawdown could also vary dependent on how the drawdown was calibrated and how thick or thin the slurry was, both of which were open to being varied and are depending on the results of the mixing process. Over or under calendaring the cathode during calendaring may also be an issue, with the cathode potentially being of uneven thickness due to the drawdown, the materials which the cathodes were calendared between, and the potential for over calendaring being present despite the use of a micrometer. Variations inherent in these processed could result in imperfections that could lead to poor performance and could also explain the differences between cells using similar or the same cathode.

3.7.5 Discussion of cycling of Li-ion cells using biotemplated NMC811 cathode powder

Cycling data has proven that NMC811 cells made with biotemplating are not only viable but that biotemplated may improve capacity retention while maintaining discharge capacity. When cycled between 4.2 and 3 V all cells have high capacity retention with a decrease of no more than 1 mAh/g per cycle, while use of sodium alginate and nitrates give cells with an initial discharge capacity of 240 mAh/g. Use of acetate precursors give initial discharge capacities for cells of 140 and 150 mAh/g when using sodium alginate and dextran respectively, indicating that while nitrates may provide higher capacities versus acetates, dextran may give slightly better discharge capacity versus. Sodium alginate. When cells are cycled between 4.5 to 2.8 V, initial discharge capacities of 200 mAh/g are possible for all biotemplates and precursors. Cells are highly prone however to failure, with the only cell maintaining capacity when cycled to 4.5 V being a cell made from sodium alginate and nitrate. Reasons for such failure may be due to issues in the cell manufacturing process such as the quality of the lithium chips or electrolyte, or issues with the mixing, drawdown, or calendaring processes. As such sodium alginate may provide improved capacity retention over dextran. Further work is therefore required in incorporating biotemplated cathodes into lithium-ion cells and refine of the cell manufacturing process.

3.8 Variation of the ratio of Li to Ni, Mn, and Co in NMC811

Previous evidence suggests that using sodium alginate as a biotemplate is used to manipulate particle morphology to form nanowires [94]. NMC811 consisting of nanowires, however, has only been synthesised once using sodium alginate during this project. As nanowires are prevalent in other non-lithium chemistries [94], [141], the presence of lithium may be one such reason that nanowires are not being formed. As such using the standard masses of nitrate precursors and sodium alginate biotemplate outlined in the method and varying the ratio of lithium in the NMC811 cathode at 0, 10, and 100% relative mass to synthesise $Ni_{0.8}Mn_{0.1}Co_{0.1}O_2$, $Li_{0.1}Ni_{0.8}Mn_{0.1}Co_{0.1}O_2$, and $LiNi_{0.8}Mn_{0.1}Co_{0.1}O_2$ respectively is investigated to determine whether lithium effects nanowire synthesis during the synthesis of layered NMC811.

3.8.1 XRD when varying the ratio of Li to Ni, Mn, and Co in NMC811

XRD patterns shown in Figure 98 show the variation in the structure of the NMC811 as lithium is removed from the structure. Using 100% relative mass of lithium, Figure 98c, the XRD pattern has the characteristics of organised, layered NMC811, with a high peak intensity ratio between reflections (003) and (104), and strong peak splitting at (006)/(012) and (018)/(110) reflections. As lithium is removed, NMC811 with 0% and 10% relative mass of lithium, Figure 98a and b, can be identified by the phase disorganised $Ni_{0.8}Mn_{0.1}Co_{0.1}O_2$. This is a rock salt structure, has no layering, and underscores that removing lithium to attempt to form nanowires would sacrifice the layered NMC811 structure. The lack of layering in the structure would drastically reduce specific discharge capacity due to a lack of lithiation sites and reduce ionic conductivity pathways across the cathode.

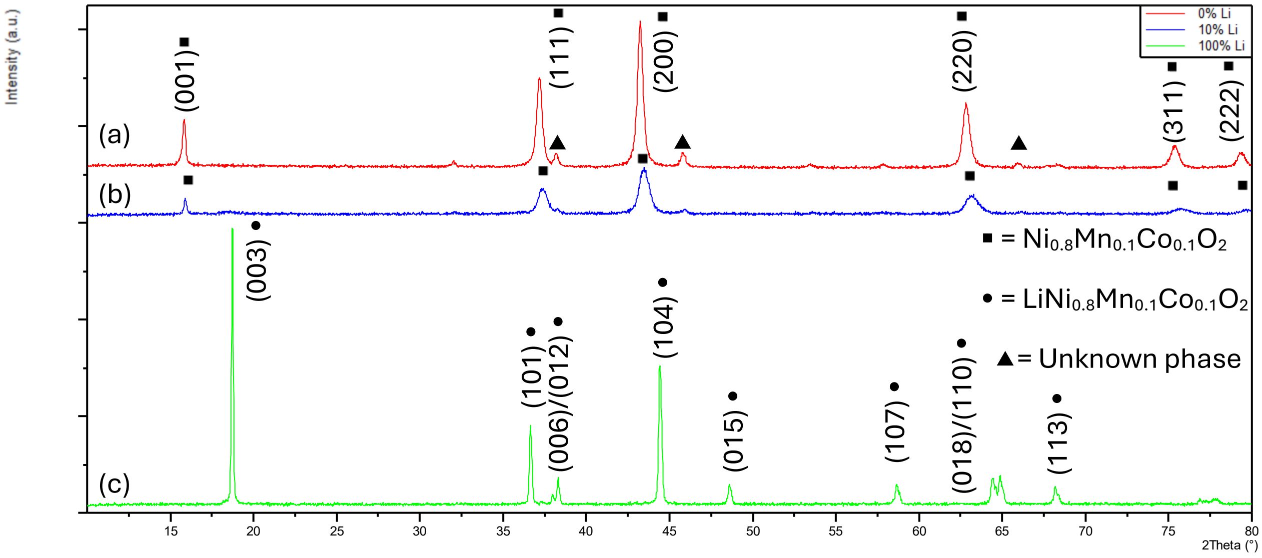

Figure 98 Calcination of NMC with 300 °C Preheat and 800 °C Calcination with a) 0%, b) 10%, and c) 100% Li relative to transition metal mass

3.8.2 SEM when varying the ratio of Li to Ni, Mn, and Co in NMC811

When analysed using SEM images of the NMC811 with different relative masses of lithium show the effect the presence of lithium appears to have on the particle morphology. While not nanoscale and requiring further refinement of the synthesis process, NMC811 synthesised with 0% and 10% relative mass of lithium, Figure 99a – c, forms microscale secondary particles with wire morphologies consisting of highly agglomerated primary particles. At 100% lithium relative mass of lithium, Figure 99d, rounded, irregular particles of average diameter 900 nm with no indication of nanowires are formed. This underscores how in the synthesis of NMC811, lithium may be detrimental to the synthesis of nanowire morphologies. Further investigations into the synthesis of NMC811 cathodes using sodium alginate biotemplating is therefore required, as well as investigations into how sodium alginate effects morphology in the synthesis of high Ni sodium-ion cathodes.

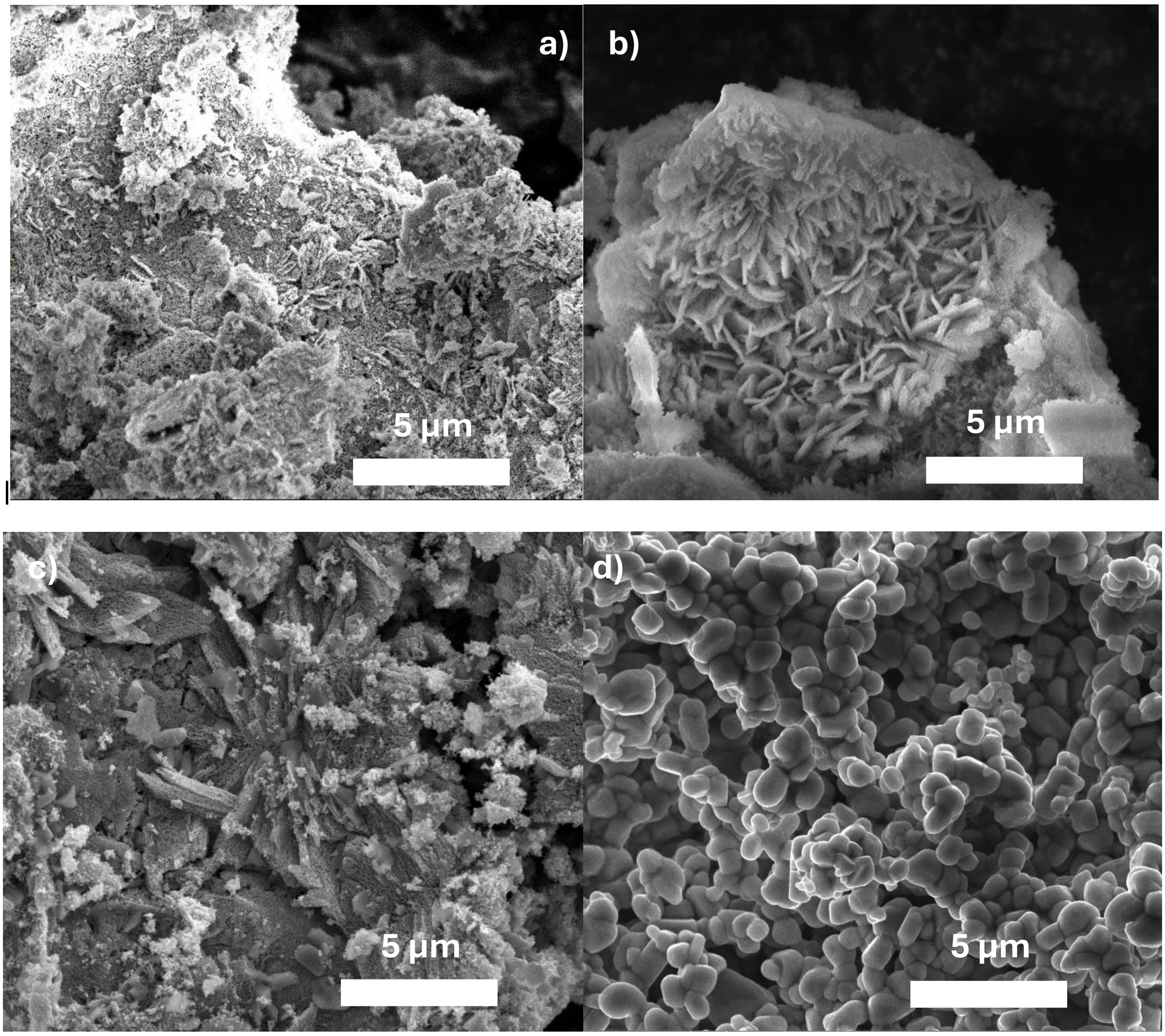

Figure 99 Morphology of NMC synthesised with 300 °C Preheat and 800 °C Calcination with a) 0%, b and c) 10%, and d) 100% Li relative to transition metal mass, with a-c) consisting of microscale secondary particles and d) consisting of irregular rounded particles

3.9 Use of Li alginate vs. Na alginate in synthesis of NMC811

3.9.1 Synthesis of lithium alginate

When increasing the relative mass of biotemplate in section 3.5, increasing the relative mass of sodium alginate results in the synthesis of a sodium carbonate secondary phase, Figure 83, with the result being that the synthesised cathode power is not a single phase. Lithium alginate is investigated as a possible replacement for sodium alginate. As one of the main reasons for selecting sodium alginate is its use in the manipulation of particle morphology to form nanowires, lithium alginate may be used as a biotemplate to replace sodium alginate and so eliminate the sodium carbonate secondary phase being formed in the NMC811.

NMC811 is synthesised using the standard masses for acetate and nitrate precursors and sodium alginate biotemplate outlined in the method, though of 0.1 g of sodium alginate is substituted for 0.1 g of lithium alginate. It was not possible to source commercial lithium alginate, and as such it was synthesised in the lab, (Eq. 5). 0.1 g Lithium alginate may be synthesised in the lab by dissolving 0.0231 g lithium hydroxide hydrate ($LiOH.H_2O$, Sigma Aldrich, 98%) in 0.0967 ml 1 mol alginic acid (Sigma Aldrich, 99%):

$$LiOH.H_2O + C_6H_8O_6 = C_6H_7O_6Li + 2H_2O$$

(Eq. 8)

This reaction produces lithium alginate dissolved in water, which is easily formed. As the lithium alginate reaction produced a byproduct of water, the already dissolved lithium alginate then is able to be added to precursor ions in the same way as sodium alginate separately dissolved in water would be added. Standard synthesis conditions outlined in the methods for NMC811 are then done, with a drying phase, preheat to 300 °C in air in a box furnace, and calcination in a tube furnace to 850 °C in oxygen, with grinding steps before and after each heating step.

3.9.2 Comparison of sodium alginate and lithium alginate biotemplated NMC811 using acetate precursors

Sodium alginate, Figure 100a, and lithium alginate, Figure 100b, biotemplated NMC811 is synthesised with acetate precursors. XRD of the NMC811 cathodes highlights how use of both biotemplates forms layered NMC811. Sodium alginate may be used to form NMC811 with a slightly greater level of organisation than when using lithium alginate, with a peak intensity ratio between (003) and (104) reflections of 1.51 and 1.39 respectively, where < 1.2 is considered high mixing of cation sites, but with similar levels of peak splitting at (006)/(012) and (018)/(110) reflections. The higher (003)/(104) peak intensity ratio of 1.51 when using sodium alginate indicate less mixing of Li^+ and Ni^{2+} ions into Ni and Li sites than when using lithium alginate, however similar peak splitting infers similar levels of layering in the NMC811 structure.

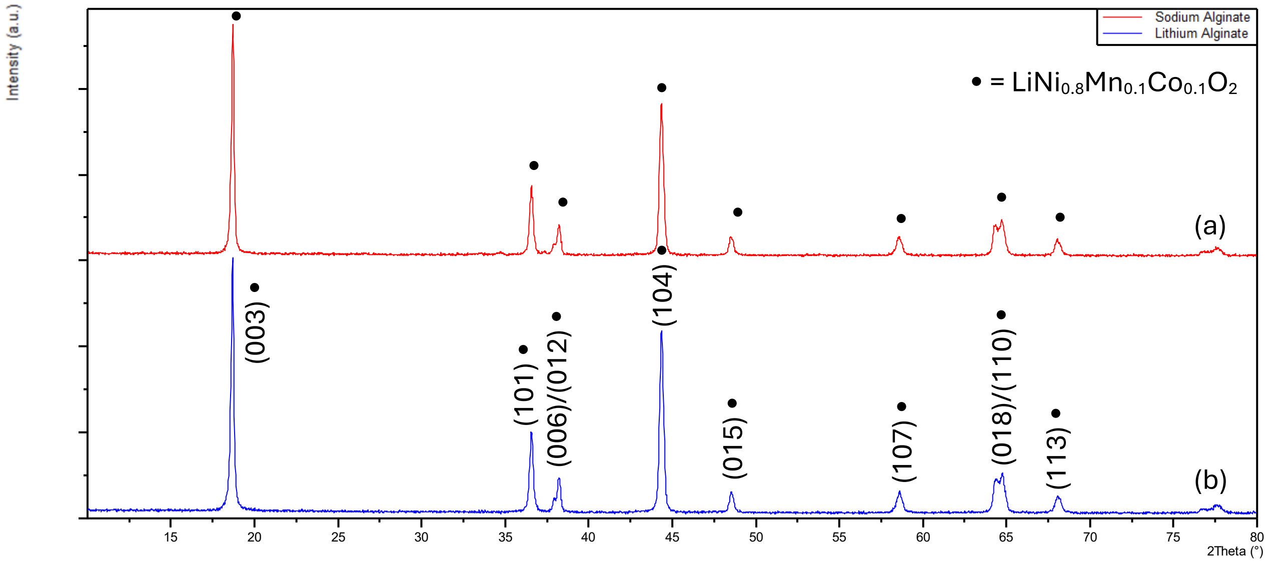

Figure 100 Calcination of NMC811 at 850 °C with a 300 °C preheat using acetate precursors and a) sodium alginate and b) lithium alginate biotemplate

3.9.2.1 Morphology of NMC811 synthesised using sodium alginate and lithium alginate using acetate precursors

When using sodium alginate, Figure 101a, and lithium alginate, Figure 101b, the average particle size when using the different biotemplates is 400 nm vs. 300 nm, respectively. This is due to similar reaction conditions providing the particles with similar time and energy to grow, resulting in similar sized particles. The use of different biotemplates leads to the synthesis of different morphologies, however, with lithium alginate forming irregular, rounded morphologies and sodium alginate forming octahedral particle morphologies. This shows the significance of sodium in the manipulation of particle morphologies, with sodium alginate being required for the synthesis of octahedral particles, while lithium alginate forms irregular, spherical particles similar to the morphology when synthesising with dextran, Figure 62.

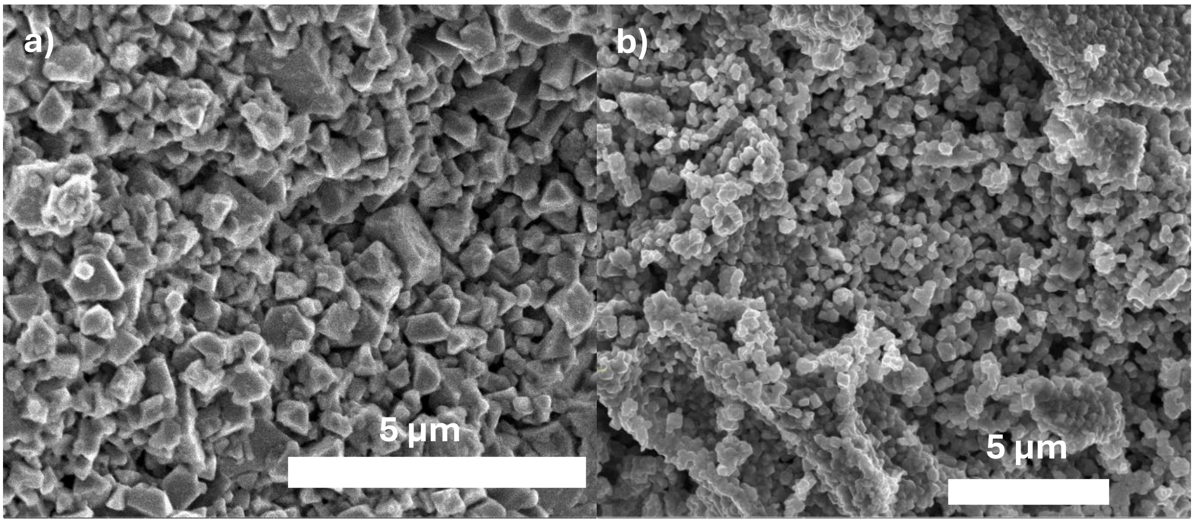

Figure 101 Morphology of NMC811 calcined at 850 °C with a 300 °C preheat using acetate precursors and a) sodium alginate and b) lithium alginate biotemplate

3.9.3 Comparison of sodium alginate and lithium alginate biotemplated NMC811 using nitrate precursors

When nitrate precursors are used with sodium alginate, Figure 102a, and lithium alginate, Figure 102b, sodium alginate synthesised NMC811 is significantly more ordered, with peak intensity ratios of 1.92 and 1.57 respectively between (003) and (104) reflections. Peak splitting for peaks at (006)/(012) and (018)/(110) reflections for sodium alginate biotemplated NMC811 is shown to be very good when compared to poor peak splitting for lithium alginate biotemplated NMC811. Sodium alginate biotemplated samples therefore have less mixing of metal cations into Li and Ni sites [133] and greater layering of the NMC811 structure. This indicates that sodium alginate is the preferred biotemplate when using nitrate precursors and use of lithium alginate is not viable without further investigation.

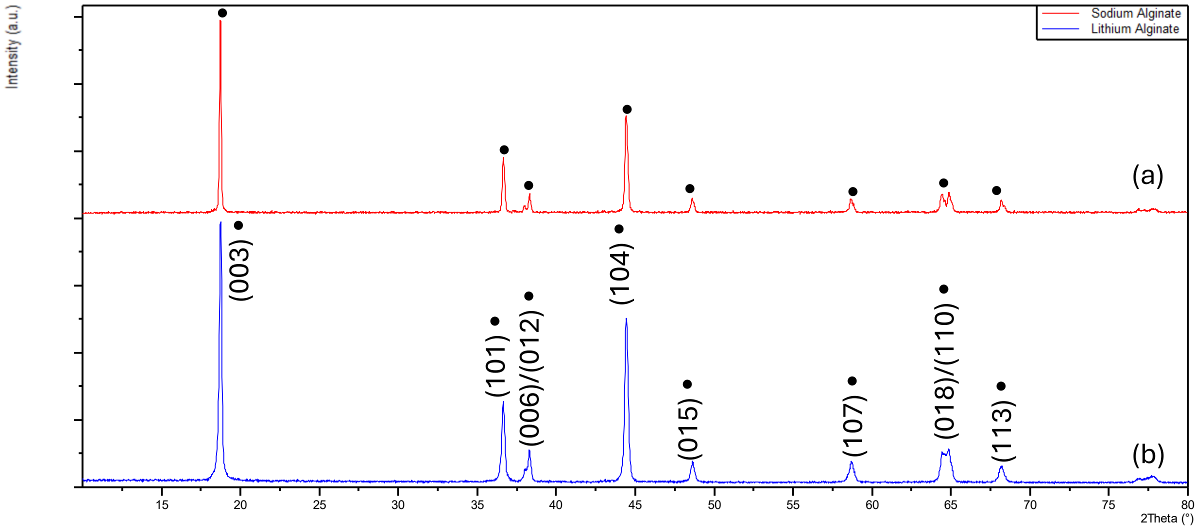

Figure 102 Calcination of NMC811 at 800 °C with a 300 °C preheat using nitrate precursors and a) sodium alginate and b) lithium alginate biotemplate

3.9.3.1 Morphology of NMC811 synthesised using sodium alginate and lithium alginate using acetate precursors

When analysed under SEM, particles formed using sodium alginate biotemplate, Figure 103a, have a 900 nm average diameter, compared to a 400 nm average diameter when biotemplated with lithium alginate, Figure 103b. A greater amount of heat is therefore present in the reaction when sodium alginate is used as opposed to lithium alginate, resulting in more energy for the growing of larger particles. That the sodium alginate biotemplated sample is reacted under greater heat can be inferred by the structure having less cation mixing [133], which is the result of a more oxidising environment in which sufficient heat must have been present to decompose some of the CO_2 in the atmosphere and free up more oxygen for the synthesis of the NMC811. Particles formed using both alginate biotemplates consist of individual, irregular primary particles, with sodium alginate particles being more rounded.

The smaller average particle diameter when using lithium alginate is however beneficial for producing greater surface area for lithium intercalation and increasing discharge capacity. Sodium alginate biotemplated particles have a greater average particle diameter and so reduction in lithiation sites, however the high organisation of the NMC811 structure results in greater ionic conductivity pathways and is more beneficial to cathode performance.

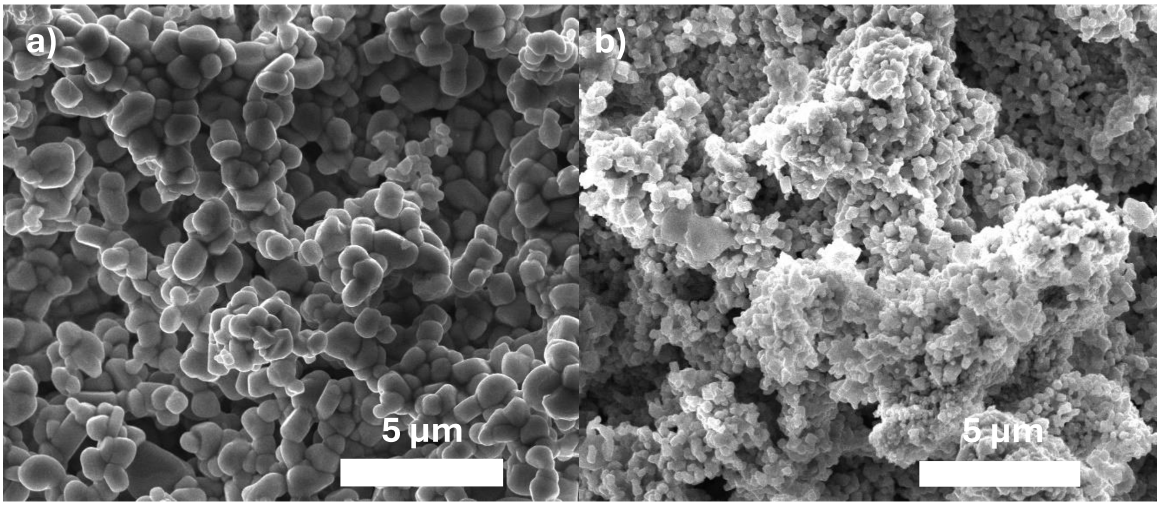

Figure 103 Morphology of NMC811 calcined at 800 °C with a 300 °C preheat using nitrate precursors and a) sodium alginate and b) lithium alginate biotemplate

3.9.4 Discussion for the comparison of using sodium alginate vs. lithium alginate

Lithium alginate is not a viable alternative to the sodium alginate biotemplate despite resulting in the elimination of a sodium carbonate secondary phase. NMC811 samples synthesised with lithium alginate have poorer layering and greater mixing of cation sites than NMC811 synthesised using sodium alginate. Furthermore, lithium alginate does not allow for any additional morphological control than that that could be obtained from using dextran, with sodium alginate required for the synthesis of octahedral morphologies. While when using nitrates the average particle diameter when biotemplating with lithium alginate is smaller, this is not a sufficient compromise due to the poor organisation of the NMC811 structure. As such further investigations into lithium alginate are required before it can be made viable, with sodium alginate being the more optimal choice of biotemplate.

3.10 Discussion for the synthesis of NMC811 biotemplating

Initial investigations into synthesising NMC811 with biotemplating using a combination of dextran and sodium alginate biotemplates and acetate and nitrate precursors has proven the technique is extremely promising. Calcination of NMC811 is required to be done under oxygen and is able to be calcined using a dwell time of 2h at 800 and 850 °C using nitrate and acetate precursors respectively with both dextran and sodium alginate biotemplates. Preheating before calcination in air using a temperature of 300 °C is optimum for structural organisation of NMC811.

When the varying the mass of biotemplates and a lower mass of dextran and sodium alginate, 0.25 g and 0.1 g respectively, is optimum for the synthesis of organised NMC811. Lithium alginate is investigated as a substitute for sodium alginate in order to eliminate the synthesis of potential sodium impurities, however no benefit was observed. When scaling up NMC811, organisation of the NMC811 is either maintained or improved depending on whether nitrates or acetates are used.

Biotemplates are also able to be used to manipulate particle morphology, with nanoscale morphologies being able to be synthesised using all combinations of biotemplates and precursors. Plates and nanowires are able to be synthesised using dextran and sodium alginate, respectively, however such morphologies are not able to be repeated and rounded morphologies and octahedral morphologies for dextran and sodium alginate are able to be synthesised regularly. Synthesis of wire morphologies using sodium alginate may be improved by the removal of lithium, however the removal of the lithium makes this unfeasible due to the presence of less lithium available to intercalate during cycling, resulting in a lower capacity.

Variation of the biotemplate and precursor may also be used to manipulate the average particle diameter in addition to the particle morphology. Further manipulation of the average particle size is also possible by varying the synthesis conditions outlined through chapter 3, such as varying the calcination and preheat temperatures and by scaling up the mass of the biotemplate and precursors. When varying calcination temperature, Table 19a, average particle diameter increases with calcination temperature when using any combination of precursor and biotemplate, with the higher calcination temperatures introducing more energy into the reaction which provides particles with more energy to grow. Furthermore, the longer ramp times as a result of the higher calcination temperatures will give particles more time to grow during the reaction. It is observed however, that the combination of acetates and dextran results in the smallest average particle diameters, with nitrate and dextran synthesised particles resulting in the largest average particles. When using sodium alginate, there appears to be little variation in average particle diameter between using acetates and nitrates.

When varying preheat temperatures, Table 19b, there appears to be no observable trend with average particle diameter varying with no discernible reason, possibly due to the preheat temperature being significantly lower than the calcination temperature and so the lesser introduction of heat to the particles having relatively little effect on the increase in average particle diameter. It can be observed though that using dextran results in smaller average particles diameters than when using sodium alginate at the same preheat temperature. This infers that sodium within the sodium alginate has an observable effect on average particle diameter, possibly due to the larger diameter of the sodium.

When scaling up the synthesis of NMC811, Table 19c, there is a doubling or greater increase of average particle diameter when using either biotemplate as a result of the large reaction size giving off more heat and so more energy for the particles to grow. It is also observed that when using sodium alginate, the average particle size is slightly greater, again possibly as a result of the larger diameter sodium present in the biotemplate. There is however a decrease in the average particle diameter when scaling up using nitrates and sodium alginate, possibly due to the lower carbon content resulting in a lesser exothermic reaction as less carbon dioxide is formed from the reaction between the carbon in the precursor and biotemplate and the oxygen atmosphere. This would result in less energy for particles to grow and result in a smaller average particle diameter. This is the opposite of what is observed when synthesising with dextran and sodium alginate, where the reaction during the preheat stage was so high energy the powder was ejected from the crucible, likely as a result of the formation of a large amount of CO_2 from the reaction between the carbon in the reactants and oxygen in the atmosphere.

Particles synthesised using lithium alginate are observed as having a significantly smaller average particle size compared to when using sodium alginate regardless of precursor used, Table 19d, possibly a result of the larger diameter of the sodium It is also noticeable that particles synthesised using nitrate again have larger average particle sizes than those synthesised using acetates. This is against evidence that suggests using acetates would produce larger average particles due to the greater carbon content and so a larger exothermic reaction as carbon in the acetates reacts with oxygen in the atmosphere to form carbon dioxide.

When biotemplated NM811 cathode powders are used to form lithium-ion coin cells, cells cycled between 4.2 V and 3 V sodium alginate and nitrate precursors give the highest initial discharge capacity of 240 mAh/g, while cells using cathodes synthesised with acetate precursors and either dextran or sodium alginate exhibit high capacity retention while having a reduction in specific discharge capacity. Between 4.5 V and 2.8 V regularly fail due to instability caused by the H2 to H3 phase change. Overall biotemplating is a viable alternative synthesis method for the synthesis of NMC811 cathodes, providing cathodes with high capacity retention and maintaining specific discharge capacity while requiring less synthesis time and comparable synthesis temperatures compared to current commercial synthesis methods revied in section 1.4.

	Dextran		**Sodium alginate**	
	Acetates	Nitrates	Acetates	Nitrates
750 °C	-	-	400 nm	450 nm
800 °C	300 nm	700 nm	600 nm	800 nm
850 °C	600 nm	1200 nm	1000 nm	1000 nm

a) Synthesis of NMC811 under oxygen using the same preheat temperature, ramp rates and dwell times

	Dextran		**Sodium alginate**	
	Acetates	Nitrates	Acetates	Nitrates
200 °C	400 nm	300 nm	600 nm	700 nm
300 °C	300 nm	400 nm	400 nm	900 nm
400 °C	300 nm	200 nm	700 nm	800 nm
500 °C	400 nm	200 nm	500 nm	500 nm

b) Varying preheat temperatures for synthesis of NMC811 under oxygen calcining at 850 °C when using acetates and 800 °C when using nitrates

	Dextran		**Sodium alginate**	
	Acetates	Nitrates	Acetates	Nitrates
x1	300 nm	-	400 nm	900 nm
x2	600 nm	-	1000 nm	600 nm

c) Scale up in mass of synthesised NMC811 from 'x1' using the method outlined in (b) and 'x2' using twice the mass of precursors and biotemplates, using a 300 °C preheat temperature and 850 °C calcination for acetates and 800 °C for nitrates

	Sodium alginate	**Lithium alginate**
Acetates	400 nm	300 nm
Nitrates	900 nm	400 nm

d) Synthesising NMC811 using 300 °C preheat and 850 °C calcination for acetates and 800 °C calcination for nitrates, using sodium alginate and lithium alginate biotemplates.

Table 19 Comparison of average particle diameters for NMC811 particles synthesised using acetate/nitrate precursors and dextran/sodium alginate/lithium alginate biotemplates

4 Results section 2 – Using sodium alginate biotemplating and sodium nitrate to introduce sodium into the NMC811 structure and the varying of Lithium-Sodium eutectics

4.1 Aims for the synthesis of NMC811 with sodium

When varying the relative mass of sodium alginate was investigated in chapter 3 it was found that increasing the relative mass of sodium alginate leads to the synthesis of secondary phases of sodium oxide, 3.5.2, in the NMC811. While this may be viewed as the NMC811 having a sodium impurity, this sodium oxide phase may be used to improve the characteristics of the NMC811 cathode in the same way NMC811 doped with sodium may. While not achieved using biotemplating, NMC532 and NMC603505 cathodes have been doped with sodium-to-lithium ratios of 3:97 and 2:98 respectively [100][101], and have exhibited both increased initial discharge capacities and capacity retentions.

While previously researched doped lithium-ion cathodes were achieved using a separate sodium dopant, it is the aim of this chapter to investigate whether doping using the biotemplate is possible while maintaining the benefits of biotemplating outlined in results chapter 3. Achieving this would allow NMC811 to be doped with sodium when being biotemplated without the need for a separate dopant.

The aims of this chapter will be investigated by comparing the feasibility of using biotemplates as a dopant vs. using a separate sodium dopant (sodium nitrate) when attempting to dope with sodium. This is to determine where high nickel NMC811 cathodes doped with sodium are viable, and if so what method of doping is most optimal.

4.2 Synthesis of NMC811 with sodium via the substitution of Na with Li, where Na = x and Li = (1 – x), using sodium alginate

In order to determine whether doping using sodium alginate is possible in the synthesis of NMC811, NMC811 is formed using acetate or nitrate precursors with sodium alginate as the biotemplate while varying the mass of the sodium alginate and lithium precursor according to the method outlined in 2.1.3. Lithium precursor is substituted for sodium alginate such that for a given increase in sodium ions in the sodium alginate, the number of lithium ions will be decreased by decreasing the mass of the lithium precursor. (i.e. Na = x and Li = (1 – x) whereby $Li_{(1-x)}Na_xNi_{0.8}Mn_{0.1}Co_{0.1}O_2$, where 0.1 g of sodium alginate would produce $Li_{0.9}Na_{0.1}Ni_{0.8}Mn_{0.1}Co_{0.1}O_2$).

This is different to the method used throughout chapter 3 when biotemplating with sodium alginate, where sodium ions in the NMC811 structure would be in addition to 100% lithium. (i.e. Na = x and Li = 1 whereby $LiNa_xNi_{0.8}Mn_{0.1}Co_{0.1}O_2$, where the established mass of 0.1 g of sodium alginate produces $LiNa_{0.1}Ni_{0.8}Mn_{0.1}Co_{0.1}O_2$). When doping with sodium, it is hypothesised that any sodium added using biotemplating with sodium alginate will substitute lithium in the structure. By varying the mass of biotemplate relative to the mass of lithium, the ratio of sodium to lithium ions can be varied. By using masses of sodium alginate of 0.1 g for x = 0.1 Na and 0.25 g for x = 0.2 Na and the established masses of Ni, Mn, and Co precursors, Table 20, NMC811 with lithium ion-to-sodium ratios where x = 0.1 and 0.2 can be synthesised. Both acetate and nitrate precursors will be used to investigate whether sodium doping was successful due to the effect the different precursors have on the synthesis process. In section 3.2.2.1 use of acetate precursors results in both the biotemplate and precursors decomposing to free up more carbon, which results with more of the oxygen atmosphere to form CO_2, a more reducing environment, and larger particle sizes due to more heat being given out. Nitrates meanwhile resulted in small particles with octahedral morphologies synthesised under a more oxidising environment as carbon is only freed up from the decomposition of the biotemplate and not the precursor. This lesser amount of carbon reacts with less oxygen, resulting in less CO_2 and less heat being given out, resulting in smaller particle sizes. This also means more oxygen is freed up in the atmosphere and so a more oxidising atmosphere.

	Acetate Hydrate	Nitrate Hydrate
Lithium, x = 0.1 (g)	0.2296	0.1552
Lithium, x = 0.2 (g)	0.2041	0.1379
Sodium alginate, x = 0.1 (g)	0.1	0.1
Sodium alginate, x = 0.2 (g)	0.25	0.25
Nickel (g)	0.4977	0.5816
Manganese (g)	0.0613	0.0447
Cobalt (g)	0.0623	0.0727

Table 20 Masses of metal precursor salts used in the attempted synthesis of Na-doped NMC811 via substitution of lithium ($Li_{(1-x)}Na_xNi_{0.8}Mn_{0.1}Co_{0.1}O_2$) using sodium alginate as a dopant

4.2.1 Synthesis of NMC811 with sodium via substitution of Na with Li using sodium alginate and nitrate precursors

4.2.1.1 X-Ray Diffraction Analysis of NMC811 synthesised with Na_2CO_3 secondary phase via substitution of Na with Li using sodium alginate and nitrate precursors

By synthesising NMC811 with Na where x = 0.1 and 0.2, Figure 104a and b, organised NMC811 can still be observed in XRD patterns. Where x = 0.1, strong peak splitting at (018)/(110) and (006)/(012) highlight good layering of the NMC811 structure while a peak intensity ratio between (003) and (104) of 1.53 show minimal mixing of cations between Li and Ni sites [133] (where < 1.2 is high mixing [130]). The structure of the NMC811 where x = 0.2 meanwhile shows some disorder, with poor peak splitting at (006)/(012) and (018)/(110) indicating poor layering of the NMC811 structure while a peak intensity ratio between (003) and (104) of 1.33 shows increased mixing of cations between Li and Ni sites. Peaks indicating a second sodium phase are present when x = 0.2 while being mostly non-present when where x = 0.1. Peaks at 19, 29 and 37 and 39 ° (201, 002, 112, 202 reflections) indicate the presence of a sodium carbonate phase within the NMC811 structure.

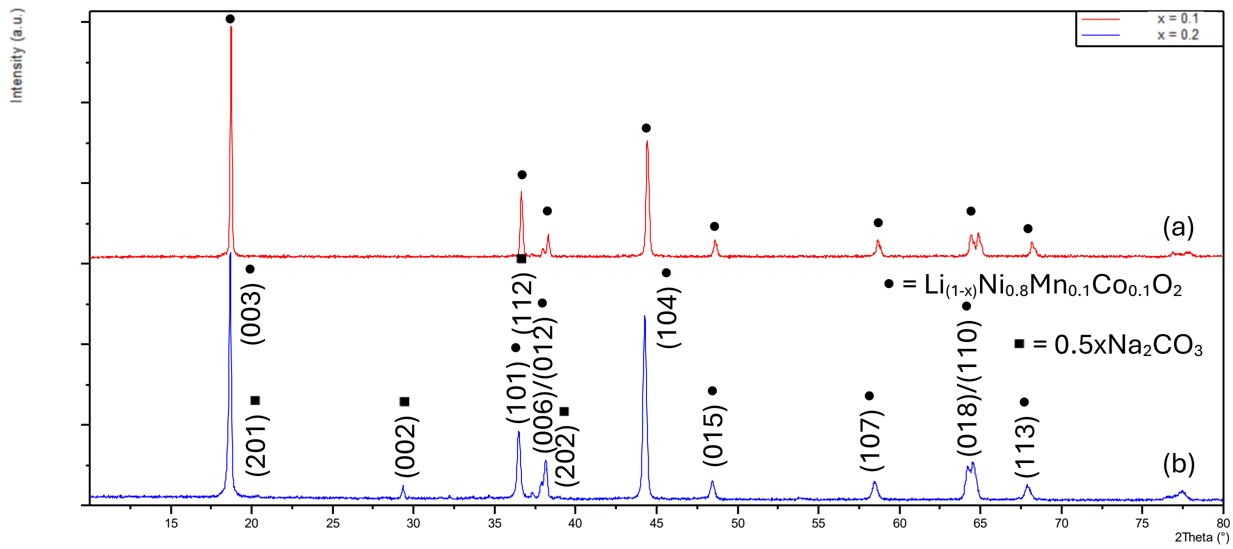

Figure 104 XRD of NMC811 synthesised with Na ($Li_{(1-x)}Ni_{0.8}Mn_{0.1}Co_{0.1}O_2.0.5xNa_2CO_3$) where Na = x and Li = (1 - x), synthesised with nitrate precursors and sodium alginate where a) x = 0.1 ($Li_{0.9}Ni_{0.8}Mn_{0.1}Co_{0.1}O_2.0.05Na_2CO_3$) and b) x = 0.2 ($Li_{0.8}Ni_{0.8}Mn_{0.1}Co_{0.1}O_2.0.1Na_2CO_3$)

4.2.1.1.1 Rietveld analysis of NMC811 with Na_2CO_3 secondary phase via substitution of Na with Li using sodium alginate and nitrate precursors and calcined at 850 °C

To determine whether NMC811 was successful doped using sodium alginate as a sodium, Rietveld analysis was done on the cathode powder calcined at 850 °C using the method, NMC CIF file, and instrument parameter file outlined in 2.2.1.1. By performing Rietveld analysis and comparing the sodium alginate biotemplated powder (obs.) to the phase data refined from the CIF file (calc), Figure 105, we can determine that sodium doping has not taken place and instead sodium has formed a secondary phase, likely Na_2CO_3. It can be observed that there is no shift in the 2Θ values of the NMC811 peaks, most significantly where peaks are denoted by the (003), (006)/(012), (104), and (018)/(110) reflections, which suggests no shift or deformation in the NMC811 lattice caused by sodium ions being present in the lattice. This is further reinforced by there being no observable change in the unit cell dimensions, with the unit cell dimensions being unchanged at *a/b* = 2.8645 Å and *c* = 14.161 Å [119]. As such the added sodium has not been doped but instead is present as a secondary phase, in this case in the form of Na_2CO_3. Such a phase however may still benefit NMC811 as observed in sodium alginate biotemplated cathodes used in cells in chapter 3.

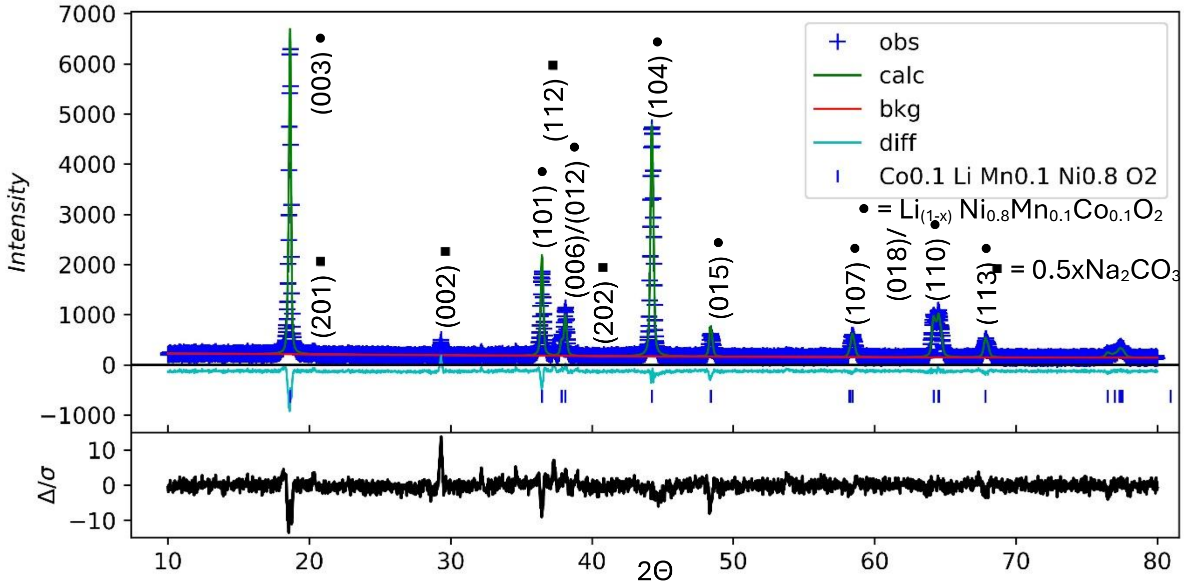

Figure 105 Rietveld analysis of NMC811 synthesised with Na ($Li_{(1-x)}Ni_{0.8}Mn_{0.1}Co_{0.1}O_2.0.5xNa_2CO_3$) where Na = x and Li = (1 - x), synthesised with nitrate precursors and sodium alginate as the Na dopant where x = 0.2 and calcined at 850 °C

4.2.1.2 Morphology of NMC811 synthesised with Na via substitution of Na with Li using sodium alginate and nitrate precursors

The morphology of the NMC811 alters significantly with an increase in the proportion of sodium, with the morphology of particles where x = 0.2, Figure 106b, being more angular with a higher proportion of tetragonal and octahedral morphologies and particles where x = 0.1, Figure 106a, being mostly rounded if irregular. Despite having different shapes particles maintain the same size, an average particle diameter of 900 nm calculated by measuring against the set scale in ImageJ. Greater agglomeration is also present when x = 0.2, likely a secondary phase of sodium carbonate. When EDAX is done on the samples, peaks at < 1 KeV when x = 0.2, Figure 107b, are present representing Na and C, but are not present when x = 0.1, Figure 107a. Sodium carbonate has a melting point of 851 °C, above the calcination temperature of 800 °C, and so is a possible secondary phase, though the detected carbon may also be that of the carbon sticky tab on which the powder is placed. A greater proportion of sodium therefore significantly alters particle morphology at the cost of greater agglomeration, and highlights the process that sodium plays in morphological control.

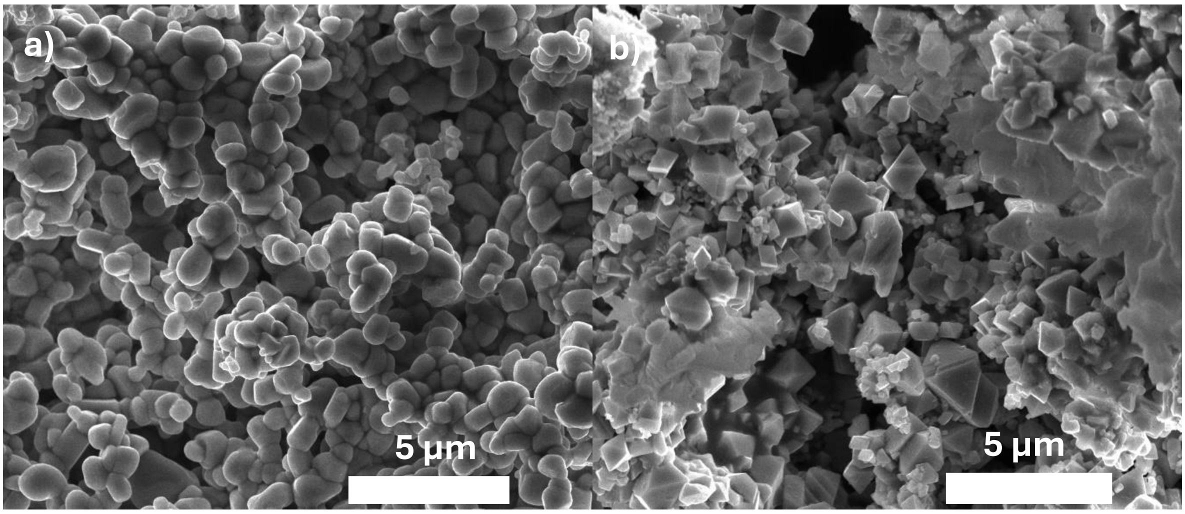

Figure 106 SEM of NMC811 synthesised with Na ($Li_{(1-x)}Ni_{0.8}Mn_{0.1}Co_{0.1}O_2.0.5xNa_2CO_3$) where Na = x and Li = (1 – x), synthesised with nitrate precursors and sodium alginate where a) x = 0.1 and exhibits rounded particles and b) x = 0.2 and exhibits angular particles

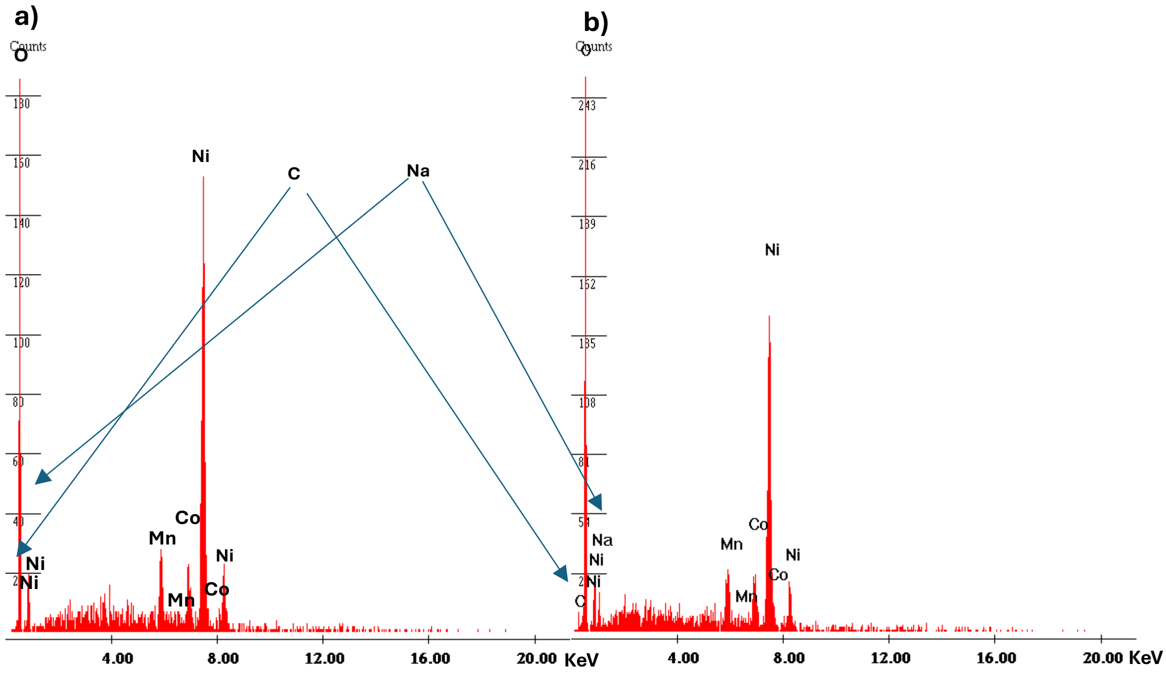

Figure 107 EDAX of NMC811with sodium secondary phase ($Li_{(1-x)}Ni_{0.8}Mn_{0.1}Co_{0.1}O_2.0.5xNa_2CO_3$) synthesised with Na where Na = x and Li = (1 – x), synthesised with nitrate precursors and sodium alginate where a) x = 0.1 and b) x = 0.2

4.2.1.3 Cell cycling of NMC811 synthesised with Na via substitution of Na with Li using sodium alginate and nitrate precursors where x = 0.2, with 4.5 to 2.8 V range

The Na containing cathode powder ($Li_{(1-x)}Ni_{0.8}Mn_{0.1}Co_{0.1}O_2.0.5xNa_2CO_3$) where x = 0.2, and so Li = 0.8, is able to be synthesised into a cathode and cycled in a lithium-ion coin cell between 4.5 V and 2.8 V at 0.1 C in order to determine how this amount of sodium effects cell performance. This cell is compared against a cell from section 3.7.3.2 synthesised using 0.1 g sodium alginate and nitrates with no substitution of lithium where Li = 1.

The Initial discharge capacity is 140 mAh/g where x = 0.2, which decreases significantly after 10 cycles to 40 mAh/g, Figure 108b, where the rate of decrease of capacity retention from cycle to cycle slows significantly. This is compared to an initial discharge capacity of 200 mAh/g and a capacity decrease to 80 mAh/g after 10 cycles, Figure 108e, for the cell where Li = 1 cycled in section 3.7.3.2.2. The lower initial discharge capacity compared to lithium-ion cell is an indication that there is less lithium available for intercalation and that the substitution of lithium with sodium is negatively affecting capacity, with sodium not intercalating. Capacity retention is poor for both x = 0.2 and Li = 1 lithium-ion cells when cycled at 4.5 V. During the initial cycle, the cell where x = 0.2 undergoes a phase change from H1 to M at 3.7 V, and the M to H2 phase change at 4.4 V during charging, with the phase transitions H2 to M occurring at 4.2 V and M to H1 happening at 3.7 V [142]. Due to the structure of the cathode, the structure does not undergo the H2 to H3 phase change, which also in part explains the lower initial discharge capacity. By comparison, the cell where Li = 1 undergoes H1 to M, M to H2, and H2 to H3 phase changes during charging at 3.7, 3.8, and 4.2 V respectively, and during discharge H3 to H2, H2 to M, and M to H1 phase transitions occurring at 4.1, 3.7, and 3.5 V, with the cell initial capacity where Li = 1 being initially higher due to going through the H2 to H3 phase transition. Both cathodes then undergo capacity fade due to the M to H2 and H2 to H3 phase transitions occurring above 4.2 V [140], which causes severe structural instability. This highlights that the cell consisting of a secondary sodium phase where lithium is substituted such that x = 0.2, there is little benefit for improving structural stability or cycling retention compared to cells where Li = 1 when using sodium alginate and nitrates.

Further reasons for the poor cyclability of the cathodes and difference in initial specific discharge capacities may be attributed to the cell manufacturing process, as discussed in 3.7.4. Oxidation and damage to the lithium chips could be one contributing factor and could affect the cathode capacity due to the loss of lithium. Aging of the electrolyte could also be a contributing factor with trace amounts of water potentially being present in the electrolyte affecting cell cycling. The difference in cycling between the two, theoretically identical cathodes could be due to errors in the manufacturing process. Inhomogeneity caused by incomplete mixing of the slurry, an uneven drawdown due to a too thick or too thin slurry, or over calendaring could result in differences in the cathode. This could result in differences in the ratio of cathode active material to carbon black or PVDF due to inhomogeneity or the cathode thickness, or even damage to the cathode caused by over calendaring. This could result in different specific capacities or cyclability for the different cells.

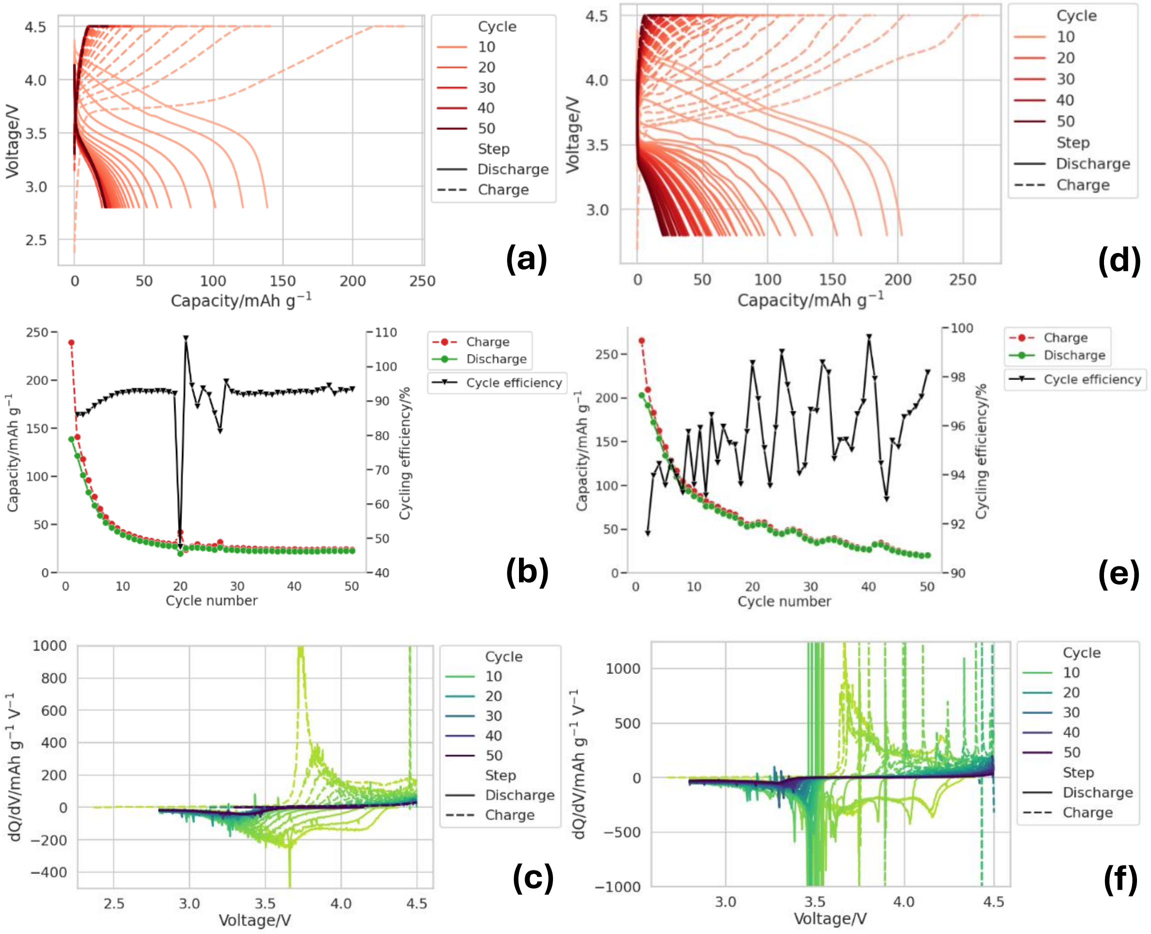

Figure 108 Charge-discharge cycling (a), Cycling efficiency and charge-discharge capacities (b), and Differential capacity vs. voltage curve (c), for Li-ion coin cell with nitrate and sodium alginate synthesised cathodes with a sodium secondary phase ($Li_{(1-x)}Ni_{0.8}Mn_{0.1}Co_{0.1}O_2.0.5xNa_2CO_3$) where x = 0.2 and Li = 0.8 between 4.5 and 2.8 V for 50 cycles, compared with a cell where Li = 1 and x = 0.1 synthesised using sodium alginate and nitrates (d, e, f)

4.2.2 Synthesis of NMC811 with sodium via substitution of Na with Li using sodium alginate and acetate Precursors

4.2.2.1 X-Ray Diffraction Analysis of Na-containing NMC811 via substitution of Na with Li using sodium alginate and acetate precursors

Use of acetate precursors appears to cause a difference in the way the sodium is incorporated into the NMC811, with peaks for a secondary phase present at 35 and 37 °, Figure 109, instead of 19, 29 and 37 and 39 °. Whereas sodium forms sodium carbonate when nitrates are used, sodium peroxide, Na_2O_2 when acetates are used as precursors. As analysed in section 3.4.3.1.1, differential scanning calorimetry done on NMC811 synthesised with sodium alginate and acetate precursors exhibits a large exothermic oxidation reaction above 300 °C where NMC hydroxide is oxidised into disorganised NMC oxide, section 3.4.3.1.2. This reaction gives out significant heat resulting in CO_2 in the atmosphere decomposing and releasing significant oxygen. Such CO_2 was formed from the reaction between carbon released from the breakdown of acetate precursors and the sodium alginate biotemplate and the oxygen atmosphere. This CO_2 is what reacts with sodium to form Na_2CO_3 when using nitrates, however when using acetates this significant increase in heat as a result exothermic reaction breaks down the CO_2 in the atmosphere to release oxygen and produce of a more oxidising environment, leading to the synthesis of the Na_2O_2.

This is in addition to more significant disorganisation of NMC811 when x = 0.2, Figure 109b, with no peak splitting at (006)/102 and (018)/(110) showing poor layering of the NMC811 and a peak intensity ratio between (003) and (104) of 0.86, highlighting a high level of cation mixing between Ni and Li sites [133] (where < 1.2 is considered a high level of mixing [130]). While the same secondary phase peaks are present when x = 0.1, Figure 109a, the improved peak splitting and (003)/(104) peak intensity ratio for the NMC811 indicate a more organised structure. This increased mixing and alternate sodium secondary phase indicates a difference of structure when synthesising Na-containing NMC811 with acetates vs. nitrates.

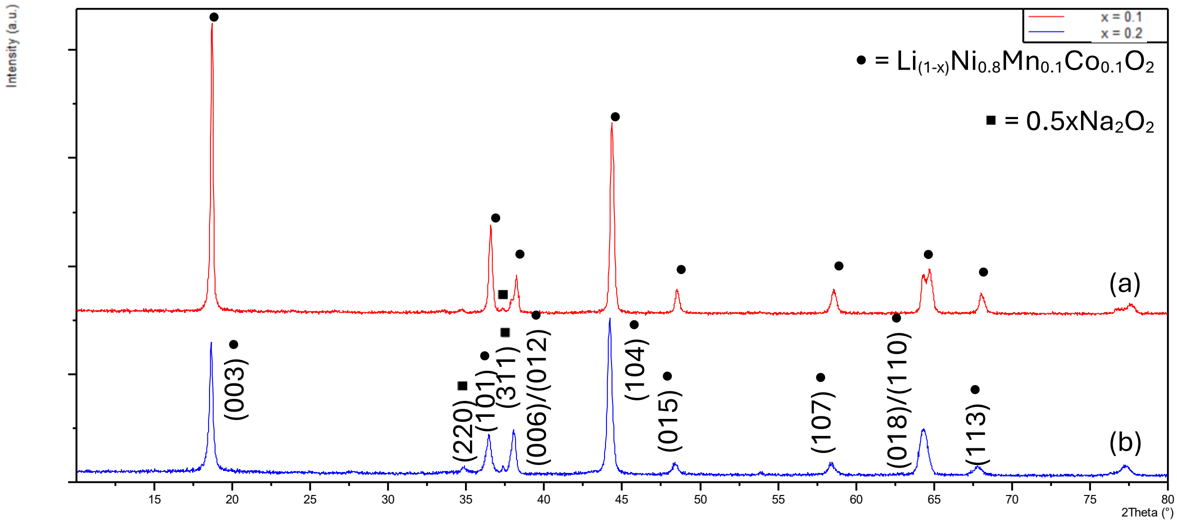

Figure 109 XRD of NMC811 ($Li_{(1-x)}Ni_{0.8}Mn_{0.1}Co_{0.1}O_2.0.5xNa_2O_2$) with a secondary xNa_2O_2 secondary phase where Na = x and Li = (1 - x), synthesised with acetate precursors and sodium alginate where a) x = 0.1 ($Li_{0.9)}Ni_{0.8}Mn_{0.1}Co_{0.1}O_2.0.05Na_2O_2$) and b) x = 0.2 ($Li_{0.8}Ni_{0.8}Mn_{0.1}Co_{0.1}O_2.0.1Na_2O_2$)

4.2.2.2 Morphology of NMC811with xNa_2O_2 via substitution of Na with Li using sodium alginate and acetate precursors

Particle morphology when using acetates have an average diameter of 400 nm when x = 0.1, Figure 110a. When x = 0.2, Figure 110b, particles have a similar average diameter of 400 nm. While having similar particle morphologies, where x = 0.2 particles have more distinct tetragonal and octahedral particles vs. more irregularly shaped particles synthesised when x = 0.1. The appearance for this is the increased proportion of sodium when x = 0.2, but also the reduction in smaller particles agglomerating into irregular particle morphology. The lack of agglomeration in comparison to when using nitrates reinforces also reinforces a different secondary sodium phase. When EDAX is done on the sample where x = 0.2, Figure 111a, Na peaks are present between 1 and 5 KeV but no carbon peaks are present as when using nitrates, Figure 111b. This infers the different sodium phase of Na_2O_2 instead of Na_2CO_3, resulting in less agglomeration, however the carbon detected previously may also be a result of the carbon tab the sample is placed on.

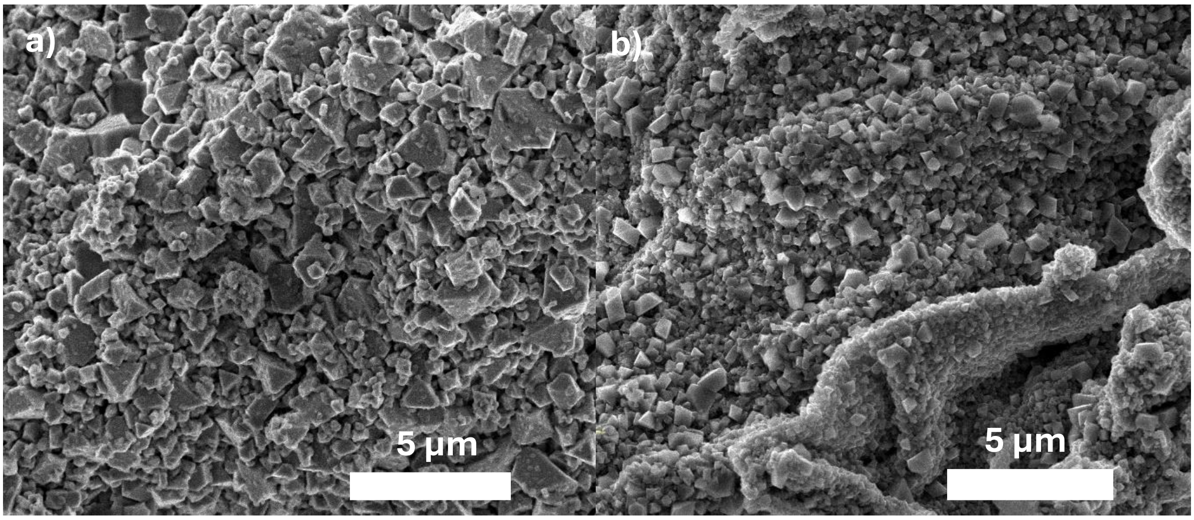

Figure 110 SEM of NMC811 ($Li_{(1-x)}Ni_{0.8}Mn_{0.1}Co_{0.1}O_2.xNa_2O_2$) and xNa_2O_2 where Na = x and Li = (1 - x), synthesised with acetate precursors and sodium alginate where a) x = 0.1 ($Li_{0.9}Ni_{0.8}Mn_{0.1}Co_{0.1}O_2.0.05xNa_2O_2$) and has tetragonal and octahedral morphologies b) x = 0.2 ($Li_{0.8}Ni_{0.8}Mn_{0.1}Co_{0.1}O_2.0.1xNa_2O_2$) and has an irregular morphology

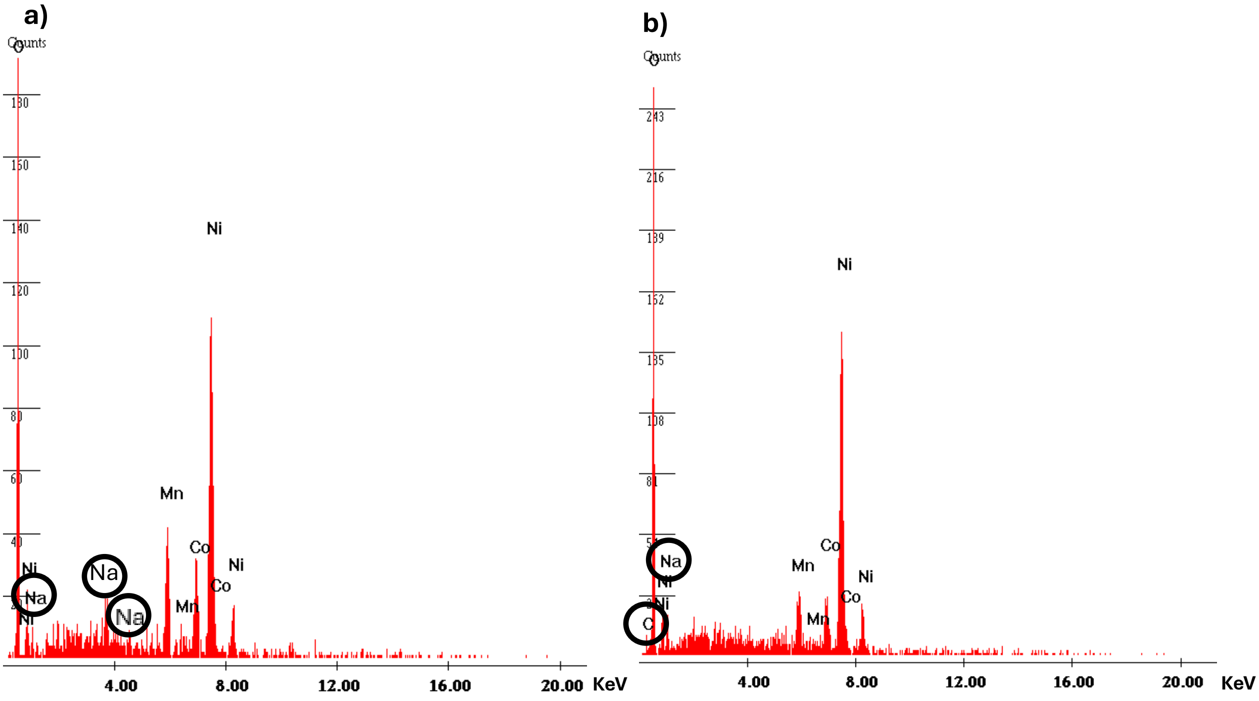

Figure 111 EDAX of NMC811 with Na ($Li_{(1-x)}Ni_{0.8}Mn_{0.1}Co_{0.1}O_2.xNa_2O_2$) where Na = x and Li = (1 – x), synthesised with sodium alginate where x = 0.2 and a) acetate precursors $Li_{0.8}Na_{0.2}Ni_{0.8}Mn_{0.1}Co_{0.1}O_2.0.1xNa_2O_2$, Figure 110a) and b) nitrate precursors $Li_{0.8}Na_{0.2}Ni_{0.8}Mn_{0.1}Co_{0.1}O_2.0.1xNa_2CO_3$, Figure 110b)

No cells so far have currently been produced with NMC811 with a secondary sodium phase ($Li_{(1-x)}Ni_{0.8}Mn_{0.1}Co_{0.1}O_2.x0.5Na_2O_2$) where x = 0.2 due to time constraints. As such there is currently no data to compare the performance of cells synthesised with a secondary sodium phase and with acetate precursors to.

4.3 Synthesis of NMC811 with sodium via the substitution of Na with Li, where Na = x and Li = (1 – x), using sodium alginate supplemented with sodium nitrate

As a ratio of sodium-to-lithium where x = 0.2 gives a high structural disorganisation in NMC811 due to the formation of sodium secondary phases, it is investigated if other sources of sodium would have the same effect on the structure. Previous evidence from results chapter 3 suggests an increase in biotemplate mass increases structural disorganisation of the NMC811. By maintaining the mass of sodium alginate to 0.1 g (equivalent to x = 0.1) and using a second source of sodium to increase the ratio of sodium-to-lithium such that x = 0.2, Table 21, structural disorganisation may be avoided. This is compared to NMC811 containing sodium secondary phases where NMC811 is synthesised using sodium alginate such that x = 0.2. Sodium nitrate is selected as a second source due to nitrates already being widely used during this research to synthesise NMC811 and due to the lack of carbon present when compared to using a source such as sodium acetate. A sodium source that does not contain carbon is selected as carbon is a common source of disorganisation. This is a result of carbon-containing reactants decomposing into carbon and reacting with oxygen in the atmosphere to form CO_2, a reducing atmosphere. This results in less oxygen being available for the synthesis of NMC811 resulting in oxygen sites not being filled and increased disorganisation of the structure. Using a sodium source that does not contain carbon ensures reducing the mass of sodium alginate to reduce the amount of carbon is not redundant.

	X = 0.2, 1:0 Sodium alginate: sodium nitrate	X = 0.2, 0.5:0.5 Sodium alginate: sodium nitrate
Lithium acetate dihydrate/Lithium nitrate (g)	0.2041/0.1379	0.2041/0.1379
Sodium alginate (g)	0.25	0.1
Sodium nitrate (g)	0	0.0213

Table 21 Masses of metal precursor salts used in the synthesis of NMC811 with Na via substitution of lithium ($Li_{(1-x)}Na_xNi_{0.8}Mn_{0.1}Co_{0.1}O_2$) using sodium alginate and sodium nitrate

4.3.1 Synthesis of NMC811 with sodium via substitution of Na with Li using sodium alginate, sodium nitrate, and nitrate precursors

4.3.1.1 X-Ray Diffraction Analysis of NMC811 with a sodium secondary phase via substitution of Na with Li using sodium alginate, sodium nitrate, and nitrate precursors

Where x = 0.2 such that NMC811 is synthesised with a half and half mixture of sodium alginate and $NaNO_3$, Figure 112a, a much more organised NMC811 structure than NMC811 synthesised only with sodium alginate, Figure 112b, is synthesised. (201), (002), (112), and (202) peaks at 19, 29, 37, and 38° when synthesising with only sodium alginate indicate a sodium carbonate secondary phase. When synthesising with half-and-half sodium alginate and $NaNO_3$ the peaks still present but with a weaker intensity, suggesting a secondary phase of sodium is still present in the NMC811 structure when using sodium nitrate but that the amount of carbonate formed may be less due to there being less carbon present due to sodium alginate being substituted for sodium nitrate.

It is however shown that there is greater organisation of the NMC811 structure when using $NaNO_3$ despite the sodium secondary phase, which is highlighted by better peak splitting at

(006)/102 and (018)/(110) when compared to NMC811 formed with only sodium alginate indicating greater layering of the NMC811 when using sodium nitrate. Peak intensity ratios between (003) and (104) of 1.31 when using only sodium alginate and 1.36 when adding sodium nitrate show similar levels of cation mixing between Li and Ni sites [133]. Use of sodium nitrate therefore shows initial promise in synthesising NMC811 than synthesising purely with sodium alginate.

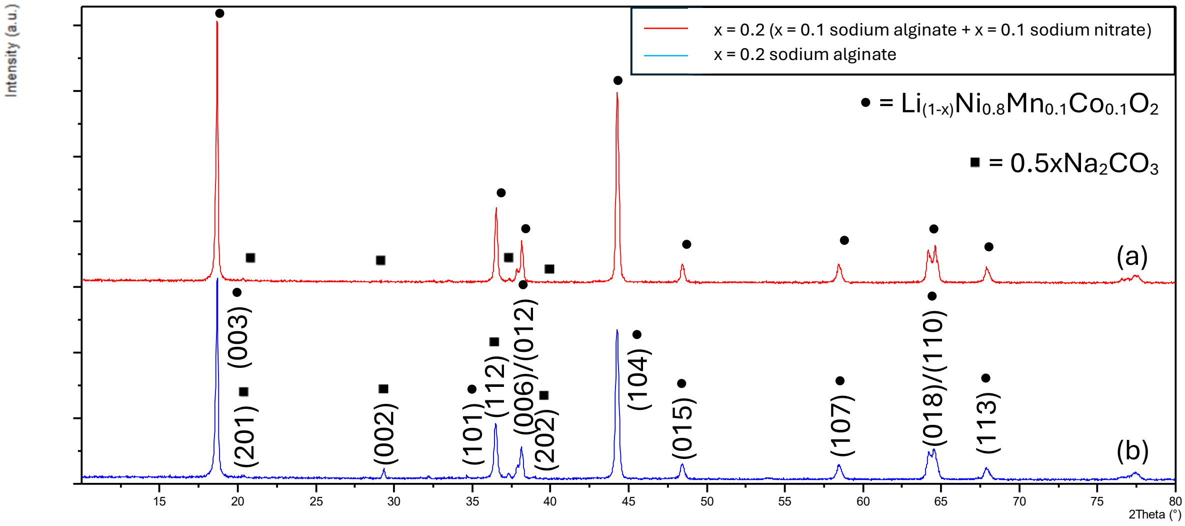

Figure 112 XRD of NMC811 with a sodium carbonate secondary phase ($Li_{(1-x)}Ni_{0.8}Mn_{0.1}Co_{0.1}O_2.0.5xNa_2CO_3$) where Na = x and Li = (1 - x), synthesised with nitrate precursors, and sodium alginate and sodium nitrate where x = 0.2 ($Li_{0.8}Ni_{0.8}Mn_{0.1}Co_{0.1}O_2.0.1Na_2CO_3$) using a) x = 0.1 sodium alginate and x = 0.1 sodium nitrate and b) using x = 0.2 sodium alginate

4.3.1.2 Morphology of NMC811 with a sodium secondary phase via substitution of Na with Li using sodium alginate, sodium nitrate, and nitrate precursors

Despite having similar levels of organisation when NMC811 is synthesised, particle morphologies of the two cathode powders show significant differences. Particles synthesised using half and half sodium alginate and sodium nitrate, Figure 113a, have a large average particle diameter of 1500 nm and have an irregular, uneven octahedral morphology with smoothed off corners. Particles synthesised only with sodium alginate, Figure 113b, have an average diameter of 900 nm with a much sharper, less irregular octahedral morphology. It is observed therefore that reducing the biotemplate, while improving the structure of the NMC811, increases average particle size and leads to a partial breakdown of the morphology. This is due to less chelation of metal ions and greater recrystallisation during synthesis, resulting in a larger particle size. EDAX taken of the two morphologies shows the absence of carbon within the particles synthesised partially using sodium nitrate, Figure 114a, when compared to particles synthesised only with sodium alginate where carbon is present, Figure 114b. Sodium carbonate is therefore much less prevalent when synthesising partially with sodium nitrate, indicating a decrease in the sodium carbonate secondary phase, though carbon observed previous may also be a result of the carbon sticky tab.

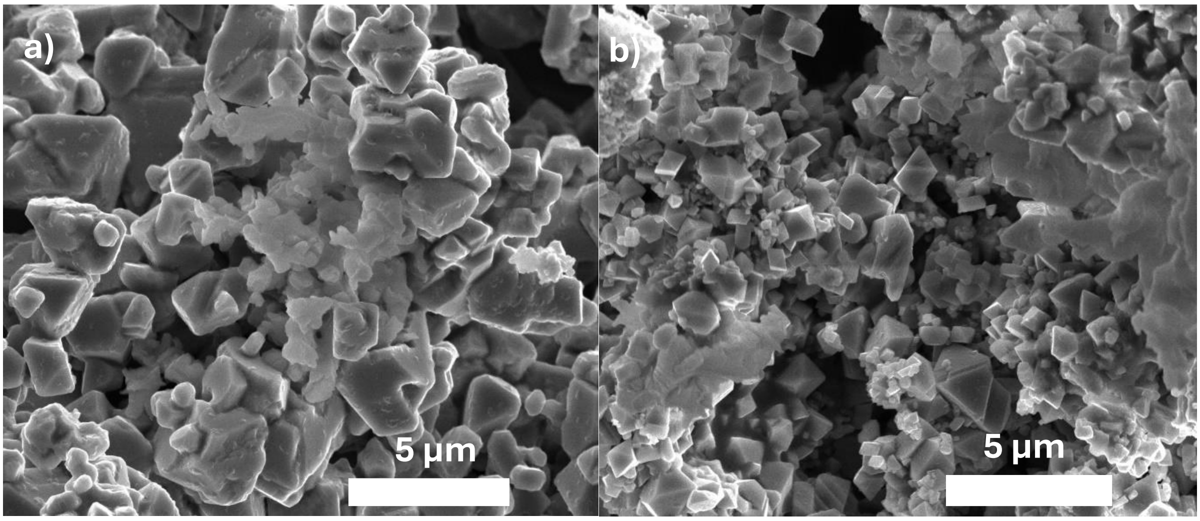

Figure 113 SEM of NMC811 with a sodium secondary phase ($Li_{(1-x)}Ni_{0.8}Mn_{0.1}Co_{0.1}O_2.0.5xNa_2CO_3$) where Na = x and Li = (1 - x), synthesised with nitrate precursors, and sodium alginate and sodium nitrate where x = 0.2 ($Li_{0.8}Ni_{0.8}Mn_{0.1}Co_{0.1}O_2.0.1Na_2CO_3$) using a) x = 0.1 sodium alginate and x = 0.1 sodium nitrate and exhbiting an irregular morphology and b) using x = 0.2 sodium alginate and exhbiiting a more regular morphology

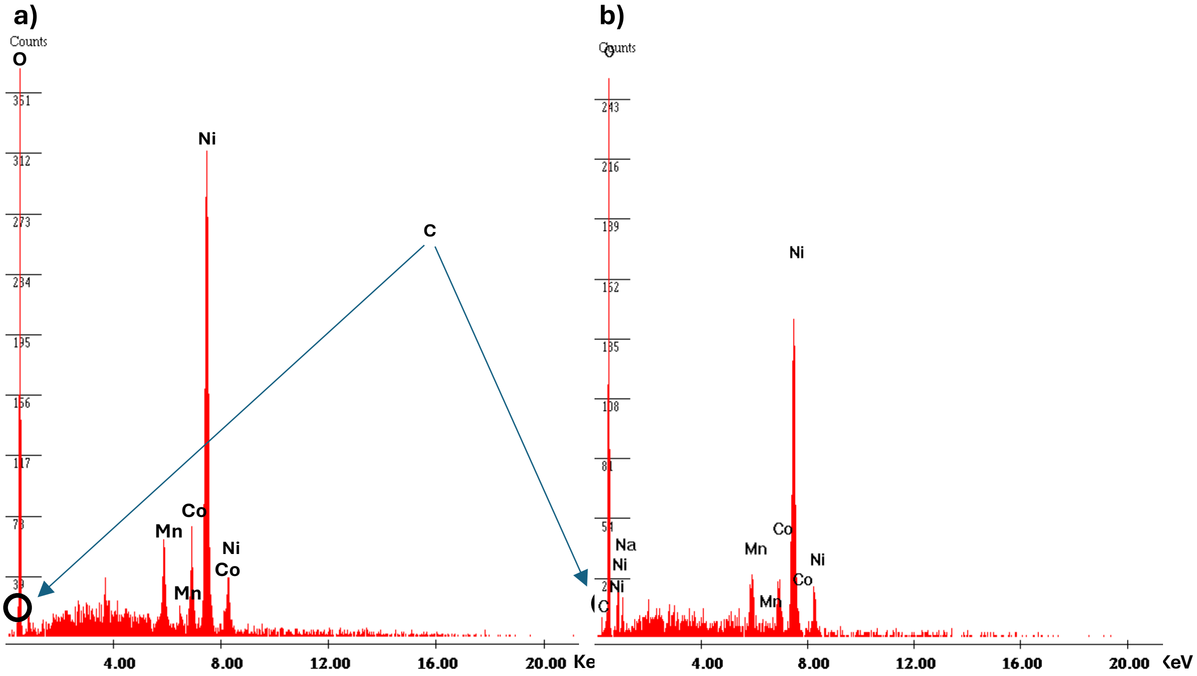

Figure 114 EDAX of NMC811 with a sodium secondary phase ($Li_{(1-x)}Ni_{0.8}Mn_{0.1}Co_{0.1}O_2.0.5xNa_2CO_3$) where Na = x and Li = (1 - x), synthesised with nitrate precursors, and sodium alginate and sodium nitrate where x = 0.2 ($Li_{0.8}Ni_{0.8}Mn_{0.1}Co_{0.1}O_2.0.1Na_2CO_3$) using a) x = 0.1 sodium alginate and x = 0.1 sodium nitrate (Figure 113a) and b) using x = 0.2 sodium alginate (Figure 113b)

4.3.1.3 *Cell cycling of NMC811 with a sodium secondary phase via substitution of Na with Li using sodium alginate, sodium nitrate, and nitrate precursors where x = 0.2, with 4.5 to 2.8 V range*

When lithium-ion cells containing with NMC811 cathodes synthesised with a mix of sodium alginate and $NaNO_3$ (where x = 0.2) are cycled between 4.5 V and 2.8 V at 0.1 C, a slightly higher initial specific discharge capacity of 150 mAh/g, Figure 115b, e, h, (vs. 140 mAh/g when synthesised with 20% Na vs. Li with only sodium alginate, Figure 115k, is present, while cycling retention is comparable to when only synthesising with sodium alginate. The potential formation of less sodium carbonate secondary phase and a slight improvement in the structural organisation between the transition metal and lithium layers when using sodium nitrate may lead to a minor improvement in the initial discharge capacity of the sodium carbonate containing NMC811.

Capacity retention when partially synthesising with sodium nitrate is still poor, Figure 115c, f, i, with the cell undergoes a phase change from H1 to M at 3.7 V, and the M to H2 phase change at 4.4 V during charging, with the phase transitions H2 to M occurring at 4.2 V and M to H1 happening at 3.5 V [142]. Due to the structure of the cathode, the structure does not undergo the H2 to H3 phase change, which also in part explains the lower initial discharge capacity. The cathode undergoes capacity fade due to the M to H2 phase transition occurring above 4.2 V [140], which causes severe structural instability. This is comparable to where the cathode is fully synthesised with sodium alginate, Figure 115l, and as such with the exception of the improved structure of the NMC811 there is little improvement for cell performance when partially synthesising using sodium nitrate and synthesising with sodium alginate and nitrate precursors.

Poor capacity retention may also be a result of the cell manufacturing process, 3.7.4. Damage to the lithium chips caused by oxidation or damage caused by removing oxidation from the chips may reduce the available lithium or compromise the stability of the lithium chip. The electrolyte may also affect performance due to similar reasons, with the electrolyte and potentially have trace amounts of water or degraded affecting cell cyclability. The oxidation of the lithium chip and potential degradation of the electrolyte is a result of the age of both products, with lithium products having undergone supply issues during the project. Poor homogeneity due to poor mixing, a poor drawdown as a result of a too thick or too thin slurry resulting in an irregular cathode thickness, or potential over calendaring of the cathode may also result in differences in the cathode thicknesses or damage to the cathode. This would further affect the cyclability of the cathodes.

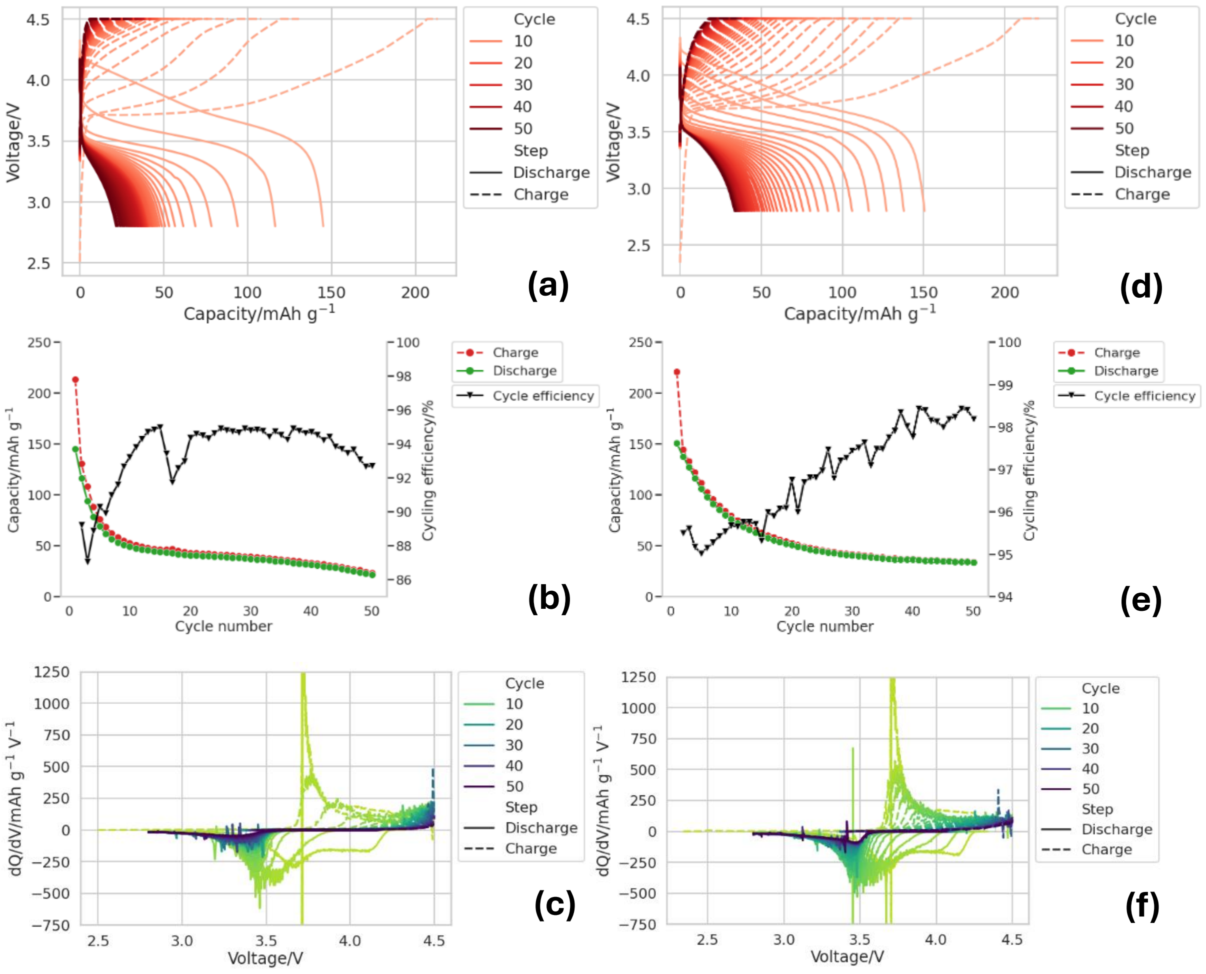
(a)
Voltage/V
Capacity/mAh g^{-1}
Cycle
10
20
30
40
50
Step
Discharge
Charge
(b)
Capacity/mAh g^{-1}
Cycling efficiency/%
Cycle number
Charge
Discharge
Cycle efficiency
(c)
dQ/dV/mAh g^{-1} V^{-1}
Voltage/V
Cycle
10
20
30
40
50
Step
Discharge
Charge
(d)
Voltage/V
Capacity/mAh g^{-1}
Cycle
10
20
30
40
50
Step
Discharge
Charge
(e)
Capacity/mAh g^{-1}
Cycling efficiency/%
Cycle number
Charge
Discharge
Cycle efficiency
(f)
dQ/dV/mAh g^{-1} V^{-1}
Voltage/V
Cycle
10
20
30
40
50
Step
Discharge
Charge

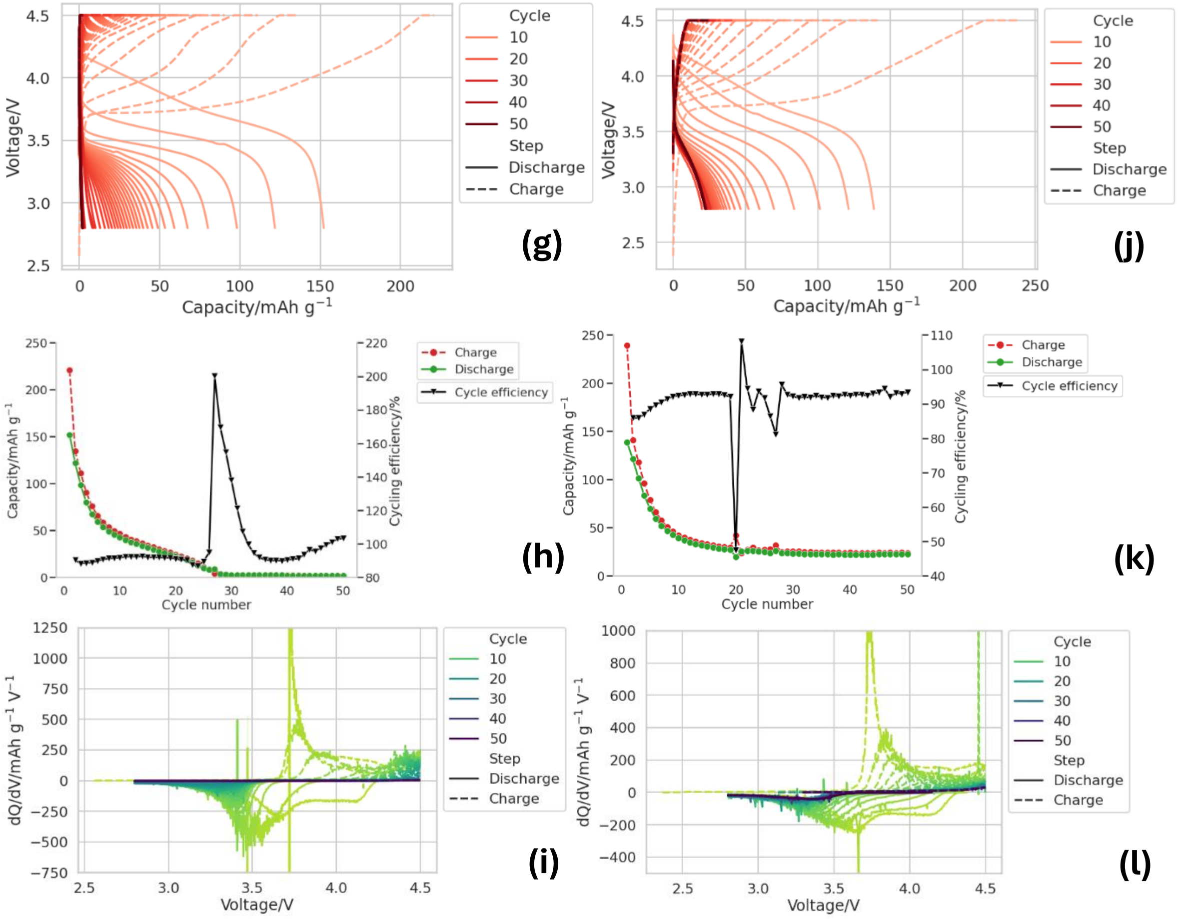

Figure 115 Charge-discharge cycling (a, d, g), Cycling efficiency and charge-discharge capacities (b, e, h), and Differential capacity vs. voltage curve (c, f, i) for Li-ion coin cells 1-3 with nitrate, sodium alginate, and sodium nitrate synthesised cathodes where x = 0.2 ($Li_{0.8}Ni_{0.8}Mn_{0.1}Co_{0.1}O_2.0.1Na_2CO_3$) between 4.5 and 2.8 V for 50 cycles, compared with a cell synthesised using only sodium alginate where x = 0.2 (j, k, l)

4.3.2 Synthesis of NMC811 with sodium via substitution of Na with Li using sodium alginate, sodium nitrate and acetate Precursors

4.3.2.1 X-Ray Diffraction Analysis of NMC811 with a sodium peroxide secondary phase via substitution of Na with Li using sodium alginate, sodium nitrate, and acetate precursors

When NMC811 is synthesised with sodium such that x = 0.2 using acetate precursors, significant disorganisation of the NMC811 occurs when NMC811 is synthesised with both a mix of sodium alginate and sodium nitrate, Figure 116a, and only sodium alginate, Figure 116b. Both powders have no peak splitting at (006)/(012) and (018)/(110) and (003)/(104) peak intensity ratios of less than 1 (where < 1.2 is considered a high level of cation mixing between Li and Ni sites [130]). Synthesising with and without sodium nitrate therefore produces poor layering of the NMC811 and mixing of Li^+ and Ni^{2+} cations in Ni and Li sites [133]. Peaks at 35 and 37 °, (220) and (311) reflections, indicate a Na_2O_2 secondary phase is present in both samples, but higher intensity peaks indicate a higher proportion when only synthesised using sodium alginate, possibly due to the higher mass of biotemplate used resulting in greater substitution of Na^+ ions with metal precursor cations. This would result in a higher proportion of the sodium peroxide secondary phase.

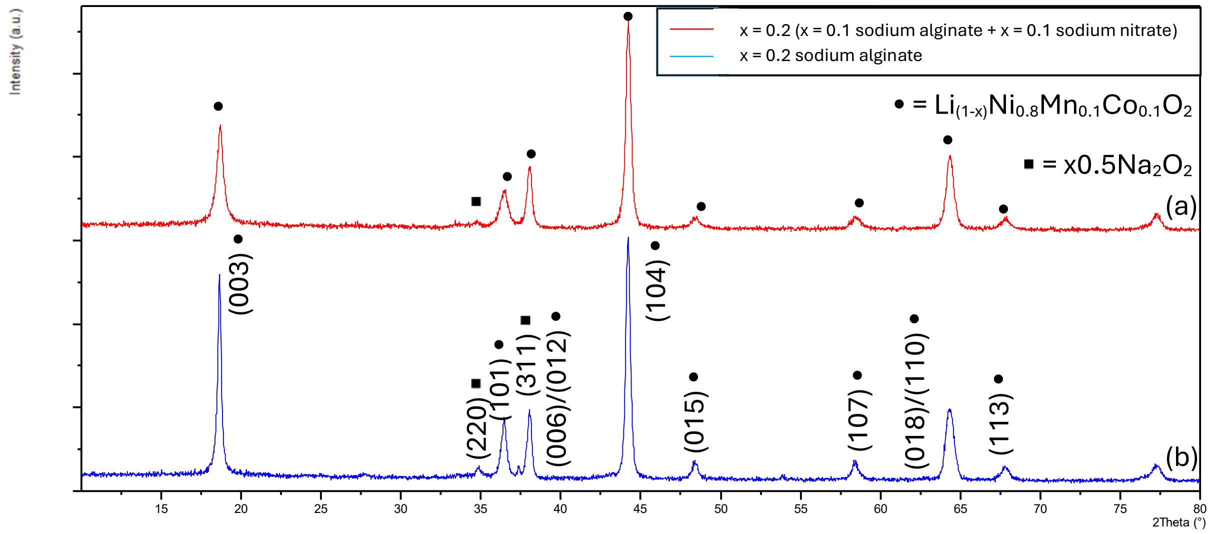

Figure 116 XRD of NMC811 with Na_2O_2 secondary phase ($Li_{(1-x)}Ni_{0.8}Mn_{0.1}Co_{0.1}O_2.x0.5Na_2O_2$) where Na = x and Li = (1 - x), synthesised with acetate precursors, and sodium alginate and sodium nitrate where x = 0.2 ($Li_{0.8}Ni_{0.8}Mn_{0.1}Co_{0.1}O_2.0.1Na_2O_2$) using a) x = 0.1 sodium alginate and x = 0.1 sodium nitrate and b) using x = 0.2 sodium alginate

4.3.2.2 Scanning Electron Microscopy of NMC811 with sodium peroxide secondary phase via substitution of Na with Li using sodium alginate and acetate precursors

Particles for both samples have similar average particle diameters of 300 nm, Figure 117a, when doing with sodium alginate and sodium nitrate and 400 nm, Figure 117b, when synthesising with only sodium alginate. The morphology of the two samples is however different, with agglomerated, rounded, and irregular particles when partially synthesised with Na_2NO_3, and individual octahedral morphologies when using only sodium alginate. Greater agglomeration of primary particles occurs when partially synthesising with sodium nitrate due to the decrease in the biotemplate mass, which results in less chelation of metal cations, while octahedral morphologies are formed when the mass of sodium alginate is increased due to the greater amount of chelation sites.

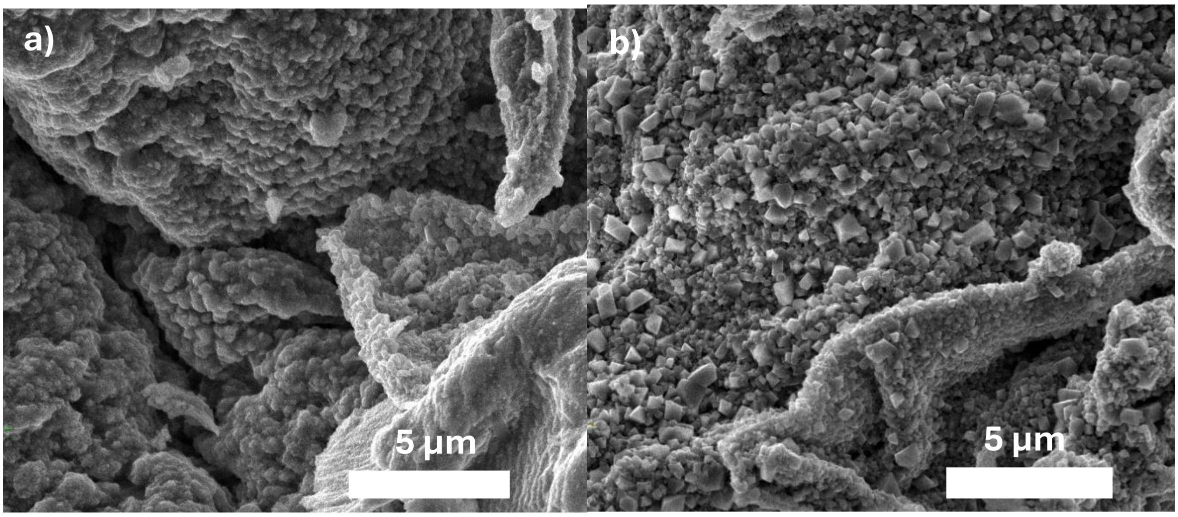

Figure 117 SEM of NMC811 with Na_2O_2 secondary phase ($Li_{(1-x)}Ni_{0.8}Mn_{0.1}Co_{0.1}O_2.x0.5Na_2O_2$) where Na = x and Li = (1 - x), synthesised with acetate precursors, and sodium alginate and sodium nitrate where x = 0.2 ($Li_{0.8}Ni_{0.8}Mn_{0.1}Co_{0.1}O_2.0.1Na_2O_2$) using a) x = 0.1 sodium alginate and x = 0.1 sodium nitrate and which exhibits agglomerated, rounded mrophologies and b) using x = 0.2 sodium alginate with individual octahedral morphologies are present

In summary, use of sodium nitrate as a partial substitute for sodium alginate leads to no overall improvement when synthesising NMC811 when using either acetates or nitrates. Despite an increased mass of sodium alginate leading to a disorganised NMC811 structure and poor cell performance due to the higher content of carbon, partial substitution of sodium nitrate results in the same level of disorganisation and cell performance. This is due to a lack of chelation of the metal cations during the dissolution phase. Evidence of this is observed using SEM, where high agglomeration of primary particles is observed when partially synthesising with sodium nitrate, but when only using sodium alginate particles have octahedral morphologies with much less agglomeration.

4.4 Synthesis of NMC811 with sodium via the substitution of Na with Li, where Na = x and Li = (1 – x), using dextran and sodium nitrate

Synthesising NMC811 using sodium alginate has shown some benefit provided the amount of sodium used does not exceed x = 0.1. When investigated in chapter 3, dextran also proved to have potential in being used as a biotemplate for the synthesis of NMC811, but when such cathodes were used in cells, they were often outperformed by cathodes synthesised using sodium alginate. As such, it is to be investigated whether synthesising dextran biotemplated cathodes using sodium will provide improvements in NMC811 structure and cell performance in the same way that sodium alginate does when used as a biotemplate and whether the substitution of a sodium-containing biotemplate with sodium-containing reactant is viable.

When using dextran as a biotemplate, there minimal sodium impurities present. As such synthesis with sodium will require a separate source of sodium, in this case sodium nitrate, Table 22. By using sodium nitrate to add sodium to NMC811 formed using dextran, a comparison between sodium containing NMC811 synthesised with both sodium alginate and dextran can be drawn.

	X = 0.1	X = 0.2
Lithium acetate dihydrate/Lithium nitrate (g)	0.2296/0.1552	0.2041/0.1379
Dextran (g)	0.25	0.25
Sodium nitrate (g)	0.0213	0.0425

Table 22 Masses of metal precursor salts used in the synthesis of Na-containing NMC811 via substitution of lithium ($Li_{(1-x)}Na_xNi_{0.8}Mn_{0.1}Co_{0.1}O_2$) when using dextran as a biotemplate and using sodium nitrate

4.4.1 Synthesis of NMC811 with sodium via substitution of Na with Li using dextran, sodium nitrate, and nitrate precursors using nitrate precursors

4.4.1.1 X-Ray Diffraction Analysis NMC811 with sodium via substitution of Na with Li using dextran, sodium nitrate, and nitrate precursors using nitrate precursors

When dextran and nitrate synthesised NMC811 is synthesised with sodium nitrate significant disorganisation occurs such that x = 0.1, Figure 118a, and x = 0.2, Figure 118b. Both samples have non-existent (006)/(012) and (018)/(110) peak splitting indicating very poor layering of the NMC811 structure and have (003)/(104) peak intensity ratios of less than or equal to 1 highlighting high mixing of Li and Ni cations in Ni and Li sites [133] (where < 1.2 is considered high levels of mixing [130]). The use of dextran, a high carbon containing biotemplate, results in the formation of the reducing carbon dioxide atmosphere as the dextran breaks down and the freed up carbon reacts with the oxygen atmosphere. This reducing atmosphere results in this more disorganised structure and greater mixing of ions due to there being less oxygen present in the atmosphere to react with the metal ions and form a stoichiometric layered NMC811 structure. When synthesising NMC811 using either mass of sodium nitrate, there is evidence of a sodium secondary phase with low intensity peaks when x = 0.1 and 0.2, showing the presence of sodium carbonate. The low intensity of the peaks is possible due to the use of sodium nitrate instead of sodium alginate, of which has a lower carbon content and so would produce less of a carbonate secondary phase.

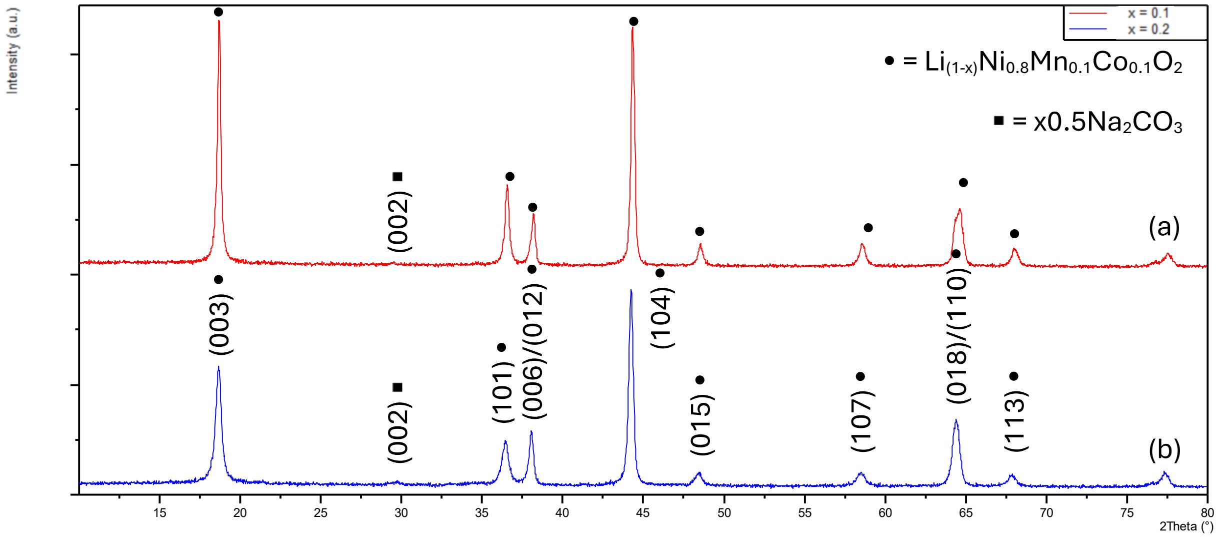

Figure 118 XRD of NMC811 with Na_2CO_3 secondary phase ($Li_{(1-x)}Ni_{0.8}Mn_{0.1}Co_{0.1}O_2.x0.5Na_2CO_3$) where Na = x and Li = (1 - x), synthesised with nitrate precursors and dextran, and sodium nitrate where a) x = 0.1 ($Li_{0.9}Ni_{0.8}Mn_{0.1}Co_{0.1}O_2.0.05Na_2CO_3$) and b) x = 0.2 ($Li_{0.8}Ni_{0.8}Mn_{0.1}Co_{0.1}O_2.0.1Na_2CO_3$)

4.4.1.2 Scanning Electron Microscopy of NMC811 with sodium via substitution of Na with Li using dextran, sodium nitrate, and nitrate precursors using nitrate precursors

Particles synthesised with dextran and sodium nitrate exhibit similar morphologies regardless of the amount of sodium used. When synthesised with sodium nitrate such that x = 0.1 or 0.2, Figure 119a and b respectively, both samples have average particle morphologies of 400 nm with a mix of individual octahedral primary particles and highly agglomerated irregularly shaped primary particles. The amount of octahedral primary particles are however indicative of sodium ions chelating to the biotemplate (with octahedral morphologies normally being observed with sodium alginate biotemplated samples). Despite this the high levels of agglomeration in both samples would significantly reduce the surface area for lithiation and lead to a reduction in specific capacity. The similarities in morphology are due to using the same mass of biotemplate in both samples, and so the same amount of chelation sites.

An increase in sodium from x = 0.1 to x = 0.2 does little to affect the overall particle morphology. Furthermore, it is not viable to use NMC811 that has been synthesised with the secondary sodium carbonate phase using dextran, sodium nitrate, and nitrate precursors in lithium-ion cells due to the high levels of agglomeration and poor organisation of the NMC811 structure.

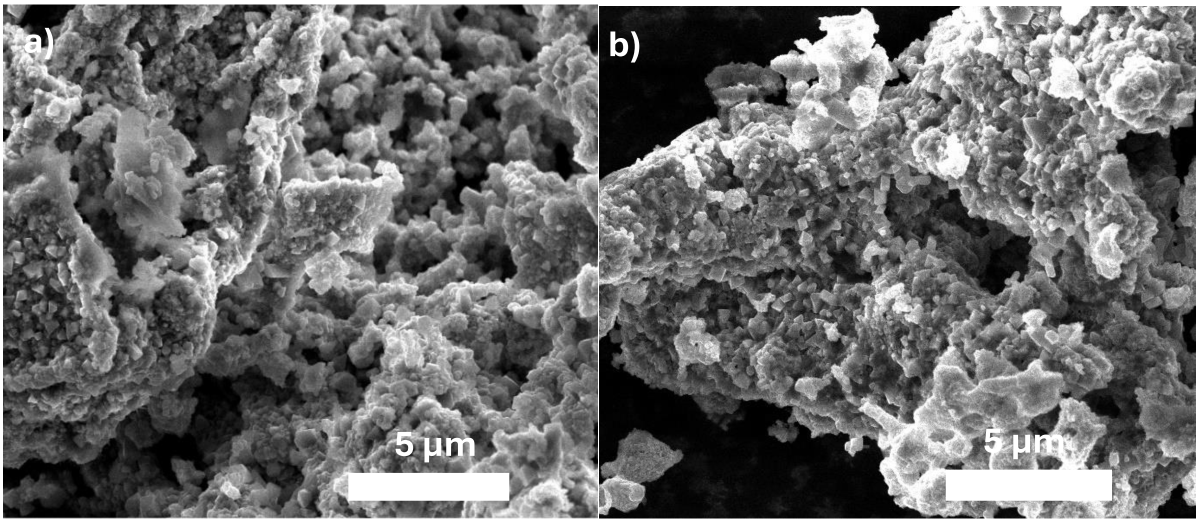

Figure 119 SEM of NMC811 with sodium carbonate ($Li_{(1-x)}Ni_{0.8}Mn_{0.1}Co_{0.1}O_2.x0.5Na_2CO_3$) where Na = x and Li = (1 - x), synthesised with nitrate precursors and dextran, and sodium nitrate where a) x = 0.1 ($Li_{0.9}Ni_{0.8}Mn_{0.1}Co_{0.1}O_2.0.05Na_2CO_3$) and b) x = 0.2 ($Li_{0.8}Ni_{0.8}Mn_{0.1}Co_{0.1}O_2.0.1Na_2CO_3$)

4.4.2 Synthesis of NMC811 with sodium via substitution of Na with Li using dextran, sodium nitrate, using acetate precursors

4.4.2.1 X-Ray Diffraction Analysis of NMC811 with sodium peroxide secondary phase via substitution of Na with Li using dextran, sodium nitrate, using acetate precursors

Similarly to when using nitrate precursors, significant disorganisation of the NMC811 is present when x = 0.1 Figure 120a, and when x = 0.2, Figure 120b. (003)/(104) peak intensity ratios of below 1.1 for both samples signify significant mixing of metal cations in lithium and nickel sites [133], with no peak splitting at (006)/(012) and (018)/(110) highlighting significant lack of layering when synthesising NMC811 where x = 0.1 or x = 0.2. While an apparent lack of peaks may indicate no secondary sodium phase and that incorporation of sodium using sodium nitrate into the NMC811 structure appears to take place as indicated, low intensity peaks are present at closer inspection indicating a secondary Na_2O_2 phase. When compared against disorganisation of NMC811 when using nitrate precursors, a similar level of disorganisation is present when using acetate precursors. Overall, synthesising NMC811 where x = 0.1 may prove viable when using acetates, though may still exhibit poor cell performance characteristics, with synthesising NMC811 where x = 0.2 producing too much disorganisation structure too much to be viable.

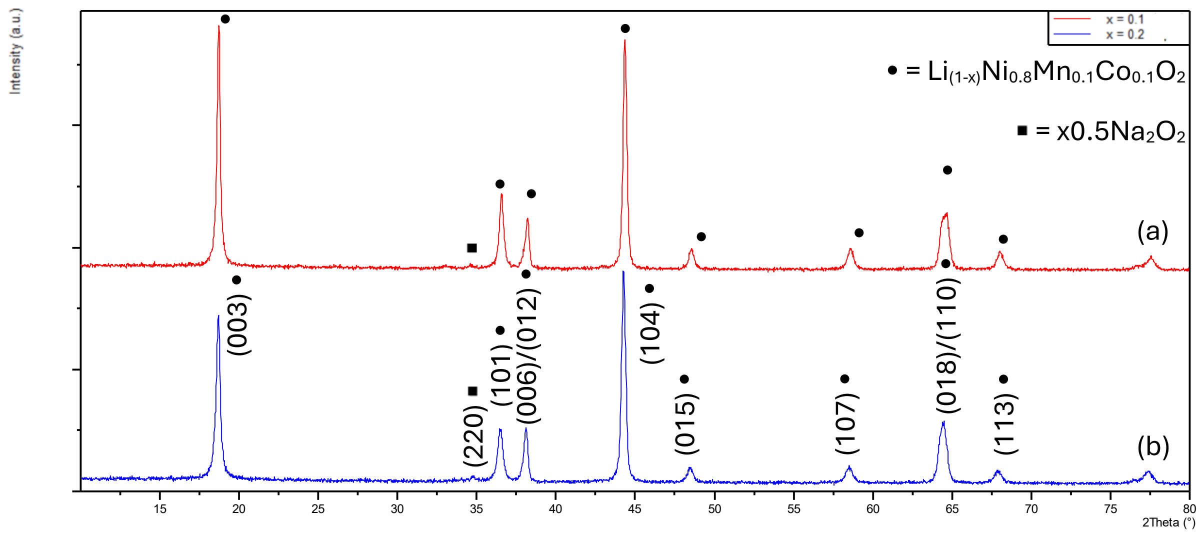

Figure 120 XRD of NMC811 with Na_2O_2 secondary phase ($Li_{(1-x)}Ni_{0.8}Mn_{0.1}Co_{0.1}O_2.x0.5Na_2O_2$) where Na = x and Li = (1 - x), synthesised with acetate precursors and dextran, and sodium nitrate where a) x = 0.1 ($Li_{0.9}Ni_{0.8}Mn_{0.1}Co_{0.1}O_2.0.05Na_2O_2$) and b) x = 0.2 ($Li_{0.8}Ni_{0.8}Mn_{0.1}Co_{0.1}O_2.0.1Na_2O_2$)

4.4.2.2 Morphology of NMC811 with sodium peroxide secondary phase via substitution of Na with Li using dextran, sodium nitrate, using acetate precursors

In terms of particle morphology, there seems to be little difference when synthesising NMC811 with sodium where x = 0.1, Figure 121a, or x = 0.2, Figure 121b. Both samples have a high level of agglomeration with few individual primary particles. The small proportion of non-agglomerated primary particles, most noticeably seen where x = 0.1 and denoted by yellow circles, have an average particle diameter of 400 nm and have octahedral morphologies. These particles proportionally make up significantly less of the sample when compared to the large number of agglomerated particles but are an indicator that chelation of some of the sodium ions onto the dextran biotemplate occurred (with such morphologies often being present when using sodium alginate biotemplates). The high level of agglomeration is possibly indicative that the samples were synthesised under a more reducing atmosphere, with a high calcination temperature and/or more oxidising atmosphere being required to provide the necessary conditions for growth of non-agglomerated primary particles. The reducing atmosphere is likely caused by the high content of carbon in the dextran and acetates, which is freed up when the decomposition of the biotemplate and precursor occurs and reacts with the oxygen atmosphere to form CO_2, a reducing atmosphere. This contributes to the high structural disorganisation and poor layering of the NMC811 as there is less oxygen available in the atmosphere for the synthesis of NMC811 resulting in unfilled oxygen sites and greater disorganisation [133] . This high level of agglomeration vs. a small number of nanoscale primary particles will likely negatively affect the performance of the cathode, specifically specific capacity, regardless of the amount of sodium used during NMC811 synthesis due to the smaller surface area available for lithium intercalation.

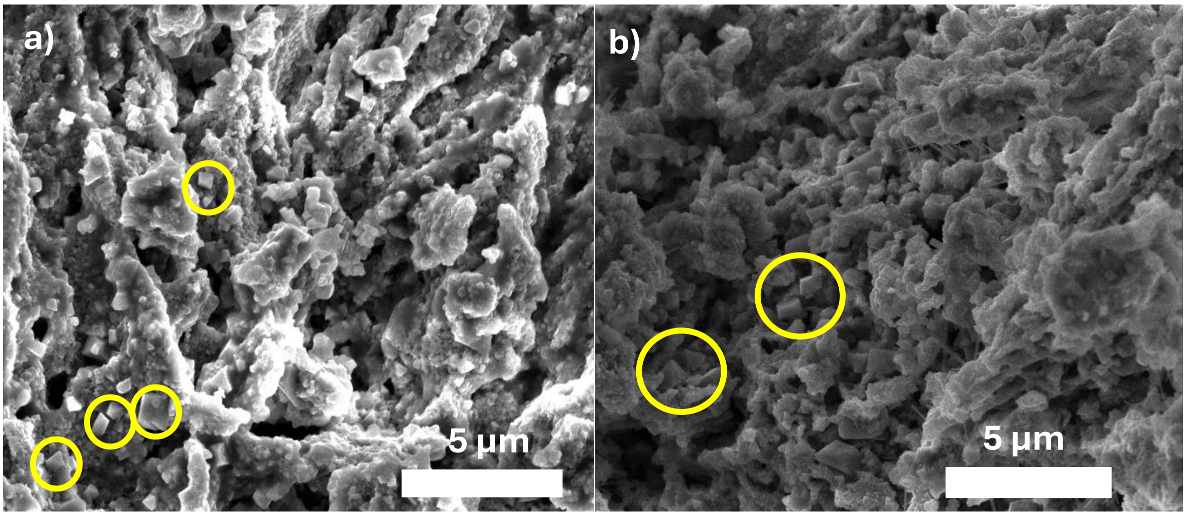

Figure 121 SEM of NMC811 with Na_2O_2 ($Li_{(1-x)}Ni_{0.8}Mn_{0.1}Co_{0.1}O_2.x0.5Na_2O_2$) where Na = x and Li = (1 - x), synthesised with acetate precursors and dextran, and sodium nitrate as the where a) x = 0.1 ($Li_{0.9}Ni_{0.8}Mn_{0.1}Co_{0.1}O_2.0.05Na_2O_2$) and b) x = 0.2 ($Li_{0.8}Ni_{0.8}Mn_{0.1}Co_{0.1}O_2.0.1Na_2O_2$), with octahedral primary particles highlighted in yellow

4.4.2.3 Cell cycling of NMC811 with sodium peroxide secondary phase via substitution of Na with Li using dextran, sodium nitrate, and acetate precursors where x = 0.1, with 4.5 to 2.8 V range

When cycled between 4.5 V and 2.8 V at 0.1C, a cell with a cathode with dextran, acetate precursors, and sodium nitrate such that x = 0.1 has comparable performance compared to a cell with a cathode synthesised using equal parts sodium alginate and sodium nitrate such that x = 0.2, Figure 115. Cycling shows an initial discharge capacity of 150 mAh/g, Figure 122b, and a capacity decrease of 100 mAh/g over 15 cycles before a significant increase in the rate of capacity retention below 50 mAh/g. The lower initial discharge capacity highlights a decrease in lithium available for intercalation and an inability for sodium to intercalate in the lithium-ion cell . Phase transitions of H1 to M at 3.8 V and M to H2 at 4.25 during charging, Figure 122c, and from H2 to M at 4.2 V and M to H1 at 3.8 V during discharge indicate two main phase changes of the structure during cycling [142]. Cycling above 4.2 V results in the breakdown of the NMC811 structure [142] with the required voltage for all phase changes exceeding 4.5 V after 50 cycles, resulting in the cell stabilising at 50 mAh/g specific discharge capacity. The high capacity fade between 150 and 50 mAh/g highlights that the addition of sodium secondary phase does not improve structural stability and that cycling above 4.2 V still leads to structural deterioration. This indicates that the substitution of lithium for sodium, which lowered the specific capacity due to less lithium being available to intercalate, is not a viable compromise however the cycling still shows the comparability between dextran biotemplated cathodes synthesised with sodium nitrate (x = 0.1) and sodium alginate biotemplated cathodes synthesised with sodium using and not using sodium nitrate (x = 0.1 and 0.2 respectively).

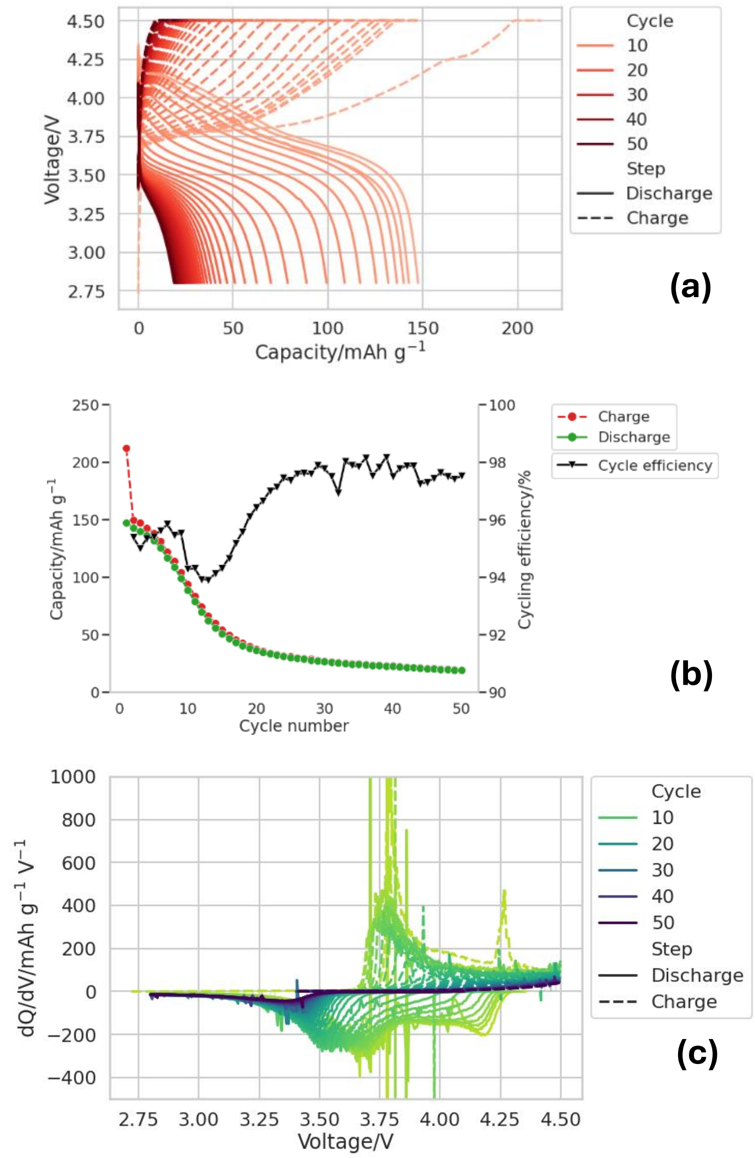

Figure 122 Charge-discharge cycling (a), Cycling efficiency and charge-discharge capacities (b), and Differential capacity vs. voltage curve (c) for Li-ion coin cell cycled between 4.5 and 2.8 V for 50 cycles with acetate and dextran, and sodium nitrate synthesised cathode where x = 0.1 ($Li_{0.9}Ni_{0.8}Mn_{0.1}Co_{0.1}O_2.0.05Na_2O_2$)

4.4.2.4 Cell cycling of NMC811 with sodium peroxide secondary phase via substitution of Na with Li using dextran, sodium nitrate, and acetate precursors where x = 0.2, with 4.5 to 2.8 V range

When the amount of sodium is increased to where x = 0.2, dextran and acetate synthesised cathodes are not able to perform viably within the lithium-ion cells. Initial specific discharge capacity ranges between 90 and (110) mAh/g, Figure 123a, d, with both cathodes also exhibiting poor capacity retention with specific discharge capacity decreasing to a maximum of 25 mAh/g well before the cell has undergone 50 cycles. The decrease in initial specific discharge capacity is due to a reduction in available lithium for intercalation, with the proportion of Li being 0.8, and an inability for the substituted sodium to intercalate due to being in the form of a Na secondary phase The differential capacity of the cells meanwhile, Figure 123c, f, shows how the structure begins to break down when cycled above 4.2 V leading to significant capacity fade [142]. During the initial charging cycle cathodes undergo phase changes from the H1 to M phase at 3.8 V and M to H2 at 4.4 V, with a phase change of H2 to M at 4.2 V and M to H1 at 3.6 V [142]. Due to the disorganised structure of the NMC811 there is no observed H2 to H3 phase change, however due to cycling over 4.2 V further deterioration of the structure occurs such that the H1 to M phase change occurs at 4.5 V after 50 cycles. As such after 50 cycles maximum specific discharge capacity is maintained at 25 mAh/g due to a further lack of phase changes, as well as sodium within the structure providing no observed benefit to improving the structure of the NMC811 during cycling.

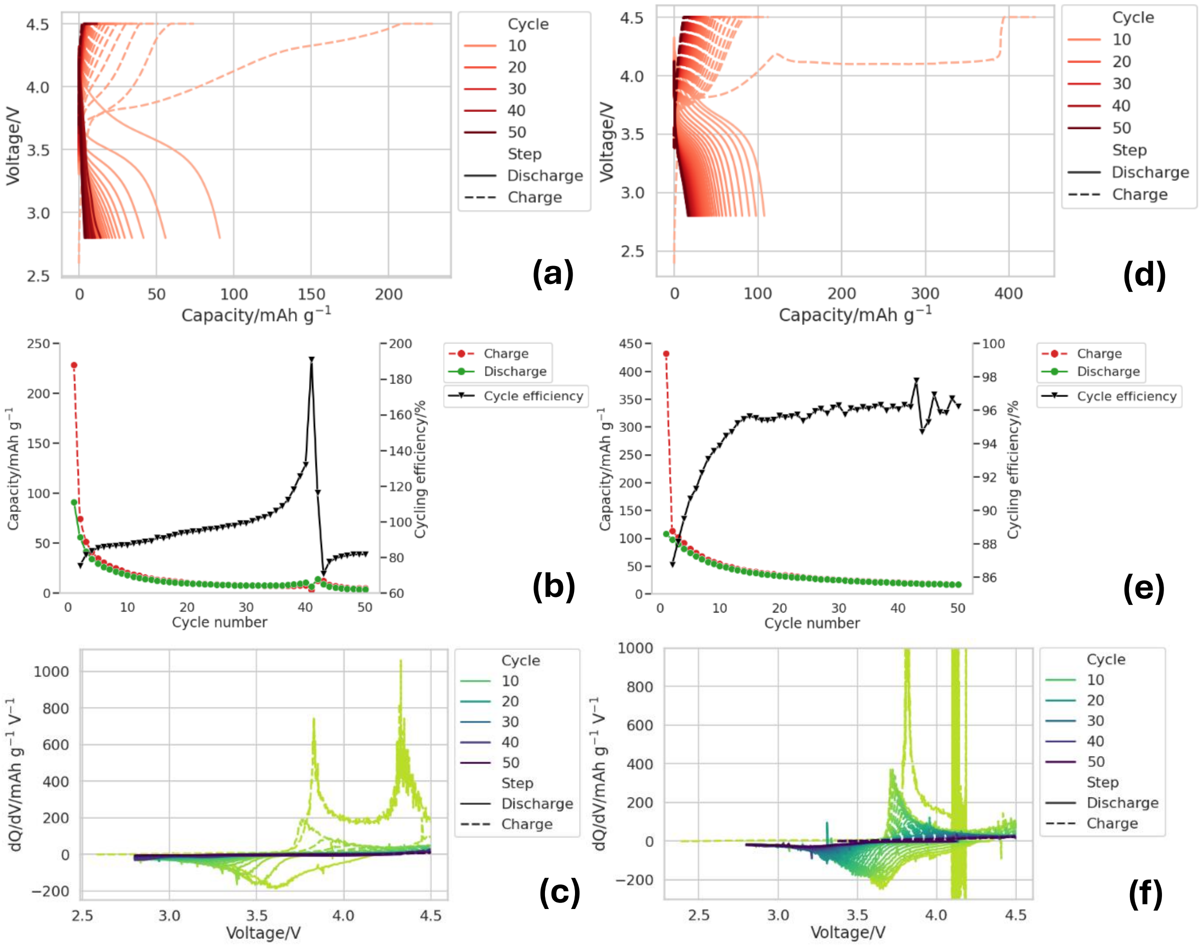

Figure 123 Charge-discharge cycling (a, d), Cycling efficiency and charge-discharge capacities (b, e), and Differential capacity vs. voltage curve (c, f) for Li-ion coin cells 1-2 cycled between 4.5 and 2.8 V for 50 cycles with acetate and dextran, and sodium nitrate synthesised cathode where x = 0.2 ($Li_{0.8}Ni_{0.8}Mn_{0.1}Co_{0.1}O_2.0.1Na_2O_2$)

4.4.2.5 Further discussion of cell cycling data

The poor cathode performance, most significantly when cycling cathodes where x = 0.2, may be further explained by issues in the cell manufacturing process, 3.7.4. The length of the storage times of the lithium chips and electrolyte, in part caused by poor supply issues of lithium products during the project, resulted in oxidation of the cathodes and potential degradation of and water being present in the electrolyte. The loss of lithium due to either the oxidation or potential damage caused by the removal of oxidation could affect cell capacity, while degradation of the electrolyte may affect cell cycling as ionic diffusivity decreases. Poor mixing of the cathode slurry, resulting in an inhomogeneous or too thick or too thin slurry, coupled with a poor drawdown and the potential for over calendaring would further hinder cell performance. The inhomogeneity of the slurry may lead to variety in the ratio of active material in the cathode between cells, resulting in different capacities as the amount of active material varies and different capabilities as the ratio of additives is varied. Meanwhile over calendaring may damage the cathode, resulting in a greater chance of early cell failure.

4.4.3 Discussion of NMC811 synthesised via the substitution of Li with Na with dextran and sodium nitrate

Dextran biotemplated cathodes synthesised where $x = 0.2$ perform worse than dextran biotemplated cathodes synthesised where $x = 0.1$. While having similar levels of capacity fade, the reduction in lithium available for intercalation and large agglomerations of particles reducing the surface area available for intercalation leads to a significant reduction in discharge capacity without any observed benefit from the sodium being substituted in. Furthermore, there is no perceived benefit to using dextran biotemplated NMC811 synthesised with sodium over NMC811 using sodium alginate as a biotemplate, with both cathodes showing similar levels of specific discharge capacity and capacity fade. While sodium was seen to give no overall benefit to improving structural stability or capacity retention, the substituting out of lithium also significantly reduced cell specific discharge capacity. As such, increasing the amount of lithium while maintaining the amount of sodium used may be an alternative way to synthesise NMC811 cathodes.

4.5 Synthesis of NMC811 with sodium via the addition of Na, where Na = x and Li = 1, using sodium alginate

Evidence suggests that the substitution of lithium with sodium produces no overall benefit in the organisation of the NMC811 structure or in improvements to cell performance. Specific capacity is lower due to the reduced the amount of lithium available for intercalation as a result of substituting out lithium for sodium. Despite a reduction in cell specific capacity, the addition of sodium gives no overall benefit to structural stability, potential due to existing in the form of a sodium carbonate or peroxide secondary phase, and results in both a more disorganised NMC811 structure formed during synthesis and significant capacity fade during cycling to 4.5 V.

One of the main problems with this synthesis of NMC811 with the addition of sodium is the removal of lithium with the subsequent replacement of sodium which led to poor specific capacity and NMC811 structure. When synthesising NMC811 using sodium alginate in chapter 3, dissolved sodium alginate was added to a mixture of dissolved metal precursor ions using the masses outlined in section 2.1.1 such that NMC811 would be $Li_1Ni_{0.8}Mn_{0.1}Co_{0.1}O_2$. Using this method no lithium was substituted or removed from the NMC811 regardless of the mass of sodium alginate

As such, the synthesis of NMC811 with sodium will be investigated using an alternative method, outlined in section 2.1.3, where sodium ions are added to NMC811 without the substitution of lithium using established masses of Ni, Mn, and Co and where Na = x and Li = 1, Table 23. The aim of synthesising NMC811 with sodium using this altered method is to improve the specific capacity of NMC811 by not reducing the amount of lithium available for intercalation while improving the structural stability and cycling of NMC811 through the addition of sodium ions.

	Acetate Hydrate	Nitrate Hydrate
Lithium (g)	0.2551	0.1724
Nickel (g)	0.4977	0.5816
Manganese (g)	0.0613	0.0447
Cobalt (g)	0.0623	0.0727
Sodium alginate, x = 0.1 (g)	0.1	0.1
Sodium alginate, x = 0.2 (g)	0.25	0.25

Table 23 Masses of metal precursor salts used in the synthesis of NMC811 with sodium via addition of sodium using sodium alginate and/or sodium nitrate

4.5.1 Synthesis of NMC811 with sodium carbonate secondary phase via the addition of Na, where Na = x and Li = 1, using sodium alginate and nitrate precursors

4.5.1.1 X-Ray Diffraction Analysis of NMC811 with sodium carbonate secondary phase via the addition of Na, where Na = x and Li = 1, using sodium alginate and nitrate precursors

By varying the mass of sodium alginate biotemplate used and so the amount of sodium present such that x = 0.1, Figure 124a, x = 0.2, Figure 124b, and x = 0.3, Figure 124c. Peak intensity ratios between (003)/(104) of 1.53 and 1.58 indicate low levels of cation mixing between Li and Ni sites [133] when x = 0.1 ($LiNi_{0.8}Mn_{0.1}Co_{0.1}O_2.0.05Na_2CO_3$) and x = 0.2 ($LiNi_{0.8}Mn_{0.1}Co_{0.1}O_2.0.1Na_2CO_3$) respectively, while the ratio where x = 0.3 ($LiNi_{0.8}Mn_{0.1}Co_{0.1}O_2.0.15Na_2CO_3$) is 1.12 indicating high levels of Li^+ and Ni^{2+} ions mixing in Ni and Li sites. Peak splitting of (006)/(012) and (018)/(110) peaks shows good layering of the NMC811 structure when x = 0.1 or 0.2, but poor layering where x = 0.3 due to minimal peak splitting being present.

When NMC811 is synthesised where x = 0.2 or 0.3, a secondary sodium phase of sodium carbonate is present highlighting a lack of incorporation of at least some of the sodium into the NMC811 structure. Such peaks are not present when x = 0.1, possibly due to the amount of sodium being present in the sample not being a high enough amount to be registered by XRD. Despite this lack on incorporation of the sodium and its existence as a secondary phase, the intensity of the peaks indicating NMC811 where x = 0.1 and 0.2 highlight an organised layered structure due to the present sodium existing as a sodium carbonate secondary phase and not incorporating into the NMC811 structure, while when x = 0.3 there is significant disorganisation of the NMC811, possibly due to a higher amount of biotemplate used in synthesis. Such an increase in biotemplate would result in more carbon being present in the reaction as carbon is freed up from the decomposition of the biotemplate and would result in a greater production of a reducing CO_2 atmosphere as the carbon reacts with the oxygen atmosphere. This would then result in less oxygen available for the formation of the NMC811 resulting in fewer oxygen sites being filled and a greater disorganisation of the structure.

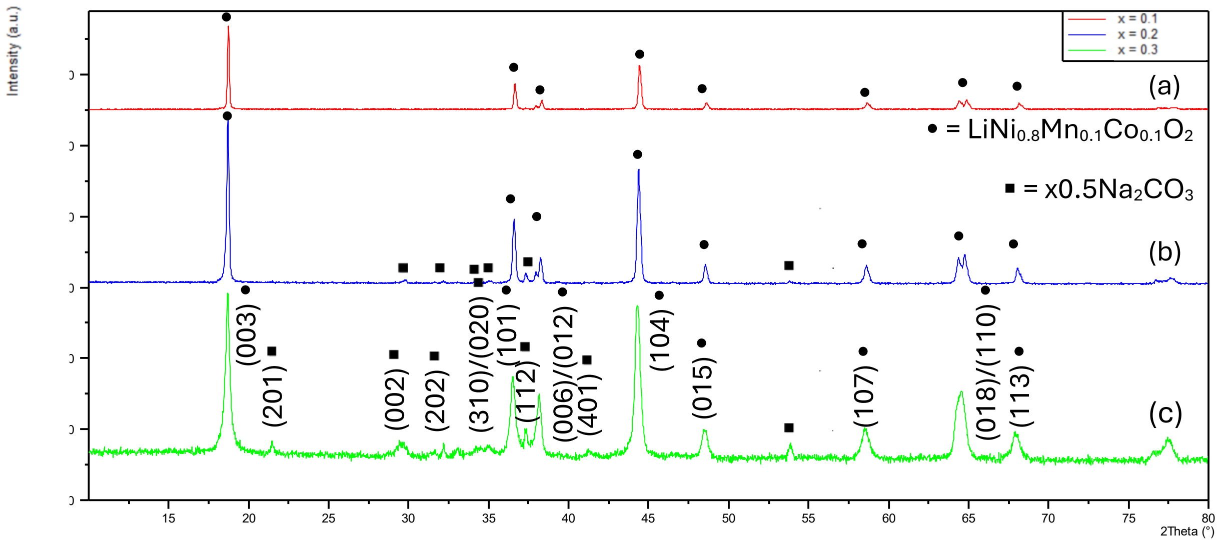

Figure 124 XRD of NMC811 with sodium carbonate ($LiNi_{0.8}Mn_{0.1}Co_{0.1}O_2.x0.5Na_2CO_3$) where Na = x and Li = 1, synthesised with nitrate precursors and sodium alginate where a) x = 0.1 ($LiNi_{0.8}Mn_{0.1}Co_{0.1}O_2.x0.05Na_2CO_3$), b) x = 0.2 ($LiNi_{0.8}Mn_{0.1}Co_{0.1}O_2.x0.1Na_2CO_3$), and c) x = 0.3 ($LiNi_{0.8}Mn_{0.1}Co_{0.1}O_2.x0.15Na_2CO_3$),

4.5.1.2 Morphology of NMC811 with sodium carbonate secondary phase via the addition of Na, where Na = x and Li = 1, using sodium alginate and nitrate precursors

As the amount of sodium is increased, particle morphology is altered significantly. With NMC811 synthesised where x = 0.1, Figure 125a, average particle diameter is 900 nm with a rounded yet irregular morphology. When the amount of sodium is increased to where x = 0.2, Figure 125b, average particle diameter remains 900 nm, the same as where x = 0.1, but with a significantly different morphology with a greater variety of particle shapes ranging from tetragonal and octahedral particles to irregular, round particles. Agglomeration is also present, highlighting not only the effect the increase in the use of sodium alginate biotemplate has on the morphology, but also how the secondary sodium carbonate phase increases the likelihood of agglomeration. Where x = 0.3, Figure 125c, formations of large octahedral particles with average particle diameter of 900 nm are present in addition to irregular, round particles of an average particle diameter of 150 nm. Large amounts of agglomeration of particles is also present as the sodium carbonate secondary phase becomes more prominent with the increase in the proportion of sodium.

The synthesis of octahedrally shaped particles from where x = 0.1 to x = 0.2 and then their synthesis where x = 0.3 highlights how the octahedral morphology is proportional to the amount of sodium alginate biotemplate being used and the increase in chelation sites for metal precursor ions to chelate to. The average particle size of the octahedral morphologies is the same across all levels of added sodium due to similar synthesis conditions resulting in similar conditions for particle growth. Synthesis conditions are similar due to the use of nitrate precursors and the increase in sodium alginate leading to an insignificant increase in carbon content, and so carbon freed up from the decomposition of the biotemplate and precursor, which reacts with the oxygen atmosphere to form CO_2. As such there is little change in the amount of CO_2 being synthesised and the reduction of the environmental conditions.

Furthermore, a significant proportion of the carbon is reacted with the sodium to form the sodium carbonate secondary phase where x = 0.2 and 0.3, causing agglomeration of primary particles. At x = 0.2, such agglomerations are minor enough that they may only lead to a minimal reduction in surface area for intercalation and so only a small decrease in cell performance.

This in addition to the organised NMC811 structure ensures this amount of sodium is still viable. Where x = 0.3 the more substantial agglomerations may lead to a significant capacity decrease due to a significant reduction in surface area and lithiation sites, which along with a disorganised NMC811 structure suggests this cathode's use in a cell would not be viable.

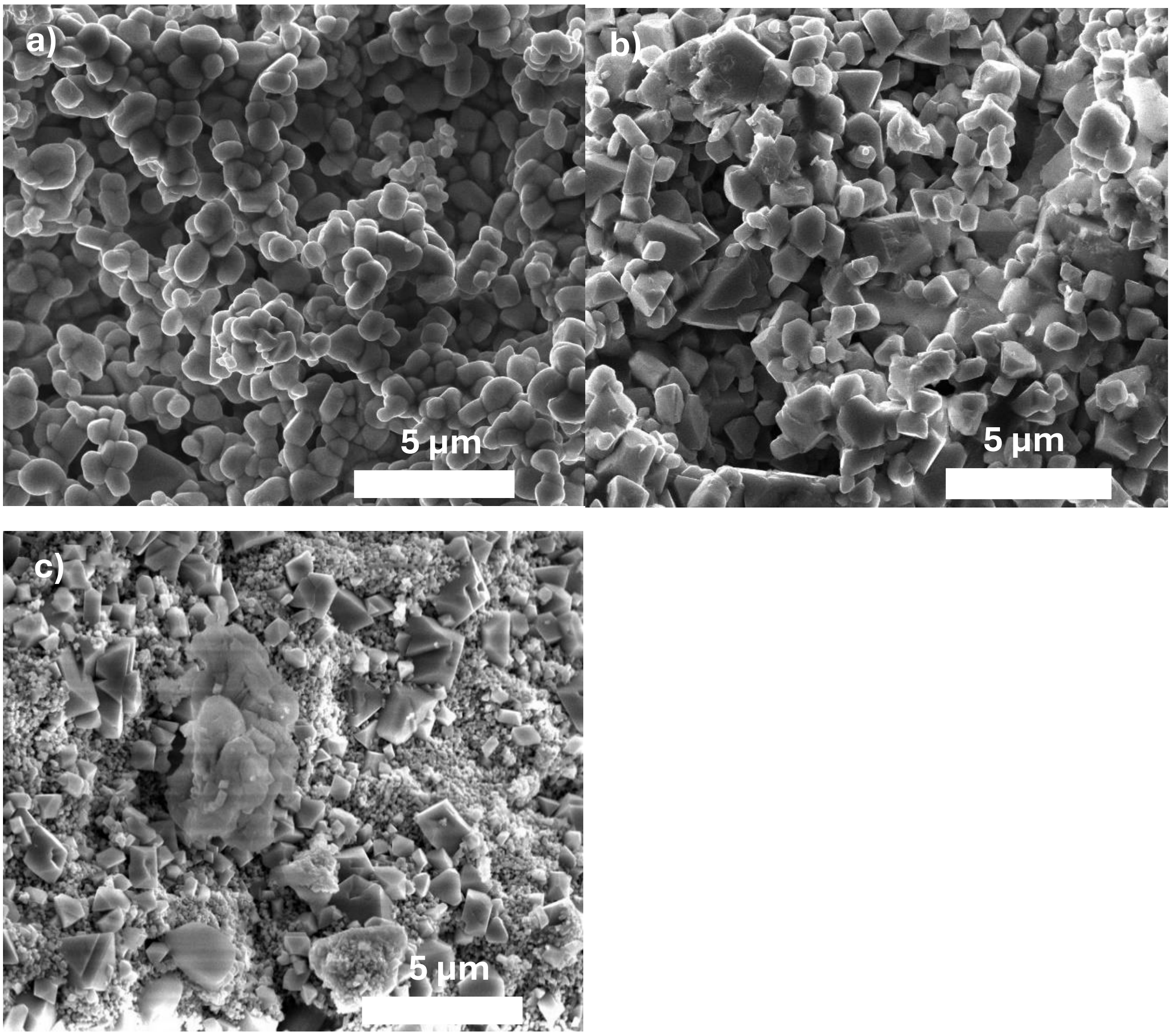

Figure 125 SEM of NMC811 with sodium carbonate ($LiNi_{0.8}Mn_{0.1}Co_{0.1}O_2.x0.5Na_2CO_3$) where Na = x and Li = 1, synthesised with nitrate precursors and sodium alginate where a) x = 0.1 ($LiNi_{0.8}Mn_{0.1}Co_{0.1}O_2.x0.05Na_2CO_3$), and exhibits rounded irregular particles, b) x = 0.2 ($LiNi_{0.8}Mn_{0.1}Co_{0.1}O_2.x0.1Na_2CO_3$), and exhibits tetragonal/octahedral morphologies and c) x = 0.3 ($LiNi_{0.8}Mn_{0.1}Co_{0.1}O_2.x0.15Na_2CO_{31}O_2$) which exhibits octahedral, rounded, and agglomerated primary particles,

4.5.1.3 Cell cycling of NMC811 with sodium carbonate via addition of Na using sodium alginate and nitrate precursors where x = 0.1, with 4.5 to 2.8 V range

When cathodes synthesised where x = 0.1 are cycled in lithium ion cells, performance is initially promising with an initial specific discharge capacity of between 130 and 200 mAh/g, Figure 126b, e, h, when cycling between 4.5 V and 2.8 V at 0.1 C. Capacity retention, while being high for one cell where capacity fade is only 30 mAh/g over 50 cycles, Figure 126d, is generally poor with significant capacity fade to 0 mAh/g after 50 cycles, Figure 126a, g. During the initial charge cycle, phase changes of H1 to M and M to H2 observed from the differential capacity curve at 3.7 and 4.2 V, and H2 to M at 4.2 V and M to H1 at 3.8 V during discharge highlight how the initial discharge capacities are reached [142]. As there is no H2 to H3 phase change observed, specific discharge capacity does not exceed 200 mAh/g. The cathodes begin to deteriorate in subsequent cycles due to the M to H2 phase change occurring at or above 4.2 V [140], leading to higher voltages being required for the phase changes such that at the 50th cycle a voltage above 4.5 V is required for the H1 to M phase change causing cell failure.

When sodium is added where Li = 1 and Na = 0.1, NMC811 shows high capacity due to plentiful lithium for intercalation, and the potential for improved capacity retention relative to other cells highlighting improved structural stability. Such capacity retention however is not a given and so the structure of the NMC811 is still prone to significant deformation.

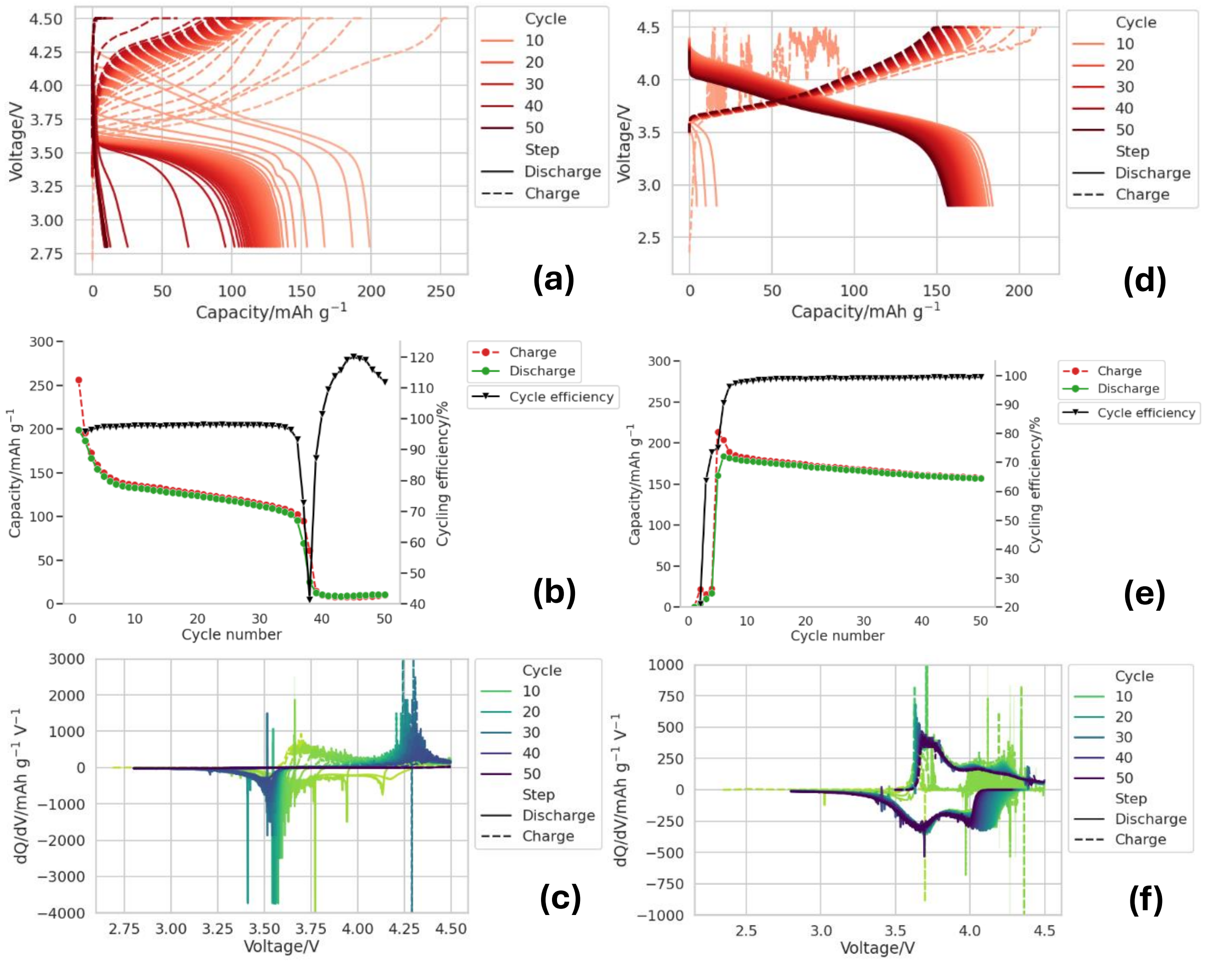

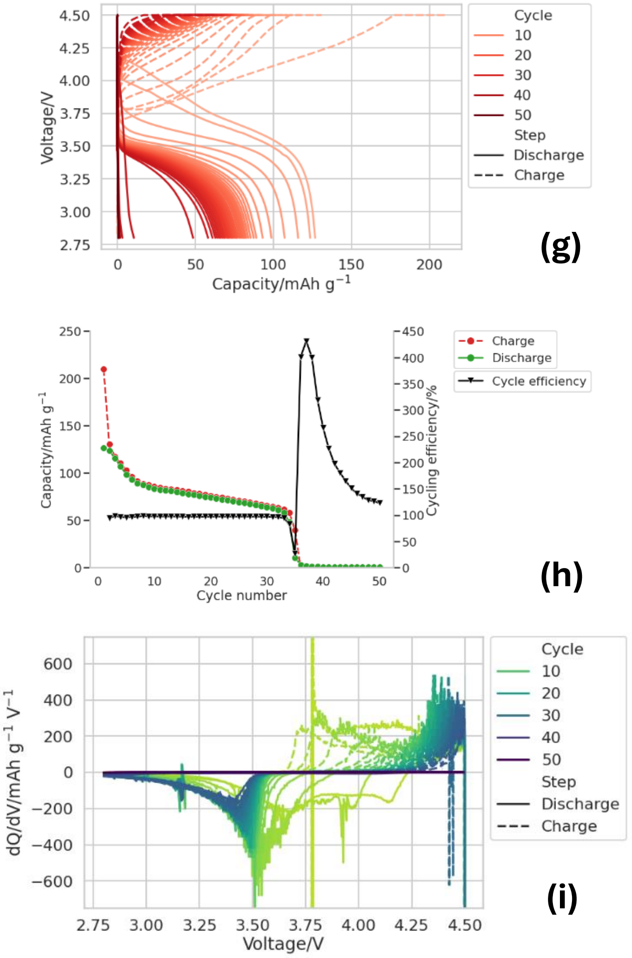

Figure 126 Charge-discharge cycling (a, d, g), Cycling efficiency and charge-discharge capacities (b, e, h), and Differential capacity vs. voltage curve (c, f, i), for Li-ion coin cells 1-3 with nitrate precursor and sodium alginate synthesised NMC811 cathodes where x = 0.1 ($LiNi_{0.8}Mn_{0.1}Co_{0.1}O_2.0.05Na_2CO_3$) between 4.5 and 2.8 V for 50 cycles

4.5.1.4 Cell cycling of NMC811 with sodium carbonate via addition of Na using sodium alginate and nitrate precursors where x = 0.1, with 4.2 to 3.0 V range

When cycled between 4.2 V and 3 V at 0.1 C, lithium ions cells with the same cathodes (x = 0.1) have a high, repeatable initial discharge capacity of 170 mAh/g, Figure 127b, e, indicating high levels of lithium intercalation is possible when synthesising NMC811 with a sodium secondary phase provided enough lithium is present. Capacity retention meanwhile varies significantly between 30 and 170 mAh/g over 50 cycles. Differential capacity plots, Figure 127c, f, show H1 to M and M to H2 phase changes at 3.7 and 3.9 V during the initial charge cycle and H2 to M and M to H1 at 4.1 and 3.7 V, with no phase change from H2 to H3 due to the cell cycling below 4.2 V. Cell failure, Figure 127a, occurs due to the required voltage for the H1 to M phase change increase to and exceeding 4.2 V as the cell undergoes cycling due to structural deformation. Provided structural deformation does not occur above 4 V, minimal capacity fade of 30 mAh/g over 50 cycles, Figure 127d, occurs due to the H1 to M and M to H2 phase changes still occurring at 3.7 and 3.9 V after 50 cycles, allowing near full intercalation of lithium to continue to occur. This shows that for the 4.2 to 3 V voltage range NMC811 with a Na_2CO_3 synthesised using sodium alginate and nitrates has promise in exhibiting high structural stability and specific capacity but still may be prone to high levels of capacity fade due to disorganisation of the NMC811 structure.

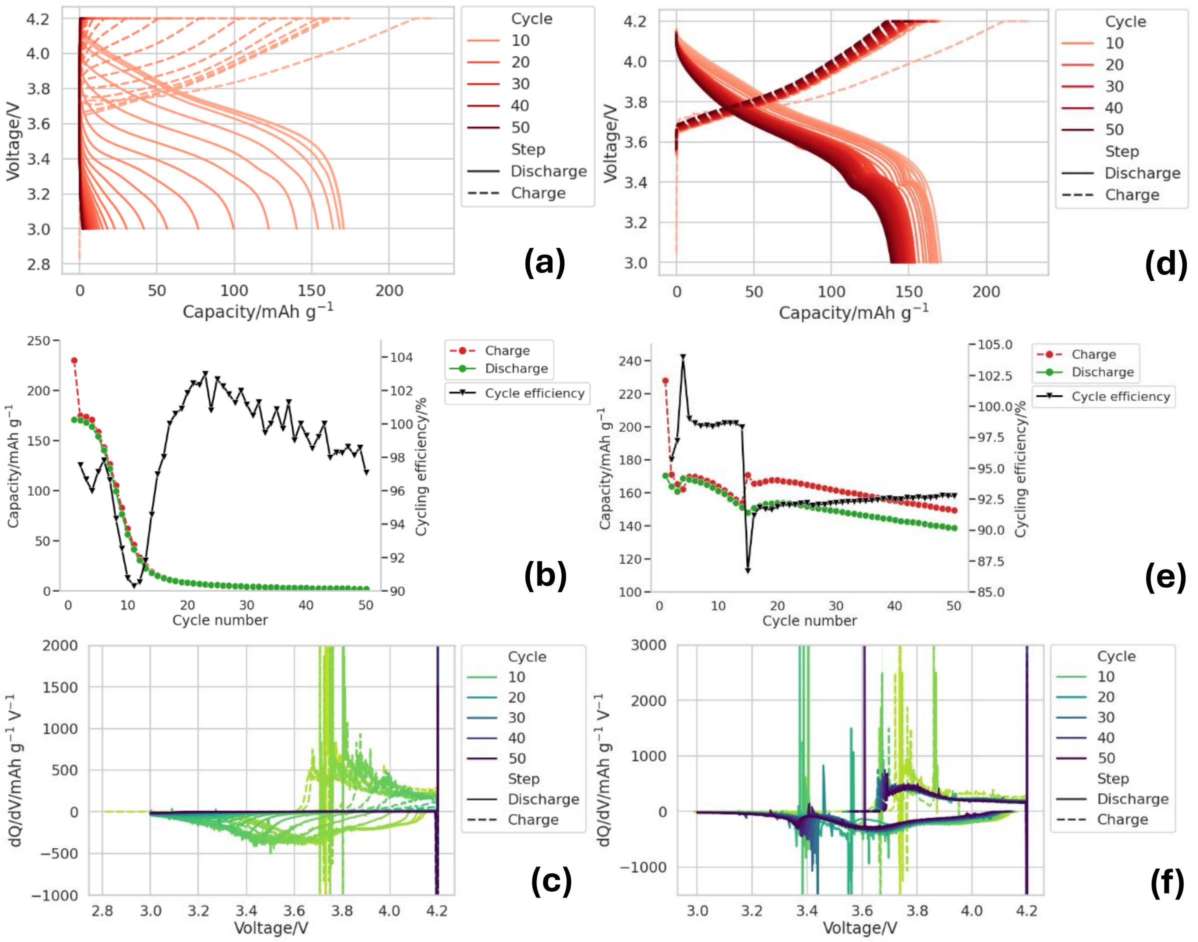

Figure 127 Charge-discharge cycling (a, d), Cycling efficiency and charge-discharge capacities (b, e), and Differential capacity vs. voltage curve (c, f), for Li-ion coin cells 1-2 with nitrate precursor and sodium alginate synthesised cathodes where x = 0.1 ($LiNi_{0.8}Mn_{0.1}Co_{0.1}O_2.0.05Na_2CO_3$) between 4.2 and 3 V for 50 cycles

4.5.1.5 Cell cycling of NMC811 with sodium carbonate via addition of Na using sodium alginate and nitrate precursors where x = 0.2, with 4.5 to 2.8 V range

NMC811 cathodes where x = 0.2 cycled in cells between 4.5 V and 2.8 V at 0.1 C show worse performance than cells with cathodes synthesised such that x = 0.1. Initial specific discharge capacities range from 150 mAh/g, Figure 128b, to 100 mAh/g, Figure 128e, indicating poorer intercalation of lithium ions. This lesser capacity is a result of there being less surface area across the more agglomerated particles as a result of the use of a greater amount of sodium alginate and a greater sodium carbonate content, Figure 125b. Cathodes also have a poor cycling retention whereby final discharge capacities are 40 or 30 mAh/g after 50 cycles. Differential capacity curves, Figure 128c, f, highlight H1 to M phase transition at 3.7 V and M to H2 phase transition at 4.2 V during the initial charge cycle, with the H2 to H3 phase change not occurring due to too low an intercalation of lithium. During discharge, the H2 to M and M to H1 phase transitions occur at 4.1 and 3.6 V, respectively. Over 50 cycles, the H1 to M phase change can be observed to occur above 4.5 V as a result of structural deterioration, causing cell failure. The increased amount of sodium used appears to directly or indirectly inhibit intercalation of the lithium as indicated by the lower discharge capacity, due to either the use of a greater amount of sodium alginate biotemplate or the formation of a large mass of sodium carbonate secondary phase, while the cathode does not benefit from greater structural stability due to this increase in sodium. When using sodium alginate and nitrates, an amount of sodium whereby x =

0.1 is therefore the limit of what is viable for NMC811 cathodes, however such cathodes are still prone to significant structural disorganisation.

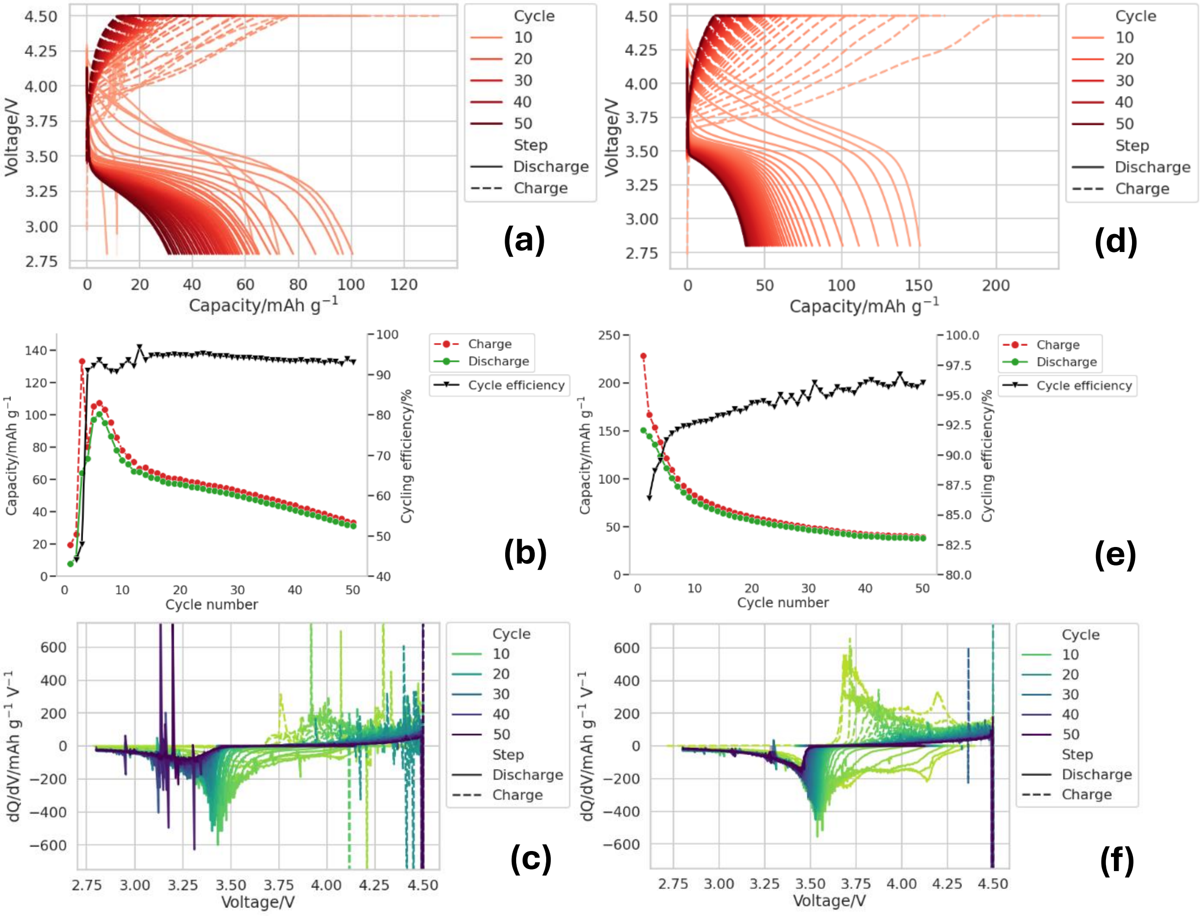

Figure 128 Charge-discharge cycling (a, d), Cycling efficiency and charge-discharge capacities (b, e), and Differential capacity vs. voltage curve (c, f), for Li-ion coin cells 1-2 with nitrate precursors and sodium alginate synthesised cathodes where x = 0.2 ($LiNi_{0.8}Mn_{0.1}Co_{0.1}O_2.0.1Na_2CO_3$) between 4.5 and 2.8 V for 50 cycles.

4.5.1.6 Further discussion of cell cycling data

Further reasons for poor capacity and cyclability of some of the cells may be due to the aforementioned issues possible during cell manufacturing, 3.7.4. Oxidation of the lithium chips or potential damage of the chips caused by attempts to remove the oxidation may result in reductions to cell capacity or cyclability as less lithium or even damage is present in the lithium chip. Cyclability may also be reduced due to degradation or water present in the electrolyte in part caused long term storage, which may result in reduced ionic diffusivity and so greater reductions in cycling stability. Variation in the capacities and cyclabilities for similar cathodes may be caused by inhomogeneity when poorly mixing, resulting in variety in the ratio of active material and additives in the cathode power. This may result in differences in the amount of NMC811 in the cathodes leading to variation in the cathodes but also variations in cycling stability as the amount of additive varies. Similarly, poor drawdowns or over calendaring may result in variety in the thicknesses of the cathodes or even damage to the cathodes, further affecting cyclability as ionic conductivity pathways are affected.

4.5.2 Synthesis of NMC811 with sodium carbonate via the addition of Na, where Na = x and Li = 1, using sodium alginate and acetate precursors

4.5.2.1 X-Ray Diffraction Analysis of NMC811 with sodium carbonate via the addition of Na, where Na = x and Li = 1, using sodium alginate and acetate precursors

When NMC811 is synthesised with acetates and sodium added using sodium alginate where Li = 1, greater disorganisation of the NMC811 is observed vs. when synthesising with nitrates. Poor layering of the NMC811 structure is observed due to poor peak splitting at reflections (006)/(012) and (018)/(110) when x = 0.1, Figure 129a, and x = 0.2, Figure 129b, with no peak splitting when x = 0.3, Figure 129c. Peak intensity ratios between (003) and (104) of 1.49, 1.32, and 1.23 for x = 0.1, 0.2, and 0.3 respectively show a high level of cation mixing between Li and Ni sites. An increase in the amount of sodium present as well as an increase in carbon content from the acetate precursors and increasing mass of sodium alginate leads to significant disorganisation of the NMC811 during synthesis. This is due to the biotemplate and precursor decomposing , releasing carbon which then reacts with the oxygen atmosphere to produce CO_2 and a reducing atmosphere as oxygen is used up in the reaction. This reducing atmosphere results in less oxygen available to fill oxygen sites during the synthesis of NMC811 and so greater organisation. As NMC811 forms a layered structure more readily in an oxidising environment due to more oxygen being available to fill oxygen sites, [133], reducing atmospheric conditions are detrimental the synthesis of layered NMC811.

Peaks present between 20 and 42 ° are indicative of a sodium carbonate secondary phase. Such peaks are present when the amount of sodium used is such that x = 0.2 or greater and indicates that sodium is not integrating into the NMC811 structure. Sodium carbonate secondary phase may also be present where x = 0.1, but due to the smaller proportion is unable to be detected using XRD. The increased amount of sodium above x = 0.2 is clearly a negative factor in the structural organisation of the NMC811 but is potentially viable at x = 0.2 or less.

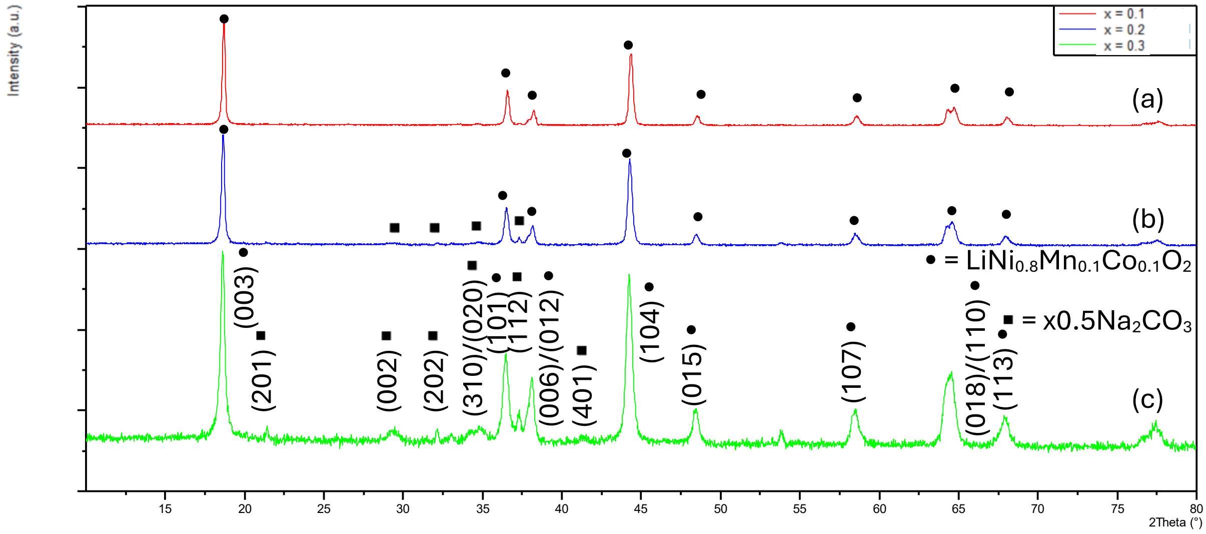

Figure 129 XRD of NMC811 with sodium carbonate ($LiNi_{0.8}Mn_{0.1}Co_{0.1}O_2.x0.5Na_2CO_3$) where Na = x and Li = 1, synthesised with acetate precursors and sodium alginate where a) x = 0.1 ($LiNi_{0.8}Mn_{0.1}Co_{0.1}O_2.x0.05Na_2CO_3$), b) x = 0.2 ($LiNi_{0.8}Mn_{0.1}Co_{0.1}O_2.x0.1Na_2CO_3$), and c) x = 0.3 ($LiNi_{0.8}Mn_{0.1}Co_{0.1}O_2.x0.15Na_2CO_3$),

4.5.2.2 Morphology of NMC811 with sodium carbonate via the addition of Na, where Na = x and Li = 1, using sodium alginate and acetate precursors

As with when synthesising with nitrates, the morphology of NMC811 synthesised with acetates leads to the synthesis of individual primary particles and larger agglomerations. When x = 0.1, Figure 130a, an average particle diameter of 400 nm is observed consisting of particle morphologies of irregularly shaped octahedral particles with smaller irregular, round particles. When x = 0.2, Figure 130b, there are two different significant morphologies, with an average particle diameter of 200 nm for small, irregular, round particles that are prone to agglomeration and an average particle diameter of 2000 nm for the larger, octahedral particles. The morphologies for particles where x = 0.3, Figure 130c, consist of small, irregular, round particles having average particle diameters of 200 nm that agglomerate into larger secondary particles, and larger octahedral particles with average particles diameters of 800 nm.

Large agglomerations of smaller primary particles are present where x = 0.2 and 0.3 as the amount of sodium alginate is increased, possibly due the sodium carbonate secondary phase and possibly due to the larger carbon content of the amount of biotemplate used. The increasing in sodium alginate also aids in the synthesis of octahedral particles due to the increased number of chelation sites for metal precursor ions to chelate. Significant proportions of sodium present from both the use of sodium alginate and formation of sodium carbonate can also lead to an increase in agglomerations that reduce the surface area and available lithiation sites, reducing specific capacity.

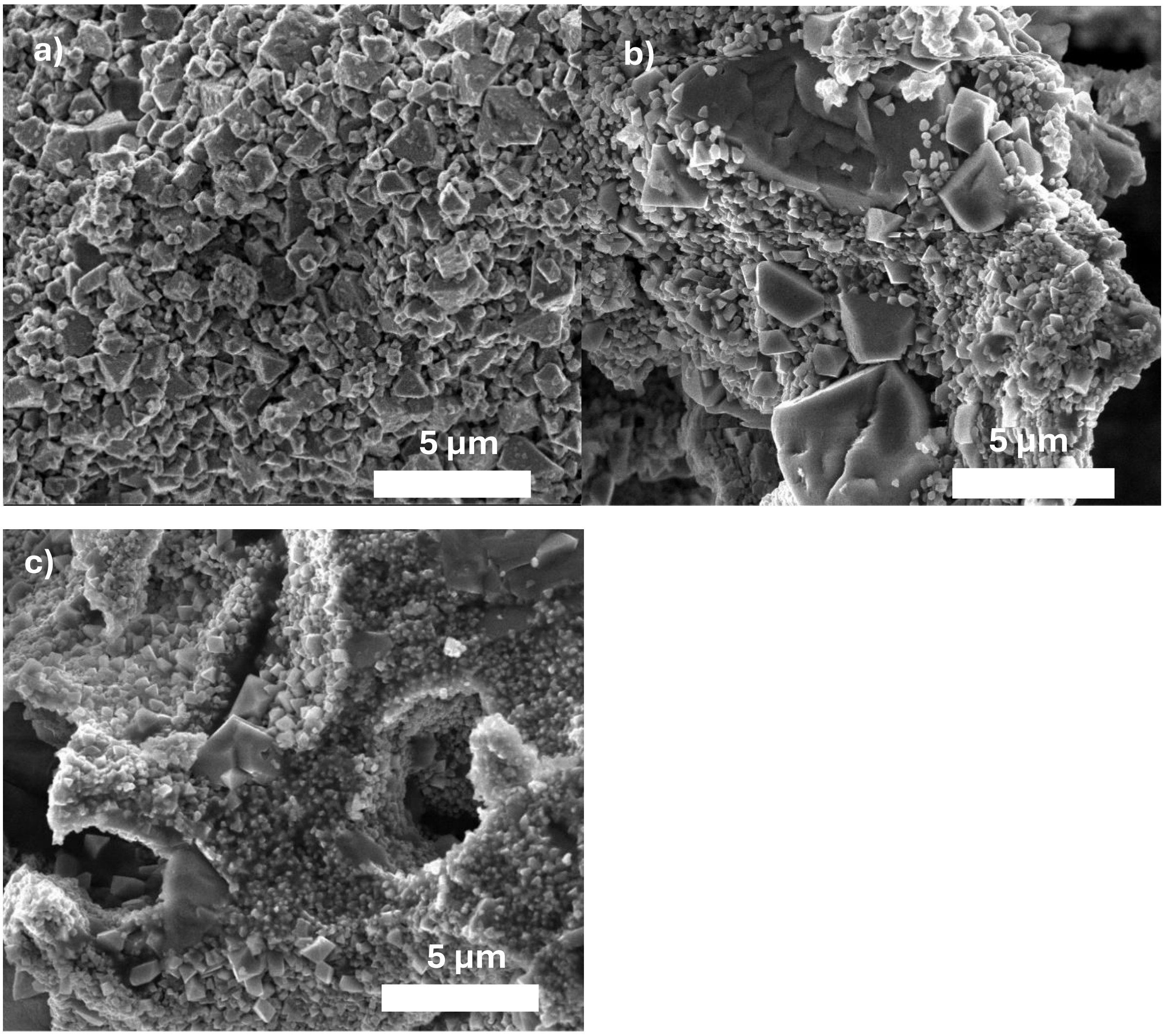

Figure 130 SEM of NMC811 ($LiNi_{0.8}Mn_{0.1}Co_{0.1}O_2.x0.5Na_2CO_3$) where Na = x and Li = 1, synthesised with acetate precursors and sodium alginate where a) x = 0.1 ($LiNi_{0.8}Mn_{0.1}Co_{0.1}O_2.x0.05Na_2CO_3$), consisting of irregular octahedral particles, b) x = 0.2 ($LiNi_{0.8}Mn_{0.1}Co_{0.1}O_2.x0.1Na_2CO_3$) consisting of larger, regular octahedral particles, and c) x = 0.3 ($LiNi_{0.8}Mn_{0.1}Co_{0.1}O_2.x0.15Na_2CO_3$) consisting of agglomerated round particles

4.5.2.3 Cell cycling of NMC811 with sodium carbonate via addition of Na using sodium alginate and acetate precursors where x = 0.1, with 4.5 to 2.8 V range

As when synthesising with nitrate precursors, NMC811 cathodes synthesised where x = 0.1 and cycled in lithium ion cells between 4.5 and 2.8 V at 0.1 C show promising capacities at the expense of poor capacity retention. Initial specific discharge capacity ranges between 150 and 180 mAh/g, Figure 131b, e, h, due to the high availability of lithium availability for intercalation. Specific discharge capacity is not higher due to the cathodes being unable to undergo the H2 to H3 phase transition which normally occurs above 4.2 V in high nickel cathodes but is not observed when synthesising with sodium [127].

Poor capacity retention is observed in all cells with discharge capacity decreasing to 10 mAh/g or below after 50 cycles. The differential capacity curves, Figure 131c, f, I, show the migration of the phase transition peaks for the H1 to M and M to H2 transitions at 3.75 and 4.1 V during the initial charge cycle and H2 to M and M to H1 transitions at 4.0 and 3.7 V during the initial discharge cycle. The structure of the cathode is seen to deteriorate as the cell is cycled, with the phase transition peaks migrating to higher voltages due to cycling above 4.2 V. As the cell approaches 50 cycles, the cathode is therefore unable to undergo the H1 to M phase transition below 4.5 V and fails.

This indicates that while 100% of the lithium is available for intercalation, the sodium is not able to provide structural stability to prevent the NMC811 structure degrading at higher voltages nor is it able to intercalate to the cathode to improve specific capacity, likely due to existing as a sodium carbonate secondary phase and not integrating into the NMC811 structure.

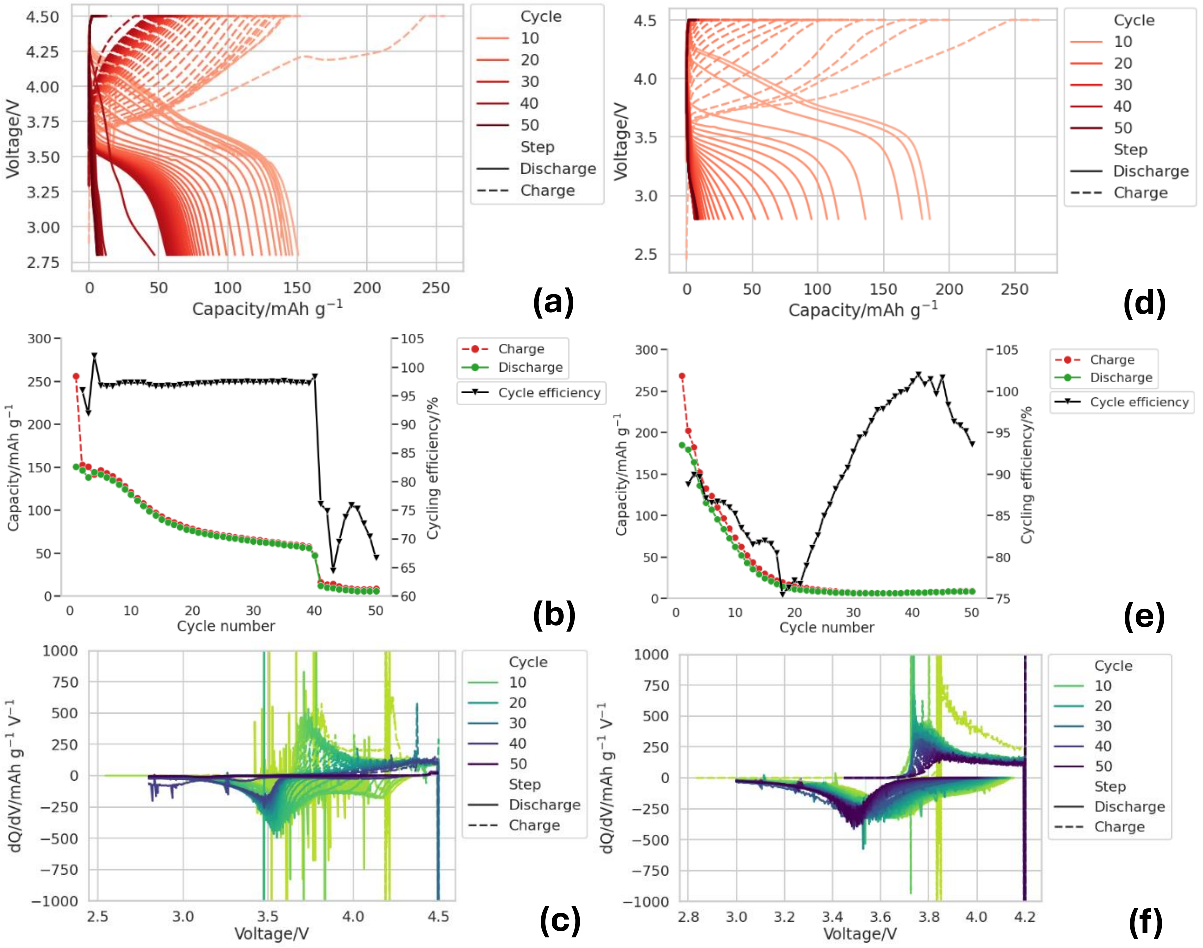

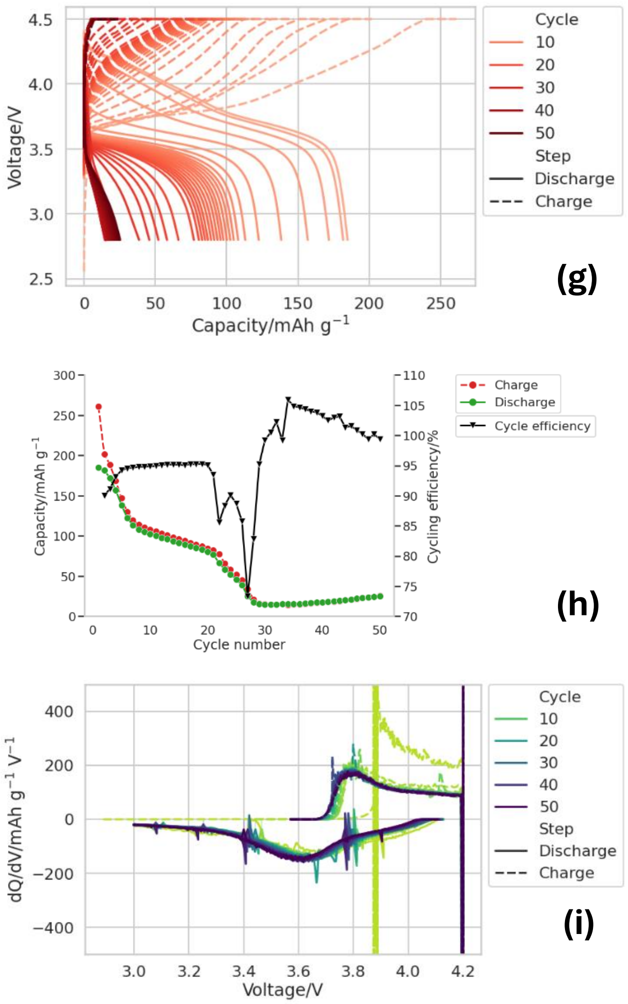

Figure 131 Charge-discharge cycling (a, d, g), Cycling efficiency and charge-discharge capacities (b, e, h), and Differential capacity vs. voltage curve (c, f, i), for Li-ion coin cells 1-3 with acetate precursors and sodium alginate synthesised cathodes where x = 0.1 ($LiNi_{0.8}Mn_{0.1}Co_{0.1}O_2.x0.05Na_2CO_3$) between 4.5 and 2.8 V for 50 cycles

4.5.2.4 Cell cycling of NMC811 and sodium carbonate via addition of Na using sodium alginate and acetate precursors where x = 0.1, with 4.2 to 3.0 V range

When lithium-ion cells with the same cathodes, where x = 0.1, are cycled only between 4.2 and 3 V at 0.1 C, high capacity retention is observed at the cost of a lower discharge capacity. Initial discharge capacities range from 120 to 70 mAh/g, Figure 127b, e, which is a significantly lower initial specific discharge capacity compared to when the cathodes are cycled between 4.5 V and 2.8 V, Figure 131. This indicates that a small proportion of the lithium is intercalating at the lower voltage range, and that the cathode is not undergoing the H2 to H3 phase transition, or potentially the M to H2 phase transition.

Capacity retention however is shown to be between 10 and 40 mAh/g over 50 cycles, a significant improvement over the same cathode cycled between 4.5 and 2.8 V. The high retention is in part due to the lower voltage range, with differential capacity plots showing that the cathode only undergoes the H1 to M and M to H1 transition during charge and discharge respectively at 3.9 V. Undergoing only the single phase changes ensures full intercalation does not occur but also negates any breakdown of the cathode structure due to cycling at high voltages. As such there is no voltage migration of the H1 to M phase transition and so there is a much more stable structure, but at the cost of specific discharge capacity.

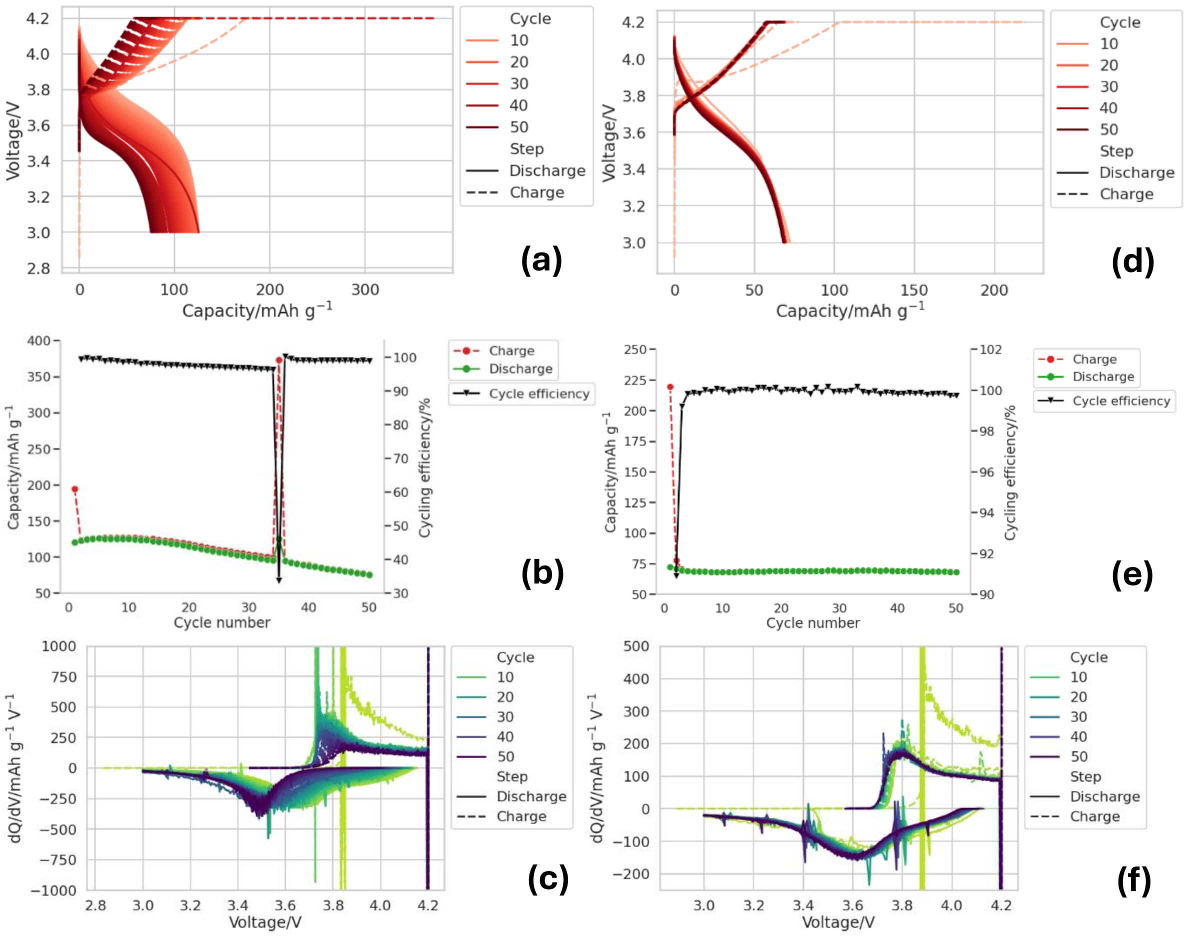

Figure 132 Charge-discharge cycling (a, d), Cycling efficiency and charge-discharge capacities (b, e), and Differential capacity vs. voltage curve (c, f), for Li-ion coin cells 1-2 with acetate precursors and sodium alginate synthesised cathodes where x = 0.1 ($LiNi_{0.8}Mn_{0.1}Co_{0.1}O_2$.x0.05$Na_2CO_3$) between 4.2 and 3 V for 50 cycles

4.5.2.5 Cell cycling of NMC811 with sodium carbonate via addition of Na using sodium alginate and acetate precursors where x = 0.2, with 4.5 to 2.8 V range

Cathodes synthesised where x = 0.2 are cycled in lithium ion cells between 4.5 and 2.8 V at 0.1 C, a low initial discharge capacity and low capacity retention is present as the significant proportion of sodium used in the cathode becomes a detriment to the cell. Initial discharge capacity is shown to range between 90 and 110 mAh/g, Figure 133b, e, indicating low intercalation of the available lithium. Capacity fade is also significant with specific discharge capacity decreasing to a maximum of 10 mAh/g after 50 cycles. Differential capacity curves, Figure 133c, f, show phase transitions during the initial charge cycle of H1 to M at 3.8 V and M to H2 at 4.5 V, with phase transitions during discharge being H2 to M at 4.2 V and M to H1 at 3.6 V. As such the M to H2 phase transition is already almost outside the voltage range during the initial cycle, further reducing lithium intercalation and specific capacity. The phase peaks migrate to higher voltages in subsequent cycles until the H to M phase transition occurs above 4.5 V as the cell approaches 50 cycles and the cell fails.

This indicates that not only is sodium not aiding in improving structural stability upon intercalation of lithium, but the lower initial discharge capacity also shows the high proportion of sodium, in the form of sodium carbonate, is likely actively restricting phase transitions inhibiting the ability for the lithium to intercalate. Such restrictions in the phase transitions are also due to an initial lower organisation of the NMC811 structure due to the use of a larger amount of sodium alginate resulting in a larger amount of the reducing carbon dioxide atmosphere as the sodium alginate undergoes decomposition and frees up carbon to react with the oxygen atmosphere to form a reducing carbon dioxide atmosphere , making less oxygen available for the formation of the NMC811 structure and resulting in decreased disorganisation as the stoichiometric ratio of oxygen to metal ions is not met. There is potential for using sodium alginate to synthesise NMC811 cathodes, where sodium is added in addition to an amount of lithium such that Li = 1, in order to improve structural stability, but any increase in structural stability comes at a compromise with a reduced specific discharge capacity.

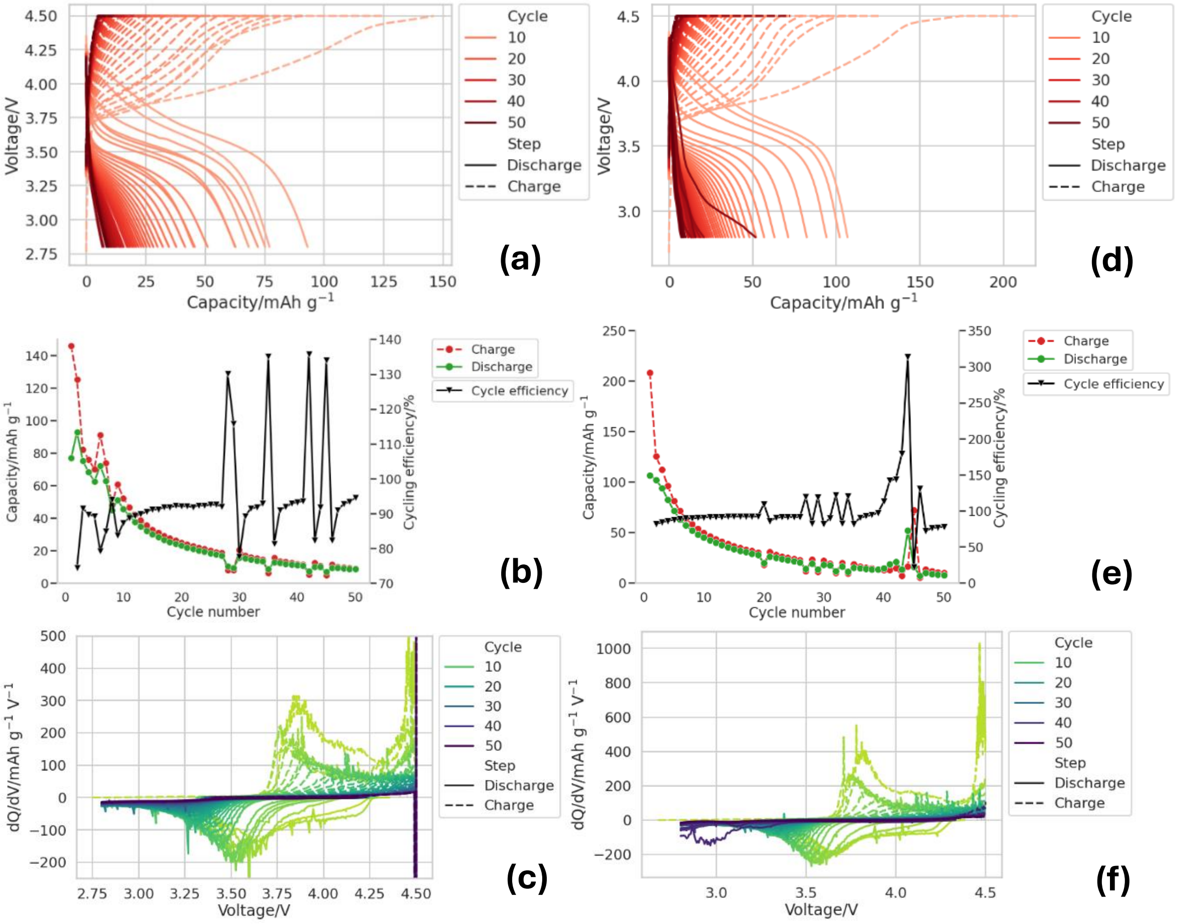

Figure 133 Charge-discharge cycling (a, d), Cycling efficiency and charge-discharge capacities (b, e), and Differential capacity vs. voltage curve (c, f), for Li-ion coin cells 1-2 with acetate precursor and sodium alginate synthesised cathodes where x = 0.2 ($LiNi_{0.8}Mn_{0.1}Co_{0.1}O_2.0.1Na_2CO_3$) between 4.5 and 2.8 V for 50 cycles

4.5.2.6 Further discussion of cell cycling data

The wide variety in cell performance may also be as a result of the potential issues within the cell manufacturing process, 3.7.4. Poor capacity may be attributed to lithium chips being either oxidisation due to long term storage issues or damage caused by the attempted removal of the oxidation, both of which reduces the available lithium during cycling. Potential degradation of the electrolyte or potential water in the electrolyte, again caused by long term storage, may affect cell cyclability as the electrolyte degrades and there is reduced ionic diffusivity. The differences between seemingly identical cathodes may be explained by a poor mixing of the slurry producing either an inhomogeneous slurry, or a slurry that is too thin or too thick. An inhomogeneous slurry may result in cathodes with different capacities due to cathodes with different ratios of active material or cathodes with greater or lesser cyclability as the ratio of additive is varied. Furthermore, a too thick or thin slurry may lead to a poor drawdown of which produces an uneven cathode. This can then potentially lead to over calendaring which can then lead to the cathode being damaged, leading to early cathode failure.

4.6 Synthesis of NMC811 with sodium via the addition of Na, where Na = x and Li = 1, using sodium alginate supplemented with sodium nitrate

While synthesising NM811 with sodium alginate without the substitution of lithium has improved structural organisation and cycling of NMC811 cathodes, synthesising with sodium where x = 0.2 or above still results in poor structural disorganisation, lack of integration of sodium into the NMC811 structure, and cell poor performance. It is investigated as to whether replacing a proportion of the sodium alginate with sodium nitrate is beneficial when sodium is added to NMC811 where Li = 1. By reducing the amount of sodium alginate and increasing the amount of sodium nitrate it is theorised that the reduction in carbon content in the reaction, due to the reduction in the mass of sodium alginate, will create a more oxidising environment and greater structural organisation of the NMC811. The method is done such that proportion of sodium alginate used is maintained (the amount of sodium alginate required such that x = 0.1) and the mass of sodium nitrate increased such that x = 0.2 and 0.3, Table 24.

	X = 0.1	X = 0.2	X = 0.3
Sodium alginate (g)	0.1	0.1	0.1
Sodium nitrate (g)	0	0.0213	0.0425

Table 24 Masses of metal precursor salts used in the synthesis of NMC811 via addition of sodium using sodium alginate and sodium nitrate

4.6.1 Synthesis of NMC811 with sodium via the addition of Na, where Na = x and Li = 1, using sodium alginate supplemented with sodium nitrate using nitrate precursors

4.6.1.1 X-Ray Diffraction Analysis of NMC811 with sodium via the addition of Na, where Na = x and Li = 1, using sodium alginate supplemented with sodium nitrate using nitrate precursors

The mass of sodium alginate is maintained to synthesis NMC811 such that x = 0.1, Figure 134a, with the mass of sodium nitrate being increased incrementally such that the amount of sodium present is x = 0.2, Figure 134b, and 0.3, Figure 134c. By substituting a portion of sodium alginate for sodium nitrate while maintaining the same mass of lithium and NMC811, there is little apparent difference in the XRD patterns as sodium nitrate is incrementally added to increase sodium from x = 0.1 to 0.3. (003)/(104) peak intensity ratios of 1.53, 1.55, and 1.64 for x = 0.1, 0.2, and 0.3 respectively indicate low mixing of Li^+ and Ni^{2+} cations across Ni and Li sites [133] and (006)/(012) and (018)/(110) peaks exhibit high peak splitting highlighting good layering of the NMC811 structure. Peaks indicating a sodium carbonate or sodium peroxide secondary phase are also not present at any amount of sodium, however this may be due to any sodium secondary phases that exists in the sample not being produced at a high amount to be registered using XRD.

One such reason for the organisation of the NMC811 and lack of a sodium carbonate phase is the reduction in carbon content by not increasing the mass of sodium alginate above where x = 0.1. Reduction in the mass of the biotemplate results in less carbon being freed up as the biotemplate decomposes, leading to the synthesis of less CO_2 as the reduced amount of carbon reacts with the oxygen atmosphere. This therefore leads to a less reducing environment with more oxygen available to fill oxygen sites during the synthesis of NMC811. Despite fewer chelation sites due to a lower mass of biotemplate used, the reduction in carbon as a result of a greater mass of sodium nitrate being used produces an organised NMC811 structure at all amounts of sodium.

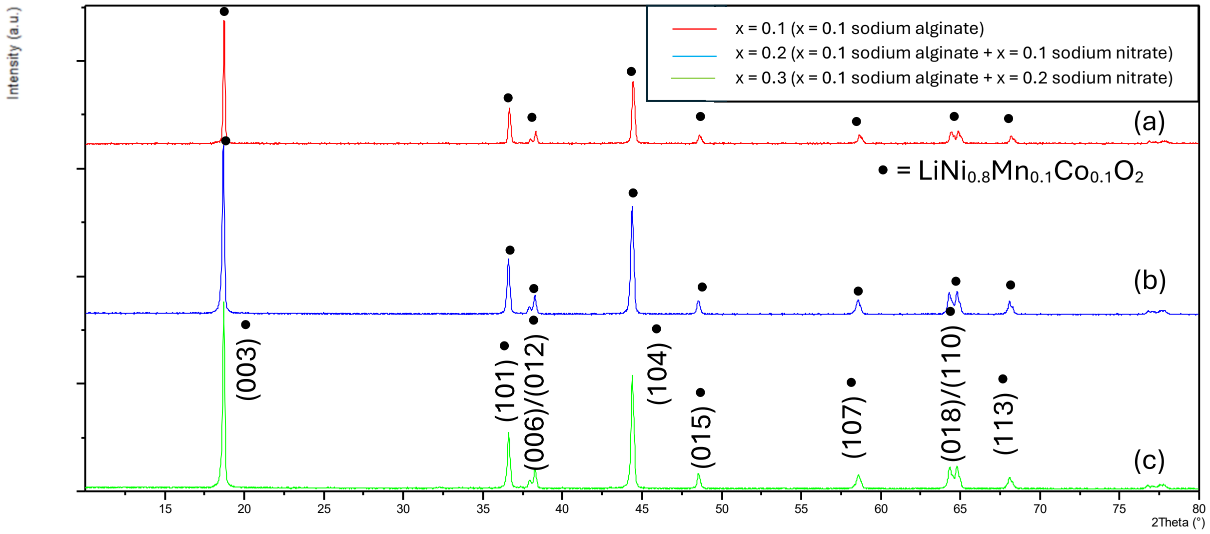

Figure 134 XRD of NMC811 with sodium ($LiNi_{0.8}Mn_{0.1}Co_{0.1}O_2.xNa$) where Na = x and Li = 1, synthesised with nitrate precursors and sodium alginate, and sodium nitrate where a) x = 0.1 ($LiNi_{0.8}Mn_{0.1}Co_{0.1}O_2.0.1Na$), b) x = 0.2 ($LiNi_{0.8}Mn_{0.1}Co_{0.1}O_2.xNa.0.2Na$), and c) x = 0.3 ($LiNi_{0.8}Mn_{0.1}Co_{0.1}O_2.0.3Na$),

4.6.1.2 Morphology of NMC811 with sodium via the addition of Na, where Na = x and Li = 1, using sodium alginate using nitrate precursors

While XRD shows that the NMC811 powders are structurally very similar, there are still noticeable differences in the morphology when the mass of sodium nitrate is increased to synthesise NMC811 with different amounts of sodium from x = 0.1 to 0.3. When synthesised with only sodium alginate such that the proportion of sodium is equal to x = 0.1, Figure 135a, an average particle diameter is 900 nm is formed with a rounded if irregular morphology. When adding sodium nitrate to where x = 0.2, Figure 135b, average particle diameter decreases to 400 nm with the morphology maintaining an irregular, round shape. When synthesised such that x = 0.3, Figure 135c, the morphology differs significantly again with morphologies ranging from small, rounded particles with 300 nm average particle diameter to octahedral particles with average particle diameters 900 nm.

Large agglomerations of primary particles are also present when x = 0.2 and 0.3 as the amount of sodium is increased while the mass of biotemplate remains constant. The increase in metal ions but the same number of chelation sites causes recrystallisation of metal ions during heating, resulting in alternate morphologies and greater agglomeration. The increase in the proportion octahedral morphologies is indicative that even with a constant mass of biotemplate, the increase in the proportion of sodium reactants lead to greater morphological control of octahedral particles and play a significant role to play in the synthesis in these morphologies. While an increase in the mass of sodium nitrate and maintaining of the mass of sodium alginate results in a more organised structure, it also results in greater agglomeration and more irregular morphologies due to a relative lack of chelation sites that may be detrimental to cell cycling.

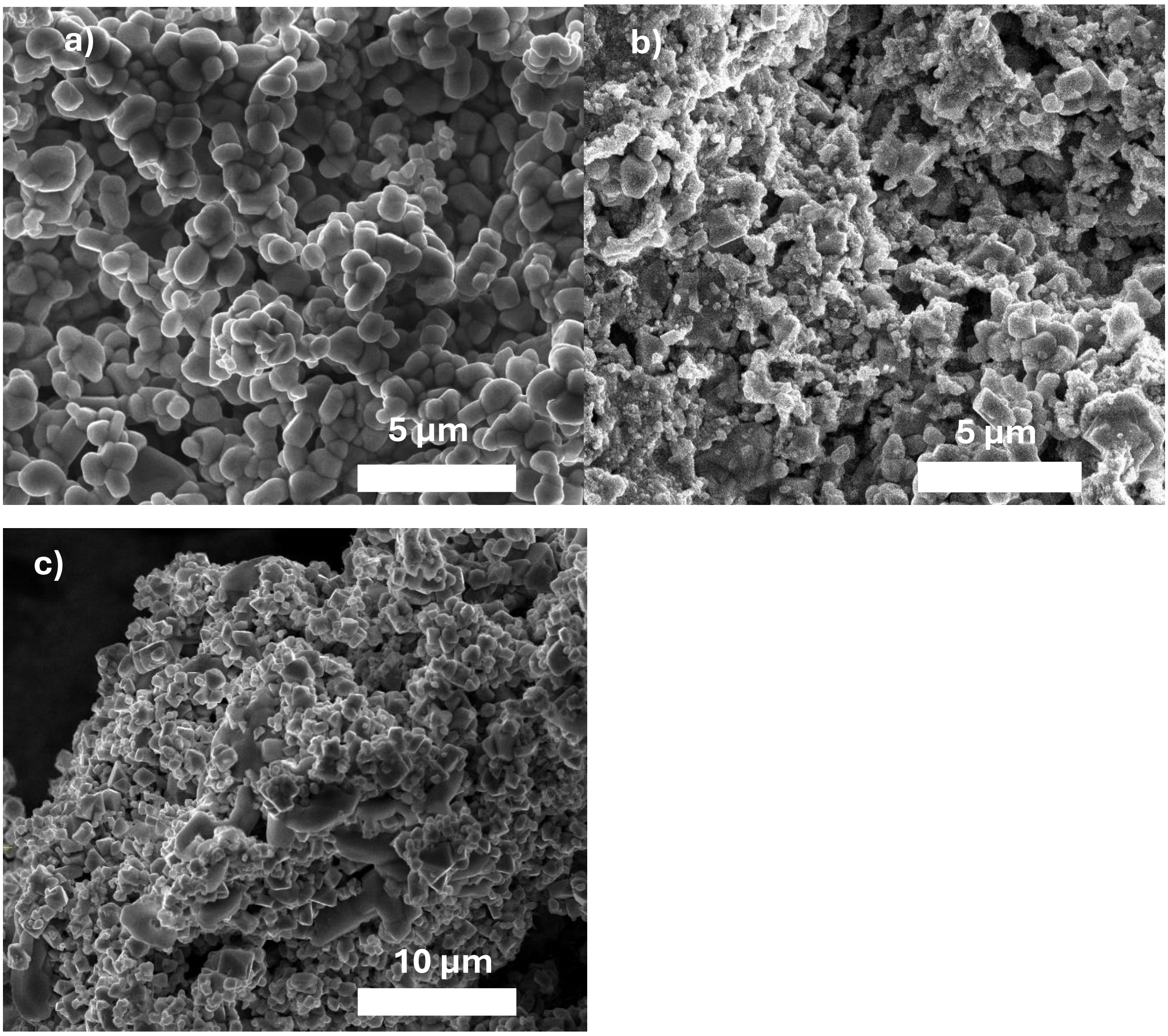

Figure 135 SEM of NMC811 with sodium ($LiNi_{0.8}Mn_{0.1}Co_{0.1}O_2.xNa$) where Na = x and Li = 1, synthesised with nitrate precursors and sodium alginate, and sodium nitrate where a) x = 0.1 ($LiNi_{0.8}Mn_{0.1}Co_{0.1}O_2.0.1Na$),exhibiting irregular rounded particles b) x = 0.2 ($LiNi_{0.8}Mn_{0.1}Co_{0.1}O_2.0.2Na$), exhibiting larger rounded particles, and c) x = 0.3 ($LiNi_{0.8}Mn_{0.1}Co_{0.1}O_2.0.3Na$),exhibiting large octahedral particles

4.6.2 Synthesis of NMC811 with sodium peroxide via the addition of Na, where Na = x and Li = 1, using sodium alginate supplemented with sodium nitrate using acetate precursors

4.6.2.1 X-Ray Diffraction Analysis of NMC811 with sodium peroxide via the addition of Na, where Na = x and Li = 1, using sodium alginate supplemented with sodium nitrate using acetate precursors

When synthesising using sodium alginate and acetates and using an increasing mass of sodium nitrate there is little difference in the XRD patterns as the amount of sodium is increased, but all powders indicate structural disorganisation. At all amounts of sodium where x = 0.1, 0.2, and 0.3, Figure 136a-c, peak intensity ratios between (003)/(104) of 1.64, 1.38, and 1.47 respectively show high levels of Li and Ni cation mixing for Ni and Li sites when synthesised such that x = 0.2 and above (where < 1.2 is considered high mixing of cation sites and 1.6 is considered low mixing [130]). Poor peak splitting of (006)/(012) and (018)/(110) peaks at all amounts of sodium used also indicate poor layering of the NMC811 structure. Use of acetate precursors leads to greater disorganisation compared to when using nitrates due to a greater amount of carbon being freed up upon the degradation of the biotemplate resulting in a greater amount of CO_2 as the increased amount of carbon reacts with the oxygen atmosphere. The greater amount of CO_2 leads results in a more reducing atmosphere as oxygen is used up in the synthesis of CO_2. Where x = 0.2 and 0.3 there are low intensity peaks indicating the presence of a secondary sodium phase, sodium peroxide. Such a phase may also be present where x = 0.1 though if so, the mass is too low to be detected. The low intensity peaks of the secondary Na_2O_2 infer that this phase is present and that a sodium was not incorporated into the NMC811 structure.

While slight disorganisation of the NMC811 structure is observed, XRD data when using acetates and the same data when using nitrates, Figure 134, points towards the addition of sodium nitrate as a partial substitute for sodium alginate producing an organised structure (provided the Na is not substituted for Li). The reduction of carbon as a result of the reduction in the mass of sodium alginate biotemplate used counters the increased carbon content of the acetate precursors and synthesises a more organised structure. This makes sodium nitrate a valuable alternative for sodium alginate when synthesising NMC811.

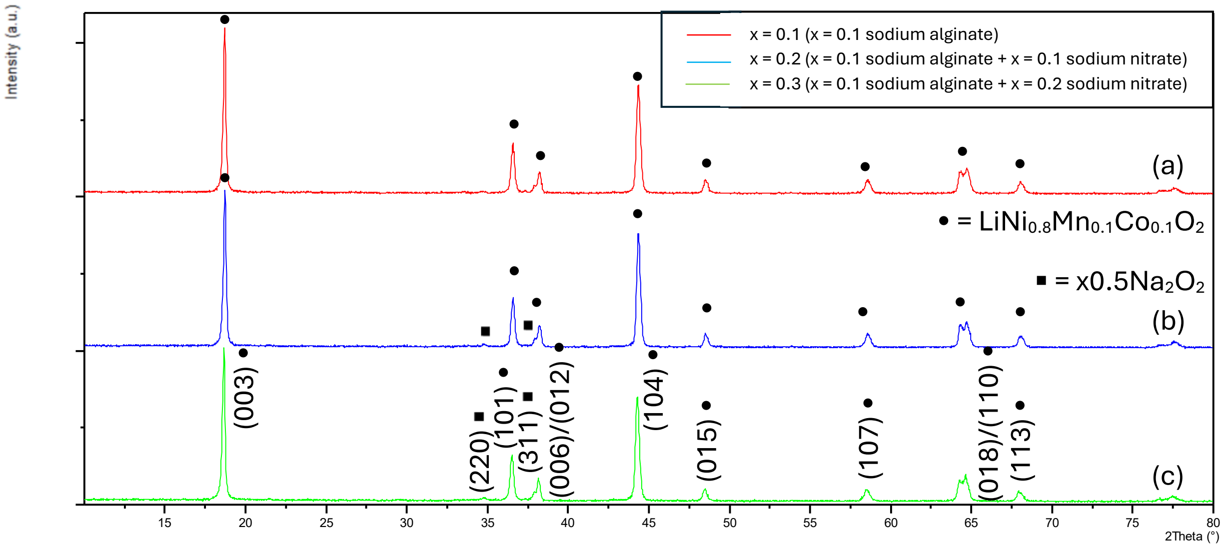

Figure 136 XRD of NMC811 with sodium peroxide ($LiNi_{0.8}Mn_{0.1}Co_{0.1}O_2.x0.5Na_2O_2$) where Na = x and Li = 1, synthesised with acetate precursors and sodium alginate, and sodium nitrate where a) x = 0.1 ($LiNi_{0.8}Mn_{0.1}Co_{0.1}O_2.x0.05Na_2O_2$), b) x = 0.2 ($LiNi_{0.8}Mn_{0.1}Co_{0.1}O_2.x0.1Na_2O_2$), and c) x = 0.3 ($LiNi_{0.8}Mn_{0.1}Co_{0.1}O_2.x0.15Na_2O_2$),

4.6.2.2 Morphology of NMC811 with sodium peroxide via the addition of Na, where Na = x and Li = 1, using sodium alginate using acetate precursors

When synthesising with acetate precursors and sodium alginate such that x = 0.1, Figure 137a, average particle diameter is 400 nm, with a with a mix of smaller, irregular, rounded particles and larger irregular octahedral particles. When sodium nitrate is added such that x = 0.2, Figure 137b, a significant proportion of particles are octahedral in shape or similar with an average particle diameter of 500 nm. This trend continues when NMC811 is synthesised with more sodium nitrate such that x = 0.3. Morphologies consist of a large number of octahedral particles with smaller, irregular particles interspersed between them and larger agglomerations with an average particle diameter of 600 nm.

An increase in sodium, particularly when using sodium nitrates, leads to a greater synthesis of octahedral particles as a result of the apparent role of sodium in the synthesis of octahedral morphologies established throughout this thesis, as well as an increase in particle agglomeration. The increase in agglomeration is a result of an increase in metal ions and the maintaining of the same number of chelation sites along the sodium alginate chain due to the use of the same mass of biotemplate. The relative lack of chelation sites leads to recrystallisation which causes greater agglomeration as well as the increase in the proportion of smaller, irregular, rounded morphologies.

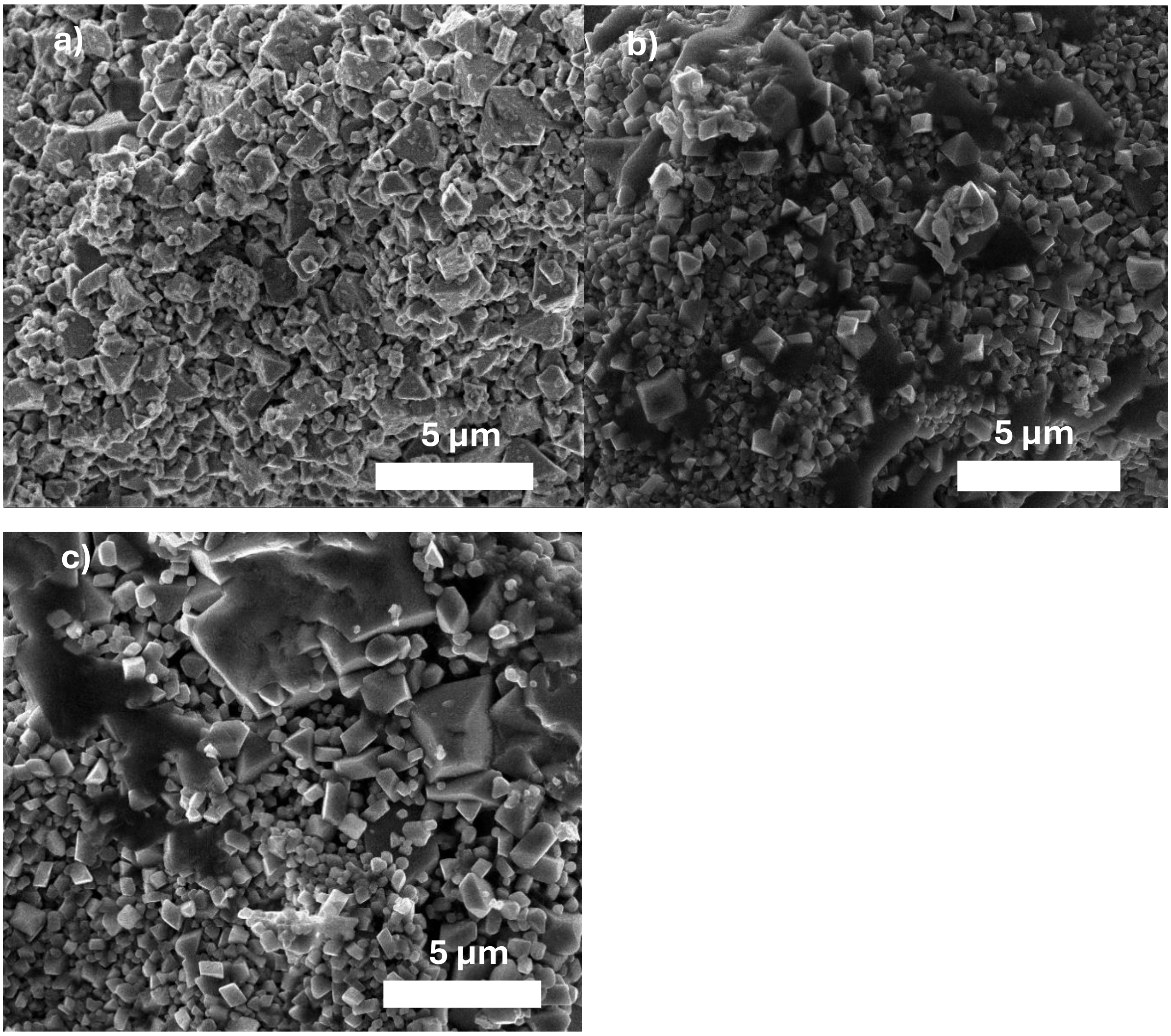

Figure 137 SEM of NMC811 with sodium peroxide ($LiNi_{0.8}Mn_{0.1}Co_{0.1}O_2.x0.5Na_2O_2$) where Na = x and Li = 1, synthesised with acetate precursors and sodium alginate, and sodium nitrate where a) x = 0.1 ($LiNi_{0.8}Mn_{0.1}Co_{0.1}O_2.x0.05Na_2O_2$), consisting of irregular octahedral particles, b) x = 0.2 ($LiNi_{0.8}Mn_{0.1}Co_{0.1}O_2.x0.1Na_2O_2$) consisting of larger, regular octahedral particles, and c) x = 0.3 ($LiNi_{0.8}Mn_{0.1}Co_{0.1}O_2.x0.15Na_2O_2$),consisting of large octahedral particles with agglomerated primary particles

4.6.3 Discussion of NMC811 synthesised with the addition of sodium, where Na = x and Li = 1, using sodium alginate and sodium nitrate

While the substitution of a proportion of sodium alginate with sodium nitrate results in an overall increase in the structure of NMC811 regardless of the precursor used, provided Li is not substituted for Na, the maintaining of the same mass of biotemplate results in worse morphological control of particles. Not increasing the mass of sodium alginate ensures the carbon content of the reaction does not increase as when the biotemplate decomposes there is no increase in the amount of carbon freed up to react with the oxygen atmosphere, reducing the amount of CO_2 formed. This maintains a more oxidising environment as more oxygen is available to fill oxygen sites during the synthesis of NMC811, which results in greater layering and less cation mixing in the NMC811 [133]. As the mass of sodium nitrate is increased, the increase in metal cations and maintaining of the same number of chelation sites results in a greater number of metal cations not being chelated which is a detriment to morphological control. While a greater mass of sodium nitrate leads to the synthesis of more octahedral morphologies and the average diameter of particles remains at nanoscale, unchelated metal cations recrystallise results in greater amount of agglomerated primary particles and smaller, irregular morphologies. Overall, however this method of synthesising NMC811 using sodium alginate and sodium nitrate shows significant promise in the synthesis of NMC811 and should be further investigated as a potential cathode in lithium-ion cells.

4.7 Synthesis of NMC811 with sodium via the addition of Na, where Na = x and Li = 1, using dextran and sodium nitrate

The last variation to be investigated in the synthesis of NMC811 with sodium is the use of sodium nitrate and dextran biotemplating, where sodium is added without the substitution of lithium such that Li = 1 and x = 0.1 and 0.2. It is compared whether NMC811 synthesised with sodium such that x = 0.1 or 0.2 ($LiNi_{0.8}Mn_{0.1}Co_{0.1}O_2.0.1Na$ and $LiNi_{0.8}Mn_{0.1}Co_{0.1}O_2.0.2Na$ respectively) without reducing the mass of lithium in the NMC811 is advantageous for structural organisation of the NMC811 cathode and whether there is improvement in capacity and/or cycling stability of the lithium ion cell. The analysis of cathode structure and cell performance is also to determine if there is any benefit over synthesising NMC811 using dextran and sodium nitrate where lithium is substituted for sodium and NMC811 synthesised with sodium alginate where no lithium is removed. NMC811 is synthesised using dextran with either acetate or nitrate precursors, Table 25, and the sodium used is exclusively introduce using sodium nitrate.

	X = 0.1	X = 0.2
Dextran (g)	0.25	0.25
Sodium nitrate (g)	0.0213	0.0425

Table 25 Masses of metal precursor salts used in the synthesis of NMC811 with sodium via addition of sodium using dextran as a biotemplate and sodium nitrate

4.7.1 Synthesis of NMC811 with sodium carbonate via the addition of Na, where Na = x and Li = 1, using dextran and sodium nitrate using nitrate precursors

4.7.1.1 X-Ray Diffraction Analysis of NMC811 with sodium carbonate via the addition of Na, where Na = x and Li = 1, using dextran and sodium nitrate using nitrate precursors

XRD performed on the dextran biotemplated NMC811 synthesised with sodium and using nitrate precursors indicates a structure with disorganisation and mixing of lithium and transition metal regardless of the amount of sodium used. Where x = 0.1, Figure 138a, peak splitting at (006)/(012) and (018)/(110) is poor indicating poor layering of the NMC811 structure, while when x = 0.2, Figure 138b, there is no visible peak splitting indicating very poor layering of the cathode structure. Peak intensity ratios between (003) and (104) are 1.27 where x = 0.1 and 0.91 for x = 0.2, highlighting significant mixing of Li^+ and Ni^{2+} cations across Ni and Li sites where both amounts of sodium are used (where when the ratio is <1.2 the cathode exhibits high mixing [130]).

Where x = 0.1 there are no peaks indicative of a second sodium phase, suggesting that the mass of the secondary phase is low enough that XRD is unable to detect it. When x = 0.2, low intensity peaks at 29 and 34° (002 and 310/020) indicate a secondary sodium carbonate phase. While significant disorganisation of the NMC811 may compound by the synthesis of the sodium secondary phase. the main cause is likely carbon content of the dextran biotemplate causing disorganisation of the NMC811. This is due to the decomposition of the dextran biotemplate releasing carbon to react with the oxygen atmosphere and form CO_2, which due to the using up of oxygen in the formation of CO_2 results in a more reducing atmosphere. The reducing atmosphere means less available oxygen available for the synthesis of NMC811 resulting in fewer filled oxygen sites and greater disorganisation of the structure.

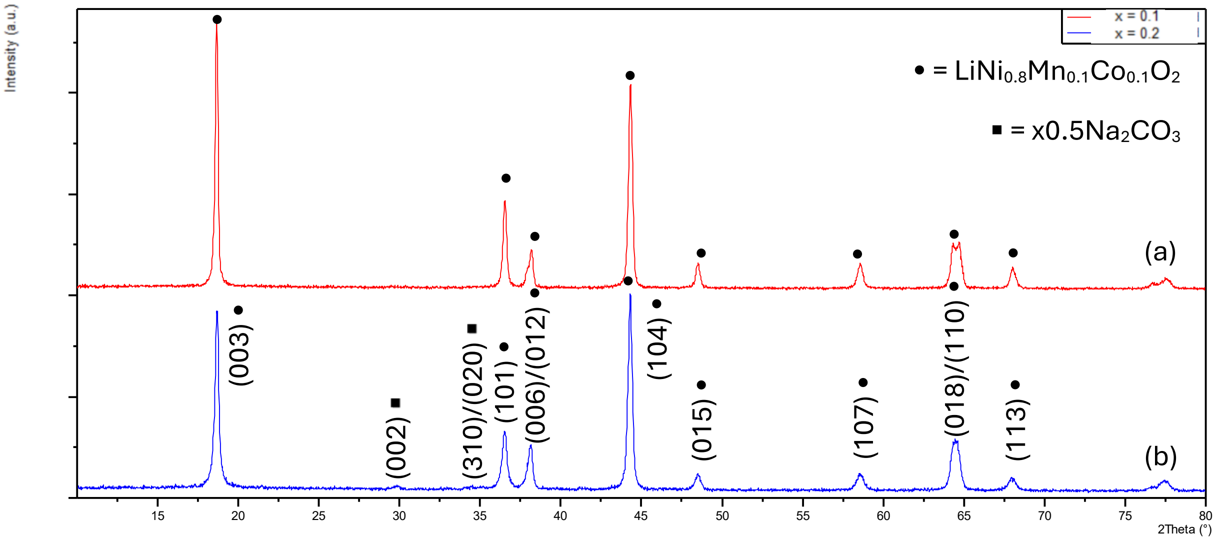

Figure 138 XRD of NMC811 with sodium carbonate ($LiNi_{0.8}Mn_{0.1}Co_{0.1}O_2.x0.5Na_2CO_3$) where Na = x and Li = 1, synthesised with nitrate precursors and dextran biotemplating, and sodium nitrate where a) x = 0.1 ($LiNi_{0.8}Mn_{0.1}Co_{0.1}O_2.x0.05Na_2CO_3$) and b) x = 0.2 ($LiNi_{0.8}Mn_{0.1}Co_{0.1}O_2.x0.1Na_2CO_3$)

4.7.1.2 Morphology of NMC811 with sodium carbonate via the addition of Na, where Na = x and Li = 1, using dextran and sodium nitrate using nitrate precursors

NMC811 synthesised with sodium where x = 0.1, Figure 139a, and x = 0.2, Figure 139b, consist of significant agglomerations of particles. Both samples contain particles with highly irregular and varied morphologies consisting of rounded, tetragonal, and octahedral shapes, with an average diameter of 300 nm when x = 0.1 and an average diameter of 200 nm for where x = 0.2, albeit that nanoscale particles exhibit significant agglomeration. Such agglomerations are due to the high content of carbon of the biotemplate producing a reducing environment and the recrystallisation of metal ions due to an increase in the amount of metal cations but no increase in the amount of chelation sites due to the mass of dextran remaining constant. The synthesis of tetragonal and octahedral morphologies however is a sign that sodium is present in the particle synthesis, inferring that sodium chelated to the dextran biotemplate even if it was not integrated into the NMC811 structure. There are also nanowire growths present when NMC811 is synthesised where x = 0.2, however the growths are likely synthesis of lithium carbonate formed as the sample aged with the SEM images being taken a year after synthesis of the cathode [143]. Significant agglomeration of the samples will negatively affect cathode performance regardless of the small average particle size, with the large agglomerations reducing surface area available for intercalation. As such this combination of biotemplate and precursors may not be suitable for synthesising NMC811 with sodium.

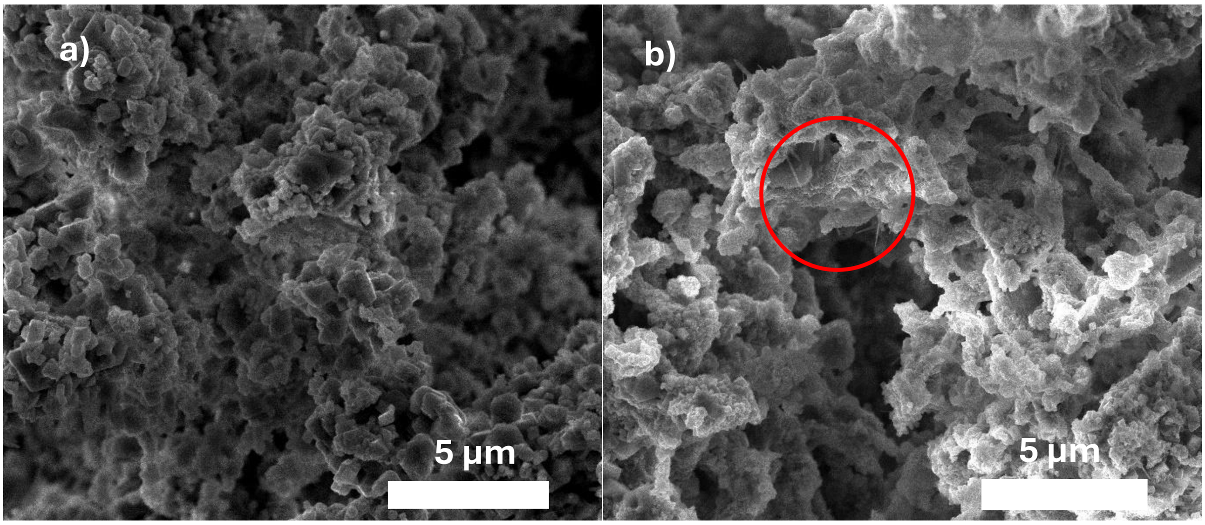

Figure 139 SEM of NMC811 with sodium carbonate ($LiNi_{0.8}Mn_{0.1}Co_{0.1}O_2.x0.5Na_2CO_3$) where Na = x and Li = 1, synthesised with nitrate precursors and dextran biotemplating, and sodium nitrate where a) x = 0.1 ($LiNi_{0.8}Mn_{0.1}Co_{0.1}O_2.x0.05Na_2CO_3$) and b) x = 0.2 ($LiNi_{0.8}Mn_{0.1}Co_{0.1}O_2.x0.1Na_2CO_3$) consisting of some nanowire growth (highlighted in red)

4.7.2 Synthesis of NMC811 with sodium carbonate via the addition of Na, where Na = x and Li = 1, using dextran and sodium nitrate using acetate precursors

4.7.2.1 X-Ray Diffraction Analysis of NMC811 with sodium carbonate via the addition of Na, where Na = x and Li = 1, using dextran and sodium nitrate using acetate precursors

When using acetate precursors, dextran biotemplated NMC811 synthesised with sodium exhibits similar levels of structural disorganisation as it does when synthesised with nitrate precursors, Figure 138. When x = 0.1, Figure 140a, and x = 0.2, Figure 140b, (where Li = 1), twin peaks at (006)/(012) and (018)/(110) reflections have poor and minimal peak splitting respectively indicating poor layering of the NMC811. (003)/(104) peak intensity ratios of 1.4 where x = 0.1 and 1.16 where x = 0.2 highlight high mixing of Li^+ and Ni^{2+} for Ni and Li sites (where <1.2 is considered high mixing of cations [130]).

Low intensity peaks with reflections of (002) at 29 ° and (310)/(020) at 34 °, where x = 0.2 and to a lesser extent where x = 0.1, indicates a secondary sodium carbonate phase, however the low intensity of the peaks infers only a small proportion of sodium has potentially formed into the secondary phase. The large carbon content from the acetates and dextran, of which is released when the biotemplate and precursor decomposes, reacts with the oxygen atmosphere to form CO_2 and forms a reducing environment. This reducing environment, a result of oxygen being used up in the synthesis of CO_2 are the causes of the disorganisation of the NMC811 structure as less oxygen is available to fill oxygen sites. From this it is apparent that, at least structurally, lithium NMC811 synthesised with dextran and sodium nitrate is not viable without significant disorganisation.

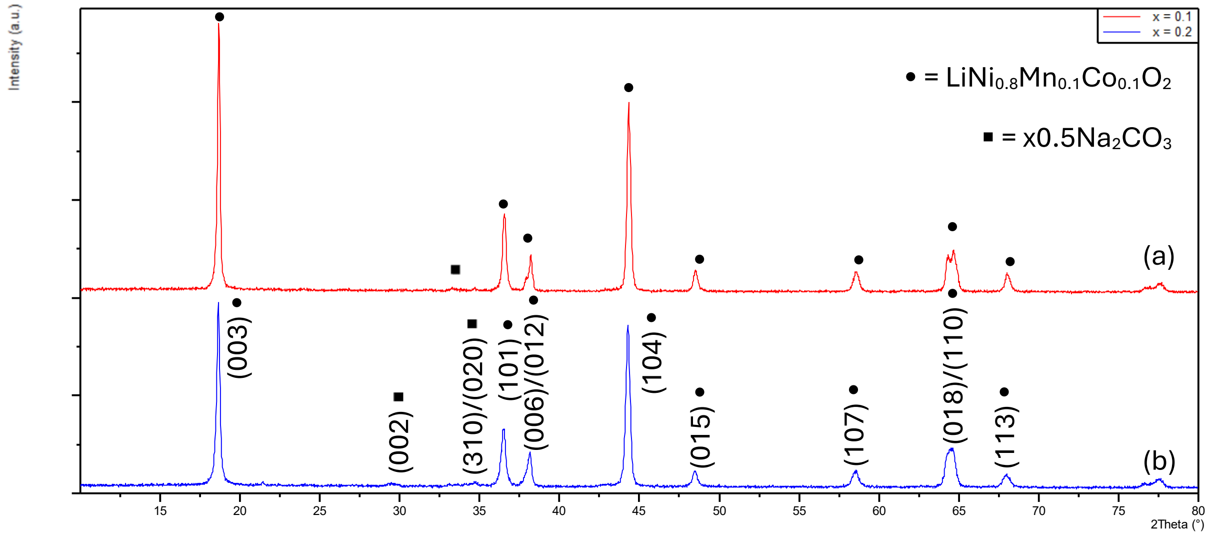

Figure 140 XRD of NMC811 with sodium carbonate ($LiNi_{0.8}Mn_{0.1}Co_{0.1}O_2.x0.5Na_2CO_3$) where Na = x and Li = 1, synthesised with acetate precursors and dextran biotemplating, and sodium nitrate where a) x = 0.1 ($LiNi_{0.8}Mn_{0.1}Co_{0.1}O_2.x0.05Na_2CO_3$) and b) x = 0.2 ($LiNi_{0.8}Mn_{0.1}Co_{0.1}O_2.x0.1Na_2CO_3$)

4.7.2.2 Morphology of NMC811 with sodium carbonate via the addition of Na, where Na = x and Li = 1, using dextran and sodium nitrate using nitrate precursors

Significant agglomeration of particles in addition to the synthesis of individual non agglomerated primary particles are present when synthesising with acetates. For both x = 0.1, Figure 141a, and x = 0.2, Figure 141b, samples particle morphology ranges from small, round, irregular particles to larger octahedral particles, where x = 0.1 and 0.2 particles have average particle diameters of 400 nm and 600 nm, respectively.

Individual octahedral particles provide high surface area for lithiation sites, with octahedral morphologies likely formed due to the chelation of the increasing amount of sodium ions onto the chelation sites of the dextran biotemplate, inferred due to the high proportion of octahedral morphologies formed using sodium alginate. Significant agglomeration of primary particles is also present across both samples which inhibits intercalation of lithium by reducing surface area and associated lithiation sites. The higher amount of metal cations and the maintaining of the same mass of dextran and associated number of chelation sites results in recrystallisation of metal cations during preheat and so greater agglomeration of particles. A large amount of agglomerated primary particles will reduce the surface area available for lithiation and so will lead to a reduction in specific capacity.

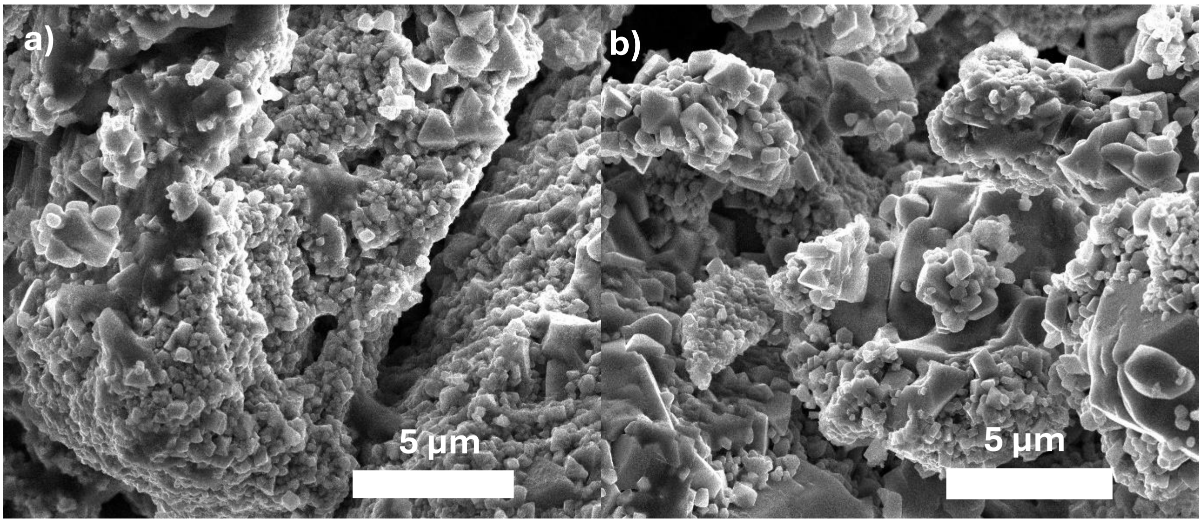

Figure 141 SEM of NMC811 with sodium carbonate ($LiNi_{0.8}Mn_{0.1}Co_{0.1}O_2.x0.5Na_2CO_3$) where Na = x and Li = 1, synthesised with acetate precursors and dextran biotemplating, and sodium nitrate where a) x = 0.1 ($LiNi_{0.8}Mn_{0.1}Co_{0.1}O_2.x0.05Na_2CO_3$) and b) x = 0.2 ($LiNi_{0.8}Mn_{0.1}Co_{0.1}O_2.x0.1Na_2CO_3$)

4.7.2.3 Cell cycling of NMC811 with sodium carbonate via addition of Na using dextran, sodium nitrate, and acetate precursors where x = 0.1, with 4.5 to 2.8 V range

Lithium-ion cell cycling performed using acetate and dextran synthesised NMC811 cathodes with sodium carbonate where Li = 1 and x = 0.1, cycled between 4.5 V and 2.8 V at 0.1 C supports evidence of poor performance suggested by XRD, Figure 140, and SEM, Figure 141, data. Initial specific discharge capacities range from 130 to 180 mAh/g, Figure 142b, e, h. While no substitution of lithium was untaken in the synthesis of the cathodes, differential capacity curves, Figure 142c, f, I, highlight how the cathodes are not able to access all of the lithium due to not undergoing the H2 to H3 phase transition.

Differential capacity curves also provide evidence for poor capacity retention, where discharge capacity decreasing at a rate of between (110) and 150 mAh/g over 50 cycles. Phase changes during the initial charge cycle of H1 to M at 3.7 V and M to H2 at 4.0 V and H2 to M at 4.2 V and M to H1 at 3.7 V during discharge [142], outlined by the differential capacity curves, occur at higher voltages in subsequent cycles due to structural deterioration as the cell is cycled above 4.2 V [140]. As of cycle 50, the H1 to M phase change occurs at 4.2 V, Figure 142c, or above 4.5 V, Figure 142I, with the M to H2 phase change also occurring above 4.5 V. This results in either cell failure or only the single H1 to M phase change occurring after 50 cycles, significantly reducing specific capacity.

As such it is observed that NMC811 with a sodium carbonate secondary phase is not able to improve structural stability during delithiation and so significant structural disorganisation occurs whereby lithium is not able to fully intercalate back onto the cathode.

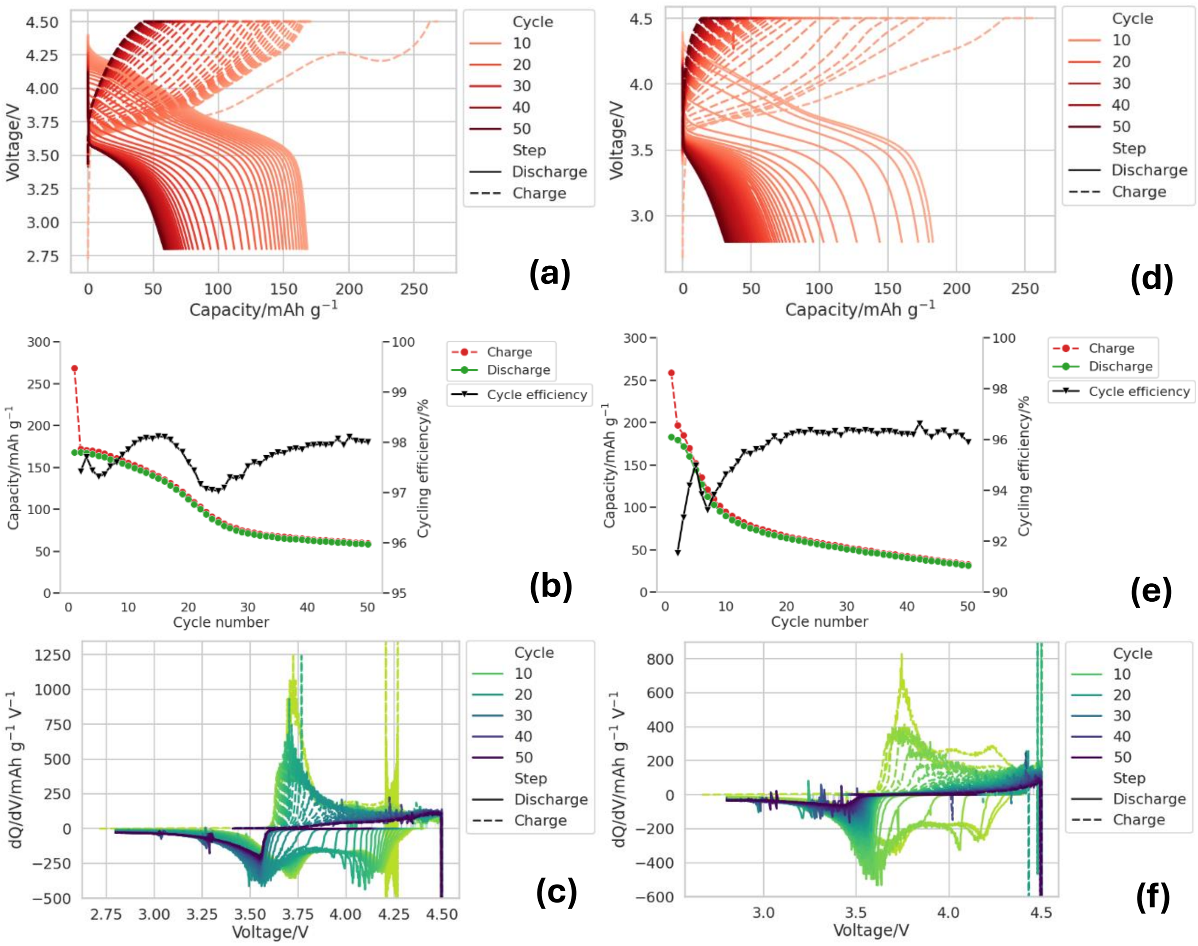(a)
Voltage/V
Capacity/mAh g^{-1}
Cycle
10
20
30
40
50
Step
Discharge
Charge
(b)
Capacity/mAh g^{-1}
Cycling efficiency/%
Cycle number
Charge
Discharge
Cycle efficiency
(c)
dQ/dV/mAh g^{-1} V^{-1}
Voltage/V
Cycle
10
20
30
40
50
Step
Discharge
Charge
(d)
Voltage/V
Capacity/mAh g^{-1}
Cycle
10
20
30
40
50
Step
Discharge
Charge
(e)
Capacity/mAh g^{-1}
Cycling efficiency/%
Cycle number
Charge
Discharge
Cycle efficiency
(f)
dQ/dV/mAh g^{-1} V^{-1}
Voltage/V
Cycle
10
20
30
40
50
Step
Discharge
Charge

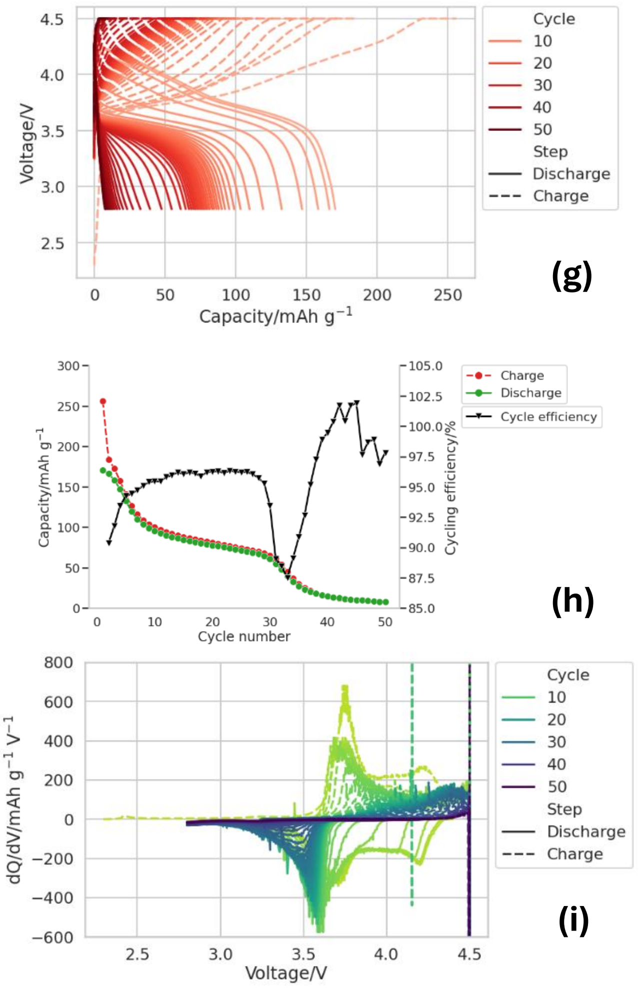

Figure 142 Charge-discharge cycling (a, d, g), Cycling efficiency and charge-discharge capacities (b, e, h), and Differential capacity vs. voltage curve (c, f, i), for Li-ion coin cells 1-3 with acetate, dextran, and sodium nitrate synthesised cathodes where x = 0.1 ($LiNi_{0.8}Mn_{0.1}Co_{0.1}O_2.x0.05Na_2CO_3$) between 4.5 and 2.8 V for 50 cycles

4.7.2.4 Cell cycling of NMC811 with sodium carbonate via addition of Na using dextran, sodium nitrate, and acetate precursors where x = 0.2, with 4.5 to 2.8 V range

Dextran biotemplated NMC811 cathodes with sodium carbonate synthesised using acetates, where Li = 1 and x = 0.2, cycled in a lithium ion cell at 4.5 V to 2.8 V at 0.1 C, are comparable to cells with cathodes synthesised with sodium alginate where x = 0.1, Figure 142. Initial specific discharge capacities range from 140 to 175 mAh/g, Figure 143b, e, h, comparable to initial specific discharge capacities where x = 0.1, Figure 142. Poor capacity retentions of between 120 and 170 mAh/g over 50 cycles are observed however with cells all exhibiting cell failure.

Initial discharge capacity is the same as dextran biotemplated cathodes were x = 0.1, Figure 142c, f, i, with cathodes synthesised with both proportions of sodium not undergoing the H2 to H3 phase transition below 4.5 V. Where x = 0.2, Figure 143c, f, i, phase transitions of H1 to M and M to H2 occur during the initial charge cycle at 3.8 V and 4.2 V [142], respectively, with H2 to M and M to H1 phase transitions occurring at 4.2 and 3.7 V, respectively. As the cells approach 50 cycles, cycling above 4.2 V causes structural deformation [140] to the point where the H1 to M phase change occurs above 4.5 V leading to no further phase changes during cell cycling and cell failure.

It is apparent that synthesising NMC811 with sodium nitrate when using dextran does not aid in the structural organisation or stability of NMC811 cathodes or aid in the improvement in specific capacity, with an increased in sodium above x = 0.1 in some cases being observed to accelerate the rate of capacity fade.

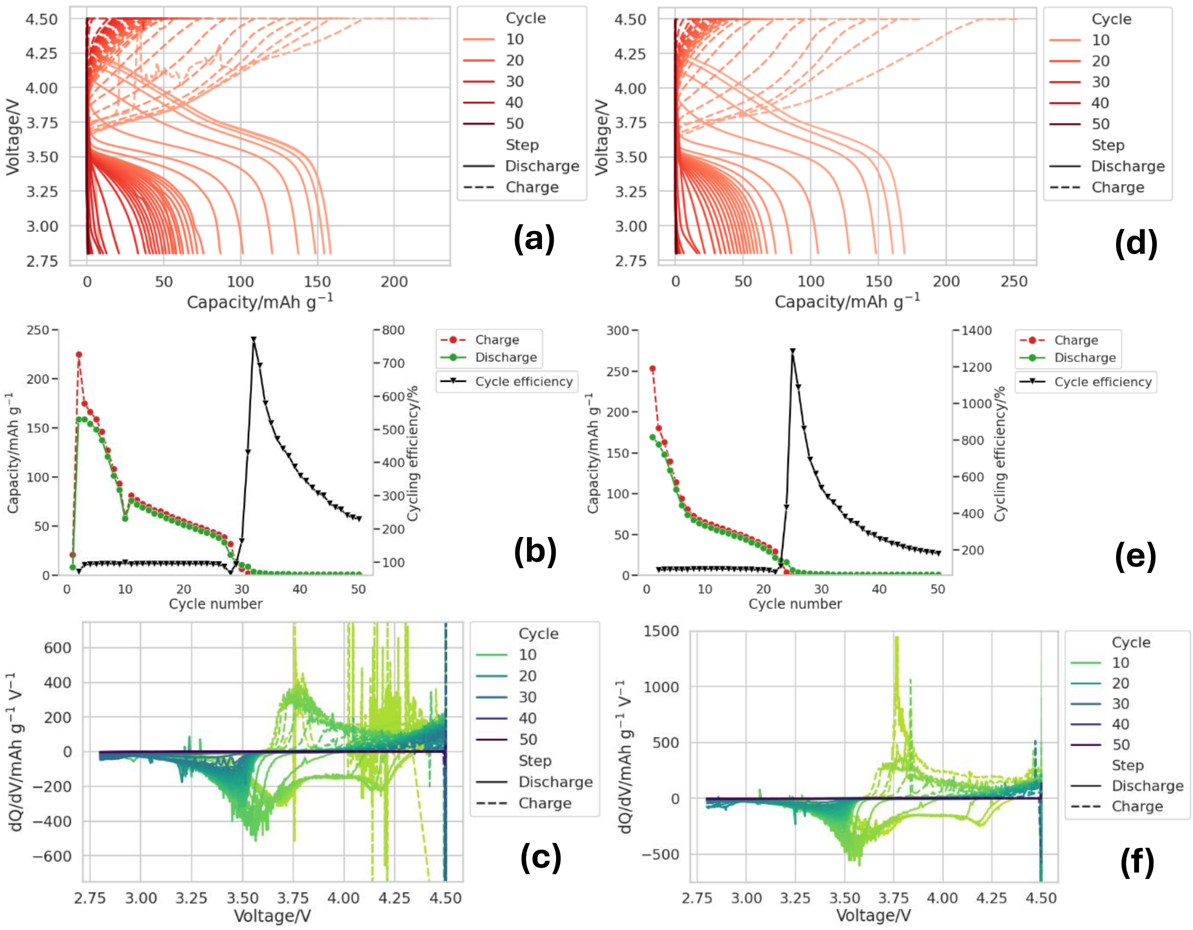
(a)
Voltage/V
4.50
4.25
4.00
3.75
3.50
3.25
3.00
2.75
Capacity/mAh g^{-1}
0
50
100
150
200
Cycle
10
20
30
40
50
Step
Discharge
Charge
(d)
Voltage/V
Capacity/mAh g^{-1}
250
(b)
Capacity/mAh g^{-1}
Cycle number
Cycling efficiency/%
Charge
Discharge
Cycle efficiency
(e)
Capacity/mAh g^{-1}
Cycle number
Cycling efficiency/%
(c)
dQ/dV/mAh g^{-1} V^{-1}
Voltage/V
(f)
dQ/dV/mAh g^{-1} V^{-1}
Voltage/V

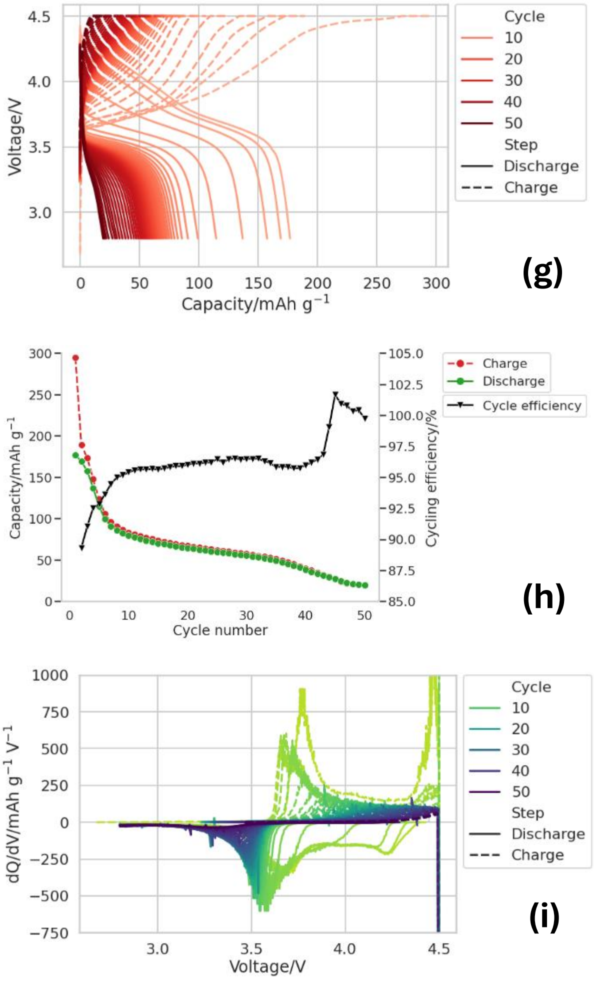

Figure 143 Charge-discharge cycling (a, d, g), Cycling efficiency and charge-discharge capacities (b, e, h), and Differential capacity vs. voltage curve (c, f, i), for Li-ion coin cells 1-3 with acetate, dextran, and sodium nitrate synthesised cathodes where x = 0.2 ($LiNi_{0.8}Mn_{0.1}Co_{0.1}O_2.x0.1Na_2CO_3$) between 4.5 and 2.8 V for 50 cycles

4.7.2.5 Further discussion of cell cycling data

The poor cyclability of the cells may also be explained by potential issues arising during the cell manufacturing process, 3.7.4. While initial specific discharge capacity appears consistent, cyclability appears to either be poor or vary significantly. This may be explained by oxidation of the lithium chip or damage caused by attempted removal of the oxidation, which may damage the lithium chip and reduce stability and cyclability, or by degradation of or water present in the electrolyte, which reduces ionic diffusivity and lead to poor cyclability. Both of these issues are as a result of long term storage of the lithium chips and electrolyte, a potential side effect of long term supply chain issues for lithium products. Cyclability may also be affected poor mixing, where an inhomogeneous slurry may lead to cathodes with less additives and so less stability, while variation in the ratios of active materials and additives in the slurry may also account for variation in cycling between seemingly identical cathodes. Further damage to the cathodes may be done by poor and uneven drawdowns due to a too thin or too thick slurry. This may potentially lead to over calendaring which can damage the cathode and further reduce cyclability.

4.8 Discussion of NMC811 with sodium via the addition of Na, where Na = x and Li = 1, using dextran and sodium nitrate

Overall, the synthesis of NMC811 with sodium via the substitution of lithium precursors with either sodium alginate and/or sodium nitrate, is not viable. The substitution of lithium reduces the availability of lithium by too significant an amount, reducing specific capacity. The sodium does not appear to integrate into the NMC811 structure but instead forms sodium carbonate or sodium peroxide secondary phase which have no effect on the structural organisation or stability of the NMC811. Capacity fade is therefore still significant regardless of the biotemplate or sodium source used, often leading to cell failure.

When sodium is added to NMC811 without the removal of lithium, resulting cathodes hold greater viability. Synthesis of NMC811 with sodium alginate at x = 0.2 or above results in too high a disorganisation of the NMC811 leading to poor cell performance while synthesising with sodium alginate where x = 0.1 results in very high capacity retention at the cost of specific capacity. When synthesising with sodium nitrate with dextran, cathode structure and cell cycling are comparable to sodium alginate biotemplated cathodes synthesised in section 3.7.3 and have the potential to exhibit improved capacity retention. When using sodium nitrate in combination with sodium alginate, high structural organisation of NMC811 is observed which shows high potential for use as cathodes in lithium-ion cells.

Morphology of NMC811 particles suffers as a result synthesis with sodium. While particles are still formed at the nanoscale and the increased use of sodium results in a greater proportion of individual octahedral morphologies with high surface areas ideal for the intercalation of lithium, the increased use of sodium results in greater agglomerations of primary particles. This is due to insufficient chelation sites for metal cations where the mass of the biotemplate is maintained but the mass of sodium is increased, resulting in recrystallisation of cations during preheating and the synthesis of agglomerations. Any attempt to rectify this by using a higher mass of biotemplate results in greater disorganisation of the NMC811 structure as the higher mass of biotemplate decomposes, freeing up more carbon to react with the oxygen atmosphere and synthesise a greater amount of CO_2. This forms a more reducing environment as oxygen is used up in the reaction and leaves less oxygen free to synthesise NMC811 and fill oxygen sites.

The average particle size of the NMC811 powder also varies with the type and mass of biotemplate used and precursor used, Table 26a, with the largest average particles of 1500 nm being synthesised from the combination of nitrate precursors, sodium alginate and sodium nitrate when using the substitution method. The smallest average particles meanwhile are synthesised from acetate precursors, sodium alginate, and sodium nitrate. When using sodium alginate, there is an observable increase in average particle size when changing the precursor from acetate to nitrate, but not from increasing the amount of the biotemplate used. An explanation for this may be that the sodium is forming a secondary phase and so is not directly affecting the average particle size of the NMC811. This is reinforced by there being no change in average particle size when using a combination of dextran and sodium nitrate, with no change in the amount of sodium nitrate used or which precursor is used.

By comparison, when using the addition method, Table 26b, there appears to be little overall trend in average particle size. When using only sodium alginate and nitrate precursors the average particle size is observed as 900 nm regardless of the amount of biotemplate used, possibly as a result of sodium forming a secondary phase and not being formed into the

NMC811 structure, and as such not affecting the particle size of the NMC811. There is also little variation when using nitrate precursors and a combination of sodium alginate and sodium nitrate, and dextran and sodium nitrate, likely for the same reason. Conversely when using acetate precursors, the greater the mass biotemplate used the greater the average particle size when using all combinations of sodium alginate, sodium nitrate, and dextran. One such reason for this may be the carbon content of the acetate precursors, with the larger carbon content reacting with the oxygen atmosphere and forming CO_2 upon the breakdown of the precursor and biotemplate, resulting in an exothermic reaction that gives out heat. The increase in the mass of the biotemplate may result in a greater exothermic reaction and a greater amount of heat, providing more energy for the particles to grow. As such, provided lithium is not removed from the NMC811 structure and the amount of sodium such that the proportion of sodium is greater than x = 0.1, NMC811 synthesised with a sodium secondary phase has promise and viability for improving capacity retention of NMC811.

Substitution, where Na = x, Li = (1-x)						
	Sodium alginate		**Sodium alginate/sodium nitrate**		**Dextran/sodium nitrate**	
	Acetates	Nitrates	Acetates	Nitrates	Acetates	Nitrates
x = 0.1	400 nm	900 nm	-	-	400 nm	400 nm
x = 0.2	400 nm	900 nm	-	-	400 nm	400 nm
Sodium alginate/sodium nitrate 50:50	-	-	300 nm	1500 nm	-	-
Sodium alginate only	-	-	400 nm	900 nm	-	-

a) Synthesis of NMC811 with sodium via the substitution of Na with Li, where Na = x and Li = (1 – x), *of sodium calcining with acetate precursors @ 850 °C or nitrate precursors @ 800 °C and either sodium alginate, sodium alginate and sodium nitrate, or dextran and sodium nitrate*

Addition, where Na = x, Li = 1						
	Sodium alginate		**Sodium alginate/sodium nitrate**		**Dextran/sodium nitrate**	
	Acetates	Nitrates	Acetates	Nitrates	400 nm	400 nm
x = 0.1	400 nm	900 nm	-	-	400 nm	300 nm
x = 0.2	1100 nm	900 nm	-	-	600 nm	200 nm
x = 0.3	800 nm	900 nm	-	-	-	-
Sodium alginate/sodium nitrate 33:67	-	-	600 nm	900 nm	-	-
Sodium alginate/sodium nitrate 50:50	-	-	400 nm	900 nm	-	-
Sodium alginate only	-	-	500 nm	400 nm	-	-

b) Synthesis of NMC811 with sodium via the addition of Na, where Na = x and Li = 1, *calcining with acetate precursors @ 850 °C or nitrate precursors @ 800 °C and either sodium alginate, sodium alginate and sodium nitrate, or dextran and sodium nitrate*

Table 26 Comparison of average particle diameters for NMC811 particles synthesised with sodium via the substitution (a) or addition (b) of sodium calcining with acetate precursors @ 850 °C or nitrate precursors @ 800 °C and either sodium alginate, sodium alginate and sodium nitrate, or dextran and sodium nitrate

5 Results section 3 - Synthesis and morphological control of NMC811 - lithium sulfate cathodes using sulfur-based κ-carrageenan

5.1 Aims for the synthesis of NMC811 - lithium sulfate cathodes using sulfur-based κ-carrageenan biotemplating

A third biotemplate, κ-carrageenan, is investigated in addition to dextran and sodium alginate as a possible biotemplate for the synthesis of NMC811. Previously used in the synthesis of yttrium barium copper oxide (YBCO) superconductors to form reticulated, blocky particle morphologies [106], κ-carrageenan shares many characteristics with sodium alginate. κ-carrageenan is obtained from red seaweed and is a long chain polysaccharide with a sulfated functional group, and like sodium alginate can be fully dissolved in 85 °C water ensuring little change to the biotemplating method is needed when using κ-carrageenan.

While use of κ-carrageenan as a biotemplate is employed to control particle morphology, use of increased masses of κ-carrageenan can result in the synthesis of sulfate impurities. One example of this is the synthesis of barium sulfate when synthesising YBCO using a high mass of κ-carrageenan [106]. While potentially detrimental, controlling the mass of the sulfate impurity may have potential benefits when used in lithium-ion cathodes. There is a large amount of interest in using sulfur with lithium chemistries, with significant work already being done into the development of lithium-sulfur cells as a cheaper alternative to NMC chemistries [9].

Another such way sulfur is being used in tandem with lithium is through the synthesis of lithium-ion chemistries such as NMC with sulfur. By using a reactant containing sulfur, a secondary Li_2SO_4 phase is formed within the cathode that gives improved cell cycling. [108]. This benefit may be gained by biotemplating, where κ-carrageenan may be used to synthesise lithium-ion cathodes with sulfur as when sodium when using sodium alginate in chapter 4.

5.2 Calcination Temperature Study of κ-carrageenan biotemplated NMC811 – lithium sulfate cathodes

An initial investigation variation of the calcination temperatures when biotemplating with κ-carrageenan is undertaken to determine the minimum calcination temperature required for the synthesis of layered, organised NMC811 when using this biotemplate. The masses, Table 27, are derived from the masses of the reactants used when synthesising YBCO with the higher ratio of κ-carrageenan to metal precursor salts [106]. The initial calcination temperature used is 850 °C, obtained by this temperature being used with dextran and sodium alginate in chapter 3 and reduced in 50 °C increments until the XRD pattern indicates significant disorganisation of the NMC811 structure.

	Acetate Hydrate	Nitrate Hydrate
Lithium (g)	0.2551	0.1158
Nickel (g)	0.04977	0.3722
Manganese (g)	0.0613	0.0286
Cobalt (g)	0.0623	0.0466
κ-carrageenan (g)	0.1	0.1

Table 27 Reactant masses for synthesising NMC811 – lithium sulfate cathodes using acetate or nitrate precursors and κ-carrageenan

5.2.1 X-Ray Diffraction of κ-carrageenan biotemplated NMC811 – lithium sulfate cathodes when varying calcination temperature

When using a calcination temperature of 850 °C, Figure 144a, the NMC811 structure is shown to have high levels of organisation. This is maintained when the calcined temperature is reduced to 800 °C, Figure 144b, before the structure becomes disorganised when 750 °C, Figure 144c, is used. Good peak splitting at (006)/(012) and (018)/(110) at 800 and 850 °C highlights more defined layering of the NMC811 structure [129] while at 750 °C poorer peak splitting indicates a less defined layered structure. The intensity ratio between peaks at (003) and (104) of 1.70, 1.56, and 1.56 using calcination temperatures of 850, 800, and 750 °C respectively, indicate low Li^+ and Ni^{2+} cation mixing between Ni and Li sites when using 800 and 750 °C and very low mixing when using 850 °C (where < 1.2 is considered high mixing [130]). When the levels of cation mixing and structural layering is compared for all three calcination temperatures, 850 °C provides the best defined layering and lowest amount of cation mixing.

Due to the high ratio of biotemplate to precursor mass when using κ-carrageenan, peaks shown at 22, 28, 31, 32, and 35 ° regardless of calcination temperature infer that sulfur was not integrated into the NMC811 structure and instead indicates a secondary phase with peaks characteristic of lithium sulfate (Li_2SO_4). This phase acts as a secondary phase in the same way Na_2O_2 or Na_2CO_3 secondary phase acts in chapter 4, and it is hypothesised that lithium sulfate will improve structural stability of the NMC811 cathode [108]. Too high a mass of lithium sulfate however will be detrimental due to Li_2SO_4 having poor electrical conductivity and so being detrimental to the performance of the cathode.

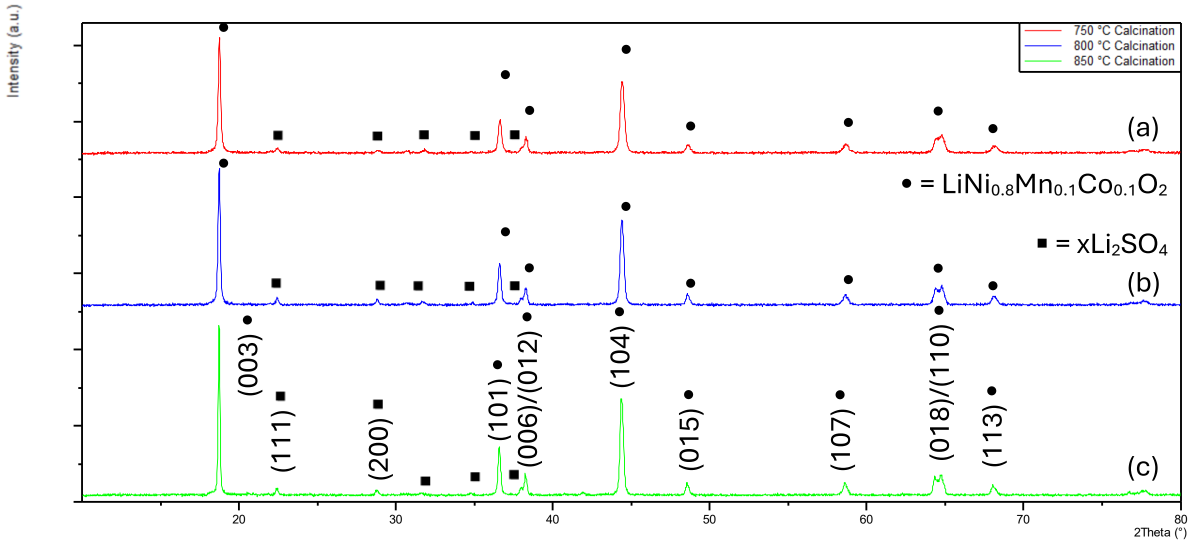

Figure 144 XRD showing NMC811– lithium sulfate cathodes synthesised using nitrate precursors and κ-carrageenan biotemplating, preheated at 300 °C in air and calcined in oxygen at a) 750 °C, b) 800 °C, and c) 850 °C

5.2.1.1 *Rietveld analysis of κ-carrageenan biotemplated NMC811 – lithium sulfate cathodes when calcined using nitrate precursors at 850 °C*

It can be confirmed as to whether any sulfur doping has taken place in addition to the formation of the Li_2SO_4 secondary phase through the use of Rietveld analysis. Refiement of κ-carrageenan biotemplated NMC811 and comparison of the powder data (obs) and refined phase data (calc), Figure 145, shows no sulfur doping in addition to the formation of the secondary phase.

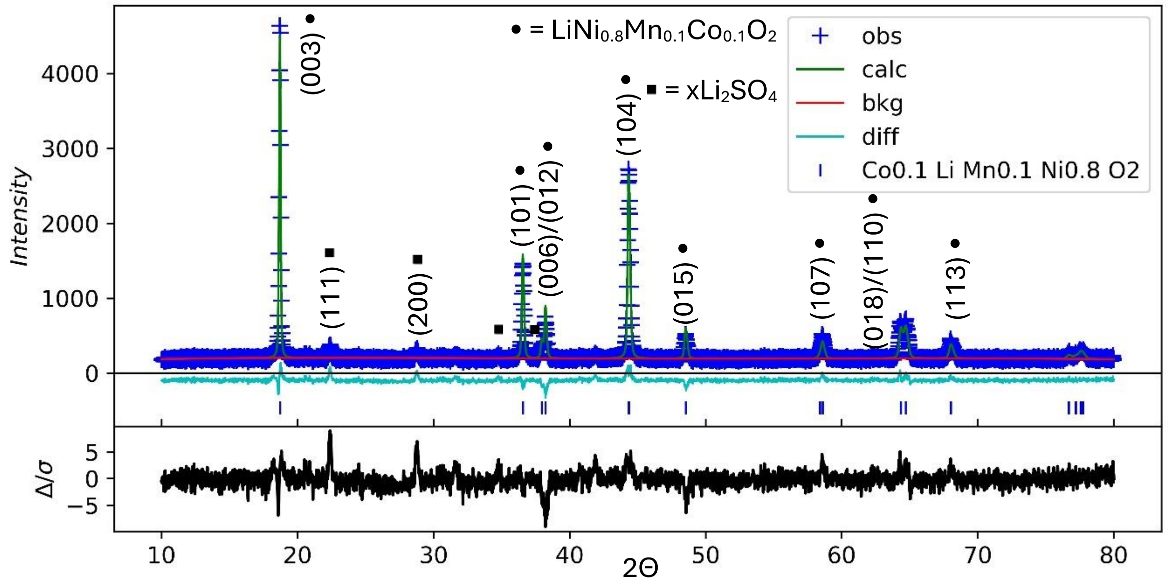

Figure 145 Rietveld analysis for NMC811– lithium sulfate cathodes synthesised using nitrate precursors and κ-carrageenan biotemplating, preheated at 300 °C in air and calcined in oxygen 850 °C

This is observed through there being no observable shift in the peaks along the 2Θ axis, which can be seen for all reflections including (003), (006)/(012), (104), and (018)/(110) reflection. This is further reinforced by there being no observable change in the unit cell dimensions, with the unit cell dimensions being unchanged at a/b = a/b = 2.8645 Å and c = 14.161 Å [119]. This supports that when an increased mass of sulfur precursor is used, secondary phases such as Li_2SO_4 are formed instead of sulfur doping taking place. Such a formation may still be beneficial, with formation of secondary lithium sulfate phases being shown to improve lithium cathodes [110].

5.3 κ-carrageenan biotemplated NMC811– lithium sulfate cathodes when varying mass of κ-carrageenan

With the calcination temperature established as 850 °C, the mass of κ-carrageenan is varied using low and high ratios of biotemplate relative to metal precursor salts, similarly to when synthesising YBCO using κ-carrageenan [106]. As it was observed that sulfur forms Li_2SO_4 as a secondary phase, $LiNi_{0.8}Mn_{0.1}Co_{0.1}O_2.xLi_2SO_4$ is synthesised using a low and high ratio of biotemplate to metal precursor salts such that x = 0.005 using the low ratio and 0.05 using acetates and 0.075 using nitrates for the high ratio.

The difference in the amount of sulfur, x, when using a high ratio of biotemplate and metal precursors is due to the use of different masses of acetate and nitrate precursors, Table 28. Such masses are similar to the masses used when biotemplating with dextran and sodium alginate in chapter 3 and is an increase in the mass of precursors and biotemplate outlined in

Table 27. This leads to a slight difference in mass for the biotemplate when using different precursor salts. The mass of lithium precursors is also increased due to some lithium during synthesis forming Li_2SO_4. Structural organisation, particle morphology, and cell performance when using low and high ratios of biotemplate to metal precursors is compared in order to determine the more optimal amounts of Sulfur for NMC811.

	Acetate Hydrate (g)	Nitrate Hydrate (g)
Lithium	0.5152	0.3482
Nickel	0.9954	1.1632
Manganese	0.1226	0.0894
Cobalt	0.1246	0.1454
K-carrageenan (low ratio of S-to-Li, x = 0.005)	0.02	0.02
K-carrageenan (high ratio of S-to-Li, x = 0.05 (Acetates), x = 0.075 (Nitrates))	0.2	0.3

Table 28 Scaled-up masses of acetate and nitrate precursors for synthesis of x2 mass of NMC811 – lithium sulfate cathodes

5.3.1 κ-carrageenan biotemplated NMC811– lithium sulfate cathodes when varying mass of κ-carrageenan using nitrate precursors

5.3.1.1 X-Ray Diffraction of κ-carrageenan biotemplated NMC811– lithium sulfate cathodes when varying mass of κ-carrageenan using nitrate precursors

The ratio of biotemplate to metal precursor is varied between low and high such that x = 0.005, Figure 146a, and x = 0.075, Figure 146b, respectively. Poor and good peak splitting at (006)/(012) and (018)/(110) reflections for low and high ratios respectively indicate good layering of the NMC811 where x = 0.075 but poor layering where x = 0.005 [129]. Peak intensity ratios between (003)/(104) are 1.82 where x = 0.005 and 1.87 where x = 0.05, highlighting minimal mixing of Li^+ and Ni^{2+} cation between Ni and LI sites for either amounts of κ-carrageenan used (where < 1.2 is a high level of mixing [130]). While using different amounts of sulfur-based κ-carrageenan exhibit similar amounts of cation mixing, a higher ratio of biotemplate to precursor salt is observed to produce a more layered NMC811 structure.

Peaks at 22, 28, and 35 ° indicate lithium sulfate as a secondary phase when using a high ratio of biotemplate to metal precursors, but no visible phase when using a low ratio. Assuming the ratio of NMC811 to Li_2SO_4 is stoichiometric and there is no loss of reactants, the mass of lithium sulfate is estimated to be 0.023 g. A greater proportion of lithium sulfate and greater layering both occur due to the use of a higher mass of biotemplate, which increases the sulfur content of the reaction leading to the synthesising of a greater amount of secondary phase but also has more chelation sites for metal precursor ions which results in greater layering of the NMC811 structure.

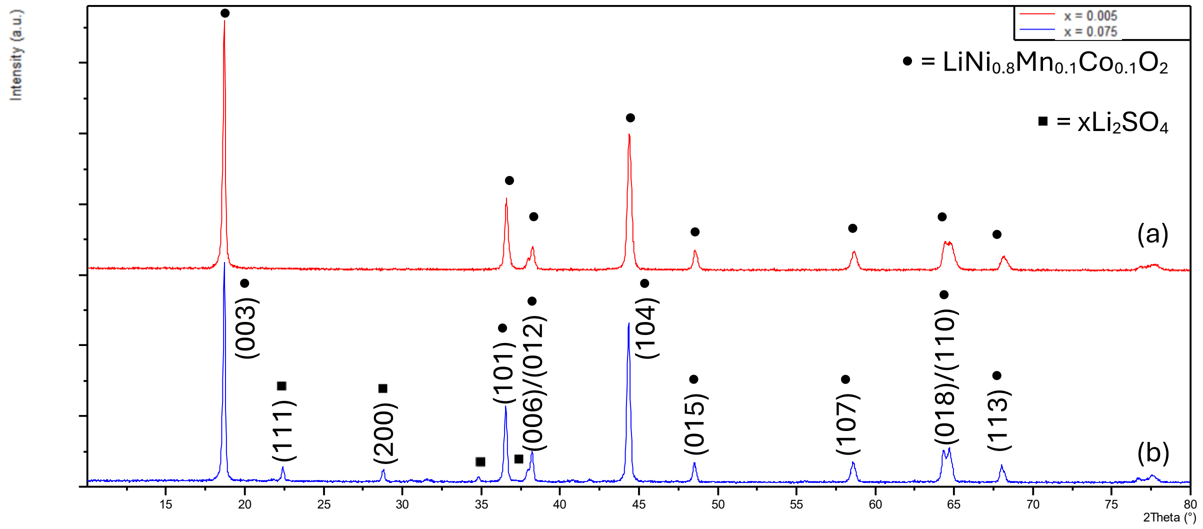

Figure 146 XRD showing $LiNi_{0.8}Mn_{0.1}Co_{0.1}O_2.xLi_2SO_4$ preheated at 300 °C in air and calcined 850 °C, using nitrate precursors and a) x = 0.005 and b) x = 0.075 κ-carrageenan biotemplating

5.3.1.2 Morphology of κ-carrageenan biotemplated NMC811 – lithium sulfate cathodes when varying mass of κ-carrageenan using nitrate precursors

The correlation between the amount of biotemplate used and organisation of NMC811 is further supported by the particle morphologies. When using a low ratio of biotemplate to metal precursor, Figure 147a, primary particles of average particle diameter 500 nm with irregular, rounded morphologies from large agglomerations. The morphology of NMC811 synthesised with a high ratio of biotemplate to metal precursors, Figure 147b, exhibits particles with a mix of smaller rounded and octahedral morphologies also of average particle diameter 500 nm of which show low levels of agglomeration. Similar average particle diameters infer the same synthesis conditions with the same amount of heating for both amounts of sulfur added such that particles would grow at the same rate. Agglomeration of the low ratio sample is a result of a low mass of biotemplate used resulting in fewer chelation sites and an ability for some metal ions to chelate. This results in recrystallisation of metal ions during drying and preheating and little morphological control, resulting in large agglomerations in addition to the synthesis of poorly layered NMC811. The increased amount of chelation sites where x = 0.075 however allows for much greater chelation of metal ions and so greater morphological control, resulting in a greater proportion of the octahedral morphology and less agglomeration of primary particles.

While examining particle morphology using SEM, EDAX is also done on particles using a low and high ratio of κ-carrageenan to metal precursors. Using a potential difference of 20 keV differences in the elemental makeup of the NMC811 – lithium sulfate cathodes are observed, with the most notable difference are the two peaks between 2 and 4 keV shown in Figure 148b (EDAX of Figure 147b), but not Figure 148a (EDAX of Figure 147a). This indicates the presence of sulfur when using the higher mass of biotemplate but when using the lower mass, the amount of sulfur present is not high enough to be detected under EDAX. The second difference present between the two figures is a relative intensity of the oxygen peak at ~ 0 keV vs. the Ni peak at 7 keV, and the presence of additional Ni peaks at 1 keV in Figure 148a. Such peaks between 0 and 1 keV in Figure 148a indicate nickel is present as a secondary phase in addition to the NMC811 phase. The existence of this secondary phase provides evidence for the poor layering of NMC811 where x = 0.005, as is a result of a lack of biotemplate and so chelation sites available for chelation of metal ions to occur, resulting in the recrystallisation of a secondary nickel phase. This phase is not able to be detected using XRD, likely due to the associated peaks occurring at the same values of 2Θ as NMC811. Such peaks are not present where x = 0.075, in part due to the higher mass of biotemplate and number of chelation sites and result in the improved layering of the structure. Such evidence proves the presence of both successful chelation due to the biotemplating method and presence of lithium sulfate when using a higher mass of biotemplate.

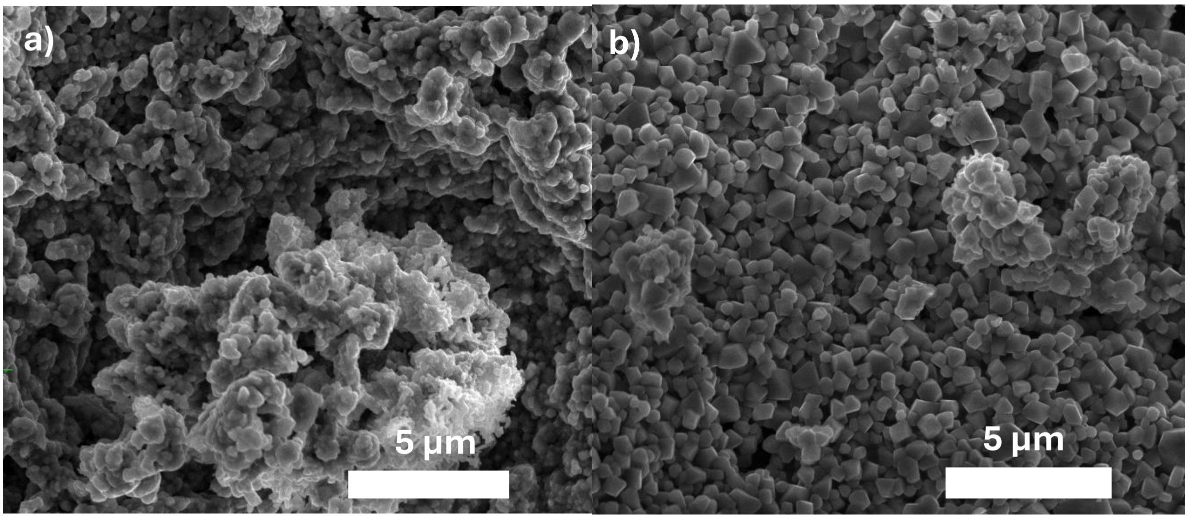

Figure 147 SEM showing $LiNi_{0.8}Mn_{0.1}Co_{0.1}O_2.xLi_2SO_4$ preheated at 300 °C in air and calcined 850 °C, using nitrate precursors and a) x = 0.005 and b) x = 0.075 κ-carrageenan biotemplating

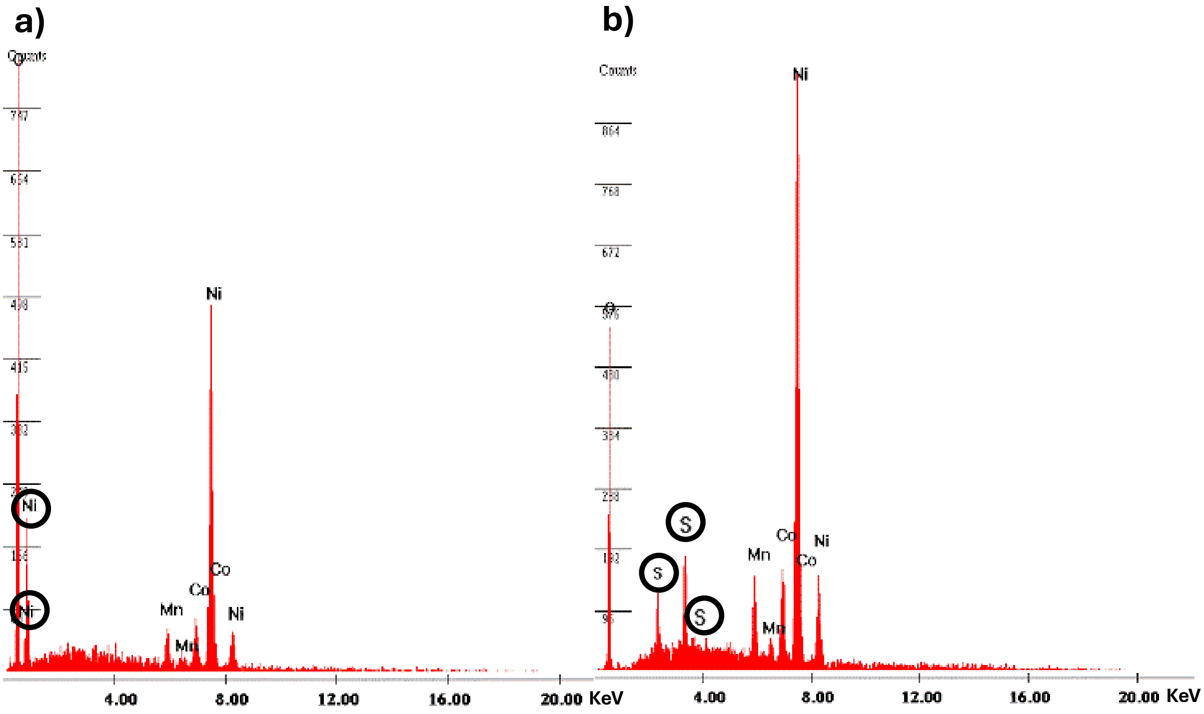

Figure 148 EDAX of $LiNi_{0.8}Mn_{0.1}Co_{0.1}O_2.xLi_2SO_4$ preheated at 300 °C in air and calcined 850 °C, using nitrate precursors and a) x = 0.005 (Figure 147a) and b) x = 0.075 (Figure 147b) κ-carrageenan biotemplating

5.3.1.3 Cell Data of κ-carrageenan biotemplated and nitrate precursor synthesised NMC811 – lithium sulfate cathodes where x = 0.005 cycled at 0.1 C between 4.5 V and 2.8 V

Despite the disorganisation of the NMC811 structure and agglomerated particle morphology when using the low ratio of κ-carrageenan to metal precursors such that x = 0.005, cycling of lithium-ion cells using NMC811 – lithium sulfate cathodes shows promising results. When cycled between 4.5 and 2.8 V at 0.1 C, 2 out of 3 cells exhibit initial specific discharge capacities of 180 mAh/g, Figure 149b, e, with a capacity fade of between 80 and 100 mAh/g over 50 cycles. Differential capacity curves, Figure 149c, f, show H1 to M and M to H2 phase transitions at 3.7 V and 4.2 V during the initial charging cycle and H2 to M and M to H1 phase transitions at 4.15 V and 3.6 V during discharge [142]. The H2 to H3 phase change does not occur below 4.5 V resulting in the cathode not exhibiting a specific discharge capacity above 200 mAh/g. After 50 cycles the H1 to M phase transition during charging and M to H1 phase change during discharge occur at 3.7 V and 3.6 V. Despite cycling above 4.2 V there is not significant breakdown of the NMC811 structure such that the H1 to M phase transition can still occur and the cell is still able to cycle to 80 mAh/g [140]. We can infer that the low proportion of lithium sulfate formed using the low ratio of biotemplate to metal precursors such that x = 0.005 may improve structural stability of the NMC811 cathode.

The third cell exhibits behaviour during the initial discharge cycle that infers some sort of significant structural change, Figure 149g, which results in cell failure after 50 cycles. As such due to structural deterioration after 50 cycles the H1 to M phase change occurs above 4.5 V and no phase changes can occur. This indicates that while lithium sulfate may benefit structural stability, structural deterioration is still possible and integrating lithium sulfate into the cathode as a secondary phase is not a guaranteed way of improving capacity fade.

Such cycling behaviour is among the best seen for cells cycled between 4.5 and 2.8 V when compared against cells in section 3.7, especially with regard to capacity retention. This is despite XRD and SEM data showing poor layering of the NMC811 structure and increased particle agglomeration. Such data shows promising results in how lithium sulfate, formed using κ-carrageenan as a biotemplate, is beneficial to the cycling of NMC811.

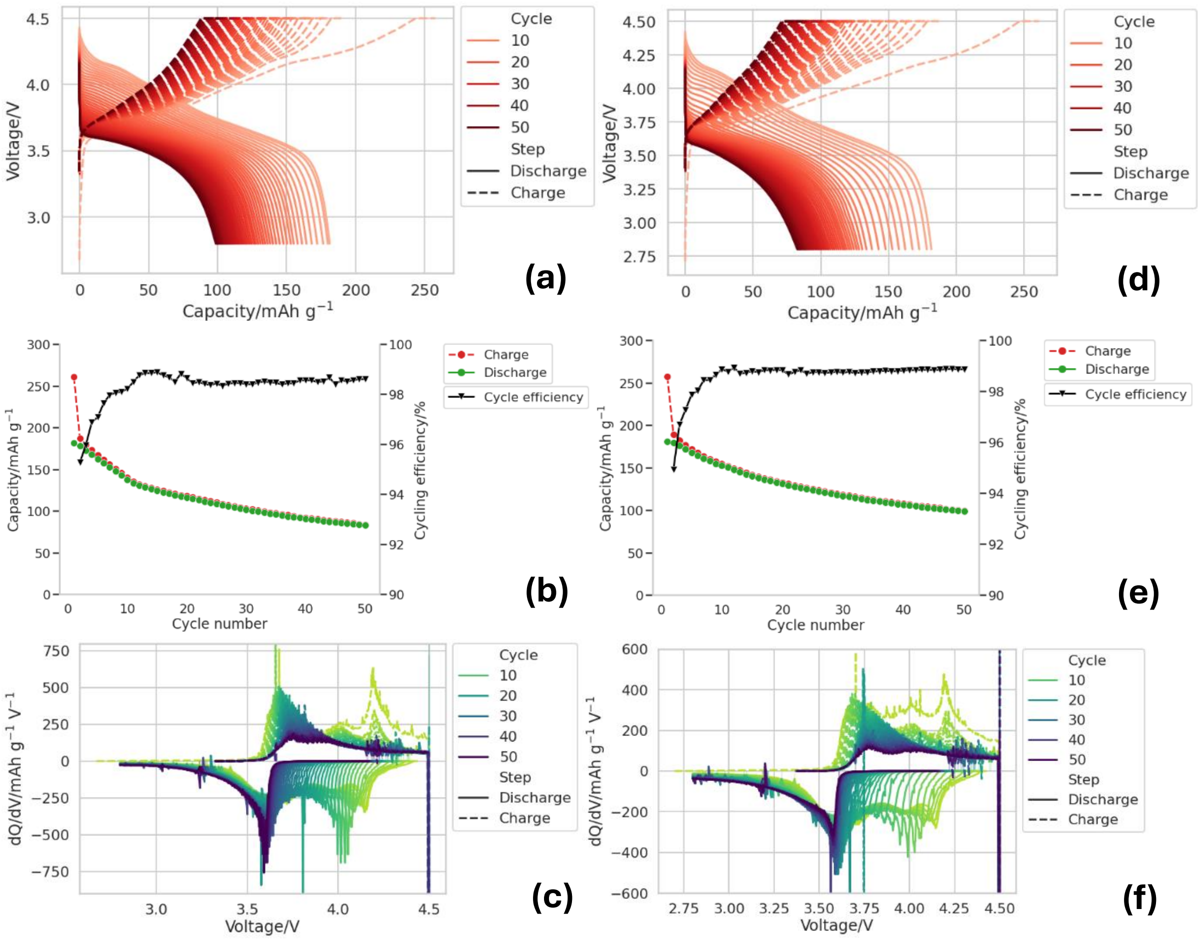
(a)
Voltage/V
4.5
4.0
3.5
3.0
Capacity/mAh g^{-1}
0
50
100
150
200
250
Cycle
10
20
30
40
50
Step
Discharge
Charge
(b)
Capacity/mAh g^{-1}
Cycling efficiency/%
Cycle number
Charge
Discharge
Cycle efficiency
300
250
200
150
100
50
0
100
98
96
94
92
90
10
20
30
40
50
(c)
dQ/dV/mAh g^{-1} V^{-1}
Voltage/V
750
500
250
0
−250
−500
−750
3.0
3.5
4.0
4.5
Cycle
10
20
30
40
50
Step
Discharge
Charge
(d)
Voltage/V
4.50
4.25
4.00
3.75
3.50
3.25
3.00
2.75
Capacity/mAh g^{-1}
0
50
100
150
200
250
Cycle
10
20
30
40
50
Step
Discharge
Charge
(e)
Capacity/mAh g^{-1}
Cycling efficiency/%
Cycle number
Charge
Discharge
Cycle efficiency
300
250
200
150
100
50
0
100
98
96
94
92
90
10
20
30
40
50
(f)
dQ/dV/mAh g^{-1} V^{-1}
Voltage/V
600
400
200
0
−200
−400
−600
2.75
3.00
3.25
3.50
3.75
4.00
4.25
4.50
Cycle
10
20
30
40
50
Step
Discharge
Charge

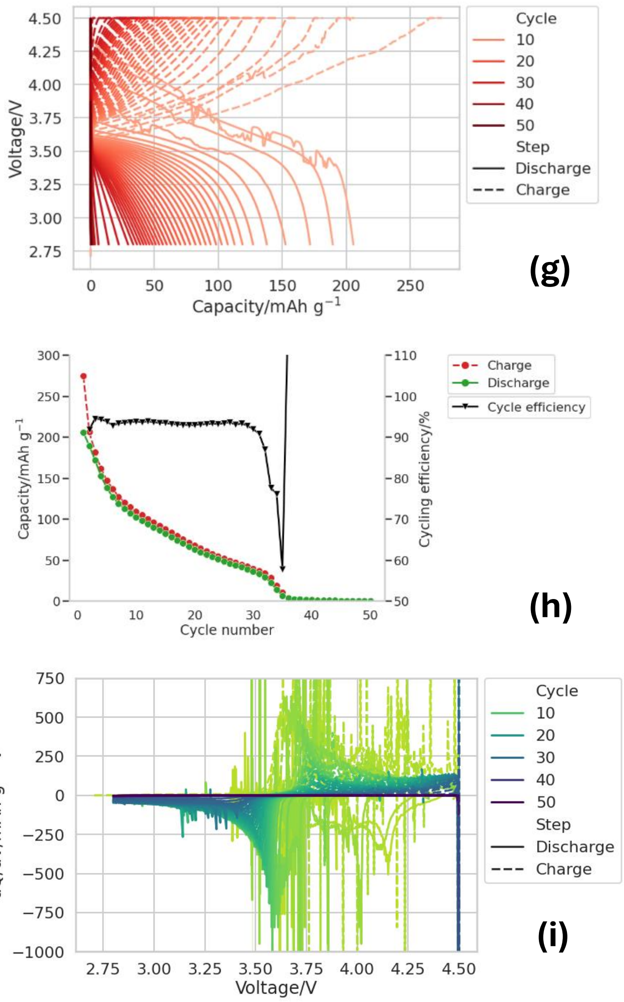

Figure 149 Charge-discharge cycling (a, d, g), Cycling efficiency and charge-discharge capacities (b, e , h), and Differential capacity vs. voltage curve (c, f, I), for Li-ion coin cells 1-3 with NMC811 – lithium sulfate cathodes synthesised with nitrates and of κ-carrageenan where x = 0.005 cycled between 4.5 and 2.8 V at 0.1 C for 50 cycles

5.3.1.4 Cell Data of κ-carrageenan biotemplated and nitrate precursor synthesised NMC811 – lithium sulfate cathodes where x = 0.005 cycled at 0.1 C between 4.2 V and 3.0 V

When a cell with the same cathode where x = 0.005 is cycled at 0.1 C between 4.2 V and 3V, the cell reaches an initial specific discharge capacity of 105 mAh/g during the first discharge cycle, Figure 150b. The cell also exhibits a capacity retention of 65 mAh/g over 50 cycles. This is compared to an initial specific discharge capacity of 180 mAh/g and capacity fade of 100 mAh/g over 50 cycles for same cathodes cycled to 4.5 V, Figure 149b, e. The reduction in specific discharge capacity and capacity retention is evidenced in the differential capacity curve, Figure 150c, where the H1 to M and M to H1 phase transitions occur at 3.75 V and 3.6 V during the initial charge and discharge cycles, respectively [142]. The phase changes M to H2 and H2 to H3 do not occur below 4.2 V with the cathode only undergoing the H1 to M phase change when cycling to 4.2 V resulting in the initial specific discharge capacity of 105 mAh/g. As the cathode structure deteriorates and voltage fade occurs, the H1 to M and M to H1 phase transitions occur at 4.2 V and 3.4 V during charging and discharging respectively after 50 cycles. While the cell does not experience cell failure, any further deterioration would result in the H1 to M phase occurring above 4.2 V and cell failure occurring. The synthesis of NMC811 using a small amount of lithium sulfate where x = 0.005 is observed to aid in capacity retention when cycled to 4.2 V however the lower initial specific discharge capacity when cycled, possibly due to the addition of the lithium sulfate, results in the cell cycling at too low a capacity to be viable when cycled at the lower voltage range.

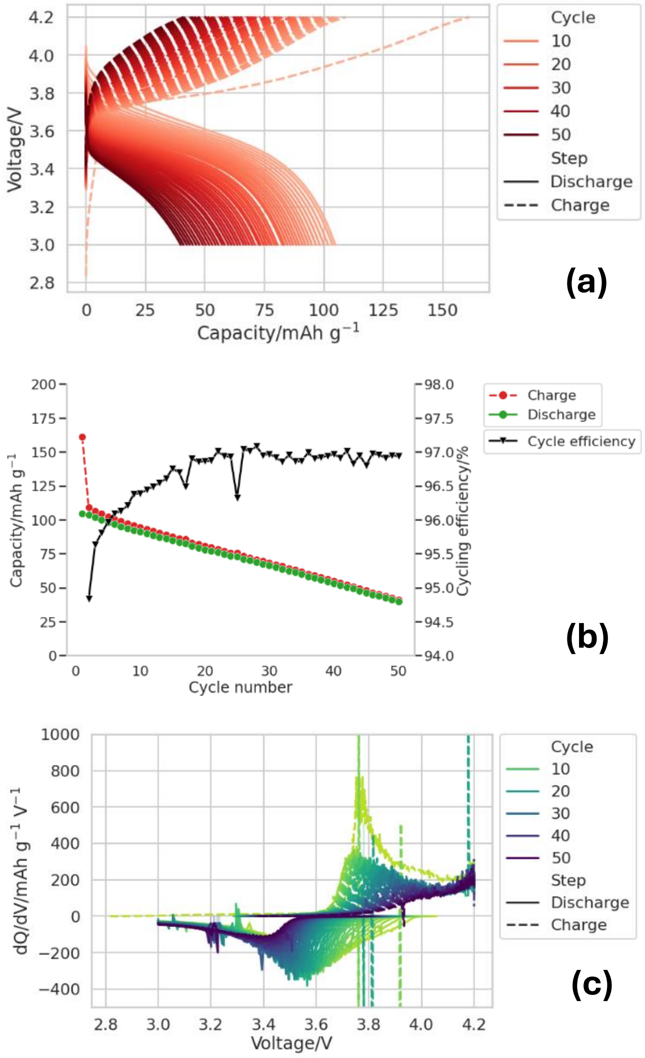

Figure 150 Charge-discharge cycling (a), Cycling efficiency and charge-discharge capacities (b), and Differential capacity vs. voltage curve (c), for Li-ion coin cell with NMC811 – lithium sulfate cathodes synthesised with nitrates and of κ-carrageenan where x = 0.005 cycled between 4.2 and 3.0 V at 0.1 C for 50 cycles

5.3.1.5 Further discussion of cell cycling data

Variety in the initial specific discharge capacities and cyclabilities of the cells may also in part be due to potential issues within the cell manufacturing process, 3.7.4. With the cells being manufactured relatively late in the project, oxidation of the lithium chips and degradation and potential uptake of water of the electrolyte due to long term storage were both issues. Oxidation of the lithium chips and damage that may have been caused by attempted removal of the oxidation could lead to a reduction in capacity as less lithium is present as well as poor cyclability as damage to the lithium chips affects its long term stability. Degradation of the electrolyte meanwhile may further reduce cyclability as a reduction of ionic diffusivity occurs. Poor mixing may also lead to poor capacity or cyclability as inhomogeneity leads to cathodes with too little ratio of NMC811, resulting in a lower capacity, or too low a ratio of additives, reducing cyclability. Poor mixing may also lead to a slurry which is either too thin or too thick, leading to an uneven drawdown. This may lead to poor calendaring or even over calendaring, which may damage the cathode and lead to further reductions in cyclability.

5.3.2 κ-carrageenan biotemplated NMC811– lithium sulfate cathodes when varying mass of κ-carrageenan using acetate precursors

5.3.2.1 X-Ray diffraction of κ-carrageenan biotemplated NMC811 – lithium sulfate cathodes when varying mass of κ-carrageenan using acetate precursors

As with previous work when using dextran and sodium alginate in chapter 3 the use of acetate precursors are investigated as a safer and cheaper alternative to using nitrates. Li^+ and Ni^{2+} cation mixing between Ni and Li sites are indicated to be similar between where $x = 0.005$, Figure 151a, and where $x = 0.05$, Figure 151b, with (003)/(104) peak intensity ratios of 1.45 and 1.51, respectively. As < 1.2 is reported to be a high level of mixing [130], this infers some but not a significantly large amount of cation mixing for both levels low and high ratios of biotemplating to metal precursors. layering of the NMC811 varies between different ratios of biotemplating to metal precursor, with where $x = 0.005$ exhibiting very good peak splitting and so good layering at peaks (006)/(012) and (018)/(110) [129] and where $x = 0.05$ showing poor peaking splitting and worse layering of the NMC811 structure. Peaks at 22, 29 and 35 ° when using a high ratio of κ-carrageenan to metal precursor indicate the presence of a secondary lithium sulfate phase. These peaks do not appear where $x = 0.005$, with the amount of lithium sulfate present being low enough such that it is not able to de detected under XRD.

While similar levels of cation mixing occur using different low and high masses of biotemplate, layering of the NMC811 is observed to decrease as the ratio of κ-carrageenan to precursors is increased. The higher mass of the biotemplate and acetate precursors used the greater the amount of carbon content released upon decomposition of the biotemplate and precursors. This carbon reacts with the oxygen atmosphere to form CO_2 and results in a reducing atmosphere as oxygen is used up in the reaction, which leads less oxygen being available for the synthesis of NMC811 and less oxygen sites being filled, leading to a reduction in the layering and structural organisation of the NMC811 [133]. Due to the use of a higher mass of biotemplate leading to a decrease of the layering of the NMC811 occurring when $x = 0.05$, the required higher ratio of biotemplate to metal precursors to synthesise lithium sulfate when using acetates will result in decreased organisation of the NMC811.

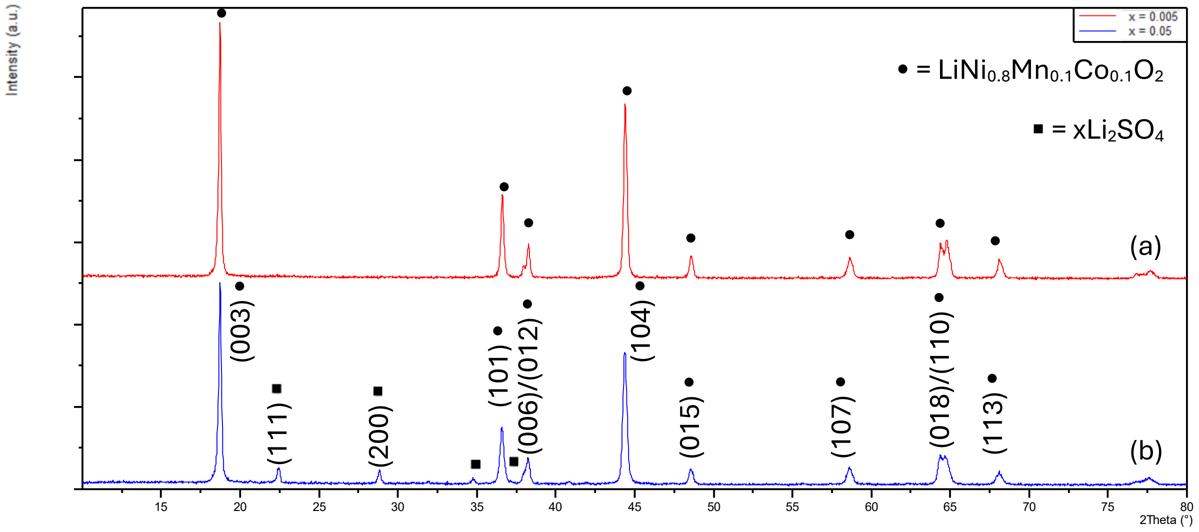

Figure 151 XRD showing $LiNi_{0.8}Mn_{0.1}Co_{0.1}O_2.xLi_2SO_4$ preheated at 300 °C in air and calcined 850 °C, using acetate precursors and a) $x = 0.005$ and b) $x = 0.05$ κ-carrageenan biotemplating

5.3.2.2 *Morphology of κ-carrageenan biotemplated NMC811 – lithium sulfate cathodes when varying mass of κ-carrageenan using acetate precursors*

When examined using SEM differences in the particle morphology are exhibited as a result of the ratio of κ-carrageenan to acetate precursors being increased. The lower mass of biotemplate used such that x = 0.005, Figure 152a, results in the synthesis of particles with a mix of irregular, rounded morphologies and octahedral morphologies with an average particles diameter of 250 nm. The lower mass of biotemplate results in the synthesis of a larger proportion of the smaller, irregular morphologies due to a lack of chelation sites resulting in fewer metal ions chelating to the biotemplate. This relative lack of chelation sites results in less morphological control of particles but still results in the small proportion of octahedral morphologies being formed as a result of morphological control as a result of metal cations chelating on the low number of chelation sites.

A larger ratio of biotemplate to precursor salts where x = 0.05, Figure 152b, results in individual primary particles ranging from smaller round particles with average particle diameters of 400 nm, to larger octahedral particles with average particle diameters of 1000 nm. The synthesis of octahedral morphologies is due to sufficient chelation sites for substitution of metal ions due to the larger mass of biotemplate used which also results in little-to-no agglomeration, while the presence of the smaller rounded particles suggests there are still metal ions which do not undergo chelation. The increase in particle diameter when compared to where x = 0.005 is possibly due to the emission of a significant amount of heat during the exothermic oxidation reaction of NMC hydroxide to disorganised NMC oxide that is observed to occur when synthesising NMC811 when using acetates, section 3.4.2.1.1. Such an increase in heat during the reaction provides greater energy allowing for the greater and faster growth of particles. Such an increase in particle size may be detrimental to cell specific capacity due to a decrease in surface area and associated lithiation sites.

When analysed using EDAX using a 20 keV potential difference the higher ratio of κ-carrageenan to acetate precursors where x = 0.05, Figure 153b (EDAX of Figure 152b), peaks between 2 and 4 keV are present indicating that sulfur is present within the cathode power. Such peaks are not present where x = 0.005, Figure 153a (EDAX of Figure 152a), with any sulfur present being of too low a mass to be detected under EDAX. When using acetates however, nickel peaks are present between 0 and 2 keV when using both masses of biotemplate, as well as oxygen and carbon peaks at ~ 0 keV. As such, when using either ratio of κ-carrageenan to acetates the presence of a secondary nitrate phase and carbon containing phase is observed, something that is not seen in the XRD. Any carbon present is likely a result of the high carbon content of the biotemplate and acetate precursors and results in the synthesis of a reducing atmosphere as the oxygen atmosphere reacts with carbon released from the decomposition of the biotemplate and precursors. The reaction of oxygen to form CO_2 results in less oxygen available for the synthesis of NMC811 and to fill oxygen sites, resulting in poorer layering and decreased organisation of the NMC811 structure [133]. Such carbon however may also be a result of the EDAX detecting carbon from the carbon sticky tab on which the powder is placed. Any secondary nickel phase present may inhabit the same values of 2Θ as NMC811 when analysed under XRD making it undetectable, however the presence of nickel under EDAX further infers poor layering and inhomogeneity in the cathode powder. This reinforces poor layering of the sample observed using XRD and further shows previous issues with structural disorganisation exhibited with biotemplating with acetates.

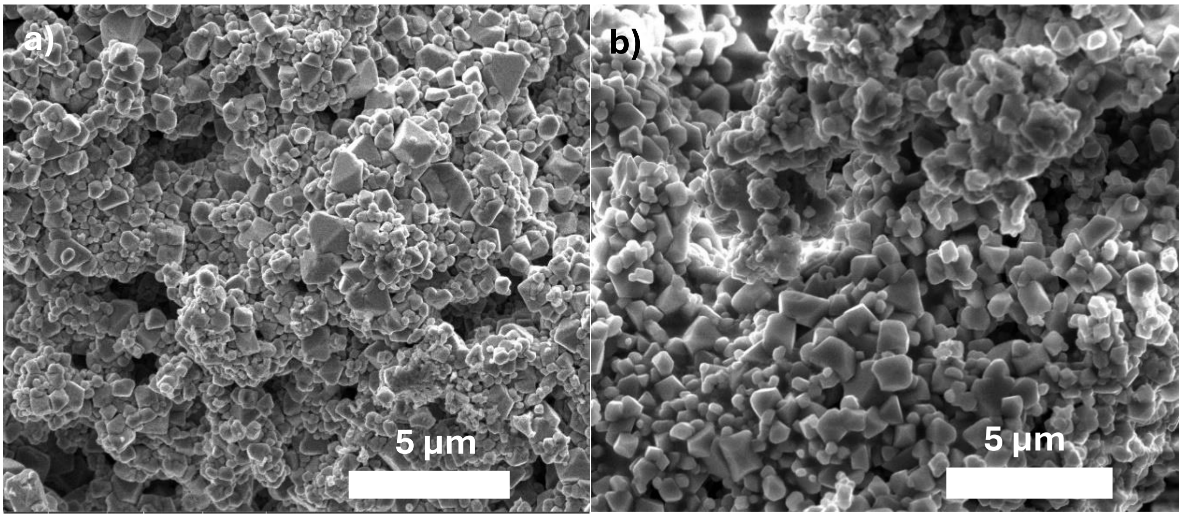

Figure 152 SEM showing $LiNi_{0.8}Mn_{0.1}Co_{0.1}O_2.xLi_2SO_4$ preheated at 300 °C in air and calcined 850 °C, using acetate precursors and a) x = 0.005 and b) x = 0.05 κ-carrageenan biotemplating

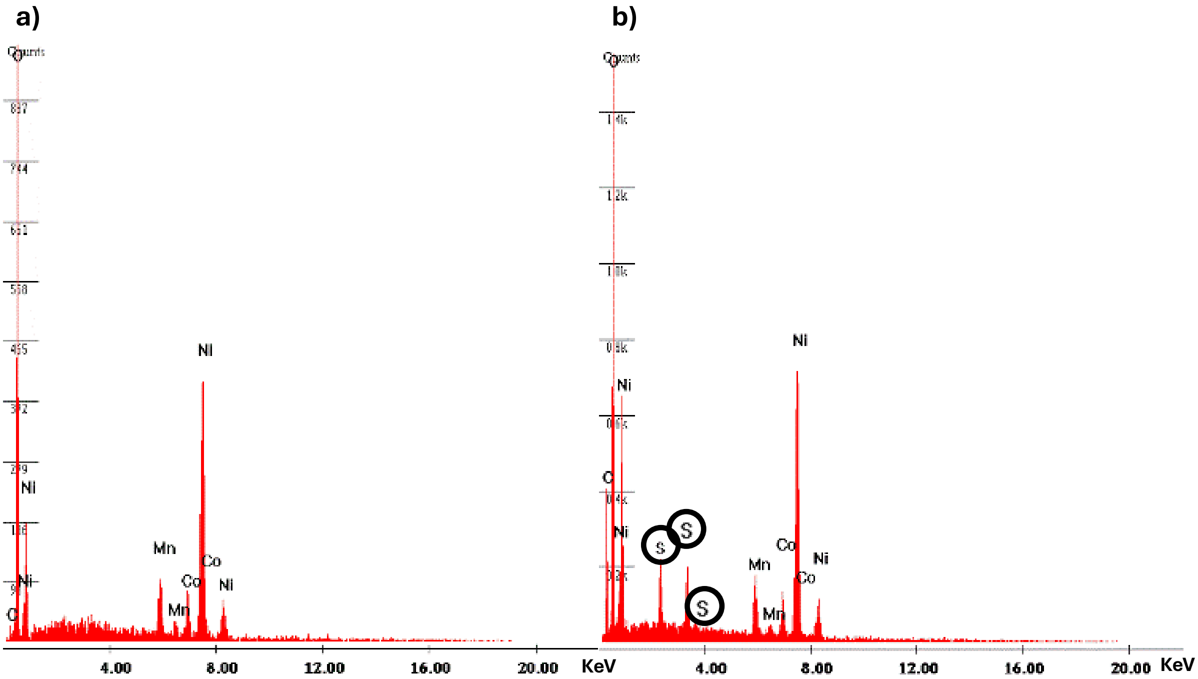

Figure 153 EDAX of $LiNi_{0.8}Mn_{0.1}Co_{0.1}O_2.xLi_2SO_4$ preheated at 300 °C in air and calcined 850 °C, using acetate precursors and a) x = 0.005 (Figure 152a) and b) x = 0.05 (Figure 152b) κ-carrageenan biotemplating

Morphology has been observed to vary using the same ratio of κ-carrageenan to acetate precursors where x = 0.05 and synthesis conditions. Despite attempts to synthesise NMC811 – lithium sulfate cathodes under the same parameters, microwire morphologies with cross-sectional diameters of between 200 and 300 nm and lengths greater than 3000 nm, Figure 154a, and octahedral primary of average particle diameter 1000 nm, Figure 154b, and were observed across two different samples, with both morphologies being observed across the entire area of the SEM stub. While octahedral morphologies have been reproduced using all biotemplates, microwire morphologies were not able to be reproduced. It is hypothesised that may be due to molten intermediate phases being formed when synthesising microwire morphologies that were not present when synthesising octahedral particles, with such phases not being able to be reproduced.

Using EDAX further differences in the elemental makeup between the particle morphologies are seen. Where both microwire and octahedral morphologies are synthesised using the same biotemplate to precursor ratio a lower intensity oxygen peak and no carbon or nickel peaks are present between 0 and 1 KeV when synthesising microwires, Figure 155a, with carbon and nickel peaks and a higher intensity oxygen peak between 0 and 1 KeV being present when synthesising octahedral morphologies, Figure 155b. Detection of carbon may be a result of the detection of the carbon sticky tab, however. Despite this it is apparent from EDAX that there is a difference in the makeup of the two morphologies.

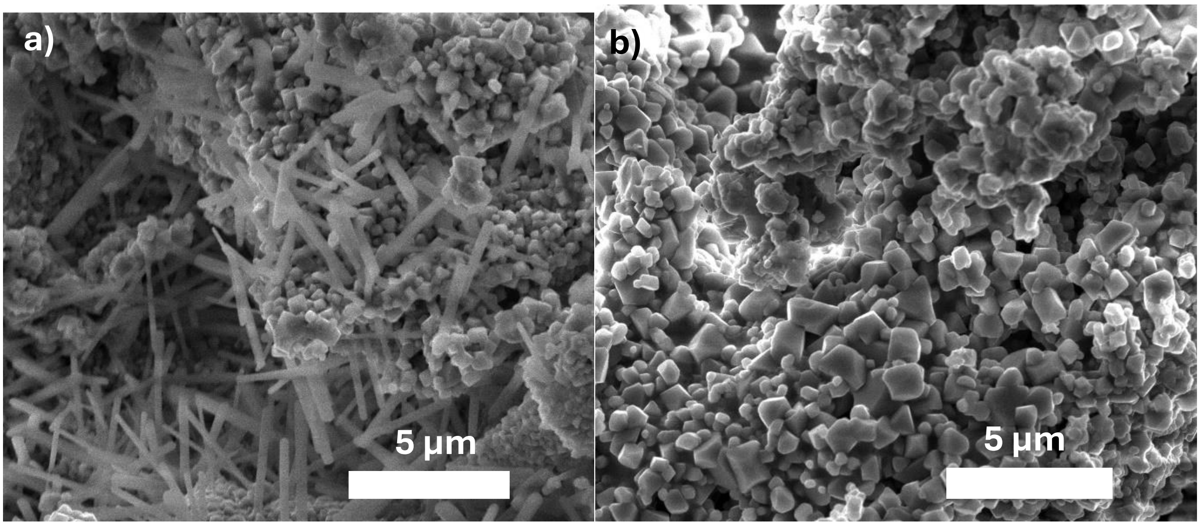

Figure 154 SEM showing $LiNi_{0.8}Mn_{0.1}Co_{0.1}O_2.xLi_2SO_4$ preheated at 300 °C in air and calcined 850 °C, using acetate precursors and κ-carrageenan where x = 0.05 forming a) microwire morphologies and b) octahedral morphologies

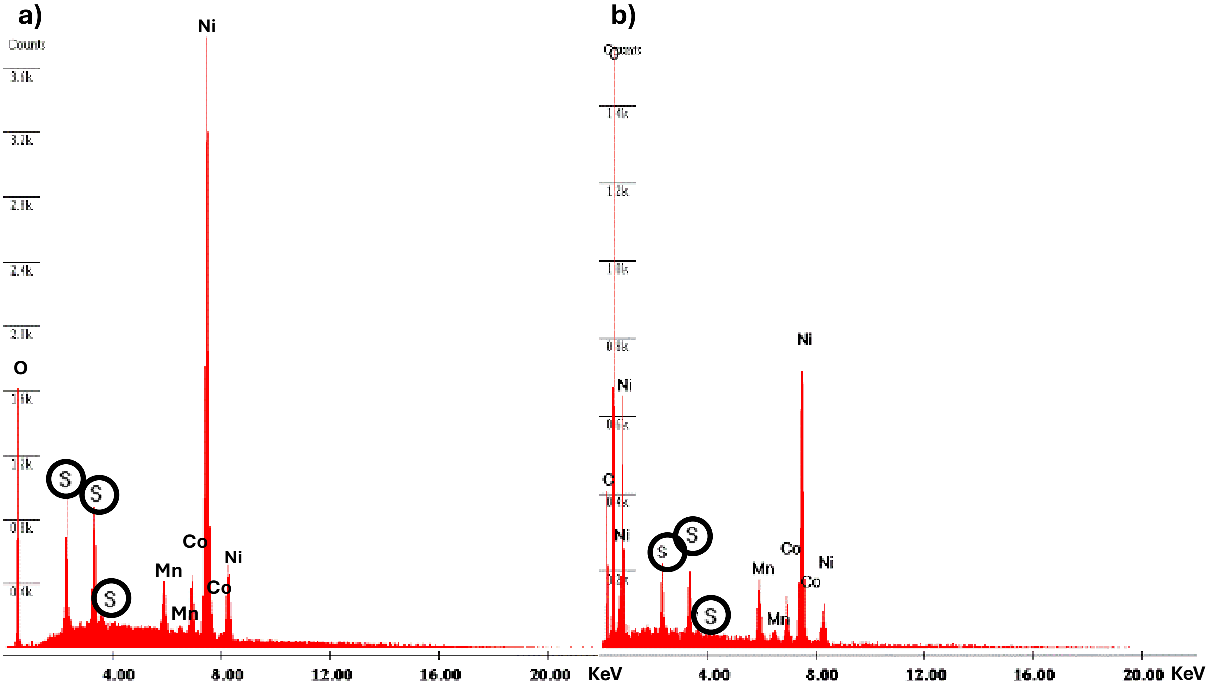

Figure 155 EDAX showing $LiNi_{0.8}Mn_{0.1}Co_{0.1}O_2.xLi_2SO_4$ preheated at 300 °C in air and calcined 850 °C, using acetate precursors and κ-carrageenan where x = 0.05 forming a) microwire (Figure 154a) and b) octahedral (Figure 154b) morphologies

XRD undertaken on the two different samples examined shows further evidence of the difference in makeup between the two particle morphologies. While poor peak splitting at (006)/(012) and (018)/(110) indicates poor layering of the NMC811 structure [129] for both microwire, Figure 156a, and octahedral morphologies, Figure 156b. (003)/(104) peak intensity ratios of 1.11 and 1.51 for microwire and octahedral morphology consisting samples indicate high and low mixing of Li^+ and Ni^{2+} cations between Ni and Li sites, respectively (where < 1.2 is representative of poor mixing [130]). As such peaks observed where the morphology is microwire shaped indicates greater disorganisation and mixing of the NMC811 than when particles are octahedral shaped.

Furthermore, different secondary phases are present for the different synthesised morphologies, with peaks at 22, 23, 30, 31, and 32 ° highlighting a different secondary phase, lithium carbonate, for the microwire particles and peaks at 22, 28, and 35 ° indicating lithium sulfate when particle morphology is octahedral. This different secondary phase may be the reason for the synthesis of microwire morphologies, with microwires being formed from the solid substrate of a solid NMC intermediate phase and the secondary lithium carbonate phase in a molten state. Further work is however required to see if such a method is reproducible.

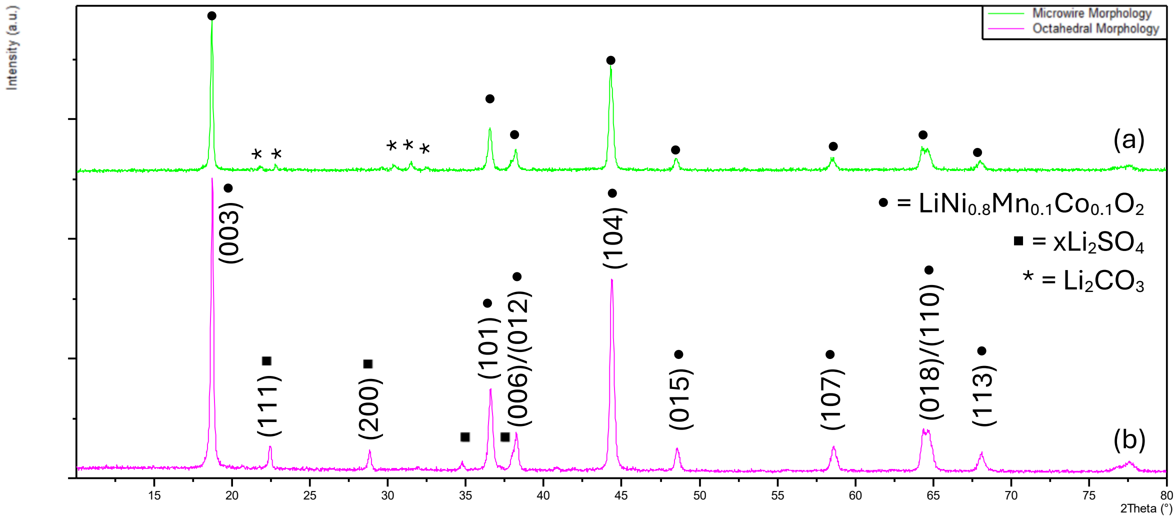

Figure 156 XRD showing $LiNi_{0.8}Mn_{0.1}Co_{0.1}O_2.xLi_2SO_4$ preheated at 300 °C in air and calcined 850 °C, using acetate precursors and κ-carrageenan where x = 0.05 forming a) microwire and b) octahedral morphologies

5.3.2.3 Cell Data of κ-carrageenan biotemplated and acetate precursor synthesised NMC811 – lithium sulfate cathodes where x = 0.05 cycled at 0.1 C between 4.5 V and 2.8 V

Cycling data for cells consisting of NMC811 cathodes synthesised with a high ratio of κ-carrageenan to acetate precursors where x = 0.05 show poor cycling capabilities. Use of the higher ratio of biotemplate to precursor results in initial specific discharge capacities of between 130 and 160 mAh/g, Figure 157b, e, h, with capacity fade resulting in a near complete drop off in specific discharge capacity over 50 cycles culminating in cell failure when cycled between 4.5 and 2.8 V at 0.1 C.

Using differential capacity curves, Figure 157b, e, h, it is observed that during the initial charge cycle the H1 to M phase transition occurs at 3.8 V and the M to H2 phase transition occurs at 4.3 V [142]. The H2 to H3 phase change does not occur below 4.5 V and accounts for the lower initial specific discharge capacity. During the initial discharge cycle H2 to M and M to H1 phase transitions occur at 4.2 V and 3.7 V respectively. Due to structural deterioration of the cathode in part caused by the cell being cycled above 4.2 V [140] voltage fade results in the H1 to M to M to H2 phase transitions occurring above 4.5 V, resulting in cell failure.

Poor layering of the NMC811, Figure 151b, and the high mass of lithium sulfate secondary phase negatively effects cell performance, with there being little evidence that the presence of lithium sulfate improves structural stability and reduces capacity fade when using acetate precursors and a high ratio of κ-carrageenan to precursors.

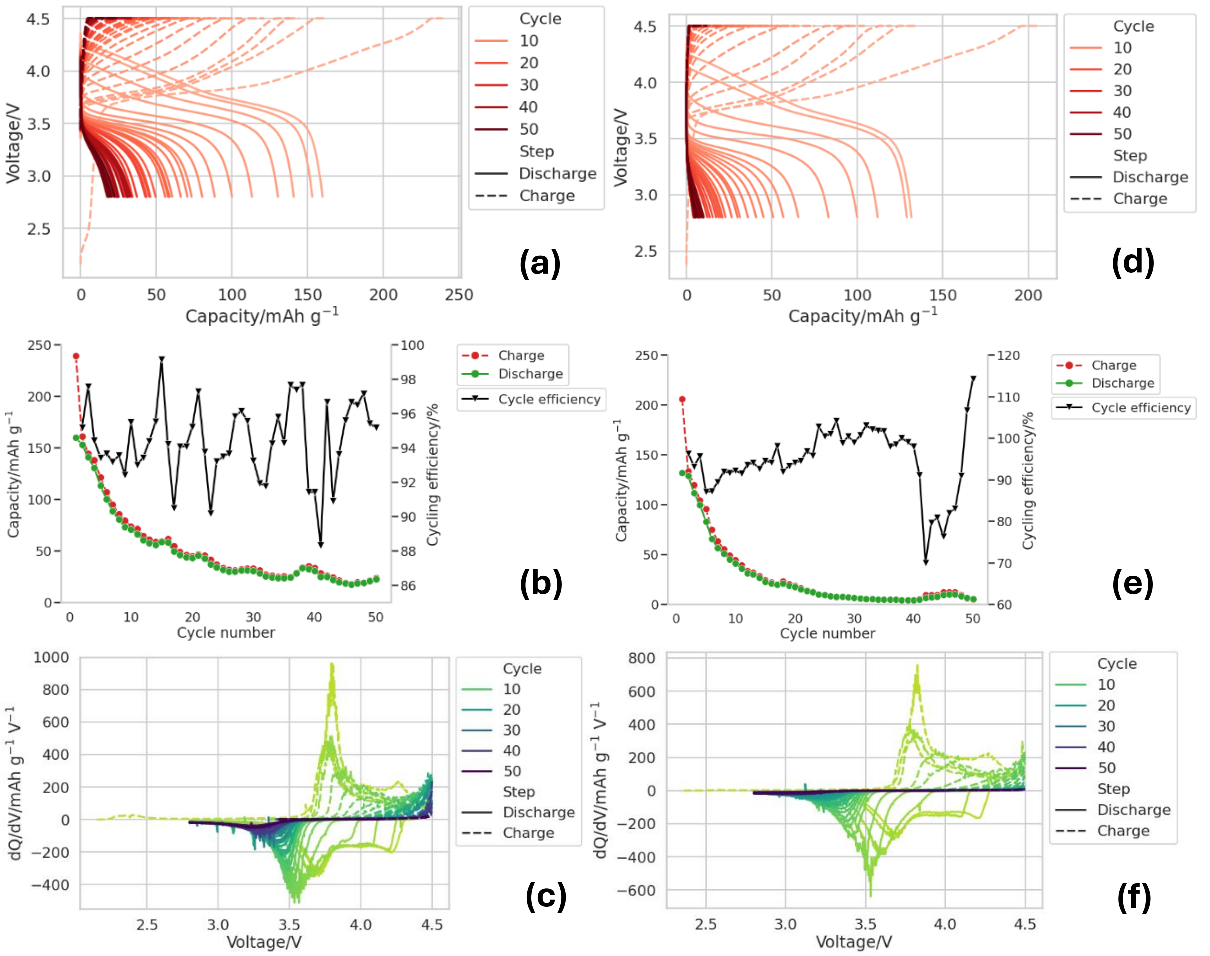
(a)
Voltage/V
Capacity/mAh g^{-1}
Cycle
10
20
30
40
50
Step
Discharge
Charge
(b)
Capacity/mAh g^{-1}
Cycling efficiency/%
Cycle number
Charge
Discharge
Cycle efficiency
(c)
dQ/dV/mAh g^{-1} V^{-1}
Voltage/V
(d)
(e)
(f)

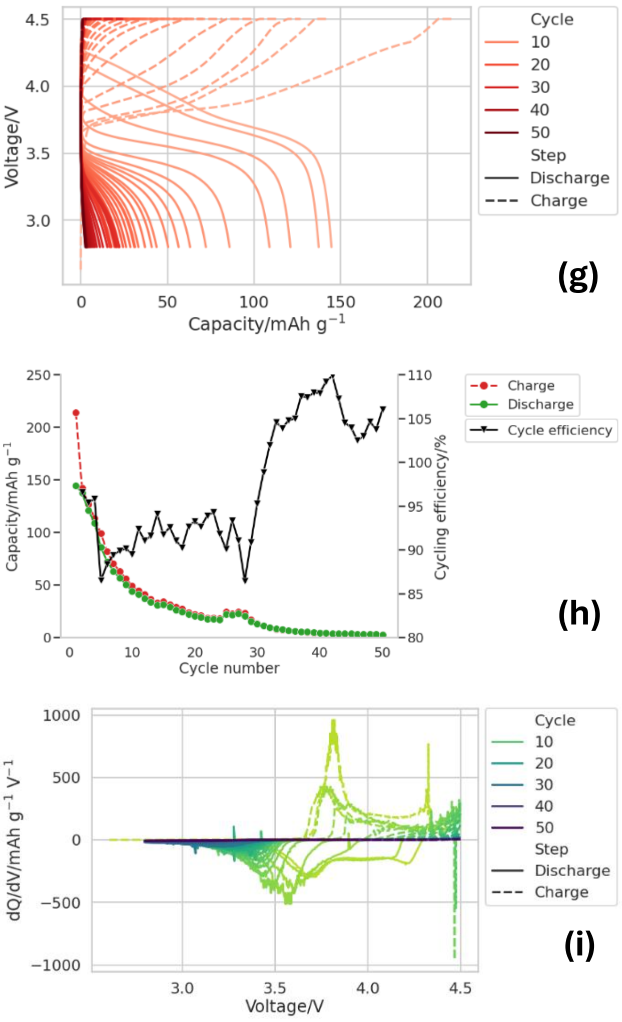

Figure 157 Charge-discharge cycling (a, d, g), Cycling efficiency and charge-discharge capacities (b, e , h), and Differential capacity vs. voltage curve (c, f, I), for Li-ion coin cells 1-3 with NMC811 – lithium sulfate cathodes synthesised with acetates and of κ-carrageenan where x = 0.05 cycled between 4.5 and 2.8 V at 0.1 C for 50 cycles

5.3.2.4 Cell Data of κ-carrageenan biotemplated and acetate precursor synthesised NMC811 – lithium sulfate cathodes where x = 0.005 cycled at 0.1 C between 4.5 V and 2.8 V

A slight increase in cell performance is observed when cells consisting of cathodes synthesised with a low ratio of biotemplate to precursors are cycled between 4.5 and 2.8 V at 0.1 C, relative to cells with a high ratio of κ-carrageenan to acetate precursors. Initial specific discharge capacity varies between 180 and 205 mAh/g, Figure 158b, e, a roughly 50 mAh/g increase from when using a high ratio of biotemplate to precursors Figure 157b, e, h. however cell failure due to significant capacity fade is still present after 50 cycles. Differential capacity curves, Figure 158c, f, indicate phase transitions during the initial charge cycle of H1 to M at 3.75 V, M to H2 at 4.2 V, and H2 to H3 at 4.5 V [142]. The presence of the H2 to H3 phase change is why the cell is able to cycle to 200 mAh/g during the initial discharge cycle. During the initial discharge cycle, H3 to H2, H2 to M, and M to H1 phase transitions occur at 4.5V, 4.15 V, and 3.55 V. Due to poor layering of the NMC811, Figure 151b, and cycling above 4.2 V [140] significant voltage fade occurs whereby the 50th cycle the H1 to M phase transition can only occur above 4.5 V. With no available phase transitions for the cathode to undergo the cell fails.

An increase in initial discharge capacity vs. cathodes synthesised with a high mass of biotemplate indicates greater surface area for lithium intercalation when using a low mass of biotemplate, but neither amount of lithium sulfate is observed to be beneficial in improving cathode stability or reducing capacity fade. When cycling between 4.5 and 2.8 V initial evidence suggests acetate synthesised NMC811 – lithium sulfate cathodes are less viable than when using nitrate synthesised NMC811 – lithium sulfate cathodes, Figure 149.

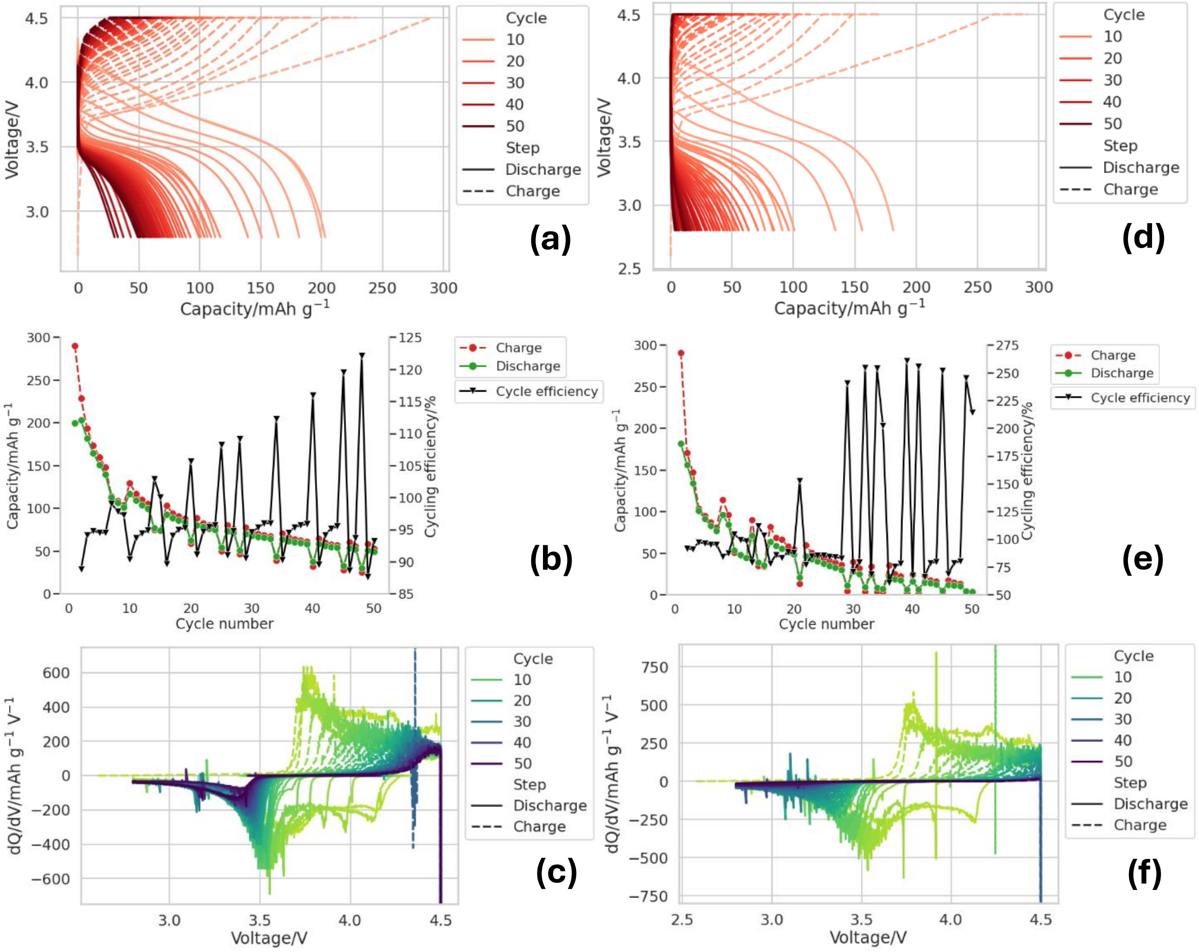

Figure 158 Charge-discharge cycling (a, d), Cycling efficiency and charge-discharge capacities (b, e), and Differential capacity vs. voltage curve (c, f), for Li-ion coin cells 1-2 with NMC811 – lithium sulfate cathodes synthesised with acetates and of κ-carrageenan where x = 0.005 cycled between 4.5 and 2.8 V at 0.1 C for 50 cycles

5.3.2.5 Cell Data of κ-carrageenan biotemplated and acetate precursor synthesised NMC811 – lithium sulfate cathodes where x = 0.005 cycled at 0.1 C between 4.2 V and 3.0 V

When cells with the same cathodes synthesised with a ratio of biotemplate to acetate precursors are cycled between 4.2 and 3 V at 0.1 C, cell performance can be seen to improve vs. when cycled between 4.5 and 2.8 V. While initial specific discharge capacity is significantly lower than when cycling between 4.5 and 2.8 V, between 90 and 150 mAh/g, Figure 159b, e, capacity retention is significantly better at between 40 and 70 mAh/g over 50 cycles. The lower initial specific discharge capacity is due to the lower upper cycling voltage, with the cathode only undergoing the H1 to M phase change. Evidenced by the differential capacity curves, Figure 159c, f, there is no evidence of either the M to H2 or H2 to H3 phase transitions occurring below 4.2 V. The H1 to M phase change occurs during the initial discharge cycle at 3.75 V, while during the initial discharge cycle the M to H1 phase occurs at 3.7 V [142]. There is also less voltage fade than when the cell is cycled to 4.5 V, Figure 158c, f, with the H1 to M phase transition occurring at 3.9 V during charging and the M to H1 phase transition occurring at 3.5 V during discharge after 50 cycles.

The greater layering of the NMC811, Figure 151a, as well as the cathode not being cycled above 4.2 V [140] results in less structural degradation and capacity fade. Structural stability may also be due to the stability produced by a low proportion of lithium sulfate secondary phase. While not detected with XRD, such a secondary phase as a result of the low ratio of biotemplate to precursors may reduce the ability of the structure to rearrange during delithiation. While capacity retention is improved when cycling between 4.2 and 3 V, evidence still shows that the benefits of lithium sulfate are most prominent when synthesis NMC811 cathodes with nitrates as opposed to acetates.

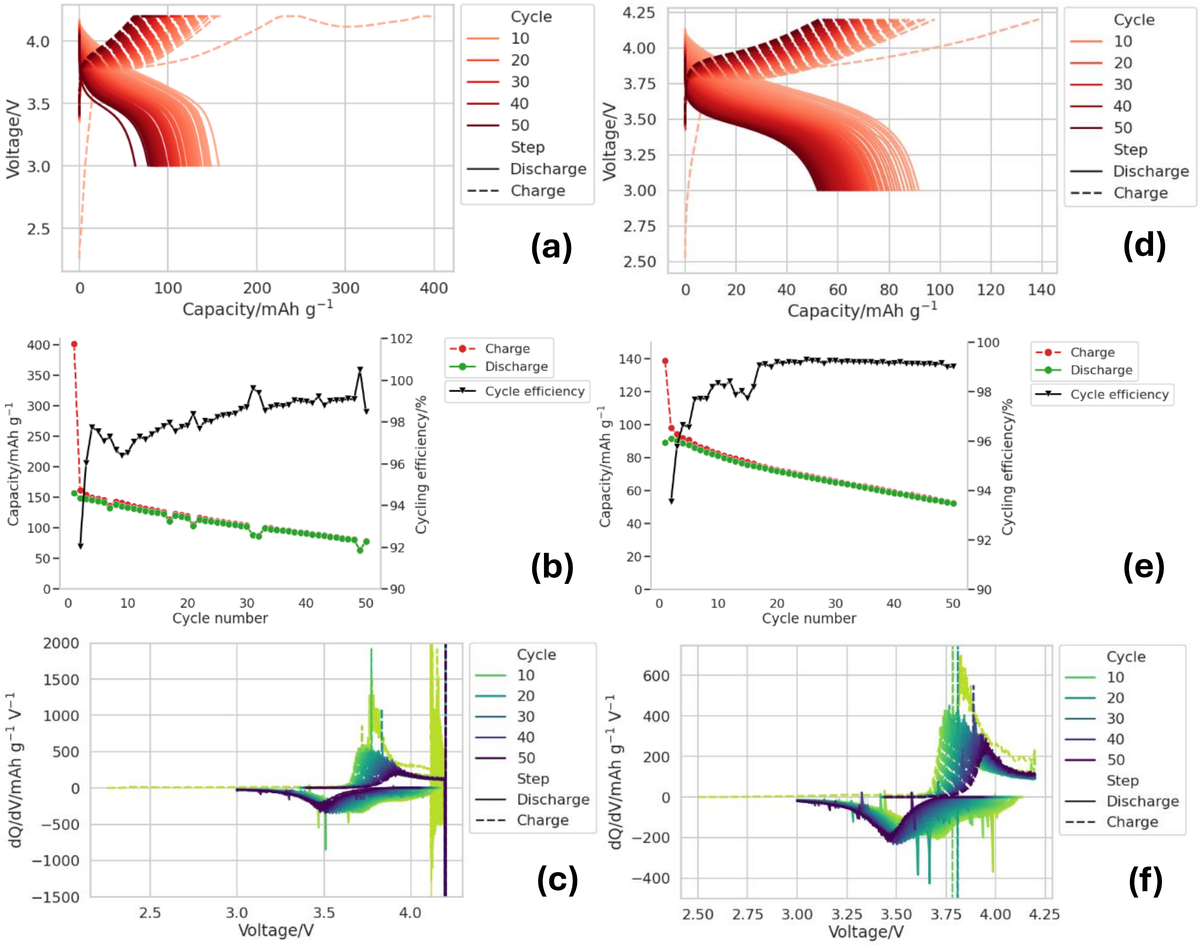

Figure 159 Charge-discharge cycling (a, d), Cycling efficiency and charge-discharge capacities (b, e), and Differential capacity vs. voltage curve (c, f), for Li-ion coin cells 1-2 with NMC811 – lithium sulfate cathodes synthesised with acetates and of κ-carrageenan where x = 0.05 cycled between 4.2 and 3.0 V at 0.1 C for 50 cycles

5.3.2.6 Further discussion of cell cycling data

Poor cyclability of some cells and poor initial specific discharge capacity of other cells may also be in part as a result of problems within the cell manufacturing process, 3.7.4. Poor cyclability may be in part explained by degradation and potential uptake of water in the electrolyte caused by long term storage, with this leading to reduced ionic diffusivity. Poor cyclability may also be caused by attempts to remove oxidation from lithium chips stored for long periods, with attempts to remove the oxidation potentially leading to damage and reducing the stability of the lithium chip during cycling. Any remaining oxidation may however lead to reductions in cell capacity as reduced amounts of lithium are available during cycling. Further reductions in cyclability may be caused by inhomogeneity of the cathode slurry due to poor mixing, as a lower ratio of additives leads to greater instability and cyclability. Comparatively, a lower ratio of

NMC811 caused by the inhomogeneity may lead to a reduction in cell capacity. Poor mixing may also lead to a slurry which is too thin or too thick, leading to a poor drawdown and poor calendaring. Should this lead to over calendaring, the cathodes may be damaged which may result in poor cyclability and potential cell failure.

5.4 Synthesis of sulfur-containing NMC811 using sulfate precursors and sodium alginate biotemplating

As well as synthesis of NMC811 - lithium sulfate cathodes by using κ-carrageenan, synthesis may also be achieved by varying the metal precursor salts used. It is investigated as to whether acetate or nitrate precursors may be substituted for sulfate precursors. By doing this, the sulfate functional group may be used to synthesise the NMC811 in the same way carbon in the acetate precursors affects synthesis of NMC811, where the decomposition of the acetate precursors frees up carbon which reacts with the oxygen atmosphere to form CO_2 and carbonate secondary phases. When using sulfates sodium alginate is selected as the biotemplate due to its similarity to κ-carrageenan and the ease of biotemplating when using it. Stated masses of sulfate reactants and the biotemplate, Table 29, are preheated and calcined at 300 in air and 850 °C under oxygen. As such the only difference when synthesising using sulfate precursors is the type of precursor salt used with all other variables kept consistent with previous sodium alginate biotemplating.

Reactant	Mass /Volume
Lithium Sulfate monohydrate (g)	0.3199
Nickel Sulfate heptahydrate (g)	0.5257
Manganese Sulfate hydrate (g)	0.0423
Cobalt Sulfate heptahydrate (g)	0.0703
Sodium Alginate (g)	0.1

Table 29 Reactant masses for synthesising NMC811 using sulfate precursors and sodium alginate

5.4.1 X-Ray Diffraction of sulfur-containing NMC811 using sulfate precursors and sodium alginate biotemplating

Following calcination XRD was performed, Figure 160, with NMC811 was not able to be synthesised using sulfate precursors under similar synthesis conditions to those using acetate or nitrate precursors. Peaks indicate a highly disorganised NMC structure of which is not able to be confirmed as having a stoichiometric ratio of 10:8:1:1 of Li, Ni, Mn, and Co cations due to the presence of multiple secondary phases. As the temperature during preheat or during calcination does not exceed 1000 °C there is no such evidence sulfur dioxide gas is formed [144]. By comparison there is evidence that CO_2 is synthesised at around 212 °C, due to the decomposition of sodium alginate [123] and the resulting reaction between the released carbon and oxygen atmosphere indicated by a large expansion of gas during calcination at this temperature. As such whereas carbon is reacted away in the form of CO_2, sulfur is not reacted off as a gas and so is present in the crucible during the whole calcination process. Significant disorder in the NMC structure occurs due to metal ions reacting with the sulfate function groups, resulting in a high proportion of sulfur secondary phases and leaving fewer metal ions available for the synthesis of NMC811.

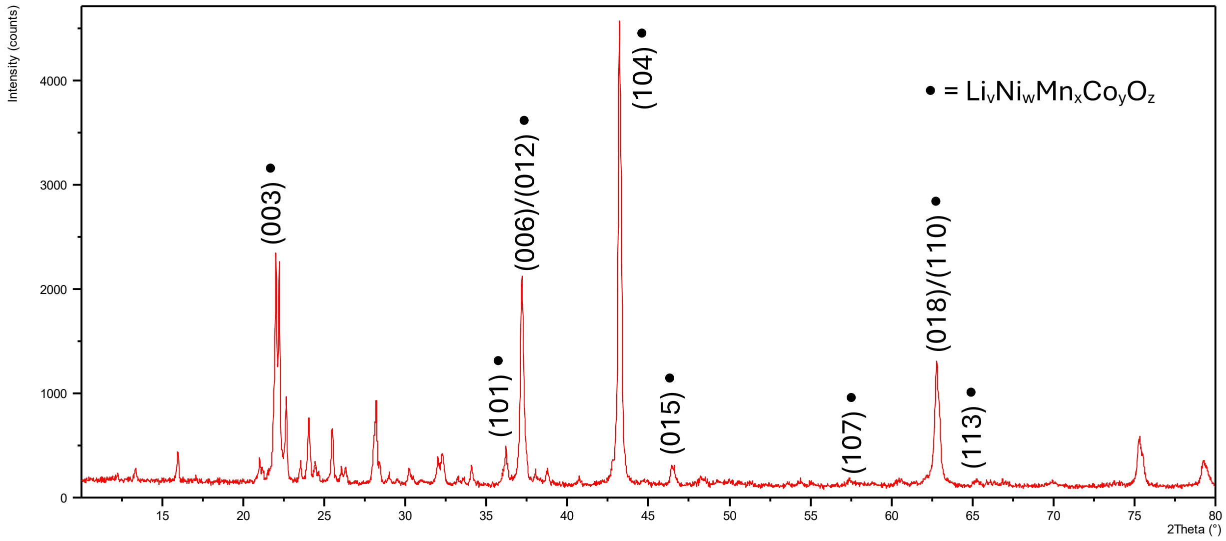

Figure 160 XRD showing NMC811 synthesised using sulfate precursors and sodium alginate biotemplating preheated at 300 °C in air and calcined in oxygen at 850 °C

5.4.2 Morphology of sulfur-containing NMC811 using sulfate precursors and sodium alginate biotemplating

The morphology present when examined under SEM, Figure 161, exhibits significant agglomeration of primary particles. Whereas NMC811 successfully synthesised using sodium alginate and either acetate or nitrates precursors may exhibit agglomerated primary particles often with round or octahedral morphologies, when calcined using sulfate precursors high levels of agglomeration are present with no defined primary particle morphologies. There is little evidence of non-agglomerated primary particles and little proof of morphological control exhibited during the reaction, with no distinctly shaped particles present. While chelation of metal ions to biotemplate may have taken place there is little evidence the sample benefitted from the biotemplating method, with recrystallisation of metal cations due to a lack of chelation or metal cations reacting with the large proportion of sulfur present during synthesis being possible. As such use of sulfate precursors has not benefitted the synthesis of morphologically controlled NMC811.

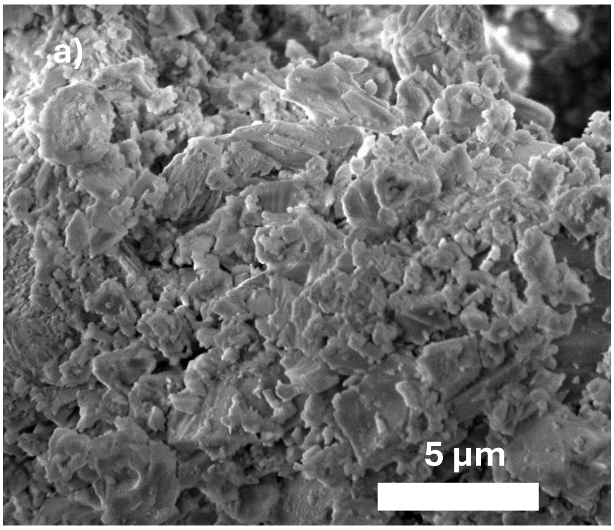

Figure 161 SEM showing NMC811 synthesised using sulfate precursors and sodium alginate biotemplating, preheated at 300 °C in air and calcined in oxygen at 850 °C

5.5 Discussion of synthesis and morphological control of NMC811 – lithium sulfate cathodes using sulfur-based κ-carrageenan

As with dextran and sodium alginate, NMC811 can be synthesised with the biotemplating method by using κ-carrageenan as a biotemplate provided correct calcination temperatures and biotemplate mass relative to precursor masses are used. When the mass of κ-carrageenan relative to the precursor mass is varied, the biotemplate may also be used to introduce sulfur into the NMC811 cathode as a secondar phase similarly to how sodium alginate was investigated to introduce sodium secondary phases.

By using a low mass of biotemplate relative to precursors, NMC811 with a secondary lithium sulfate phase may be synthesised with nanoscale non-agglomerated primary particles. When used in a lithium-ion coin cell NMC811 – lithium sulfate cathodes gives improved cycling stability vs. some dextran or sodium alginate biotemplated NMC811 cathodes while not sacrificing discharge capacity. When increased ratios of κ-carrageenan to precursor salts are used, larger masses of lithium sulfate leads to greater disorganisation of the NMC811 as well as more particle agglomeration, with the increased amount of lithium sulfate not improving structural stability leading to poor capacity retention, specific discharge capacity, and ultimately cell failure.

When particle size is analysed it is observed that when synthesis is done using acetate precursors with a low mass of biotemplate the average particle diameter is half that of particles synthesised using nitrate precursors, and also smaller than those synthesised using acetate precursors and a high mass of biotemplate,

Table 30. The low mass of acetates introduces a low amount of carbon into the reaction, resulting in a smaller exothermic reaction as CO_2 is formed from carbon from the breakdown of the precursor and biotemplate and the oxygen atmosphere. This results in a low amount of heat introduced into the reaction and a low amount of energy available for particles to grow. When paired with the low amount of sulfur introduced by the low mass of biotemplate, which forms a secondary phase and is likely not being formed into the NMC811 particles, this results in smaller particles. When using nitrate precursors there is no noticeable difference in average size when using either a low or high mass of biotemplate, with one possible reason being the

sulfur from the biotemplate forming a secondary phase and so not affecting the particle size of the NMC811.

As such a low ratio of κ-carrageenan is recommended the synthesis of NMC811 – lithium sulfate cathodes such that a viable cathode may be produced. While κ-carrageenan may be used a substitute for dextran or sodium alginate in order to synthesise NMC811 – lithium sulfate cathodes, initial studies indicate sulfate precursors are not a suitable replacement for acetates or nitrates with significant agglomeration and no observed synthesis of layered NMC811 occurring.

	κ-carrageenan	
	Acetates	Nitrates
Low mass	250 nm	500 nm
High mass	400 nm	500 nm

Table 30 Comparison of average particle diameters for NMC811 particles synthesised at 300 °C preheat and 850 °C calcination with acetate and nitrate precursors and low and high masses of κ-carrageenan biotemplate

6 Conclusions

Use of the novel biotemplating method to synthesise $LiNi_{0.8}Mn_{0.1}Co_{0.1}O_2$ (NMC811) cathodes and manipulate the particle morphology has shown some significant promise. In chapter 3 NMC811 was synthesising using a combination of either acetate or nitrate precursor salts and dextran or sodium alginate biotemplate. When NMC811 was synthesised using acetate precursors using either dextran or sodium alginate biotemplating, NMC811 was able to be synthesised by drying overnight at 85 °C, preheating in air at 300 °C for 2 h, and calcining in O_2 at 850 °C for 2 h. NMC811 was required to be synthesised under O_2 with previous research highlighting the necessity of an oxidising atmosphere to improve layering and reducing mixing of Li^+ and Ni^{2+} cations across Ni and Li sites [133]. Nitrates were similarly able to be used to synthesise NMC811 but with a lower calcination temperature of 800 °C. The calcination temperature is higher when using acetate precursors due to the high content of carbon within the precursors. The carbon is freed up to react with the oxygen atmosphere upon the decomposition of the biotemplate and precursors, forming CO_2 and a more reducing environment as a result of oxygen being used up to synthesise CO_2. This then requires a higher calcination temperature in order to decompose the CO_2 and ensure there is sufficient oxygen to fill oxygen sites during the synthesis of layered NMC811 and increase the structural organisation.

X-ray diffraction of biotemplated NMC811 synthesised under these conditions indicated layered, organised NMC811, with the combinations of acetates and dextran, nitrates and dextran, acetates and sodium alginate, and nitrates and sodium alginate having minimal mixing of Li^+ and Ni^{2+} cations between Li and Ni sites [130] as indicated by (003)/(104) peak intensity ratios of 1.55, 1.57, 1.5, and 1.68 respectively (where a ratio of < 1.2 indicates high mixing of Li and Ni sites). This is compared to a commercial NMC811 sample which exhibited a (003)/014 peak intensity ratio of 1.68. NMC811 synthesised with all combinations of precursors and biotemplate also shows good peak splitting at peaks (006)/(012) and (018)/(110), indicating good layering of the NMC811 structure [129].

Morphology of NMC811 particles is primarily shown to be nanoscale, non-agglomerated primary particles despite calcination temperatures above 800 °C. Using acetates produced irregularly shaped primary particles of average diameter 600 nm, while primary particles formed using nitrates and dextran also had irregular morphologies with average diameters of 700 nm. Particles synthesised with acetates and sodium alginate exhibited octahedral morphologies with 1000 nm average diameter, while nitrates and sodium alginate synthesised NMC811 was formed of 900 nm average diameter particles with a mix of octahedral and rounded morphologies. The larger particle sizes, most significantly exhibited when synthesising NMC811 using acetates and sodium alginate, was identified as being due to an exothermic reaction between 350 and 400 °C whereby an NMC hydroxide phase oxidised into disorganised NMC oxide, releasing a large amount of heat which provided energy for particles to grow to a larger diameter. As such, preheat temperature was maintained at 300 °C to ensure the possible synthesis of the NMC hydroxide phase, of which would likely be formed from the reaction of transition metal ions and hydroxide functional groups that were freed up during the decomposition of the biotemplate during preheat, but allow it to oxidise during calcination under O_2.

Novel morphologies were also observed. When calcined at 800 °C using acetates and dextran, plates with microscale diameters and nanoscale thicknesses were synthesised, while when sodium alginate and nitrates were synthesised at 850 °C nanowires were observed. Plate morphologies are beneficial for their high surface area and conductivity across the cross-section of the plate, however the 800 °C is below what is required to synthesise organised, layered NMC811 when using acetates. Nanowires also exhibit high surface area and ionic conductivity, as well as improved structural stability. Both morphologies were not able to be replicated and appeared sporadically and in small quantities in the cathodes they were observed in. It is theorised that an intermediate lithium carbonate intermediate phase was in some way involved in either the synthesis or final content of the morphologies, with nanowires requiring a molten intermediate phase (lithium carbonate) and solid substrate (NMC oxide) to form. This infers some inhomogeneity was required to form the novel particles. It is also theorised that the difficulty in synthesising these novel morphologies was due to the synthesis requirements to form the particles being different from those being required to form layered, organised NMC811 when using biotemplating. As such a compromise would have to be made between organisation of the NMC811 structure and particle morphology. This is further reinforced by the synthesis of NMC811 cathodes with 0 and 10% lithium content, which exhibits microwire morphologies not present when using a 100% proportion of lithium. This indicates that compromise would be required between the conditions to form a layered NMC811 structure with lithium and transition metal layers and to form novel morphologies.

When biotemplated NMC811 cathodes were used in lithium-ion coin cells, a range of performance was observed. When cycled between 4.2 V and 3 V at 0.1 C, cells with cathodes synthesised with nitrates and sodium alginate and nitrates exhibited an initial specific discharge capacity of 240 mAh/g with a capacity fade of 30 mAh/g over 50 cycles. Cathodes synthesised using acetates and dextran exhibited an initial specific discharge capacity of between 150 and 160 mAh/g with capacity fade of only 10 mAh/g over 10 cycles, while NMC811 cathodes synthesised using acetates and sodium alginate had an initial specific discharge capacity of 140 mAh/g with 10 mAh/g capacity fade over 10 cycles. The low capacity fade with good to high specific discharge capacity can be in part attributed to the cathode not having access to the H2 to H3 phase transition below 4.2 V. While this results in a slight loss of capacity, it ensures higher structural stability of the cathode [140].

When the same cathodes are cycled between 4.5 V and 2.8 V at 0.1 C, dextran and acetate synthesised cathodes show an initial specific discharge capacity between 160 mAh/g and 200 mAh/g with high capacity fade of (110) to 160 mAh/g over 50 cycles. When biotemplating with sodium alginate, acetate synthesised cathodes exhibit initial discharge capacities of between 160 and 200 mAh/g with capacity fade between 150 and 170 mAh/g over 50 cycles with nitrate synthesised cathodes having initial specific discharge capacities and capacity fades of between 170 mAh/g with 30 mAh/g capacity fade over 50 cycles and 200 mAh/g with capacity fades of 190 mAh/g over 50 cycles. This highlights how when cycled above 4.2 V the access to the H2 to H3 phase change may lead to an improvement in specific capacity as more lithium is accessible, however this also results in significant structural deterioration and capacity fade [127]. It is also observed that of the different combinations of precursors and biotemplate, sodium alginate and nitrates provide the best compromise of specific discharge capacity and capacity fade when cycled to both 4.2 V and 4.5 V.

It is worth noting that due to time restrictions however, refinement of the cell manufacturing process was able to be fully done. As such oxidation of lithium chips, and potential damage caused by the removal of the oxidation, and degradation of the electrolyte and potential uptake of water as a result of long term storage may lead to reductions in capacity due to loss of lithium and poor cyclability due to reduced ionic diffusivity. Furthermore, poor mixing may lead to inhomogeneity of the slurry resulting in not only differences in cathode performance between theoretically identical cathodes but also poor capacities due to a lower ratio of NMC811 or poor cyclability due to a lower ratio of additives. Poor mixing may also produce slurries that are too thin or too thick leading to uneven drawdowns and potentially poor calendaring, resulting in variations in cathode thickness and so variation in cyclability caused by differences in ionic pathways. Furthermore, poor calendaring may lead to over calendaring, which may result in damage to the cathodes leading to reduced cyclability and even cell failure.

With the benefits of biotemplating using sodium alginate established, it was investigated as to whether the presence of sodium within the sodium alginate biotemplate and by association NMC811 was beneficial to the cathode performance. This was achieved by substituting out lithium with sodium using sodium alginate to investigate whether the biotemplate could be used as dopant, and if not whether the formation of a sodium secondary phase would be beneficial. Firstly, sodium alginate was used such that the ratio of lithium-to-sodium was 10:90 and 10:80, then sodium nitrate was substituted for half of the sodium alginate where the lithium-to-sodium ratio was 20:80, then sodium alginate was substituted for dextran with sodium nitrate used at lithium-to-sodium ratios of 10:90 and 20:80.

It was found that substituting lithium for sodium resulted in a poor NMC811 structure regardless of whether acetates or nitrates were used or the amount of sodium substituted, with poor peak splitting at (006)/(012) and (018)/(110) for both ratios of lithium-to-sodium of 10:90 and 20:80 indicating poor layering of the NMC811 structure, and (003)/(104) peak intensity ratios not exceeding 1.36 highlighting a high level of Li^+ and Ni^{2+} cation mixing between Ni and Li sites [133] (where < 1.2 is considered a high level of mixing [130]). When using a 20:80 ratio of lithium-to-sodium, either sodium carbonate when using nitrates or sodium peroxide when using acetates is formed as a secondary indicating little incorporation of sodium into the NMC811 structure. When particles were analysed, particles synthesised using sodium alginate at lithium-to-sodium ratios of 20:80 had agglomerated, octahedral nanoscale primary particles of average particle diameters of 400 and 900 nm when using acetates and nitrates to synthesis cathodes respectively. Particles synthesised with dextran meanwhile were highly agglomerated with no noticeable primary particle morphology. This highlights the morphological control sodium alginate has on the synthesis of octahedral morphologies even without the synthesis of layered NMC811.

When made into cells, NMC811 cathodes with sodium carbonate or peroxide secondary phases cycled between 4.5 V and 2.8 V at 0.1 C all exhibited poor performance, with initial specific discharge capacities of between 140 and 200 mAh/g and capacity fade between 120 and 190 mAh/g over 50 cycles when using sodium alginate and/or sodium nitrate, and 90 to 150 mAh/g with capacity fade of 90 to 125 mAh/g over 50 cycles when using dextran and sodium nitrate. There is no observed improvement in specific capacity vs. NMC811 with no sodium secondary phases cathodes and high deterioration of the NMC811 as cells cycle above 4.2 V and access the H2 to H3 phase change resulting in cell failure [127]. As such it appears when substituting lithium for sodium there is no overall benefit in capacity or structure stability when introducing sodium into the NMC811 cathode. Such deterioration however may also be due to lack of refinement in the cell manufacturing process as poor quality lithium chips or electrolyte, or poor mixing, drawdowns, or calendaring may result in reduced capacities and cyclability.

The same cathodes, synthesised using sodium alginate, sodium alginate and sodium nitrate, and dextran and sodium nitrate, are repeated but without lithium being removed and instead sodium being added to a full NMC811 cathode. Results show an improvement in the NMC811 structure with improved peak splitting at (006)/(012) and (018)/(110) for all methods of synthesis up to 20% sodium with both acetate and nitrate precursors indicating improved layered of the NMC811 structure, and (003)/(104) peak intensity ratios of between 1.32 and 1.58 highlighting reduced mixing of Li^+ and Ni^{2+} between Ni and Li [133] sites (where < 1.2 is considered high mixing [130]). Morphologies remain similar however, with agglomerated primary particles of average diameter 900 nm up to 2000 nm being formed with morphologies ranging from smaller, rounded, irregular morphologies to larger octahedral morphologies. This again highlights the morphological control sodium-containing biotemplates have on the synthesis of octahedral particles.

When cathodes are cycled in lithium-ion coin cells between 4.5 V and 2.8 V at 0.1 C, poor performance is again observed with all cells regardless of biotemplate used, precursor used, or whether sodium nitrate was used. While exhibiting initial specific discharge capacities of between 130 and 200 mAh/g when synthesised with 10% sodium and between 100 and 180 mAh/g when synthesised with 20% sodium, poor capacity fade of between 70 to 200 mAh/g over 50 cycles is observed regardless of the amount of sodium alginate and/or nitrate used, with only one cell exhibiting capacity fade of only 30 mAh/g over 50 cycles. This is again likely due to structural failure caused by the cell cycling over 4.5 V and undergoing the H2 to H3 phase change [127]. It is a different story when cells are cycled between 4.2 V and 3 V at 0.1, however. While there are some cells that exhibit cell performance similar to that when cycled to 4.5 V, cathodes synthesised with 10% sodium exhibit initial specific discharge capacities as high as 170 mAh/g with capacity fade between 10 and 30 mAh/g over 50 cycles. As the cell is only cycled to 4.2 V, it does not undergo the H2 to H3 phase change and does undergo structural deterioration [140]. This further shows how the addition of sodium to NMC811 may improve the structural stability of NMC811, however once again poor cell capacities and cyclability may also be in part due to degraded lithium chips or electrolyte or issues with slurry mixing, drawdowns, and calendaring.

The third investigation was using κ-carrageenan in tandem with acetate and nitrate precursors as both a biotemplate and to introduce lithium sulfate as a secondary phase to synthesis NMC811 - lithium sulfate cathodes. It was found early on in the process that sulfur liked to form lithium sulfate as a secondary phase instead of fully incorporating into the NMC811 structure. As such masses acetate and nitrate precursors and high and low masses of κ-carrageenan were used to produced $LiNi_{0.8}Mn_{0.1}Co_{0.1}O_2.xLi_2SO_4$, where x = 0.005 and 0.05, respectively. When synthesising NMC811 - lithium sulfate cathodes using nitrates, (003)/(104) peak intensity ratios of 1.82 where x = 0.005 and 1.87 where x = 0.05 indicating low mixing of Li^+ and Ni^{2+} cations across Ni and Li sites [130], while the lower and higher proportions of lithium sulfate results in poor and good peak splitting at (006)/(012) and (018)/(110) respectively, indicating poor and good layering of the NMC811 structure [129]. Lithium sulfate secondary phase is also observed where x=0.05, indicating little integration of sulfur into the NMC811 structure. While having an organising structure, it is apparent that when using nitrates, sufficient biotemplate must be used such that layering of the NMC811 structure can be achieved. When using acetate precursors, the opposite is true with (003)/(104) peak intensity ratios of 1.45 and 1.51 and poor and good peak splitting at (006)/(012) and (018)/(110) for where x = 0.005 and 0.05 respectively. A significant lithium sulfate secondary phase is also present where x = 0.05. The poorer layering where x = 0.05 is likely due to the higher amount of biotemplate and use of acetate precursors introducing a higher carbon content into the reaction. The carbon is released upon the decomposition of the biotemplate and precursors which then reacts with the oxygen environment to synthesise greater amount of CO_2. This results in a more reducing environment as oxygen reacts with carbon, [133], and leads to a more disorganised structure as less oxygen is available during the synthesis of NMC811 to fill oxygen sites.

When morphologies are analysed, it was observed that when using both acetate and nitrate precursors a lower mass of κ-carrageenan irregular, rounded primary particles with average diameter 250 to 500 nm were formed. When the mass of κ-carrageenan was increased, morphology changed to individual octahedral primary particles with average diameter between 500 and 1000 nm showing the effect biotemplating has on the synthesis of octahedral morphologies. In one instance when using acetate precursors microwires were formed with cross-sectional diameter 200 – 300 nm and length of roughly 3000 nm. While not able to be reproduced the microwires were found across the entire sample, and when analysed using XRD were found to have a lithium carbonate secondary phase instead of a lithium sulfate secondary phase. This further reinforces the importance of intermediate phases formed during synthesis in the growth of different morphologies.

NMC811 cathodes were also synthesised using sulfate precursors as the source of sulfur and sodium alginate as the biotemplate. This resulted in highly disorganised NMC cathodes with no observed layering and a high amount of Li^+ and Ni^{2+} cation mixing. This is likely due to the presence of too much sulfur being present in the precursors and it not being able to be reacted off during the biotemplating method, resulting in a significant proportion of sulfur secondary phases. The morphology is also highly agglomerated, with no noticeable individual primary particles.

When cathodes using a low mass of κ-carrageenan such that $x = 0.005$ are cycled between 4.5 V and 2.8 V at 0.1 C, initial specific discharge capacities of between 180 to 200 mAh/g are observed, but with significant capacity fade of between 100 and 200 mAh/g over 50 cycles. A similar result can be seen when using a high mass of κ-carrageenan such that $x = 0.05$ with the cell showing an initial specific discharge capacity of between 130 and 160 mAh/g and a capacity fade or between 130 to 160 mAh/g over 50 cycles. This indicates that when cycled to 4.5 V, the lithium sulfate does little to suppress structural instability, with the cathode undergoing significant disorganisation as it cycles above 4.2 V and goes through the H2 to H3 phase change [127]. When cycled between 4.2 V and 3 V at 0.1 C, cells with both high and low proportions of lithium sulfate exhibit initial specific discharge capacities of between 90 and 150 mAh/g with capacity fade of between 40 and 70 mAh/g over 50 cycles. While the specific capacity is lower as a result of cycling to 4.2 V and not undergoing the H2 to H3 phase change, this also results in less structural deterioration [140] with the lithium sulfate secondary phase potentially improving structural stability when cycling between 4.2 V and 3 V. Such a lower capacity or cycling stability however may again be explained by issues in the cell manufacturing technique, specifically during mixing, drawdown, and calendaring, and degradations in the lithium chips and electrolyte.

In summary, the novel biotemplating method has been found to be a viable synthesis method in the production of NMC811 cathodes. Biotemplating can be used to produce NMC811 cathodes with only 2 h preheat and calcination times with calcination temperatures as low as 800 °C when using nitrate precursors, resulting in a quicker and more inexpensive synthesis method. Using biotemplating layered, organised NMC811 with octahedral, nanoscale morphologies can be reproduced reliable with further scope to optimise for novel plate and nanowire morphologies. When made into a cell, cathodes synthesised with sodium alginate and nitrate precursors can be cycled as high as 240 mAh/g to 4.2 V at 0.1 C with 30 mAh/g capacity fade over 50 cycles. Sodium alginate and κ-carrageenan biotemplates can also be used to synthesise NMC811 with both sodium and lithium sulfate secondary phases respectively, with both being able to be used to produce cathodes with layered, organised structures and nanoscale octahedral morphologies. When made into cells both NMC811 - lithium sulfate cathodes and NMC811 containing a sodium secondary phase are able to be cycled to 4.2 V at 0.1 C to specific discharge capacities above 150 mAh/g with capacity fade of 1 mAh/g per cycle. The novel biotemplating method therefore provides an alternative synthesis route to produce NMC811 with improved specific capacity and capacity retention while reducing synthesis times and costs. This is with the goal of using improved NMC811 cathodes in devices and EVs, increasing the uptake of green technologies and bringing us closer to the goal of net zero emissions.

7 Future Work

The novel biotemplating method provides significant scope for optimisation within this project, within other projects in the wider research community, and outside of academia for both industry and global energy and reduction in environmental damage as a whole.

Within the synthesis of NMC811 cathodes, there is further investigation and optimisation into the use of dextran, sodium alginate, and κ-carrageenan that is able to be undertaken. While initial results are promising, with lithium-ion cells using sodium alginate biotemplated NMC811 cathodes resulting in an initial discharge capacity of 220 mAh/g and lithium-ion cells produced using dextran resulting in highly stable capacities with capacity fade < 1mAh/g during cycling, the wide scope of the project means that there is still further room for refinement. With more time further biotemplates such as chitosan, Avicel (cellulose), pollen, wood, cotton, or even bacteria may also be investigated as suitable biotemplates and how they may be used to produce novel morphologies and improve the performance of NMC811 cathodes. Such biotemplates were initially investigated early in the project and researched as part of the literature review, 1.4.3.5, but there was not enough time to investigate the use of these biotemplates in NMC811 in any greater depth.

With further time, work in refining the synthesis methods using dextran, sodium alginate, and κ-carrageenan to enable both an organised and layered NMC811 structure while also allowing the manipulation into particle morphologies such as nanowires and plates on a reproducible basis is a possibility. It is theorised that there is a calcination temperature where both the layered structure and particle morphologies are possible but further work is required to confirm this. Furthermore, further refinement of synthesis methods using higher masses of sodium and sulfur may allow for actual doping of NMC811 cathodes as opposed to the formation of secondary phases. Sodium and sulfur doped cathodes, compared to cathodes with sodium and lithium sulfate secondary phases, may lead to cathodes with alternative characteristics or improved performance and so further investigation should be considered.

The optimisation of the cell manufacturing process is also a part of the project that required greater dedication. With greater emphasis placed on the powder synthesis during the project, which was further hampered by issues due to Covid-19 in the first two years, there was insufficient time to refine the cell manufacturing process to allow for the production of reproducible cells. Problems with reproducibility have led to a number of issues including poor mixing of the slurry, leading to inhomogeneous slurries that either have a lower ratio of NMC811 leading to a reduced capacity or a lower ratio of additives leading to a reduced cycling stability. The poor mixing may also lead to slurries that are too thin or too thick, leading to a poor and uneven drawdown and so a poor calendaring which may result in variation in the thickness of the cathodes and so differing cyclabilities due to different length ionic conductivity pathways. In worse cases over calendar may occur which can damage the cathode and lead to significant reductions in cyclability and cell failure.

Separate to the processes, supply chain issues surrounding lithium have led to too much of a reliance on lithium chips and electrolytes stored for significant periods of time. Lithium chips were oxidised reducing the amount of lithium available during cycling, and while the oxidation may be removed doing so may also damage the chips reducing the stability of the lithium chips and the cyclability. The electrolyte by comparison may have degraded or taken on water, reducing ionic diffusivity and reducing cyclability. Furthermore, due to time constraints, only one type of electrolyte was used, and so there was not time to compare electrolytes to determine the optimum electrolyte or even if the electrolyte used was beneficial or detrimental to the cell performance. By placing greater emphasis on cell manufacture and the source and quality of the cell components used, and by investigating how altering the mixing, drawdown, calendaring, and the electrolyte used may impact the final cell, greater reproducibility and performance in biotemplating NMC811 cells could be achieved.

The optimisation of is also beneficial from an environmental position. The production of electric vehicles is often criticised for its high levels of environmental damage and emissions, with an increased amount of mining to meet demand being one such contributor [145]. Use of biotemplates, of which are environmentally sustainable and green, being derived from sugars and algae of which are widely available, would help alleviate this by increasing the viability of cathodes previously considered too unstable or underpowered, such as NMC811 or LNO. This would help reduce the requirements for mining of more environmentally damaging materials used in cathodes such as cobalt, of which there is an increasing pressure to reduce due to the high cost and ethical reasons, [44].

Outside of academic research it should be the aim of the electrochemical industry that serious consideration is given to the scaling up of biotemplating and their incorporation into the synthesis process, with biotemplating allowing for quicker syntheses at lower synthesis temperatures while still producing the required cathodes. This aids future industry which if synthesising cathodes using biotemplating would be able to run furnaces quicker and at lower temperatures, reducing the cost of synthesis and the stress on furnaces while also reducing the emissions from running said furnaces.

The increased capacity and performance of lithium-ion cells produced by biotemplating would also further expand their applications. The primary application for stable and higher capacity lithium-ion cells synthesised via biotemplating is for use in electric vehicles, and research should be undertaken to access the viability of using biotemplated cells in electric vehicles. Use of more stable cells with higher capacities synthesised with the less expensive biotemplating method in future electric vehicles would lead to safer, higher range, and less expensive electric vehicles. This is with the aim of electric vehicles more closely matching the current equivalent internal combustion engine (ICE) vehicles in cost and performance as the upcoming ICE ban approaches [4].

It would also be researched whether a more stable and safe lithium-ion cell would lend itself to energy storage, with an increase in the cell capacity potentially providing greater storage capacity to such facilities. While the main focus of lithium-ion cells tends to be for electric vehicles, energy storage is equally as important as the world tends towards renewable energies such and solar and wind power and the need for energy storage facilities increases [146]. While current sodium-ion cells are often tapped for use in stationary energy storage, [147], it should be researched whether a less expensive, higher capacity, and more stable lithium-ion cell may be a viable alternative.

Outside of lithium-ion, the novel biotemplating has significant scope to be used elsewhere. Further use of biotemplates in sodium-ion and lithium-sulfate cells, among other chemistries, may also be investigated to further optimise upcoming chemistries and bring them to market quicker. While biotemplating for use in sodium-ion is already being investigated, [92], there is scope to research biotemplating for use with many different sodium-ion cathode in a similar to how it has been investigated in lithium-ion cells. Once this process is refined, scale-up in order to manufacture biotemplated sodium-ion cells in energy storage should be considered especially given sodium-ion cells currently being tapped for a role in this area [147].

In addition to investigating using alternative biotemplates such as sodium alginate in other applications such as YBCO superconductors [106]. Given the superconductors increased reliance in medicine and particle accelerators, as well as their developing role in mag-lev train technology and nuclear fusion, [148], investigations into synthesising superconductors with biotemplates should take place in order to aid in lowering the cost of superconductor synthesis in these already high-cost applications.

Biotemplating remains a relatively niche and untapped area of research in electrochemistry, though the limited research undertaken has highlighted its potential. By building on existing research and by further refinement and optimisation of cathodes and other applications synthesised using biotemplating, such as lithium and sodium-ion cathodes, there is a large scope for the improvement and scaling up of the biotemplating technique. This is with the aim of improving existing and upcoming technologies that rely on electrochemical storage in order to reach net zero [1].

8 References

[1] A. Olhoff *et al.*, *Emissions Gap Report 2024: No more hot air … please! With a massive gap between rhetoric and reality, countries draft new climate commitments*. United Nations Environment Programme, 2024. doi: 10.59117/20.500.11822/46404.

[2] Department for Energy Security & Net Zero, "2023 UK greenhouse gas emissions, provisional figures," Mar. 2024. Accessed: Feb. 27, 2025. [Online]. Available: https://assets.publishing.service.gov.uk/media/6604460f91a320001a82b0fd/uk-greenhouse-gas-emissions-provisional-figures-statistical-release-2023.pdf

[3] Department for Energy Security & Net Zero, "Net Zero Government Initiative: UK roadmap to net zero government emissions," Dec. 2023. Accessed: Feb. 27, 2025. [Online]. Available: https://assets.publishing.service.gov.uk/media/6569cb331104cf000dfa7352/net-zero-government-emissions-roadmap.pdf

[4] R. Tyers *et al.*, "Electric vehicles and infrastructure CBP-7480," Jul. 2024. Accessed: Feb. 27, 2025. [Online]. Available: https://commonslibrary.parliament.uk/research-briefings/cbp-7480/

[5] N. Chawla, N. Bharti, and S. Singh, "Recent advances in non-flammable electrolytes for safer lithium-ion batteries," *Batteries*, vol. 5, no. 1, Feb. 2019, doi: 10.3390/batteries5010019.

[6] A. Barai *et al.*, "A comparison of methodologies for the non-invasive characterisation of commercial Li-ion," *Prog Energy Combust Sci*, vol. 72, pp. 1–31, May 2019, doi: 10.1016/j.pecs.2019.01.001.

[7] L. Zhao *et al.*, "Engineering of Sodium-Ion Batteries: Opportunities and Challenges," *Engineering*, vol. 24, pp. 172–183, May 2023, doi: 10.1016/j.eng.2021.08.032.

[8] M. L. Soria, J. Ân, C. Ân, J. Carlos Herna Ândez, D. Moreno, and A. Ojeda, "Nickel metal hydride batteries for high power applications," *J Power Sources*, vol. 96, pp. 68–75, Jun. 2001, doi: 10.1016/S0378-7753(00)00677-7.

[9] J. Robinson, "Lithium-sulfur batteries: lightweight technology for multiple sectors," *Faraday Insights*, vol. 8, Jul. 2020, Accessed: Feb. 27, 2025. [Online]. Available: https://faraday.ac.uk/wp-content/uploads/2020/07/Faraday_Insights_8_FINAL.pdf

[10] N. Nitta, F. Wu, J. T. Lee, and G. Yushin, "Li-ion battery materials: Present and future," *Materials Today*, vol. 18, no. 5, pp. 252–264, Jun. 2015, doi: 10.1016/j.mattod.2014.10.040.

[11] A. Manthiram, "An Outlook on Lithium Ion Battery Technology," *ACS Cent Sci*, vol. 3, no. 10, pp. 1063–1069, Oct. 2017, doi: 10.1021/acscentsci.7b00288.

[12] E. Kallitsis, J. J. Lindsay, M. Chordia, B. Wu, G. J. Offer, and J. S. Edge, "Think global act local: The dependency of global lithium-ion battery emissions on production

location and material sources," *J Clean Prod*, vol. 449, Apr. 2024, doi: 10.1016/j.jclepro.2024.141725.

[13] C. Grosjean, P. Herrera Miranda, M. Perrin, and P. Poggi, "Assessment of world lithium resources and consequences of their geographic distribution on the expected development of the electric vehicle industry," *Renewable and Sustainable Energy Reviews*, vol. 16, no. 3, pp. 1735–1744, Apr. 2012, doi: 10.1016/j.rser.2011.11.023.

[14] Battery Design, "Battery Chemistry." Accessed: Feb. 27, 2025. [Online]. Available: https://www.batterydesign.net/chemistry/

[15] M. Schirber, "Sodium as a Green Substitute for Lithium in Batteries," *Physics (College Park Md)*, vol. 17, Apr. 2024, doi: 10.1103/physics.17.73.

[16] T. Yu *et al.*, "The research and industrialization progress and prospects of sodium ion battery," *J Alloys Compd*, vol. 958, Oct. 2023, doi: 10.1016/j.jallcom.2023.170486.

[17] K. Chayambuka, G. Mulder, D. L. Danilov, and P. H. L. Notten, "From Li-Ion Batteries toward Na-Ion Chemistries: Challenges and Opportunities," *Adv Energy Mater*, vol. 10, no. 38, Oct. 2020, doi: 10.1002/aenm.202001310.

[18] Z. X. Chen, M. Zhao, L. P. Hou, X. Q. Zhang, B. Q. Li, and J. Q. Huang, "Toward Practical High-Energy-Density Lithium–Sulfur Pouch Cells: A Review," *Advanced Materials*, vol. 34, no. 35, Sep. 2022, doi: 10.1002/adma.202201555.

[19] A. Manthiram, Y. Fu, and Y. S. Su, "Challenges and prospects of lithium-sulfur batteries," *Acc Chem Res*, vol. 46, no. 5, pp. 1125–1134, May 2013, doi: 10.1021/ar300179v.

[20] M. Zhao, B. Q. Li, X. Q. Zhang, J. Q. Huang, and Q. Zhang, "A Perspective toward Practical Lithium-Sulfur Batteries," *ACS Cent Sci*, vol. 6, no. 7, pp. 1095–1104, Jul. 2020, doi: 10.1021/acscentsci.0c00449.

[21] L. F. Nazar, M. Cuisinier, and Q. Pang, "Lithium-sulfur batteries," *MRS Bull*, vol. 39, no. 5, pp. 436–442, 2014, doi: 10.1557/mrs.2014.86.

[22] V. Arun *et al.*, "Review on Li-Ion Battery vs Nickel Metal Hydride Battery in EV," *Advances in Materials Science and Engineering*, vol. 2022, no. 1, Aug. 2022, doi: 10.1155/2022/7910072.

[23] D. Steward, G. Saur, M. Penev, and T. Ramsden, "Lifecycle Cost Analysis of Hydrogen Versus Other Technologies for Electrical Energy Storage," Nov. 2009, Accessed: Feb. 27, 2025. [Online]. Available: http://www.osti.gov/servlets/purl/968186-wRSjx1/

[24] F. R. Kalhammer, B. M. Kopf, D. H. Swan, V. P. Roan, and M. P. Walsh, "Status and Prospects for Zero Emissions Vehicle Technology Report of the ARB Independent Expert Panel 2007 Prepared for State of California Air Resources Board Sacramento, California," 2007.

[25] M. Malpede, “The dark side of batteries: Child labor and cobalt mining in the Democratic Republic of Congo,” Mar. 2023. Accessed: Feb. 27, 2025. [Online]. Available: http://dx.doi.org/10.2139/ssrn.3680730

[26] L. Fischer, F. Rupalla, S. Sahdev, A. Tanweer, and Mckinsey, “A new EV survey_ What consumers want in charging _ McKinsey.” Accessed: Dec. 15, 2024. [Online]. Available: https://www.mckinsey.com/features/mckinsey-center-for-future-mobility/our-insights/exploring-consumer-sentiment-on-electric-vehicle-charging#/

[27] Kantar, “Understanding Consumer Attitudes Towards Electric Vehicles.” Accessed: Dec. 15, 2024. [Online]. Available: https://www.kantar.com/inspiration/research-services/understanding-consumer-attitudes-towards-electric-vehicles-pf#:~:text=The%20primary%20motivators%20for%20current,of%20EVs%20in%20the%20market.

[28] J.-J. Marie, “Developments in Lithium-Ion Battery Cathodes,” *Faraday Insights*, vol. 18, Sep. 2023, Accessed: Feb. 27, 2025. [Online]. Available: https://www.faraday.ac.uk/wp-content/uploads/2023/09/Faraday_Insights_18_FINAL.pdf

[29] M. H. Hossain, M. A. Chowdhury, N. Hossain, M. A. Islam, and M. H. Mobarak, “Advances of lithium-ion batteries anode materials—A review,” *Chemical Engineering Journal Advances*, vol. 16, Nov. 2023, doi: 10.1016/j.ceja.2023.100569.

[30] T. Wang *et al.*, “Synthesis and Manipulation of Single-Crystalline Lithium Nickel Manganese Cobalt Oxide Cathodes: A Review of Growth Mechanism,” *Front Chem*, vol. 8, Sep. 2020, doi: 10.3389/fchem.2020.00747.

[31] J. Bai *et al.*, “Kinetic Pathways Templated by Low-Temperature Intermediates during Solid-State Synthesis of Layered Oxides,” *Chemistry of Materials*, vol. 32, no. 23, pp. 9906–9913, Dec. 2020, doi: 10.1021/acs.chemmater.0c02568.

[32] M. Jiang, D. L. Danilov, R. A. Eichel, and P. H. L. Notten, “A Review of Degradation Mechanisms and Recent Achievements for Ni-Rich Cathode-Based Li-Ion Batteries,” *Adv Energy Mater*, vol. 11, no. 48, Dec. 2021, doi: 10.1002/aenm.202103005.

[33] K. Taehoon, “The origin of the aggressive degradation of Ni-rich transition metal oxide cathodes for high-energy density lithium-ion batteries,” *J Solid State Chem*, vol. 310, Jun. 2022, doi: 10.1016/j.jssc.2022.123040.

[34] K. Taehoon, “Implication of magnetic property on the degradation process of layered Ni-rich transition metal oxide cathode for high-capacity lithium-ion batteries,” *J Magn Magn Mater*, vol. 562, Dec. 2022, doi: 10.1016/j.jmmm.2022.170107.

[35] A. Manthiram, “A reflection on lithium-ion battery cathode chemistry,” *Nat Commun*, vol. 11, no. 1, Dec. 2020, doi: 10.1038/s41467-020-15355-0.

[36] J.-P. Schmiegel *et al.*, “Improving the Cycling Performance of High-Voltage NMC111 || Graphite Lithium Ion Cells By an Effective Urea-Based Electrolyte Additive,” *J Electrochem Soc*, vol. 166, no. 13, pp. A2910–A2920, 2019, doi: 10.1149/2.0691913jes.

[37] LithiumStorageBattery, “Lithium Ion Battery Classification And Future Trend（2）.” Accessed: Dec. 11, 2024. [Online]. Available: https://www.lithiumstoragebattery.com/news-lithium-ion-battery-classification-future-trend.html

[38] R. Jung *et al.*, “Effect of Ambient Storage on the Degradation of Ni-Rich Positive Electrode Materials (NMC811) for Li-Ion Batteries,” *J Electrochem Soc*, vol. 165, no. 2, pp. A132–A141, 2018, doi: 10.1149/2.0401802jes.

[39] K. Elong, M. Firdaus Kasim, A. Azahidi, and Z. Osman, “$LiNi_{0\cdot3}Mn_{0\cdot3}Co_{0\cdot3}O_2$ (NMC 111) cathode material synthesize via combustion Method: Effect of combustion fuel on Structure, morphology and their electrochemical performances,” *Mater Today Proc*, Mar. 2023, doi: 10.1016/j.matpr.2023.02.283.

[40] J. Li, H. Li, W. Stone, R. Weber, S. Hy, and J. R. Dahn, “Synthesis of Single Crystal $LiNi_{0\cdot5}Mn_{0\cdot3}Co_{0\cdot2}O_2$ for Lithium Ion Batteries,” *J Electrochem Soc*, vol. 164, no. 14, pp. A3529–A3537, Nov. 2017, doi: 10.1149/2.0401714jes.

[41] R. Weber, C. R. Fell, J. R. Dahn, and S. Hy, “Operando X-ray Diffraction Study of Polycrystalline and Single-Crystal $Li_xNi_{0\cdot5}Mn_{0\cdot3}Co_{0\cdot2}O_2$,” *J Electrochem Soc*, vol. 164, no. 13, pp. A2992–A2999, Sep. 2017, doi: 10.1149/2.0441713jes.

[42] L. Wang *et al.*, “Single-crystal $LiNi_{0\cdot6}Co_{0\cdot2}Mn_{0\cdot2}O_2$ as high performance cathode materials for Li-ion batteries,” *J Alloys Compd*, vol. 674, pp. 360–367, Jul. 2016, doi: 10.1016/j.jallcom.2016.03.061.

[43] L. Xu *et al.*, “Progress in Preparation and Modification of $LiNi_{0\cdot6}Mn_{0\cdot2}Co_{0\cdot2}O_2$ Cathode Material for High Energy Density Li-Ion Batteries,” *International Journal of Electrochemistry*, vol. 2018, pp. 1–12, Jul. 2018, doi: 10.1155/2018/6930386.

[44] P. Kalungi, Z. Yao, and H. Huang, “Aspects of Nickel, Cobalt and Lithium, the Three Key Elements for Li-Ion Batteries: An Overview on Resources, Demands, and Production,” *Materials*, vol. 17, no. 17, Sep. 2024, doi: 10.3390/ma17174389.

[45] R. Pan, E. Jo, Z. Cui, and A. Manthiram, “Degradation Pathways of Cobalt-Free $LiNiO_2$ Cathode in Lithium Batteries,” *Adv Funct Mater*, vol. 33, no. 10, Mar. 2023, doi: 10.1002/adfm.202211461.

[46] C. Song *et al.*, “Improving the electrochemical performance of $LiNi_{0\cdot80}Co_{0\cdot15}Al_{0\cdot05}O_2$ in lithium ion batteries by $LiAlO_2$ surface modification,” *Applied Sciences (Switzerland)*, vol. 8, no. 3, Mar. 2018, doi: 10.3390/app8030378.

[47] W. Li, S. Lee, and A. Manthiram, “High-Nickel NMA: A Cobalt-Free Alternative to NMC and NCA Cathodes for Lithium-Ion Batteries,” *Advanced Materials*, vol. 32, no. 33, Aug. 2020, doi: 10.1002/adma.202002718.

[48] G. W. Nam *et al.*, "Capacity Fading of Ni-Rich NCA Cathodes: Effect of Microcracking Extent," *ACS Energy Lett*, vol. 4, no. 12, pp. 2995–3001, Dec. 2019, doi: 10.1021/acsenergylett.9b02302.

[49] D. Jugović and D. Uskoković, "A review of recent developments in the synthesis procedures of lithium iron phosphate powders," *J Power Sources*, vol. 190, no. 2, pp. 538–544, May 2009, doi: 10.1016/j.jpowsour.2009.01.074.

[50] L. X. Yuan *et al.*, "Development and challenges of $LiFePO_4$ cathode material for lithium-ion batteries," *Energy Environ Sci*, vol. 4, no. 2, pp. 269–284, Jul. 2010, doi: 10.1039/c0ee00029a.

[51] Z. Yang, Y. Dai, S. Wang, and J. Yu, "How to make lithium iron phosphate better: a review exploring classical modification approaches in-depth and proposing future optimization methods," *J Mater Chem A Mater*, vol. 4, no. 47, pp. 18210–18222, Oct. 2016, doi: 10.1039/C6TA05048D.

[52] L. Najmam, "Why We're Excited about LFP Batteries for Electric Cars", Accessed: Dec. 08, 2024. [Online]. Available: https://www.recurrentauto.com/research/lfp-battery-in-your-next-ev-tesla-and-others-say-yes

[53] K. Wang *et al.*, "Recent advances and historical developments of high voltage lithium cobalt oxide materials for rechargeable Li-ion batteries," *J Power Sources*, vol. 460, Jun. 2020, doi: 10.1016/j.jpowsour.2020.228062.

[54] D. Uxa, E. Hüger, K. Meyer, L. Dörrer, and H. Schmidt, "Lithium-Ion Diffusion in Near-Stoichiometric Polycrystalline and Monocrystalline $LiCoO_2$," *Chemistry of Materials*, vol. 35, no. 8, pp. 3307–3315, Apr. 2023, doi: 10.1021/acs.chemmater.3c00359.

[55] K. Mizushima, P. C. Jones, P. J. Wiseman, and J. B. Goodenough, "Li_xCoO_2 ($0<x\leq1$): A New Cathode Material for Batteries of High Energy Density," *Mat. Res. Bull*, vol. 15, pp. 783–789, Apr. 1980, doi: 0025-5408/80/060783-07502,00/0.

[56] Y. Shao-Horn, L. Croguennec, C. Delmas, E. C. Nelson, and M. A. O'Keefe, "Atomic resolution of lithium ions in $LiCoO_2$," *Nat Mater*, vol. 2, no. 7, pp. 464–467, Aug. 2003, doi: 10.1038/nmat922.

[57] A. Manthiram, "A reflection on lithium-ion battery cathode chemistry," *Nat Commun*, vol. 11, no. 1, Dec. 2020, doi: 10.1038/s41467-020-15355-0.

[58] A. H. Marincaş, F. Goga, S. A. Dorneanu, and P. Ilea, "Review on synthesis methods to obtain $LiMn_2O_4$-based cathode materials for Li-ion batteries," *Journal of Solid State Electrochemistry*, vol. 24, no. 3, pp. 473–497, Mar. 2020, doi: 10.1007/s10008-019-04467-3.

[59] Y. Mao, S. Xiao, and J. Liu, "Nanoparticle-assembled $LiMn_2O_4$ hollow microspheres as high-performance lithium-ion battery cathode," *Mater Res Bull*, vol. 96, pp. 437–442, Dec. 2017, doi: 10.1016/j.materresbull.2017.03.005.

[60] K. Mukai *et al.*, "Pressure dependence of magnetic transition temperature in $Li[Li_xMn_{2-x}]O_4$ ($0 \leq x \leq 1/3$) studied by muon-spin rotation and relaxation," *J Appl Phys*, vol. 113, no. 5, Feb. 2013, doi: 10.1063/1.4790377.

[61] M. Bianchini, M. Roca-Ayats, P. Hartmann, T. Brezesinski, and J. Janek, “There and Back Again-The Journey of $LiNiO_2$ as a Cathode Active Material,” *Angewandte Chemie International Edition*, vol. 58, no. 31, pp. 10434–10458, Jul. 2019, doi: 10.1002/anie.201812472.

[62] M. Malik, K. H. Chan, and G. Azimi, “Review on the synthesis of $LiNi_xMn_\gamma Co1_{-x-\gamma}O_2$ (NMC) cathodes for lithium-ion batteries,” *Mater Today Energy*, vol. 28, Aug. 2022, doi: 10.1016/j.mtener.2022.101066.

[63] N. Reeves-McLaren *et al.*, “The Spinel $LiCoMnO_4$: 5V Cathode and Conversion Anode,” *Energy Procedia*, vol. 151, pp. 158–162, Oct. 2018, doi: 10.1016/j.egypro.2018.09.041.

[64] H. Zhao *et al.*, “A simple, low-cost and eco-friendly approach to synthesize single-crystalline $LiMn_2O_4$ nanorods with high electrochemical performance for lithium-ion batteries,” *Electrochim Acta*, vol. 166, pp. 124–133, Jun. 2015, doi: 10.1016/j.electacta.2015.03.040.

[65] S. K. Young, “Overview of Sol-Gel Science and Technology,” Jan. 2002. Accessed: Feb. 28, 2025. [Online]. Available: https://apps.dtic.mil/sti/pdfs/ADA398036.pdf

[66] R. Dominko *et al.*, “Porous olivine composites synthesized by sol-gel technique,” *J Power Sources*, vol. 153, no. 2, pp. 274–280, Feb. 2006, doi: 10.1016/j.jpowsour.2005.05.033.

[67] R. Thirunakaran, G. H. Lew, and W. S. Yoon, “Synthesis and electrochemical properties of dual doped spinels $LiNi_xAl_\gamma Mn_{2-x-\gamma}O_4$ via facile novel chelated sol–gel method as possible cathode material for lithium rechargeable batteries,” *Journal of Energy Chemistry*, vol. 26, no. 1, pp. 101–114, Jan. 2017, doi: 10.1016/j.jechem.2016.08.006.

[68] R. Thirunakaran, T. Kim, and W. S. Yoon, “Effects of multi-dopants (Zn and Ho) in stabilizing spinel structure for cathode materials in lithium rechargeable batteries - Novel chelated sol-gel synthesis,” *Particuology*, vol. 24, pp. 87–95, Feb. 2016, doi: 10.1016/j.partic.2015.03.003.

[69] H. Lu *et al.*, “High capacity $Li[Ni_{0\cdot8}Co_{0\cdot1}Mn_{0\cdot1}]O_2$ synthesized by sol-gel and co-precipitation methods as cathode materials for lithium-ion batteries,” *Solid State Ion*, vol. 249–250, pp. 105–111, Nov. 2013, doi: 10.1016/j.ssi.2013.07.023.

[70] G. Yang and S. J. Park, “Conventional and microwave hydrothermal synthesis and application of functional materials: A review,” *Materials*, vol. 12, no. 7, Apr. 2019, doi: 10.3390/ma12071177.

[71] J. Chen and M. S. Whittingham, “Hydrothermal synthesis of lithium iron phosphate,” *Electrochem commun*, vol. 8, no. 5, pp. 855–858, May 2006, doi: 10.1016/j.elecom.2006.03.021.

[72] C. Xu, J. Lee, and A. S. Teja, “Continuous hydrothermal synthesis of lithium iron phosphate particles in subcritical and supercritical water,” *Journal of Supercritical Fluids*, vol. 44, no. 1, pp. 92–97, Feb. 2008, doi: 10.1016/j.supflu.2007.09.001.

[73] G. Huang, S. Xu, S. Lu, L. Li, and H. Sun, “Micro-/nanostructured Co_3O_4 anode with enhanced rate capability for lithium-ion batteries,” *ACS Appl Mater Interfaces*, vol. 6, no. 10, pp. 7236–7243, May 2014, doi: 10.1021/am500452t.

[74] S. W. Bian and L. Zhu, “Template-free synthesis of mesoporous Co_3O_4 with controlled morphologies for lithium ion batteries,” *RSC Adv*, vol. 3, no. 13, pp. 4212–4215, Apr. 2013, doi: 10.1039/c3ra40333e.

[75] B. Wu *et al.*, “Morphology controllable synthesis and electrochemical performance of $LiCoO_2$ for lithium-ion batteries,” *Electrochim Acta*, vol. 209, pp. 315–322, Aug. 2016, doi: 10.1016/j.electacta.2016.05.085.

[76] S. H. Ye, J. K. Bo, C. Z. Li, J. S. Cao, Q. L. Sun, and Y. L. Wang, “Improvement of the high-rate discharge capability of phosphate-doped spinel $LiMn_2O_4$ by a hydrothermal method,” *Electrochim Acta*, vol. 55, no. 8, pp. 2972–2977, Mar. 2010, doi: 10.1016/j.electacta.2010.01.018.

[77] J. Zhu and G. Chen, “Single-crystal based studies for correlating the properties and high-voltage performance of $Li[Ni_xMn_\gamma Co_{1-x-\gamma}]O_2$ cathodes,” *J Mater Chem A Mater*, vol. 7, no. 10, pp. 5463–5474, Feb. 2019, doi: 10.1039/c8ta10329a.

[78] G. Arnold, J. Garche, R. Hemmer, S. Ströbele, C. Vogler, and M. Wohlfahrt-Mehrens, “Fine-particle lithium iron phosphate $LiFePO_4$ synthesized by a new low-cost aqueous precipitation technique,” *J Power Sources*, vol. 119–121, pp. 247–251, Jun. 2003, doi: 10.1016/S0378-7753(03)00241-6.

[79] A. Li, Z. Shao, S. Yang, X. Li, and A. Zhang, “Precipitation synthesis and enhanced electrochemical performance of graphene-modified $LiMn_2O_4$ for lithium-ion batteries,” *Ionics (Kiel)*, vol. 26, pp. 3231–3238, Jan. 2020, doi: 10.1007/s11581-019-03432-4.

[80] L. Dimesso, “Pechini processes: An alternate approach of the sol-gel method, preparation, properties, and applications,” in *Handbook of Sol-Gel Science and Technology: Processing, Characterization and Applications*, Springer International Publishing, 2018, pp. 1067–1087. doi: 10.1007/978-3-319-32101-1_123.

[81] H. Xia, H. Wang, W. Xiao, L. Lu, and M. O. Lai, “Properties of $LiNi_1/_3Co_1/_3Mn_1/_3O_2$ cathode material synthesized by a modified Pechini method for high-power lithium-ion batteries,” *J Alloys Compd*, vol. 480, no. 2, pp. 696–701, Jul. 2009, doi: 10.1016/j.jallcom.2009.02.023.

[82] S. P. Lin, K. Z. Fung, Y. M. Hon, and M. H. Hon, “Crystallization mechanism of $LiNiO_2$ synthesized by Pechini method,” *J Cryst Growth*, vol. 226, pp. 148–157, Jun. 2001, doi: 10.1016/S0022-0248(01)01363-X.

[83] W. Liu, G. C. Farrington, F. Chaput, and B. Dunn, “Synthesis and Electrochemical Studies of Spinel Phase $LiMn_2O_4$ Cathode Materials Prepared by the Pechini Process,” *J. Electrochem. Soc*, vol. 143, pp. 879–884, Mar. 1996, doi: 10.1149/1.1836552.

[84] T. Kimijima, N. Zettsu, and K. Teshima, “Growth manner of octahedral-shaped $Li(Ni_1/_3Co_1/_3Mn_1/_3)O_2$ single crystals in molten $Na2SO_4$,” *Cryst Growth Des*, vol. 16, no. 5, pp. 2618–2623, May 2016, doi: 10.1021/acs.cgd.5b01723.

[85] B. Pişkin, C. S. Uygur, and M. K. Aydınol, “Morphology effect on electrochemical properties of doped (W and Mo) 622NMC, 111NMC, and 226NMC cathode materials,” *Int J Hydrogen Energy*, vol. 45, no. 14, pp. 7874–7880, Mar. 2020, doi: 10.1016/j.ijhydene.2019.07.249.

[86] M. Konarova and I. Taniguchi, “Preparation of $LiFePO_4$/C composite powders by ultrasonic spray pyrolysis followed by heat treatment and their electrochemical properties,” *Mater Res Bull*, vol. 43, no. 12, pp. 3305–3317, Dec. 2008, doi: 10.1016/j.materresbull.2008.02.014.

[87] M. Almazrouei, S. Park, M. Houck, M. De Volder, S. Hochgreb, and A. Boies, “Synthesis Pathway of Layered-Oxide Cathode Materials for Lithium-Ion Batteries by Spray Pyrolysis,” *ACS Applied Materials and Interfaces* , vol. 16, no. 26, pp. 33633–33646, Jul. 2024, doi: 10.1021/acsami.4c06503.

[88] A. E. Danks, S. R. Hall, and Z. Schnepp, “The evolution of ‘sol-gel’ chemistry as a technique for materials synthesis,” *Mater Horiz*, vol. 3, no. 2, pp. 91–112, Mar. 2016, doi: 10.1039/c5mh00260e.

[89] E. Yuba, S. Uesugi, M. Miyazaki, Y. Kado, A. Harada, and K. Kono, “Development of pH-sensitive dextran derivatives with strong adjuvant function and their application to antigen delivery,” *Membranes (Basel)*, vol. 7, no. 3, Sep. 2017, doi: 10.3390/membranes7030041.

[90] T. Watanabe, A. Ohtsuka, N. Murase, P. Barth, and K. Gersonde, “NMR studies on water and polymer diffusion in dextran gels. Influence of potassium ions on microstructure formation and gelation mechanism,” *Magn Reson Med*, vol. 35, no. 5, pp. 697–705, 1996, doi: 10.1002/mrm.1910350511.

[91] D. Walsh, L. Arcelli, T. Ikoma, J. Tanaka, and S. Mann, “Dextran templating for the synthesis of metallic and metal oxide sponges,” *Nat Mater*, vol. 2, no. 6, pp. 386–390, May 2003, doi: 10.1038/nmat903.

[92] S. Zilinskaite, A. J. R. Rennie, R. Boston, and N. Reeves-Mclaren, “Biotemplating: A sustainable synthetic methodology for Na-ion battery materials,” *J Mater Chem A Mater*, vol. 6, no. 13, pp. 5346–5355, 2018, doi: 10.1039/c7ta09260a.

[93] S. C. Wimbush, W. Marx, A. Barth, and S. R. Hall, “On the incorporation of beryllium into the biotemplated synthesis of $YBa_2Cu_3O_{7-}\delta$,” *Supercond Sci Technol*, vol. 23, no. 9, Sep. 2010, doi: 10.1088/0953-2048/23/9/095003.

[94] Z. Schnepp, S. C. Wimbush, S. Mann, and S. R. Hall, “Alginate-mediated routes to the selective synthesis of complex metal oxide nanostructures,” *CrystEngComm*, vol. 12, no. 5, pp. 1410–1415, 2010, doi: 10.1039/b923543b.

[95] J. Zhang, T. L. Peppard, and G. A. Reineccius, “Double-layered emulsions as beverage clouding agents,” *Flavour Fragr J*, vol. 30, no. 3, pp. 218–223, May 2015, doi: 10.1002/ffj.3231.

[96] Z. A. C. Schnepp, S. C. Wimbush, S. Mann, and S. R. Hall, “Structural evolution of superconductor nanowires in biopolymer gels,” *Advanced Materials*, vol. 20, no. 9, pp. 1782–1786, May 2008, doi: 10.1002/adma.200702679.

[97] X. Zhou, G. Chen, J. Tang, Y. Ren, and J. Yang, “One-dimensional $NiCo_2O_4$ nanowire arrays grown on nickel foam for high-performance lithium-ion batteries,” *J Power Sources*, vol. 299, pp. 97–103, Dec. 2015, doi: 10.1016/j.jpowsour.2015.08.085.

[98] P. Shao *et al.*, “Non-chloride in situ preparation of nano-cuprous oxide and its effect on heat resistance and combustion properties of calcium alginate,” *Polymers (Basel)*, vol. 11, no. 11, Oct. 2019, doi: 10.3390/polym11111760.

[99] N. Vanitha *et al.*, “Effect of graphene quantum dot on sodium alginate with ammonium formate (NH4HCO2) biopolymer electrolytes for the application of electrochemical devices,” *Ionics (Kiel)*, vol. 28, no. 6, pp. 2731–2749, Mar. 2022, doi: 10.1007/s11581-022-04522-6.

[100] W. Hua *et al.*, “Na-doped Ni-rich $LiNi_{0\cdot5}Co_{0\cdot2}Mn_{0\cdot3}O_2$ cathode material with both high rate capability and high tap density for lithium ion batteries,” *Dalton Transactions*, vol. 43, no. 39, pp. 14824–14832, Oct. 2014, doi: 10.1039/c4dt01611d.

[101] Y. Shen *et al.*, “Sodium doping derived electromagnetic center of lithium layered oxide cathode materials with enhanced lithium storage,” *Nano Energy*, vol. 94, Apr. 2022, doi: 10.1016/j.nanoen.2021.106900.

[102] Y. Y. Wang, Y. Y. Sun, S. Liu, G. R. Li, and X. P. Gao, “Na-Doped $LiNi_{0\cdot8}Co_{0\cdot15}Al_{0\cdot05}O_2$ with Excellent Stability of Both Capacity and Potential as Cathode Materials for Li-Ion Batteries,” *ACS Appl Energy Mater*, vol. 1, no. 8, pp. 3881–3889, Aug. 2018, doi: 10.1021/acsaem.8b00630.

[103] J. Wang, W. Lin, B. Wu, and J. Zhao, “Syntheses and electrochemical properties of the Na-doped $LiNi_{0\cdot5}Mn_{1\cdot5}O_4$ cathode materials for lithium-ion batteries,” *Electrochim Acta*, vol. 145, pp. 245–253, Nov. 2014, doi: 10.1016/j.electacta.2014.07.140.

[104] M. Sadeghi, “SYNTHESIS OF A BIOCOPOLYMER CARRAGEENAN-g-POLY(AAm-co-IA)/ MONTMORILONITE SUPERABSORBENT HYDROGEL COMPOSITE,” *Brazilian Journal of Chemical Engineering*, vol. 29, no. 2, pp. 295–305, Jun. 2012, doi: 10.1590/S0104-66322012000200010.

[105] A. Mirzaei, M. Esmkhani, M. Zallaghi, Z. Nezafat, and S. Javanshir, “Biomedical and Environmental Applications of Carrageenan-Based Hydrogels: A Review,” *J Polym Environ*, vol. 31, no. 5, pp. 1679–1705, May 2023, doi: 10.1007/s10924-022-02726-5.

[106] R. Boston, K. Awaya, T. Nakayama, W. Ogasawara, and S. R. Hall, “Formation of superconducting yttrium barium copper oxide using sulphur-containing templates,” *RSC Adv*, vol. 4, no. 51, pp. 26824–26828, 2014, doi: 10.1039/c4ra04745a.

[107] A. Mirzaei, M. Esmkhani, M. Zallaghi, Z. Nezafat, and S. Javanshir, “Biomedical and Environmental Applications of Carrageenan-Based Hydrogels: A Review,” *J Polym Environ*, vol. 31, no. 5, pp. 1679–1705, May 2023, doi: 10.1007/s10924-022-02726-5.

[108] S. H. Park, Y.-K. Sun, K. S. Park, K. S. Nahm, Y. S. Lee, and M. Yoshio, “Synthesis and electrochemical properties of lithium nickel oxysulfide ($LiNiS_{\gamma}O_{2-\gamma}$) material for lithium secondary batteries,” *Electrochim Acta*, vol. 47, no. 11, pp. 1721–1726, Mar. 2002, doi: 10.1016/S0013-4686(02)00023-3.

[109] J. Li *et al.*, “Stabilizing $LiNi_{0\cdot 8}Co_{0\cdot 15}Mn_{0\cdot 05}O_2$ Cathode by Doping Sulfate for Lithium-Ion Batteries,” *ChemSusChem*, vol. 14, no. 13, pp. 2721–2730, Jul. 2021, doi: 10.1002/cssc.202100595.

[110] B. Dong *et al.*, “Effects of sulfate modification of stoichiometric and lithium-rich $LiNiO_2$ cathode materials,” *J Mater Chem A Mater*, vol. 12, no. 19, pp. 11390–11402, Apr. 2024, doi: 10.1039/d4ta00284a.

[111] J. Konne, S. A. Davis, S. Glatzel, M. R. Lees, and S. R. Hall, “A new stoichiometry of cuprate nanowires,” *Supercond Sci Technol*, vol. 25, no. 11, Nov. 2012, doi: 10.1088/0953-2048/25/11/115005.

[112] D. C. Green, S. Glatzel, A. M. Collins, A. J. Patil, and S. R. Hall, “A new general synthetic strategy for phase-pure complex functional materials,” *Advanced Materials*, vol. 24, no. 42, pp. 5767–5772, Nov. 2012, doi: 10.1002/adma.201202683.

[113] Y. S. Kang *et al.*, “Shape control of hierarchical lithium cobalt oxide using biotemplates for connected nanoparticles,” *J Power Sources*, vol. 436, Oct. 2019, doi: 10.1016/j.jpowsour.2019.226836.

[114] G. F. Harrington and J. Santiso, “Back-to-Basics tutorial: X-ray diffraction of thin films,” *J Electroceram*, vol. 47, no. 4, pp. 141–163, Dec. 2021, doi: 10.1007/s10832-021-00263-6.

[115] The Editors of Encyclopaedia Britannica, “Bragg law _ Definition, Equation, Diagram, & Facts _ Britannica.” Accessed: Mar. 22, 2025. [Online]. Available: https://www.britannica.com/science/Bragg-law

[116] J. P. Foley, “Resolution equations for column chromatography,” *Analyst*, vol. 116, no. 12, pp. 1275–1279, 1991, doi: 10.1039/AN9911601275.

[117] Shimadzu, “About Resolution, Part 1.” Accessed: Apr. 18, 2025. [Online]. Available: https://www.shimadzu.com/an/service-support/technical-support/analysis-basics/basic/resol-1.html

[118] “Crystallography Open Database”.

[119] H. Arai, M. Tsuda, and Y. Sakurai, “Lithium nickelate electrodes with enhanced high-temperature performance and thermal stability,” *J Power Sources*, vol. 90, pp. 76–81, Sep. 2000, doi: 10.1016/S0378-7753(00)00451-1.

[120] S. J. Pennycook and P. D. Nellist, *Scanning Transmission Electron Microscopy Imaging and Analysis*, 1st Edition. New York: Springer, 2011.

[121] VacCoat, “What Is An Electron Microscope.” Accessed: Feb. 28, 2025. [Online]. Available: https://vaccoat.com/blog/electron-microscope/#:~:text=Electron%20Microscope%20(EM),biological%20and%20non%2Dbiological%20samples.

[122] O. Strbak *et al.*, “Influence of dextran molecular weight on the physical properties of magnetic nanoparticles for hyperthermia and MRI applications,” *Nanomaterials*, vol. 10, no. 12, pp. 1–18, Dec. 2020, doi: 10.3390/nano10122468.

[123] C. G. Flores-Hernández, M. de los A. Cornejo-Villegas, A. Moreno-Martell, and A. Del Real, “Synthesis of a biodegradable polymer of poly (Sodium alginate/ethyl acrylate),” *Polymers (Basel)*, vol. 13, no. 4, pp. 1–12, Feb. 2021, doi: 10.3390/polym13040504.

[124] H & M Analytical Services, “Thermal Analysis - Thermal Gravimetric Analysis (TGA)”, Accessed: Nov. 22, 2024. [Online]. Available: h-and-m-analytical.com/thermal-analysis/

[125] C. M. Lopez, X. Yao, R. Samajdar, and K. Vajaria, “Assembling coin cells in half cell format. Measurement Good Practice Guide. 153,” National Physics Laboratory, Apr. 2024. doi: 10.47120/npl.mgpg153.

[126] Metrohm, “Constant current constant voltage (CCCV) cycling with INTELLO.” Accessed: Apr. 14, 2025. [Online]. Available: https://www.metrohm.com/en_gb/applications/application-notes/autolab-applikationen-anautolab/an-bat-014.html

[127] J. Choi, L. Dong, C. Y. Yu, C. O’Meara, E. Lee, and J. H. Kim, “Relationship of Chemical Composition and Moisture Sensitivity in $LiNi_xMn_YCo_{1-x-Y}O_2$ for Lithium-Ion Batteries,” *Journal of Electrochemical Energy Conversion and Storage*, vol. 18, no. 4, Nov. 2021, doi: 10.1115/1.4051208.

[128] Metrohm, “Differential capacity analysis (DCA) for battery research with INTELLO.” Accessed: Apr. 14, 2025. [Online]. Available: https://www.metrohm.com/en_gb/applications/application-notes/autolab-applikationen-anautolab/an-bat-015.html

[129] M. Shang, X. Chen, and J. Niu, “Nickel-rich layered $LiNi_{0.8}Mn_{0.1}Co_{0.1}O_2$ with dual gradients on both primary and secondary particles in lithium-ion batteries,” *Cell Rep Phys Sci*, vol. 3, no. 2, Feb. 2022, doi: 10.1016/j.xcrp.2022.100767.

[130] T. E. Ashton *et al.*, “Stoichiometrically driven disorder and local diffusion in NMC cathodes,” *J Mater Chem A Mater*, vol. 9, no. 16, pp. 10477–10486, Apr. 2021, doi: 10.1039/d1ta01639c.

[131] I. Crawford and J. Miller, “Can taking carbon dioxide from the atmosphere and splitting it into carbon and oxygen help stem the tide of rising greenhouse gases_ _ MIT Climate Portal.” Accessed: Feb. 28, 2025. [Online]. Available: https://climate.mit.edu/ask-mit/can-taking-carbon-dioxide-atmosphere-and-splitting-it-carbon-and-oxygen-help-stem-tide

[132] A. S. Wijareni, H. Widiyandari, A. Purwanto, A. F. Arif, and M. Z. Mubarok, “Morphology and Particle Size of a Synthesized NMC 811 Cathode Precursor with Mixed Hydroxide Precipitate and Nickel Sulfate as Nickel Sources and Comparison of Their Electrochemical Performances in an NMC 811 Lithium-Ion Battery,” *Energies (Basel)*, vol. 15, no. 16, Aug. 2022, doi: 10.3390/en15165794.

[133] T. Entwistle, E. Sanchez-Perez, G. J. Murray, N. Anthonisamy, and S. A. Cussen, "Co-precipitation synthesis of nickel-rich cathodes for Li-ion batteries," *Energy Reports*, vol. 8, pp. 67–73, Nov. 2022, doi: 10.1016/j.egyr.2022.06.110.

[134] Z. Fang *et al.*, "Formation of Surface Impurities on Lithium-Nickel-Manganese-Cobalt Oxides in the Presence of CO_2 and H_2O," *J Am Chem Soc*, vol. 143, no. 27, pp. 10261–10274, Jul. 2021, doi: 10.1021/jacs.1c03812.

[135] S. R. Hall, "Biotemplated syntheses of anisotropic nanoparticles," *Proceedings of the Royal Society A: Mathematical, Physical and Engineering Sciences*, vol. 465, no. 2102, pp. 335–366, Feb. 2009, doi: 10.1098/rspa.2008.0384.

[136] C. S. Carney, R. E. Chinn, Ö. N. Doğan, and M. C. Gao, "Isothermal Decomposition Kinetics of Nickel (II) Hydroxide Powder," *J Alloys Compd*, vol. 644, pp. 968–974, Sep. 2015, doi: 10.1016/j.jallcom.2015.03.256.

[137] M. Morozov, S. Ivanov, M. Kadirov, and A. Bund, "Facile synthesis of a binder-free 3D Ni/NiO microwire network with a nanostructured fiber surface for a negative electrode in Li-ion battery," *J Appl Electrochem*, vol. 51, no. 5, pp. 815–828, May 2021, doi: 10.1007/s10800-021-01541-5.

[138] J. Zhang, J. Qiao, K. Sun, and Z. Wang, "Balancing particle properties for practical lithium-ion batteries," *Particuology*, vol. 61, pp. 18–29, Feb. 2022, doi: 10.1016/j.partic.2021.05.006.

[139] K. Märker, P. J. Reeves, C. Xu, K. J. Griffith, and C. P. Grey, "Evolution of Structure and Lithium Dynamics in $LiNi_{0.8}Mn_{0.1}Co_{0.1}O_2$ (NMC811) Cathodes during Electrochemical Cycling," *Chemistry of Materials*, vol. 31, no. 7, pp. 2545–2554, Mar. 2019, doi: 10.1021/acs.chemmater.9b00140.

[140] G. Nuroldayeva, D. Adair, Z. Bakenov, and B. Uzakbaiuly, "Revealing Phase Transition in Ni-Rich Cathodes via a Nondestructive Entropymetry Method," *ACS Omega*, vol. 8, no. 41, pp. 37899–37907, Oct. 2023, doi: 10.1021/acsomega.3c03245.

[141] S. R. Hall, "Biomimetic synthesis of high-Tc, type-ii superconductor nanowires," *Advanced Materials*, vol. 18, no. 4, pp. 487–490, Feb. 2006, doi: 10.1002/adma.200501971.

[142] M. Hendrickx *et al.*, "The Influence of Synthesis Method on the Local Structure and Electrochemical Properties of Li-Rich/Mn-Rich NMC Cathode Materials for Li-Ion Batteries," *Nanomaterials*, vol. 12, no. 13, Jul. 2022, doi: 10.3390/nano12132269.

[143] C. Liang *et al.*, "Unravelling the room-temperature atomic structure and growth kinetics of lithium metal," *Nat Commun*, vol. 11, no. 1, Dec. 2020, doi: 10.1038/s41467-020-19206-w.

[144] Gerhard. Kreysa and Michael. Schütze, *Corrosion handbook : corrosive agents and their interaction with materials. Vol. 10, Sulfur dioxide, sodium sulfate*. Wiley-VCH ; John Wiley [distributor], 2008.

[145] J. Amos, “Move to net zero ‘inevitably means more mining.’” Accessed: May 11, 2025. [Online]. Available: https://www.bbc.co.uk/news/science-environment-57234610

[146] S. Stokes and S. Jones, “UK’s largest battery energy storage site goes live.” Accessed: May 11, 2025. [Online]. Available: https://www.bbc.co.uk/news/articles/cy94y7vrj2wo

[147] O. Gordon, “Exclusive: sodium batteries to disrupt energy storage market.” Accessed: May 11, 2025. [Online]. Available: Exclusive: sodium batteries to disrupt energy storage market

[148] The Electrochemical Society, “Superconductors and the Future.” Accessed: May 11, 2025. [Online]. Available: https://www.electrochem.org/superconductors